

# Rotordynamic Analysis of Tapered Composite Driveshaft Using Conventional and Hierarchical Finite Element Formulations

Majed AL Muslmani

A thesis

In the Department

Of

Mechanical and Industrial Engineering

Presented in Partial Fulfillment of the Requirements

For the Degree of

Master of Applied Science (Mechanical Engineering) at

Concordia University

Montreal, Quebec, Canada

March 2013

©Majed Saleh AL Muslmani 2013

**CONCORDIA UNIVERSITY**  
**SCHOOL OF GRADUATE STUDIES**

This is to certify that the Thesis prepared,

By: **Majed Al Muslmani**

Entitled: **“Rotordynamic Analysis of Tapered Composite Driveshaft Using  
Conventional and Hierarchical Finite Element Formulations”**

and submitted in partial fulfillment of the requirements for the Degree of

**Master of Applied Science (Mechanical Engineering)**

complies with the regulations of this University and meets the accepted standards with respect to originality and quality.

Signed by the final Examining Committee:

\_\_\_\_\_ Chair  
Dr. M. K. Zanjani

\_\_\_\_\_ Examiner  
Dr. S. V. Hoa

\_\_\_\_\_ Examiner  
Dr. K. Galal (external)

\_\_\_\_\_ Supervisor  
Dr. R. Ganesan

Approved by:

\_\_\_\_\_ Dr. S. Narayanswamy, MASc Program Director  
Department of Mechanical and Industrial Engineering

\_\_\_\_\_ Dean Dr. Robin Drew  
Faculty of Engineering & Computer Science

Date: \_\_\_\_\_

## **Abstract**

### **Rotordynamic Analysis of Tapered Composite Driveshaft Using Conventional and Hierarchical Finite Element Formulations**

Majed Al Muslmani

In the aerospace and automotive applications driveshafts are manufactured using fiber reinforced composite materials. Compared to a conventional metallic driveshaft, a composite driveshaft gives higher natural frequencies and critical speeds, and lower vibration. The design of the driveshaft is dependent on its fundamental natural frequency and its first critical speed, and tapering the driveshaft can substantially improve the values of the natural frequency and first critical speed. In this thesis, the rotordynamic analysis of the tapered composite driveshaft is carried out using three finite element formulations: the conventional-Hermitian finite element formulation, the Lagrangian finite element formulation, and the hierarchical finite element formulation. These finite element models of the tapered composite shaft are based on Timoshenko beam theory, so transverse shear deformation is considered. In addition, the effects of rotary inertia, gyroscopic force, axial load, coupling due to the lamination of composite layers, and taper angle are incorporated in the conventional-Hermitian, the Lagrangian, and the hierarchical finite element models. The strain energy and the kinetic energy of the tapered composite shaft are obtained, and then the equations of motion are developed using Lagrange's equations. Explicit expressions for the mass matrix, the gyroscopic matrix

and the stiffness matrix of the tapered composite shaft are derived to perform rotordynamic analysis. The Lagrangian beam finite element formulation has three nodes and four degrees of freedom per each node while the conventional-Hermitian beam and the hierarchical beam finite element formulations have two nodes. The three finite element models are validated using the approximate solution based on the Rayleigh-Ritz method. A comprehensive parametric study is conducted based on the finite element models, which shows that tapering the composite driveshaft can increase considerably the natural frequency and first critical speed, and that they have nonlinear variation with the taper angle.

## **Acknowledgements**

I would like to express my sincere gratitude to Prof. Rajamohan Ganesan for his guidance, continuous encouragement, and valuable advices throughout this research. Also, I would like to be grateful to him for his time and constructive comments during writing my thesis.

In addition, I would like to acknowledge Ministry of Higher Education in Saudi Arabia for the financial support. Special thank to my colleagues at office EV 13.167 for their help and support.

Last but not least, I would like express my sincere appreciation to my family members and my friends for their support and encouragement.

## Table of Contents

List of Figures .....	x
List of Tables .....	xv
Nomenclature .....	xix
Chapter 1 Introduction and literature survey .....	1
1.1 Rotordynamic analysis .....	1
1.2 Composite materials .....	2
1.3 Finite element method (FEM) .....	3
1.4 Literature survey .....	4
1.4.1 Rotordynamic analysis of conventional metallic shaft .....	5
1.4.2 Rotordynamic analysis of composite shaft .....	7
1.5 Objectives of the thesis .....	10
1.6 Layout of the thesis .....	11
Chapter 2 Rotordynamic Analysis of Rotor-Bearing System Using Conventional Finite Element Method .....	13
2.1 Introduction .....	13
2.2 Coordinate system .....	13
2.3 Rigid disk element .....	17

2.4 Bearing element.....	21
2.5 Shaft element.....	22
2.5.1 Shape functions based on Euler - Bernoulli beam theory .....	24
2.5.2 Shape Functions based on Timoshenko Beam theory .....	26
2.5.3 Energy equations .....	31
2.5.4 Tapered driveshaft .....	33
2.6 System equations of motion and analysis .....	34
2.6.1 Whirl speeds analysis .....	35
2.6.2 Campbell Diagram and Critical Speeds.....	36
2.6.3 Steady-State Synchronous Response.....	38
2.7 Numerical Examples .....	39
2.8 Summary .....	54

### Chapter 3 Rotordynamic Analysis of Uniform Composite Shaft Using Finite Element

Method .....	55
3.1 Introduction .....	55
3.2 Stress - strain relations for a composite material layer .....	56
3.1 Strain-displacement relations .....	60
3.2 Kinetic and strain energy expressions.....	62
3.3 Conventional-Hermitian finite element formulation.....	70
3.4 Numerical examples .....	77
3.5 Summary .....	101

Chapter 4 Rotordynamic Analysis of Tapered Composite Shaft Using Finite Element Method .....	102
4.1 Introduction .....	102
4.2 Stress-strain relations for tapered cylinder layer .....	102
4.3 Kinetic and potential energy expressions .....	108
4.4 Finite element formulation .....	115
4.4.1 Hierarchical composite shaft element formulation .....	115
4.4.2 Lagrangian composite shaft element formulation .....	123
4.4.3 Conventional-Hermitian composite shaft element formulation .....	130
4.5 Rayleigh – Ritz solution .....	141
4.6 Validation .....	146
4.7 Summary .....	150
Chapter 5 Parametric Study of Tapered Composite Shaft .....	151
5.1 Introduction .....	151
5.2 Tapered composite shaft case A .....	152
5.3 Tapered composite shaft Case B .....	166
5.3.1 Effect of length on natural frequencies and first critical speed .....	167
5.3.2 Effect of shaft diameter on natural frequencies and first critical speed .....	172
5.3.3 Effect of fiber orientation on the natural frequencies and first critical speed .....	176
5.3.4 Effect of the stiffness of the bearing on the first critical speed .....	183

5.3.5 Effect of axial load on natural frequencies and first critical speed .....	185
5.3.6 Effect of the disk on the natural frequencies and first critical speed.....	191
5.4 Summary .....	194
Chapter 6 Conclusions, contributions, and future work .....	195
6.1 Conclusions .....	195
6.2 Contributions.....	197
6.3 Future work .....	197
References.....	199
Appendix A Uniform Composite shaft-Conventional finite element.....	204
Appendix B Hierarchical shaft element formulation .....	215
Appendix C Lagrange's interpolation formulation.....	234
Appendix D Conventional finite element .....	248

## List of Figures

Figure 2.1 Typical rotor-bearing system.....	14
Figure 2.2 Cross-section rotation angles.....	16
Figure 2.3 Typical rotating rigid disk. ....	18
Figure 2.4 Rotating shaft supported at its ends by two bearings. ....	21
Figure 2.5 Typical finite shaft element.....	23
Figure 2.6 The displacements and the rotations in the two bending planes .....	24
Figure 2.7 Deformed geometry of an edge of beam under the assumption of Timoshenko beam theory.....	27
Figure 2.8 Typical Campbell diagram of rotor-bearing system.....	38
Figure 2.9 The rotor system configuration with two bearings and two disks.....	40
Figure 2.10 The Campbell diagram of the rotor system for isotropic bearings (case 1). .	42
Figure 2.11 The mode shape of the rotor at 4000 rpm supported by isotropic bearings (case 1).....	43
Figure 2.12 The Campbell diagram of the rotor system supported by anisotropic bearings (case 2).....	45
Figure 2.13: The mode shape of the rotor system supported by anisotropic bearings (case 2). ....	46
Figure 2.14: Steady-state response of the rotor-bearing system at node 3 in y and z directions case 1 (isotropic bearings).....	47

Figure 2.15: Steady-state response of the rotor-bearing system at node 5 in y and z directions for case 1 (isotropic bearings).....	48
Figure 2.16: Steady-state response of the rotor-bearing system at node 3 and node 5 in y direction for case 1 (isotropic bearings).....	48
Figure 2.17 Campbell diagram of the rotor system supported by isotropic bearings .....	49
Figure 2.18 The configuration of the overhung rotor with one disk and two bearings ....	50
Figure 2.19 The stepped shaft-disk system.....	52
Figure 3.1 Single composite material lamina deformed into a uniform cylinder. ....	57
Figure 3.2 Single layer of composite material in the principal material coordinates. ....	58
Figure 3.3 The forces and moments on the cross-section of the composite shaft .....	65
Figure 3.4 Deformed geometry of an edge of beam under the assumption of Timoshenko Beam theory .....	71
Figure 3.5 Campbell diagram of boron/epoxy composite shaft.....	81
Figure 3.6 Mode shapes of the boron/epoxy composite shaft at 5000 rpm. ....	82
Figure 3.7 The Campbell diagram of the graphite/epoxy composite shaft-disk system...	86
Figure 3.8 The mode shapes of the graphite/epoxy composite shaft-disk system at 6000 rpm. ....	87
Figure 3.9 Unbalance response and phase angle of the graphite/epoxy composite shaft at the disk position in y and z directions.....	88
Figure 3.10 The stepped composite shaft-disk system. ....	89
Figure 3.11 The stepped composite shaft under the axial load.....	97

Figure 3.12 The natural frequencies of the stepped composite shaft at 0 rpm under different axial loads.....	98
Figure 3.13 The backward natural frequencies of the stepped composite shaft at 5000 rpm under different axial loads.....	99
Figure 3.14 The forward natural frequencies at 5000 rpm under different axial loads. .	100
Figure 4.1 Single composite lamina deformed into tapered cylinder .....	103
Figure 4.2 Typical tapered shaft element.....	109
Figure 4.3 Hierarchical beam finite element with two nodes .....	115
Figure 4.4 Beam element with three nodes.....	124
Figure 4.5 The configuration of the tapered graphite - epoxy composite shaft.....	147
Figure 5.1 The configuration of the tapered composite shaft with disk in the middle ...	152
Figure 5.2 The first critical speeds of the tapered composite shaft for different taper angles obtained using Hermitian finite element model.....	155
Figure 5.3 The first critical speeds of the tapered composite shaft for different taper angles determined using Lagrangian finite element model .....	155
Figure 5.4 The first critical speeds of the tapered composite shaft for different taper angles determined using Hierarchical finite element model.....	156
Figure 5.5 $Q_{11}, Q_{15}, Q_{16}, Q_{55}$ , and $Q_{66}$ for the layer of graphite-epoxy with fiber orientation angle of $0^\circ$ .....	156
Figure 5.6 $Q_{11}, Q_{15}, Q_{16}, Q_{55}$ , and $Q_{66}$ for the layer of graphite-epoxy with fiber orientation angle of $90^\circ$ .....	157

Figure 5.7 Q11, Q15, Q16, Q55, and Q66 for the layer of graphite-epoxy with fiber orientation angle of 45° .....	157
Figure 5.8 Q11, Q15, Q16, Q55, and Q66 for the layer of graphite-epoxy with fiber orientation angle of -45° .....	158
Figure 5.9 Tapered composite shaft with different positions of the disk.....	159
Figure 5.10 The mode shapes of the tapered composite shaft with taper angle of 0° at 6000 rpm .....	163
Figure 5.11 Campbell diagram of the tapered composite shaft with taper angle of 0° ..	163
Figure 5.12 The mode shapes of the tapered composite shaft with taper angle of 3° at 6000 rpm .....	164
Figure 5.13 Campbell diagram of the tapered composite shaft with taper angle of 3° ..	164
Figure 5.14 The mode shapes of the tapered composite shaft with taper angle of 5° at 6000 rpm .....	165
Figure 5.15 Campbell diagram of the tapered composite shaft with taper angle of 5° ..	165
Figure 5.16 Different lengths of the tapered composite shaft.....	166
Figure 5.17 First critical speeds for different lengths determined using hierarchical finite element.....	171
Figure 5.18 First critical speeds for different diameters obtained using hierarchical finite element.....	175
Figure 5.19 First critical speeds for different fiber orientation angles based on hierarchical finite element.....	182

Figure 5.20 First critical speed for different bearing stiffness values determined using hierarchical finite element.....	184
Figure 5.21 First critical speed of the tapered composite shaft with taper angle of $0^\circ$ for different axial loads obtained using hierarchical finite element .....	188
Figure 5.22 First critical speed of the tapered composite shaft with taper angle of $1^\circ$ for different axial loads obtained using hierarchical finite element .....	188
Figure 5.23 First critical speed of the tapered composite shaft with taper angle of $2^\circ$ for different axial loads obtained using hierarchical finite element .....	189
Figure 5.24 First critical speed of the tapered composite shaft with taper angle of $3^\circ$ for different axial loads obtained using hierarchical finite element .....	189
Figure 5.25 First critical speed of the tapered composite shaft with taper angle of $4^\circ$ for different axial loads obtained using hierarchical finite element .....	190
Figure 5.26 First critical speed of the tapered composite shaft with taper angle of $5^\circ$ for different axial loads obtained using hierarchical finite element .....	190
Figure 5.27 The tapered composite shaft with the attached disk .....	191

## **List of Tables**

Table 2.1 Eigenvalues and natural frequencies of the rotor supported by isotropic bearings at two different speeds (case 1). .....	41
Table 2.2 The first seven critical speeds of the rotor supported by isotropic bearings (case 1). .....	41
Table 2.3 Eigenvalues and natural frequencies of the rotor supported by anisotropic bearings at two different speeds (case 2). .....	44
Table 2.4 The first seven critical speeds of the rotor supported by anisotropic bearings (case 2). .....	44
Table 2.5 The natural frequencies in Hz under the effect of different tensile and compression axial loads .....	51
Table 2.6 The properties of the stepped shaft-disk system.....	52
Table 2.7 The natural frequencies in Hz of the stepped shaft with different lengths $L_2$ ..	53
Table 2.8: The natural frequencies in Hz of the stepped shaft with different diameters $d_2$ . .....	54
Table 3.1 The dimensions of the composite shaft and the properties of the bearing [20].	79
Table 3.2 Properties of the composite materials [20] .....	79
Table 3.3 The first critical speed of the boron-epoxy composite shaft.....	80
Table 3.4 The first five critical speeds of the boron-epoxy composite shaft.....	81
Table 3.5 The dimensions and properties of the composite shaft-disk system [20] .....	83

Table 3.6 The first five critical speeds of the graphite/epoxy composite shaft-disk system. ....	84
Table 3.7 The lowest five eigenvalues in rad/s of the graphite/epoxy composite shaft-disk system running at 6000 rpm and 0 rpm. ....	85
Table 3.8 The geometric dimensions and properties of the composite shaft-disk system	90
Table 3.9 Natural frequencies in Hz of stepped composite rotor with different lengths ..	91
Table 3.10 Natural frequencies in Hz of stepped composite rotor with different fiber orientation angles .....	92
Table 3.11 The natural frequencies of the stepped composite shaft-disk system with different lengths of segment 1 and segment 2 .....	93
Table 3.12 The geometric dimensions of segment 2 of the stepped shaft .....	94
Table 3.13 The natural frequencies of the stepped composite shaft-disk system with different diameters of the segment 2.....	95
Table 3.14 The natural frequencies of the stepped composite shaft-disk system with different densities of the disk .....	96
Table 3.15 The geometric dimensions of the composite shaft-disk system .....	97
Table 4.1 Properties of the composite materials [20] .....	147
Table 4.2 First critical speed in rpm of the tapered composite shaft with different taper angles using finite element method and Rayleigh-Ritz method .....	148

Table 4.3 The natural frequencies in Hz of the tapered composite shaft at 10000 rpm with different taper angles obtained using finite element method and Rayleigh-Ritz method. .....	149
Table 5.1 The geometric dimensions and properties of the tapered composite shaft .....	153
Table 5.2 The first critical speed in rpm of the tapered composite shaft for different taper angles. ....	154
Table 5.3 First critical speed in rpm of the tapered composite shaft for different taper angles and positions of the disk .....	159
Table 5.4 The first critical speed in rpm of the tapered composite shaft for different taper angles and stacking sequences obtained using Hermitian finite element model .....	161
Table 5.5 The first critical speed in rpm of the tapered composite shaft for different taper angles and stacking sequences determined using Lagrangian finite element model .....	161
Table 5.6 The first critical speed in rpm of the tapered composite shaft for different taper angles and stacking sequences determined using Hierarchical finite element model ....	162
Table 5.7 Natural frequencies in Hz of the tapered composite shaft with different lengths .....	168
Table 5.8 First critical speed in rpm of the tapered composite shaft with different lengths and taper angles.....	170
Table 5.9 Natural frequencies in Hz of the tapered composite shaft at 5000 rpm for different diameters obtained using hierarchical finite element. ....	173

Table 5.10 First critical speed in rpm of the tapered composite shaft for different diameters.....	174
Table 5.11 Natural frequencies in Hz of the tapered composite shaft at 5000 rpm with different fiber orientation angles obtained using hierarchical finite element - I.....	177
Table 5.12 Natural frequencies in Hz of the tapered composite shaft at 5000 rpm with different fiber orientation angles obtained using hierarchical finite element - II .....	178
Table 5.13 First critical speed in rpm of the tapered composite shaft with different fiber orientation angles .....	179
Table 5.14 Natural frequencies in Hz of the tapered composite shaft at 5000 rpm with different tensile loads using the hierarchical finite element .....	186
Table 5.15 Natural frequencies in Hz of the tapered composite shaft at 5000 rpm with different compressive loads using hierarchical finite element.....	187
Table 5.16 Natural frequencies in Hz of the tapered composite shaft at 5000 rpm with different material densities of the disk.....	192
Table 5.17 The first critical speed in rpm of the tapered composite shaft for different material densities of the disk.....	193

## Nomenclature

$v$	Displacement of the shaft in y direction
$w$	Displacement of the shaft in z direction
$\beta_y$	Rotation of the shaft around y direction
$\beta_z$	Rotation of the shaft around z direction
$\Omega$	Rotational speed of the shaft
$[M_d]$	Mass matrix of the disk
$[G_d]$	Gyroscopic matrix of the disk
$k_{yy}$	Stiffness of bearing in y direction
$k_{zz}$	Stiffness of bearing in z direction
$c_{yy}$	Damping of bearing in y direction
$c_{zz}$	Damping of bearing in z direction
$G$	Shear modulus
$E$	Young's modulus

$k_s$	Shape factor depending on the shape of the cross-section and the Poisson ratio
I	Second moment of area of the cross-section about the neutral plane
A	Area of cross-section of the shaft element
$\phi_{xz}$	Shear angle in x-z plane
$\phi_{xy}$	Shear angle in x-y plane
$P$	Axial load
$[M_T]$	Translational mass matrix of uniform metal shaft
$[M_R]$	Rotational mass matrix of uniform metal shaft
$[G_{\text{shaft}}]$	Gyroscopic matrix of uniform metal shaft
$[K_B]$	Bending stiffness matrix of uniform metal shaft
$[K_S]$	Shear stiffness matrix of uniform metal shaft
$[K_F]$	Geometric stiffness matrix due to axial load of uniform metal shaft

$[\Psi_{EB}]$	Translational shape function matrix based on Euler-Bernoulli beam theory
$[\Phi_{EB}]$	Rotational shape function matrix based on Euler-Bernoulli beam theory
$[\Psi_{Tim}]$	Translational shape function matrix based on Timoshenko beam theory
$[\Phi_{Tim}]$	Rotational shape function matrix based on Timoshenko beam theory
$M_y$	Moment of the composite shaft around y axis
$M_z$	Moment of the composite shaft around z axis
$Q_y$	Shear force in y direction
$Q_z$	Shear force in z direction
$[Q]$	Stiffness matrix of a single lamina
$U_{BS}$	Strain energy of the composite shaft due to bending moments and shear forces
$U_F$	Strain energy due to axial load

$U_{comp}$	Total strain energy of the composite shaft
$[M_{Tc}]$	Translational mass matrix of uniform composite shaft
$[M_{Rc}]$	Rotational mass matrix of uniform composite shaft
$[G_{Shaft_c}]$	Gyroscopic matrix of uniform composite shaft
$[K_{Bc}]$	Bending stiffness matrix of uniform composite shaft
$[K_{Shc}]$	Shear stiffness matrix of uniform composite shaft
$[K_{Fc}]$	Geometric stiffness matrix due to axial load of uniform composite shaft
$[\bar{Q}]$	Transformed stiffness matrix of layer due to fiber orientation angle $\eta$
$[\bar{\bar{Q}}]$	Transformed stiffness matrix of layer due to taper angle $\alpha$
$[\sigma_{x\theta r}]$	Stress matrix corresponding to cylindrical coordinate system $(x, \theta, r)$
$[\varepsilon_{x\theta r}]$	Strain matrix corresponding to cylindrical coordinate system $(x, \theta, r)$

$[\sigma_{1'2'3'}]$	Stress matrix corresponding to coordinate system (1', 2', 3')
$[\varepsilon_{1'2'3'}]$	Strain matrix corresponding to coordinate system (1', 2', 3')
$[N_v], [N_w], [N_{\beta_y}], [N_{\beta_z}]$	Shape functions matrix - Hierarchical finite element formulation
$N_{11}, N_{22}, N_{33}$	Shape functions - Lagrangian finite element formulation
$\eta$	Fiber orientation angle
$\alpha$	Taper angle
$[\sigma_{123}]$	Stress matrix corresponding to coordinate system (1, 2, 3)
$[\varepsilon_{123}]$	Strain matrix corresponding to coordinate system (1, 2, 3)
$[T_1]$	Stress Transformation matrix of layer due to angle $\eta$
$[T_2]$	Strain Transformation matrix of layer due to angle $\eta$
$[T_3]$	Stress Transformation matrix of layer due to angle $\alpha$
$[T_4]$	Strain Transformation matrix of layer due to angle $\alpha$

# Chapter 1

## Introduction and literature survey

### 1.1 Rotordynamic analysis

Today, rotating machines play an important role in aerospace and power industries. They are used in applications such as aircraft engines, power plant stations, medical equipment, automobiles, and helicopters. Designing rotating machines requires determining their dynamic behavior, so it is essential to use modern techniques to model and analyze the rotating machines. Studying the dynamic behavior of rotating machines to determine their dynamic characteristics such as critical speeds, bending natural frequencies and unbalance response, usually is defined as rotordynamic analysis.

Typically, any rotating machine has three main components: rotor, bearings, and attached disks or blades. The rotor is considered the heart of rotating machines; and since the rotating machine interacts with its surroundings, such as a high-pressure fluid or unbalance of an attached disk or blade, the rotor experiences a high level of vibration. This unacceptable level of vibration can lead to high stresses in the rotor, noise, a bad surface finish in machining tools, and damage or failure in bearing or seals.

In fact, vibration of the rotor can happen in different ways: lateral vibration, axial vibration, and torsional vibration. In lateral vibration, the rotor moves in orbital motion, which is the result of a combination of motions in horizontal and vertical directions. Axial vibration happens along the rotor's axis, while torsional vibration appears as a twisting in the rotor around its axis. Lateral vibration has a more significant effect on the

rotor than axial or torsional vibration, because lateral vibration has more amount of energy than axial or torsional vibration [1].

Moreover, lateral forces, such as unbalance force that exists in attached disks or blades, are considered the main reason for lateral vibration. When rotor speed is equal to any bending natural frequencies of the rotor, the rotor undergoes violent vibration and the corresponding speed of the rotor is referred to as a critical speed.

## **1.2 Composite materials**

When two or more materials with different properties and mechanical performance come together to make a new material, the performance and properties of which are designed to be more advanced than those of the individual materials, the new material is defined as a composite material [2]. On macroscopic scale, advanced composite materials consist of two phases: fiber reinforcement material and matrix material. Fiber reinforcement is stiffer and stronger than the matrix and provides composite materials with high strength and stiffness, while the matrix holds the fibers in their direction, protects them from environmental effects, and transfers the load between the fibers [3].

Advanced composite materials have a high specific strength and specific stiffness -to-weight ratio compared to conventional metallic materials, such as steel and aluminum; in addition, advanced composite materials have a high fatigue life, good capability to resist corrosion, and low thermal expansion [3]. As a result of their characteristics, advanced composite materials are extensively used in the aerospace and automobile industries.

Recently, driveshafts in helicopters and vehicles have started to be manufactured with composite materials rather than conventional metallic materials, because composite materials improve the dynamic characteristics of the driveshaft. Also, the advanced composite materials give the driveshaft higher critical speeds and higher bending natural frequencies compared to conventional metallic materials.

However, an advanced composite shaft cannot transfer the same amount of torque as conventional metallic shaft that has the same size as the composite shaft; and at certain level of torsional load, torsional buckling happens in the advanced composite shaft before the conventional metallic shaft. To overcome this problem, a hybrid metallic composite shaft can be used; where the composite materials increase the bending natural frequency and the metallic materials improve the capability of transferring a high amount of torque.

### **1.3 Finite element method (FEM)**

FEM is the most popular computational method, and it is used to solve and analyze a large range of engineering problems, such as structural dynamics, stress analysis, heat transfer, and fluid flow. The concept behind FEM is simple. Instead of defining the approximation functions over the complete domain, as the Rayleigh-Ritz method does, FEM defines the admissible function only over a finite number of subdomains, named *finite elements*. Nowadays, there are many types of computer software based on finite element method, and the most famous softwares in industry and academics being ANSYS<sup>®</sup>, NASTRAN<sup>®</sup>, and ABAQUS<sup>®</sup>.

Finite element method can be divided into two categories: conventional and advanced finite element method. In conventional finite element method, the rotor usually is modeled by a beam element that has two nodes in total, one node for each of its ends; each node has four degrees of freedom, that are two displacements and two rotations. Since finite element method gives an approximation solution, the rapid convergence of solutions depends on increasing the number of elements. Today, with fast improvement in computer capabilities, it is possible to use large number of elements to obtain an accurate solution. However, for some complex engineering problems, increasing the number of elements can be expensive and time consuming, even with a sophisticated computer.

An example of an advanced finite element method is the hierarchical finite element method. The idea behind the hierarchical finite element is to keep the mesh unchanged and increase the degree of the admissible functions; this can be achieved by adding polynomial and trigonometric terms inside the admissible functions to increase the degrees of freedom that resulted in fast convergence. Moreover, it is possible to obtain a combination of the conventional finite element and the hierarchical finite element, where the mesh of the elements and the degree of the admissible functions are changeable; this combination usually is referred to as an *hp*- version of finite element method [22].

#### **1.4 Literature survey**

Driveshaft design depends on predicting critical speeds and bending natural frequencies. Different analytical and computational methods have been used to study the behaviour of

rotordynamic systems. Herein, the literature survey is divided into two parts. The first part presents some important rotordynamic analyses of conventional metallic driveshafts. The second part presents rotordynamic analysis of driveshafts made of composite materials.

#### **1.4.1 Rotordynamic analysis of conventional metallic shaft**

As mentioned before, the finite element method (FEM) is the most popular computational method, and with advanced computer technology it becomes easier to apply FEM on complex problems. In fact, there is vast literature on rotordynamic analysis of driveshafts using FEM.

In his PhD thesis, Ruhl [4] used FEM to model a turbo-rotor system; the model did not account for rotary inertia, axial load, gyroscopic moments, shear deformation or internal damping. However, his early investigation, of using FEM for a rotor-bearing system is considered seminal. Ruhl used his model to predict the instability region and unbalance response of a rotor-bearing system.

Nelson and McVaugh [5] introduced a procedure to model a rotordynamic system using FEM; their system consisted of a flexible shaft, rigid disks, and discrete bearings. Equations of motion of each part of the system (disk, rotor and bearing) were derived separately and then the general equation of the system was obtained by assembling the equations of each component (disk, rotor and bearing). The model included the effects of rotary inertia, gyroscopic moments, and axial load. The finite element had two nodes; each node had four degrees of freedom, two translations and two rotations.

In addition, Nelson and Zorzi [6] studied the effect of a constant axial torque on dynamic characteristics of a rotor-bearing system, and they found that the critical speeds of the rotor system were not affected by the level of axial torque. However, when the rotordynamic system was operated at high speed, the effect of the axial torque on the stability, reliability and safety cannot be neglected.

Nelson and Zorzi [7] studied the internal damping effect on the dynamic behavior of a rotor-bearing system. The internal damping was represented in two linear damping forms: viscous and hysteretic damping. The researchers found that the internal damping had a negative effect on the stability of system: the viscous damping led the rotor-bearing system to instability at the first critical speed, while hysteretic damping made the system unstable at all critical speeds. Nelson [8] used Timoshenko beam theory to include the effects of transverse shear deformation, gyroscopic moment, rotary inertia, and axial load. In addition, Chen and Ku [9] used a Ritz finite element technique to predict the regions of dynamic instability of a rotor-bearing system subjected to periodic axial force; the rotating shaft was modeled based on Timoshenko beam theory.

Moreover, the tapered shaft captured an interest among rotordynamics researchers. Greenhill et al. [10] extended the linearly tapered Timoshenko beam theory to develop a tapered finite element formulation for a shaft; they included the shear deformation in the finite element as a degree of freedom. The conical element had two nodes and each one of them had six degrees of freedom: two translations, two rotations, and two shear deformations. Genta and Gugliotta [11] introduced an axisymmetrical conical beam finite

element with two complex degrees of freedom at each node. Also, Khuief and Mohiuddin [12] developed an equation of coupled bending and torsional motions using Lagrange's equation; they derived a conical finite element with two nodes and ten degrees of freedom for each node. The conical finite element was derived based on Timoshenko beam theory.

#### **1.4.2 Rotordynamic analysis of composite shaft**

Recently, composite materials have been used on a large scale for different structural applications. Since composite materials have high strength- and stiffness-to-weight ratios, composite materials have become more attractive to manufacturers in the aerospace and automobile industries. Advanced composite materials dramatically improve the dynamic characteristics of shafts in terms of critical speeds, bending natural frequencies, and unbalance response.

Zinberg and Symonds [13] developed an advanced composite tail rotor for helicopters. They experimentally studied a boron/epoxy composite shaft and determined its critical speeds; their results show an improvement in the dynamic behavior of composite shafts over aluminum shafts. Also, Hetherington et al. [14] experimentally investigated the dynamic performance of supercritical helicopter power transmission composite shafts; their experiment indicated that composite shafts can be operated above at least the second critical speed. Also, it was observed that external damping is required for safe and stable supercritical operation.

Singh and Gupta [15] published formulations for the rotordynamics of composite shafts by using two different theories: the conventional equivalent modulus beam theory (EMBT) and a layerwise beam theory (LBT). Performance rotordynamics parameters such as critical speed, unbalance response, bending natural frequencies, and threshold of stability were more accurately predicted using LBT than using EMBT. In fact, EMBT has some limitations that LBT does not. Specifically, EMBT does not measure the effects of bending-stretching coupling, shear-normal coupling, bending-twisting coupling, cross-sectional deformations, or out-of-plane warping. In another study, Guبران and Gupta [16] published a modification of the equivalent modulus beam theory to include the effect of the stacking sequence and coupling mechanisms of composite materials. The bending natural frequencies of the composite shaft that was analyzed using the modified EMBT showed a good agreement with LBT results.

Kim and Bert [17] studied the vibration of cylindrical hollow composite shafts using the Sanders best first approximation shell theory. They investigated the critical speeds of different types of composite rotors and compared the results to those obtained using the classical beam theory, and the compared results well agreed. Hu and Wang [18] performed vibration analysis on rotating laminated cylindrical shells using the ABAQUS<sup>®</sup> finite element program. They studied the influences of rotating speed, end conditions, shell thickness, shell length, and shell radius on the fundamental bending natural frequency.

Chen and Peng [19] studied the stability of rotating uniform composite shafts. The composite rotor was studied using the shaft finite element, based on Timoshenko beam theory, by considering the EMBT. Chang et al. [20] developed a finite element model to study the dynamic behavior of uniform composite shaft. Their model incorporated rotary inertia, gyroscopic moments and shear deformation as well as the coupling mechanisms in composite materials. The shaft was modeled based on a first-order shear deformation beam theory. Also, Chang et al. [21] performed a vibration analysis of rotating uniform composite shafts containing randomly oriented reinforcements. Boukhalfa et al. [22] applied a p-version hierarchical finite element to model a composite shaft; the hierarchical beam finite element contained two nodes, and each node had six degrees of freedom. The model included the effects of rotary inertia, gyroscopic moments, and shear deformation as well as the coupling mechanisms in composite materials, and it was modeled as Timoshenko beam. In addition, Boukhalfa and Hadjoui [23] published free vibration analysis of uniform composite shaft using the hp-version of finite element, which is a combination of the conventional version of finite element (h-version) and the hierarchical finite element.

Kim Wonsuk, in his PhD dissertation [24], developed a mechanical model for a tapered composite Timoshenko shaft. The model represented an extended length tool holder at high speed in end milling or boring operation. The structure of the shaft had clamped – free supports. Kim used the general Galerkin method to obtain the spatial solutions of the equations of motion. He studied forced torsion, dynamic instability, forced vibration

response, and static strength of a tapered composite shaft subjected to deflection-dependent cutting forces.

### **1.5 Objectives of the thesis**

Eventhough Kim [24] developed a mechanical model for a tapered composite Timoshenko shaft and studied forced torsion, dynamic instability, and forced vibration response of a tapered composite shaft, he did not use the finite element method. In fact Kim used the general Galerkin method to obtain the spatial solutions of the equations of motion, and the solution was only under clamped-free condition of the tapered composite shaft. Based on the author's knowledge there is no work that has been carried out on the rotordynamic analysis of tapered composite driveshaft based on the finite element method. In this thesis, the tapered composite shaft means that the inner and outer diameters of one end are constant while the inner and outer diameters of the other end increase with increasing the taper angle.

The objectives of the present thesis are: (1) to develop three different finite element models: conventional-Hermitian, hierarchical, and conventional-Lagrangian finite element models for rotordynamic analysis of tapered composite shaft; (2) to investigate the bending natural frequencies, critical speeds and mode shapes of tapered and uniform composite shafts; (3) to validate the developed finite element models using the approximate solution that is obtained based on the Rayleigh-Ritz method; and (4) to conduct a comprehensive parametric study on uniform and tapered composite driveshafts.

Moreover, rotordynamic analysis of metal driveshaft based on conventional-Hermitian finite element is very well established, so the conventional-Hermitian finite element is used for rotordynamic analysis of the uniform and the tapered composite driveshaft in this thesis. In addition, the conventional-Lagrangian finite element model [20] and hierarchical finite element model [22] of uniform composite driveshaft have already been developed; but no work has been done on tapered composite driveshaft using these finite element methods. Therefore, in the present thesis, the conventional-Hermitian, the conventional-Lagrangian, and hierarchical finite element models are developed to establish a comparison between finite element solutions. Furthermore, these finite element models are validated using the Rayleigh-Ritz method.

## **1.6 Layout of the thesis**

This chapter presents introductory information on rotordynamic analysis, composite materials, and finite element method. Also, it provides a literature survey on rotordynamic analysis of conventional metallic driveshafts and composite material driveshaft.

Chapter 2 presents the rotordynamic analysis of conventional metallic shafts using conventional finite element.

In chapter 3 a formulation based on conventional-Hermitian finite element is developed and applied to the rotordynamic analysis of uniform composite driveshafts based on Timoshenko Beam Theory; the effect of axial load is considered in the formulation.

Chapter 4 provides four different formulations for tapered composite driveshafts: conventional-Hermitian, hierarchical, and Lagrangian finite elements as well as Rayleigh-Ritz formulation

Chapter 5 gives a detailed parametric study on rotordynamics of tapered composite shafts. The study includes the effects of stacking sequence, axial load, fiber orientation, length of the driveshaft and taper angle.

Chapter 6 closes the thesis by providing an overall conclusion of the present work and by suggesting recommendations for future work.

## **Chapter 2**

# **Rotordynamic Analysis of Rotor-Bearing System Using Conventional Finite Element Method**

### **2.1 Introduction**

In this chapter, vibration analysis of conventional metal driveshaft using conventional finite element formulation is presented. A finite shaft element is developed for this purpose. Two different models are developed based on two different beam theories; one is based on Euler -Bernoulli beam theory and the other model is based on Timoshenko beam theory. In Euler –Bernoulli beam theory rotary inertia and shear deformation are ignored, while in Timoshenko beam theory they are considered. Also, the effect of the axial load is included in both the models. Moreover, rotor-bearing system with tapered shaft is modeled based on Timoshenko theory. Rotordynamic analysis including determination of natural frequencies, critical speeds, mode shapes and steady-state response is conducted and applications to example systems are provided. Rotordynamic analysis of conventional metal driveshaft is a very well established topic, so the equations in this chapter are borrowed from References [1, 25, 26] to provide basic information and introduction about rotordynamic analysis.

### **2.2 Coordinate system**

A typical rotor-bearing system consists of three main parts: rotor, disk and bearing. Figure 2.1 shows a typical rotor-bearing system. The equations of motion of the rotor-

bearing system depend on the equations of motion of each component. Thus, it is necessary to develop the individual equations of motion of the rotor, bearing and disk. Then, one can assemble them to obtain general equations of motion for the rotor-bearing system. Moreover, in order to develop the equations of motion of rotor-bearing system using finite element method, it is required to divide the rotor into number of elements which are connected together with nodes. Each element has two nodes located at the ends where disks and bearings are attached to the rotor. Since the vibration analysis in this work is focus only on lateral vibration, each node has four degrees of freedom: two translations in the y and z directions and two rotations about the y- and z-axes. The translational motions of any node on the rotor are defined from the equilibrium position by displacements v and w in y and z directions, respectively, while the rotational motions are defined by rotations  $\beta_y$  and  $\beta_z$  about y- and z-axes, respectively. Here, it is assumed that the rotations  $\beta_y$  and  $\beta_z$  are small [1].

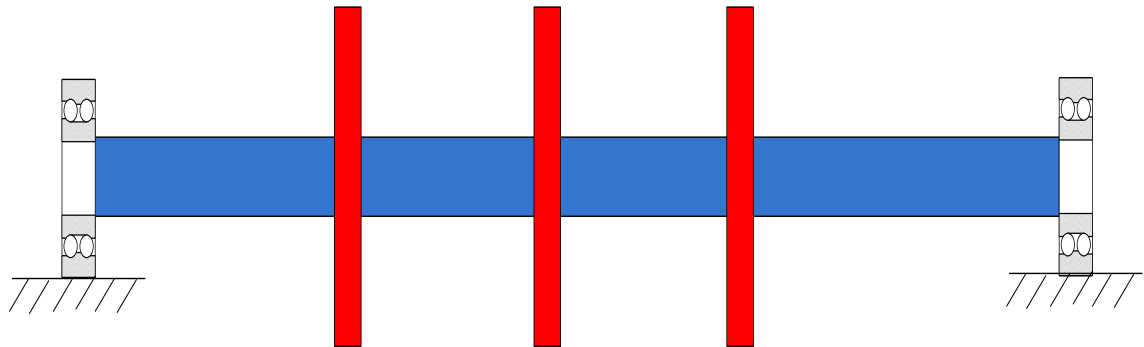


Figure 2.1 Typical rotor-bearing system

In addition, rotor-bearing system is described by two coordinate systems: (a)  $xyz$  which is fixed to the space (b)  $\bar{x}\bar{y}\bar{z}$  which is fixed to the cross-section of the disk and the shaft and rotates with them; the two coordinate systems are related through a set of rotation angles. The kinetic energy of the shaft element and the disk are function of the instantaneous angular velocities in  $\bar{x}\bar{y}\bar{z}$  frame. So, it is assumed that the instantaneous angular velocities in  $xyz$  frame are  $\dot{\beta}_y$  about the y-axis,  $\dot{\beta}_z$  about the z-axis and  $\dot{\phi}$  about the x-axis, and they have to be transferred to  $\bar{x}\bar{y}\bar{z}$  frame. In order to do this, it is necessary to choose an order of rotations as it is shown in Fig 2.2, and the rotations are applied in the following order [1]:

- 1)  $\beta_y$  about y-axis (it makes  $x'y'z'$  coordinate)
- 2)  $\beta_z$  about the new z-axis (it makes  $x''y''z''$  coordinate)
- 3)  $\phi$  about the new x-axis(it makes  $\bar{x}\bar{y}\bar{z}$  coordinate)

So, the instantaneous angular velocities in  $\bar{x}\bar{y}\bar{z}$  frame are [1]:

$$\begin{aligned}
 \begin{bmatrix} \omega_{\bar{x}} \\ \omega_{\bar{y}} \\ \omega_{\bar{z}} \end{bmatrix} &= \begin{bmatrix} \dot{\phi} \\ 0 \\ 0 \end{bmatrix} + \begin{bmatrix} 0 & 0 & 1 \\ \cos \phi & \sin \phi & 0 \\ -\sin \phi & \cos \phi & 1 \end{bmatrix} \begin{bmatrix} 0 \\ \dot{\beta}_z \\ 0 \end{bmatrix} \\
 &+ \begin{bmatrix} 0 & 0 & 1 \\ \cos \phi & \sin \phi & 0 \\ -\sin \phi & \cos \phi & 1 \end{bmatrix} \begin{bmatrix} 0 & -\sin \beta_z & \cos \beta_z \\ 1 & 0 & 0 \\ 0 & \cos \beta_z & \sin \beta_z \end{bmatrix} \begin{bmatrix} 0 \\ \dot{\beta}_y \\ 0 \end{bmatrix}
 \end{aligned} \tag{2.1}$$

$$\begin{bmatrix} \omega_{\bar{x}} \\ \omega_{\bar{y}} \\ \omega_{\bar{z}} \end{bmatrix} = \begin{bmatrix} \dot{\phi} - \dot{\beta}_y \sin \beta_z \\ \dot{\beta}_z \cos \phi + \dot{\beta}_y \sin \phi \cos \beta_z \\ -\dot{\beta}_z \sin \phi + \dot{\beta}_y \cos \phi \cos \beta_z \end{bmatrix} \quad (2.2)$$

where  $\omega_{\bar{x}}$ ,  $\omega_{\bar{y}}$  and  $\omega_{\bar{z}}$  are the instantaneous angular velocities about  $\bar{x}$ ,  $\bar{y}$  and  $\bar{z}$  respectively.

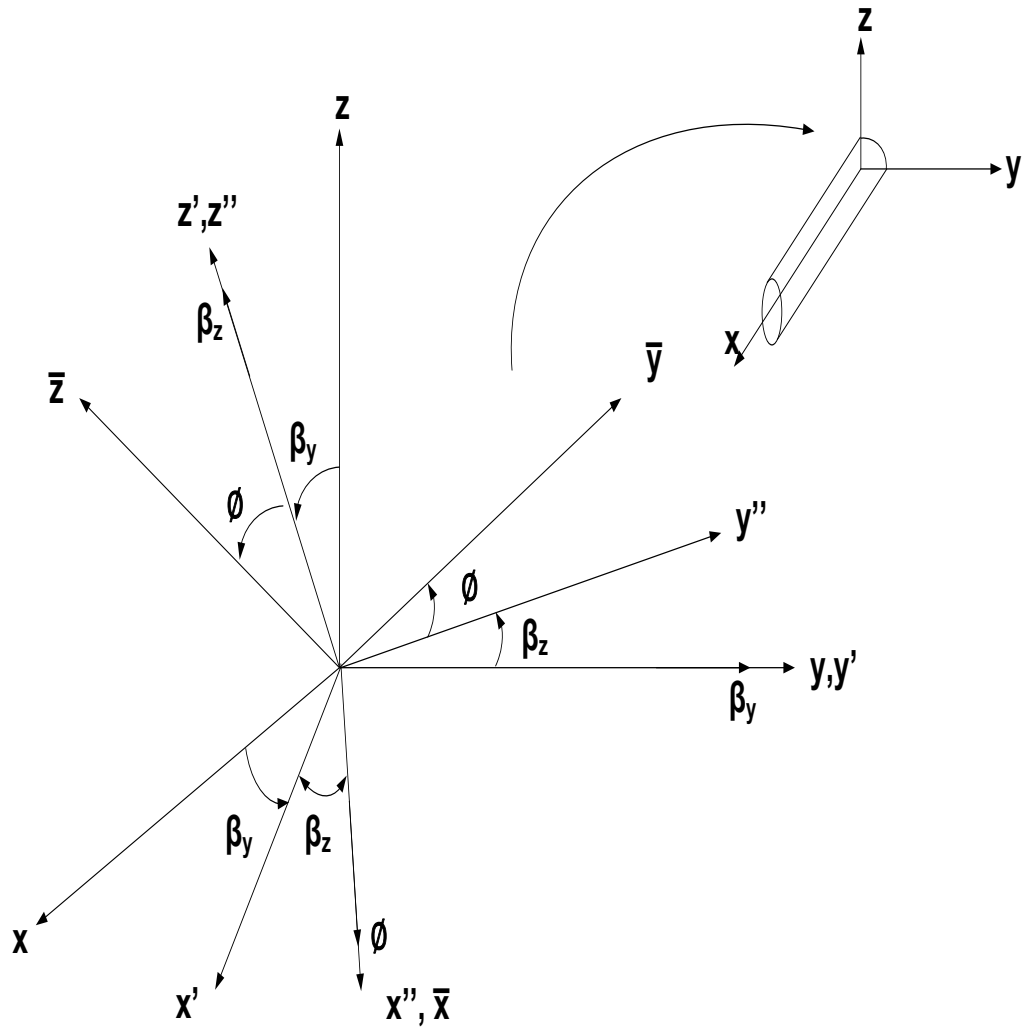


Figure 2.2 Cross-section rotation angles

Furthermore, the general equations of rotor-bearing system can be developed using the following approach:

- a. Establishing the kinetic energy  $T$  and the strain energy  $U$  for the element rotor-bearing system.
- b. Developing the lateral displacements and the rotations fields of the rotor using the finite element method.
- c. Using the Lagrange's Equation to obtain the equation of motion of the shaft element.

$$\frac{d}{dt} \left( \frac{\partial T}{\partial \dot{q}} \right) - \frac{\partial T}{\partial q} + \frac{\partial U}{\partial q} = Q$$

where  $q$  is the vector of the generalized coordinates,  $Q$  is the vector of generalized forces .

- d. Assembling the individual equations of the shaft element, disks, and bearings to obtain the general equations of motion of rotor-bearing system.

### 2.3 Rigid disk element

Energy method is used here to obtain the equation of motion of the disk. The disk is assumed to be a rigid body made of metallic material as it is illustrated in Fig 2.3, so the strain energy is neglected and the disk is described only by its kinetic energy. Herein, the rotational part of the kinetic energy is calculated with respect to  $\bar{x}\bar{y}\bar{z}$  frame that is fixed to the disk. The kinetic energy that results from the translation of the disk is

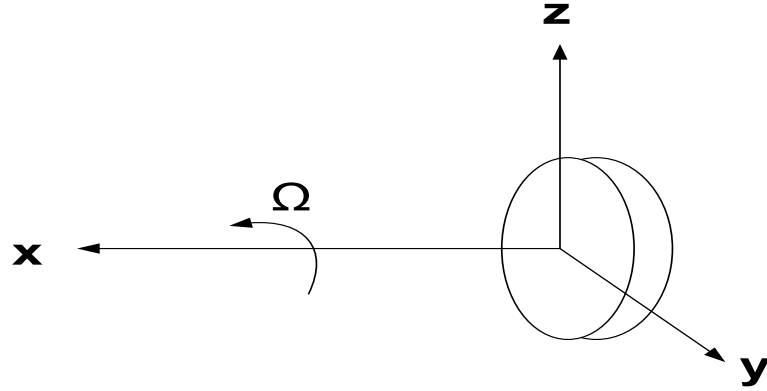


Figure 2.3 Typical rotating rigid disk.

$$T_{dt} = \frac{1}{2} (\text{disk mass}) (\text{linear velocity})^2 = \frac{1}{2} m_d (\dot{v}^2 + \dot{w}^2) \quad (2.3)$$

where  $m_d$  is the mass of the disk and  $\dot{v}$  and  $\dot{w}$  are the translational velocities in y and z directions. The kinetic energy due to disk rotation is [1]

$$T_{dr} = \frac{1}{2} I_d (\omega_{\bar{y}}^2 + \omega_{\bar{z}}^2) + \frac{1}{2} I_p \omega_{\bar{x}}^2 \quad (2.4)$$

where  $\omega_{\bar{x}}$ ,  $\omega_{\bar{y}}$  and  $\omega_{\bar{z}}$  are the angular velocities of the disk around  $\bar{x}$ ,  $\bar{y}$  and  $\bar{z}$ , respectively.  $I_p$  and  $I_d$  are the polar moment of inertia and diametral moment of inertia, respectively. The total kinetic energy is

$$T_d = \frac{1}{2} m_d (\dot{v}^2 + \dot{w}^2) + \frac{1}{2} I_d (\omega_{\bar{y}}^2 + \omega_{\bar{z}}^2) + \frac{1}{2} I_p \omega_{\bar{x}}^2 \quad (2.5)$$

$$\begin{aligned}
T_d = & \frac{1}{2} m_d (\dot{v}^2 + \dot{w}^2) + \frac{1}{2} I_d (\dot{\beta}_z^2 + \dot{\beta}_y^2 \cos^2 \beta_z) \\
& + \frac{1}{2} I_p (\dot{\phi}^2 - 2\dot{\phi} \dot{\beta}_y \sin \beta_z + \dot{\beta}_y^2 \sin^2 \beta_z)
\end{aligned} \tag{2.6}$$

Since the rotations  $\beta_z$  and  $\beta_y$  are small,  $\sin \beta_z \approx \beta_z$  and  $\cos \beta_z \approx 1$ , and the higher order terms can be neglected. Thus [1],

$$T_d = \frac{1}{2} m_d (\dot{v}^2 + \dot{w}^2) + \frac{1}{2} I_d (\dot{\beta}_z^2 + \dot{\beta}_y^2) - I_p \Omega \dot{\beta}_y \beta_z + \frac{1}{2} I_p \dot{\phi}^2 \tag{2.7}$$

where  $\frac{1}{2} I_p \dot{\phi}^2$  is a constant term and has no effect on the equation of the disk;  $-I_p \Omega \dot{\beta}_y \beta_z$  represents the gyroscopic (Coriolis) effects of the disk where  $\Omega$  is the rotation speed and equals to  $\dot{\phi}$ . The equations of motion of the disk are obtained by applying Lagrange's equation to Equation (2.7) [1]:

$$\begin{bmatrix} \frac{d}{dt} \left( \frac{\partial T_d}{\partial \dot{v}} \right) - \frac{\partial T_d}{\partial v} \\ \frac{d}{dt} \left( \frac{\partial T_d}{\partial \dot{w}} \right) - \frac{\partial T_d}{\partial w} \\ \frac{d}{dt} \left( \frac{\partial T_d}{\partial \dot{\beta}_y} \right) - \frac{\partial T_d}{\partial \beta_y} \\ \frac{d}{dt} \left( \frac{\partial T_d}{\partial \dot{\beta}_z} \right) - \frac{\partial T_d}{\partial \beta_z} \end{bmatrix} = \begin{bmatrix} m_d & 0 & 0 & 0 \\ 0 & m_d & 0 & 0 \\ 0 & 0 & I_d & 0 \\ 0 & 0 & 0 & I_d \end{bmatrix} \begin{Bmatrix} \ddot{v} \\ \ddot{w} \\ \ddot{\beta}_y \\ \ddot{\beta}_z \end{Bmatrix} + \Omega \begin{bmatrix} 0 & 0 & 0 & 0 \\ 0 & 0 & 0 & 0 \\ 0 & 0 & 0 & I_p \\ 0 & 0 & -I_p & 0 \end{bmatrix} \begin{Bmatrix} \dot{v} \\ \dot{w} \\ \dot{\beta}_y \\ \dot{\beta}_z \end{Bmatrix} \tag{2.8}$$

The governing equation of motion for rotating rigid disk is

$$[M_d]\{\ddot{q}\} + \Omega[G_d]\{\dot{q}\} = \{Q_d\} \tag{2.9}$$

where  $[M_d]$  and  $[G_d]$  are the mass matrix and the gyroscopic matrix of the disk, respectively.

$$[M_d] = \begin{bmatrix} m_d & 0 & 0 & 0 \\ 0 & m_d & 0 & 0 \\ 0 & 0 & I_d & 0 \\ 0 & 0 & 0 & I_d \end{bmatrix} \quad (2.9.a)$$

$$[G_d] = \begin{bmatrix} 0 & 0 & 0 & 0 \\ 0 & 0 & 0 & 0 \\ 0 & 0 & 0 & I_p \\ 0 & 0 & -I_p & 0 \end{bmatrix} \quad (2.9.b)$$

$Q_d$  in equation (2.9) represents the forces and moments terms that act on the disk that result from mass unbalance, skew position of the disk on the shaft, interconnection forces and other external effects [1]. In an unbalanced disk, the unbalanced forces come into play because the mass center of the disk is shifted from its geometric center by an eccentricity of  $e$  and a phase angle of  $\delta$ . The unbalance forces in the disk are [1,26]

$$F_y = m_d e \Omega^2 \cos(\Omega t + \delta) \quad (2.10)$$

$$F_z = m_d e \Omega^2 \sin(\Omega t + \delta) \quad (2.11)$$

Also, the out of balance moments can exist on the shaft. The resulting moments are [1,29]

$$M_y = \tau(I_p - I_d) \Omega^2 \cos(\Omega t + \gamma) \quad (2.12)$$

$$M_z = \tau(I_p - I_d) \Omega^2 \sin(\Omega t + \gamma) \quad (2.13)$$

where  $\tau$  is the angle between the center line of the rotor and the axis of rotation, and  $\gamma$  is a phase angle. So, the force and moment matrix  $Q_d$  is

$$\{Q_d\} = \begin{Bmatrix} F_y \\ F_z \\ M_y \\ M_z \end{Bmatrix} = \begin{Bmatrix} m_d e \Omega^2 \cos \delta \\ m_d e \Omega^2 \sin \delta \\ \tau(I_p - I_d) \Omega^2 \cos \gamma \\ \tau(I_p - I_d) \Omega^2 \sin \gamma \end{Bmatrix} \cos \Omega t + \begin{Bmatrix} m_d e \Omega^2 \cos \delta \\ m_d e \Omega^2 \sin \delta \\ -\tau(I_p - I_d) \Omega^2 \sin \gamma \\ \tau(I_p - I_d) \Omega^2 \cos \gamma \end{Bmatrix} \sin \Omega t \quad (2.14)$$

## 2.4 Bearing element

Mostly, bearings are considered as flexible elements and they are represented in a mathematical model as springs and dampers as shown in Figure 2.4. The nonlinear relationship between load and deflection in most categories of bearing makes the analysis more complex, and to avoid this complexity in rotordynamic analysis one can assume linear load-deflection relationship of the bearing [1].

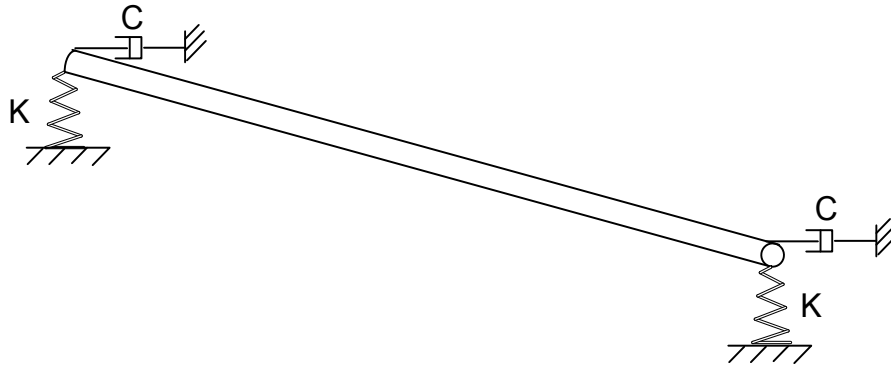


Figure 2.4 Rotating shaft supported at its ends by two bearings.

The virtual work of the bearing acting on the shaft is [1]

$$\begin{aligned} \delta W = & -k_{yy}v\delta v - k_{yz}w\delta v - k_{zz}w\delta w - k_{zy}v\delta w - c_{yy}\dot{v}\delta v - c_{yz}\dot{w}\delta v \\ & - c_{zz}\dot{w}\delta w - c_{zy}\dot{v}\delta w \end{aligned} \quad (2.15)$$

Or

$$\delta W = f_y\delta v + f_z\delta w \quad (2.16)$$

where  $f_y$  and  $f_z$  are the components of the generalized force that acts on the shaft by the bearing [1]

$$\begin{Bmatrix} f_y \\ f_z \end{Bmatrix} = - \begin{bmatrix} k_{vv} & k_{vw} \\ k_{wv} & k_{ww} \end{bmatrix} \begin{Bmatrix} v \\ w \end{Bmatrix} - \begin{bmatrix} c_{vv} & c_{vw} \\ c_{wv} & c_{ww} \end{bmatrix} \begin{Bmatrix} \dot{v} \\ \dot{w} \end{Bmatrix} \quad (2.17)$$

Equation (2.17) can be written in form

$$[C_b]\{\dot{q}_b\} + [K_b]\{q_b\} = \{Q_b\} \quad (2.18)$$

Or, in a general form when the damping and stiffness of a bearing are function of the shaft speed [1] :

$$\{Q_b\} = -K(\Omega)\{q_b\} - C(\Omega)\{\dot{q}_b\} \quad (2.19)$$

where

$$\{Q_b\} = \begin{Bmatrix} f_y \\ f_z \end{Bmatrix} \quad \text{and} \quad \{q_b\} = \begin{Bmatrix} v \\ w \end{Bmatrix}$$

## 2.5 Shaft element

Figure 2.5 shows finite shaft element. The shaft is modeled as a rotating beam element with distributed mass and stiffness. The element has two nodes located at its ends and each node has four degrees of freedom; the four degrees of freedom are two translational displacements in y and z directions and two rotational displacements about y- and z- axes. Furthermore, the internal displacements of the element are functions of time and the position along the length of the shaft, and the displacement of any point in the element can be expressed by the displacements of the end nodes and shape function as [26]

$$\begin{Bmatrix} v(x, t) \\ w(x, t) \\ \beta_y(x, t) \\ \beta_z(x, t) \end{Bmatrix} = \begin{bmatrix} \Psi(x) \\ \Phi(x) \end{bmatrix} \{q(t)\} \quad (2.20)$$

$\{q(t)\}$  is the vector of the time-dependent displacements of the nodes in the finite shaft element.

$$q(t) = [v_1 \ w_1 \ \beta_{y1} \ \beta_{z1} \ v_2 \ w_2 \ \beta_{y2} \ \beta_{z2}]^T \quad (2.21)$$

The shape functions (  $\Psi(x)$  and  $\Phi(x)$  ) are established by using two different beam theories, that are Euler-Bernoulli beam theory and Timoshenko beam theory.

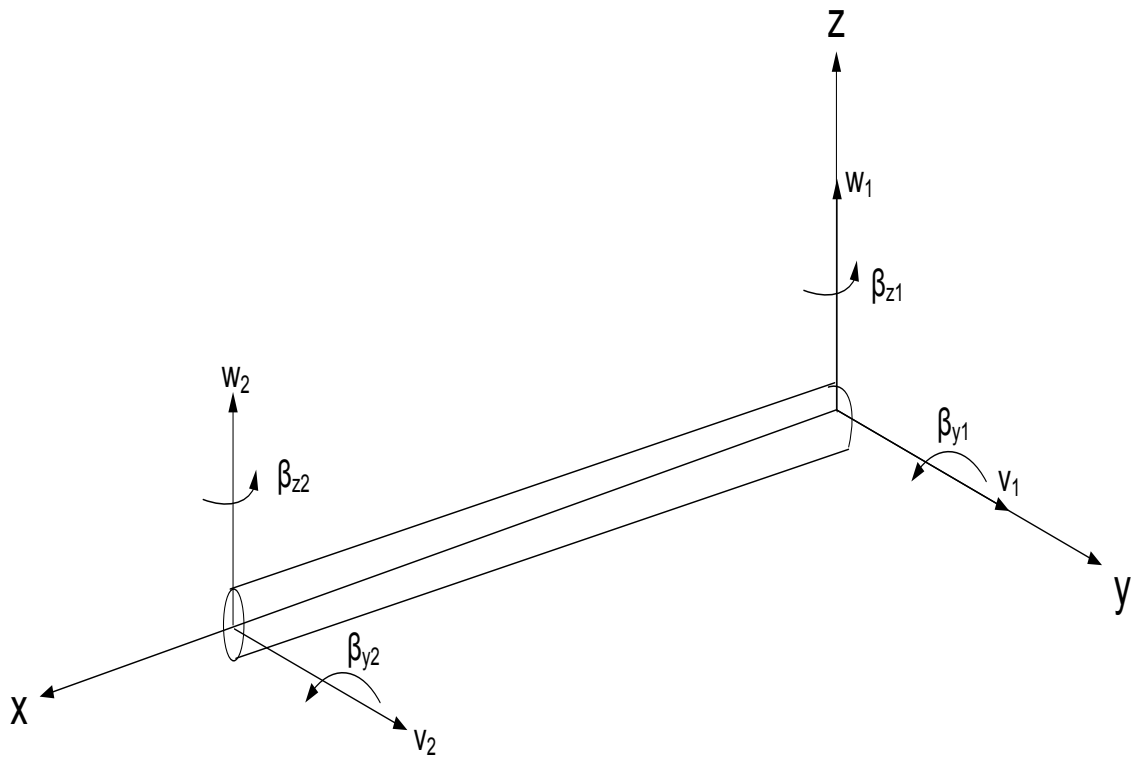


Figure 2.5 Typical finite shaft element

### 2.5.1 Shape functions based on Euler - Bernoulli beam theory

In Euler-Bernoulli beam theory, shear deformation and rotary inertia are ignored, and the translational displacements and rotational displacements, as shown in Figure 2.6, are related by [26]

$$\beta_z = \frac{\partial v}{\partial x} \quad (2.22)$$

$$\beta_y = -\frac{\partial w}{\partial x} \quad (2.23)$$

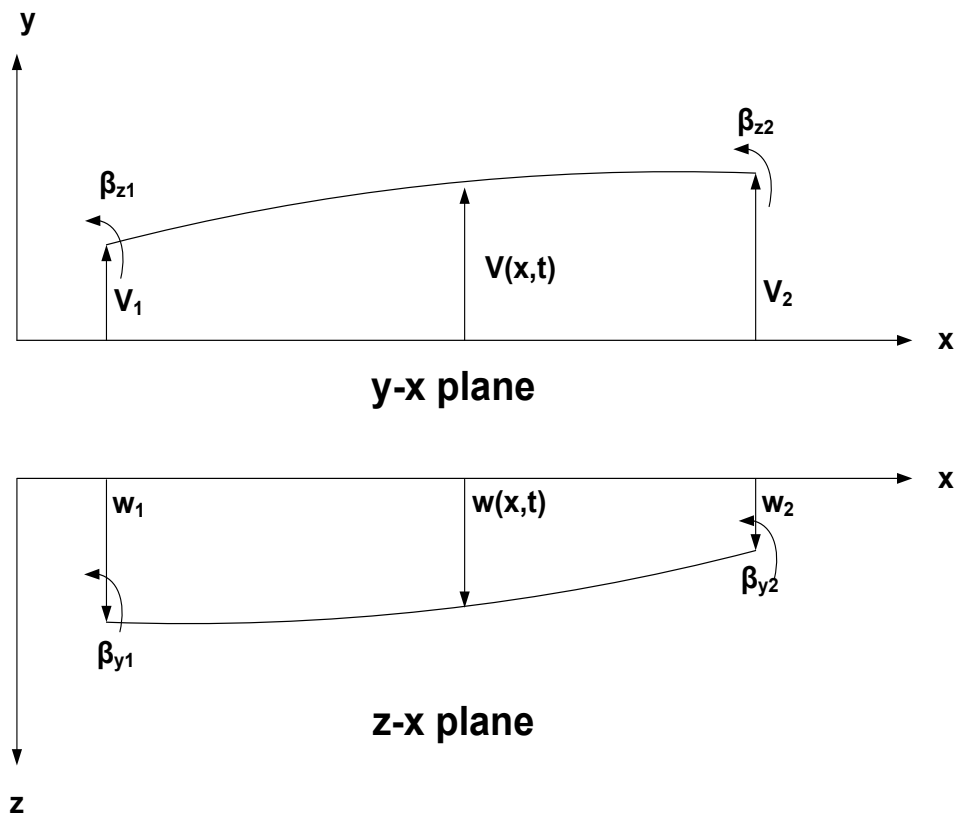


Figure 2.6 The displacements and the rotations in the two bending planes

The deflection within the shaft element in y-x plane is defined by the end displacements and shape functions. To derive the shape functions, one can consider the y-x plane and represent the lateral displacement  $v(x, t)$  by a cubic polynomial with four parameters because there are four boundary conditions [1,26] :

$$v(x, t) = C_0 + C_1x + C_2x^2 + C_3x^3 \quad (2.24)$$

The translation and rotation boundary conditions in y-x plane are:

$$v(0, t) = v_1(t) \quad \beta_z(0, t) = \beta_{z1}(t) \quad (2.25)$$

$$v(L, t) = v_2(t) \quad \beta_z(L, t) = \beta_{z2}(t)$$

Applying the lateral and the rotational boundary conditions gives

$$v_1 = a_0 \quad (2.26)$$

$$v_2 - v_1 = a_1L + a_2L^2 + a_3L^3 \quad (2.27)$$

$$a_1 = \beta_{z1} + \phi_{xy} \quad (2.28)$$

$$\beta_{z2} - \beta_{z1} = 2a_2L + 3a_3L^2 \quad (2.29)$$

Solving for  $C_0, C_1, C_2$  and  $C_3$ , and substituting back into Equation (2.24) gives [1,26]

$$v(x, t) = N_1(x)v_1(t) + N_2(x)\beta_{z1}(t) + N_3(x)v_2(t) + N_4(x)\beta_{z2}(t) \quad (2.30)$$

where

$$\begin{aligned} N_1 &= 1 - 3\xi^2 + 2\xi^3 & N_3 &= 3\xi^2 - 2\xi^3 \\ N_2 &= L(\xi - 2\xi^2 + \xi^3) & N_4 &= L(-\xi^2 + \xi^3) \end{aligned} \quad (2.31)$$

where  $\xi$  is the non-dimensional parameter:  $\xi = \frac{x}{L}$ . Substituting Equation (2.30) into Equation (2.22) gives [1,26]

$$\beta_z(x, t) = \dot{N}_1(x)v_1(t) + \dot{N}_2(x)\beta_{z1}(t) + \dot{N}_3(x)v_2(t) + \dot{N}_4(x)\beta_{z2}(t) \quad (2.32)$$

where

$$\begin{aligned} \dot{N}_1 &= \frac{1}{L}(-6\xi + 6\xi^2) & \dot{N}_2 &= 1 - 4\xi + 3\xi^2 \\ \dot{N}_3 &= \frac{1}{L}(6\xi - 6\xi^2) & \dot{N}_4 &= -2\xi + 3\xi^2 \end{aligned} \quad (2.33)$$

For symmetric shaft, the shape functions for one plane of motion can be used for the other plane, so the displacement field of the shaft element can be approximated as [26]

$$\begin{bmatrix} v \\ w \\ \beta_y \\ \beta_z \end{bmatrix} = \begin{bmatrix} \Psi_{EB}(x) \\ \Phi_{EB}(x) \end{bmatrix} \{q(t)\} = \begin{bmatrix} N_1 & 0 & 0 & N_2 & N_3 & 0 & 0 & N_4 \\ 0 & N_1 & -N_2 & 0 & 0 & N_3 & -N_4 & 0 \\ 0 & -\dot{N}_1 & \dot{N}_2 & 0 & 0 & -\dot{N}_3 & \dot{N}_4 & 0 \\ \dot{N}_1 & 0 & 0 & \dot{N}_2 & \dot{N}_3 & 0 & 0 & \dot{N}_4 \end{bmatrix} \begin{bmatrix} v_1 \\ w_1 \\ \beta_{y1} \\ \beta_{z1} \\ v_2 \\ w_2 \\ \beta_{y2} \\ \beta_{z2} \end{bmatrix} \quad (2.34)$$

### 2.5.2 Shape Functions based on Timoshenko Beam theory

Euler - Bernoulli beam theory is a reasonable approximation for a thin beam, but not for a thick beam which has two important effects: shear deformation and rotary inertia. Timoshenko beam theory includes shear effect and rotary inertia. The main concept of the theory is to remove the assumption that the beam cross-section remains perpendicular to the beam centerline. Moreover, in Timoshenko beam theory, the rotations of the cross-

section centerline consist of two parts: one is caused by the bending and the other one by the shear deformation [26], as illustrated in Figure 2.7.

$$\beta_z = \frac{\partial v}{\partial x} - \phi_{xy} \quad (2.35)$$

$$\beta_y = -\frac{\partial w}{\partial x} + \phi_{xz} \quad (2.36)$$

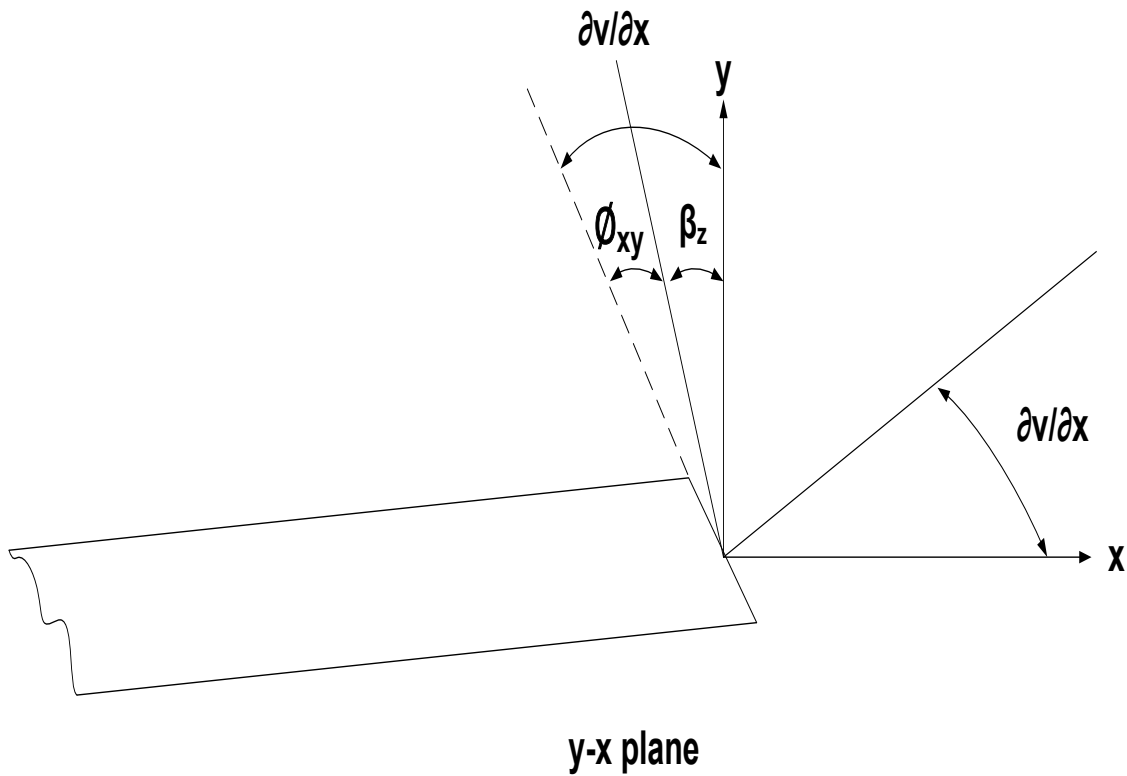


Figure 2.7 Deformed geometry of an edge of beam under the assumption of Timoshenko beam theory

And, the rotation and translation boundary conditions in y-x plane are

$$\begin{aligned} v(0, t) = v_1 & & \beta_z(0, t) = \beta_{z1} = \frac{\partial v}{\partial x} \Big|_{x=0} - \phi_{xy} \\ v(L, t) = v_2 & & \beta_z(L, t) = \beta_{z2} = \frac{\partial v}{\partial x} \Big|_{x=L} - \phi_{xy} \end{aligned} \quad (2.37)$$

The shear angle  $\phi_{xy}$  and the lateral displacement  $v$  should be related together, and to obtain the relationship between them, the moment equilibrium of the beam must be considered. The bending moments and the internal shearing forces are [1, 25, 26]

$$M_z = EI \frac{\partial \beta_y}{\partial x} \quad Q_y = k_s AG \phi_{xy} = k_s AG \left( \frac{\partial v}{\partial x} - \beta_z \right) \quad (2.38)$$

where

I: Second moment of area of the cross-section about the neutral plane

A: Area of the cross-section of the shaft element

G: shear modulus

E: Young's modulus

$k_s$ : Shape factor depending on the shape of the cross-section and the Poisson ratio

For a hollow circular shaft section [1]:

$$k_s = \frac{6(1 + \nu)^2(1 + \mu^2)^2}{(7 + 12\nu + 4\nu^2)(1 + \mu^2)^2 + 4(5 + 6\nu + 2\nu^2)\mu^2} \quad (2.39)$$

where,  $\mu = r_i/r_o$  and for a solid shaft [1]:

$$k_s = \frac{6(1 + \nu)^2}{(7 + 12\nu + 4\nu^2)} \quad (2.40)$$

The static equilibrium of the beam in y-x plane can be written as [1, 25, 26]:

$$\frac{\partial}{\partial x} \left( EI \frac{\partial \beta_z(x, t)}{\partial x} \right) = -k_s GA \phi_{xy} \quad (2.41)$$

Substituting Equation (2.35) in Equation (2.41) gives

$$\frac{\partial^2 \phi_{xy}(x, t)}{\partial x^2} + \frac{\partial^3 v(x, t)}{\partial x^3} = -\frac{k_s GA}{EI} \phi_{xy}(x, t) \quad (2.42)$$

Substituting Equation (2.24) in Equation (2.42) to obtain the shear angle  $\phi_{xy}$ [1]

$$\phi_{xy} = \frac{6EI}{k_s GA} C_3(t) = \frac{\Gamma L^2}{2} C_3(t) = -\frac{\Gamma L^2}{12} \frac{\partial^3 v(x, t)}{\partial x^3} \quad (2.43)$$

$\Gamma$  is the shear deformation parameter, and it represents the ratio between bending stiffness and shear stiffness, and  $\xi = \frac{x}{L}$  is the non-dimensional parameter [12]. Now, substituting the boundary conditions from Equation (2.37) in Equations (2.24) and (2.35) and finding the four parameters ( $C_0, C_1, C_2, C_3$ ), one can get [1,26]

$$v(x, t) = N_{t1}(x)v_1(t) + N_{t2}(x)\beta_{z1}(t) + N_{t3}(x)v_2(t) + N_{t4}(x)\beta_{z2}(t) \quad (2.44)$$

where

$$N_{t1} = \frac{1}{1 + \Gamma} [1 + \Gamma - \Gamma\xi - 3\xi^2 + 2\xi^3] \quad (2.45)$$

$$N_{t2} = \frac{L}{1 + \Gamma} \left[ \frac{2 + \Gamma}{2} \xi - \frac{4 + \Gamma}{2} \xi^2 + \xi^3 \right]$$

$$N_{t3} = \frac{1}{1 + \Gamma} [\Gamma \xi + 3\xi^2 - 2\xi^3]$$

$$N_{t4} = \frac{L}{1 + \Gamma} \left[ -\frac{\Gamma}{2} \xi + \frac{\Gamma - 2}{2} \xi^2 + \xi^3 \right]$$

Substituting Equation (2.44) and Equation (2.43) into Equation (2.35) gives [1,26]

$$\beta_y(x, t) = N_{r1}(x)v_1(t) + N_{r2}(x)\beta_{z1}(t) + N_{r3}(x)v_2(t) + N_{r4}(x)\beta_{z2}(t) \quad (2.46)$$

where

$$N_{r1} = \frac{1}{L(1 + \Gamma)} [-6\xi + 6\xi^2]$$

$$N_{r2} = \frac{1}{1 + \Gamma} [1 - 4\xi + 3\xi^2 + \Gamma(1 - \xi)]$$

$$N_{r3} = \frac{1}{L(1 + \Gamma)} [6\xi - 6\xi^2] \quad (2.47)$$

$$N_{r4} = \frac{1}{1 + \Gamma} [\Gamma \xi - 2\xi + 3\xi^2]$$

$$\Gamma = \frac{12 EI}{k_s GAL^2}$$

The displacement field of the shaft element can be approximated as [26]

$$\begin{bmatrix} v \\ w \\ \beta_y \\ \beta_z \end{bmatrix} = \begin{bmatrix} \Psi_{\text{Tim}}(x) \\ \Phi_{\text{Tim}}(x) \end{bmatrix} \{q(t)\} = \begin{bmatrix} N_{t1} & 0 & 0 & N_{t2} & N_{t3} & 0 & 0 & N_{t4} \\ 0 & N_{t1} & -N_{t2} & 0 & 0 & N_{t3} & -N_{t4} & 0 \\ 0 & -N_{r1} & N_{r2} & 0 & 0 & -N_{r3} & N_{r4} & 0 \\ N_{r1} & 0 & 0 & N_{r2} & N_{r3} & 0 & 0 & N_{r4} \end{bmatrix} \begin{bmatrix} v_1 \\ w_1 \\ \beta_{y1} \\ \beta_{z1} \\ v_2 \\ w_2 \\ \beta_{y2} \\ \beta_{z2} \end{bmatrix} \quad (2.48)$$

### 2.5.3 Energy equations

Herein, the equations of motions are obtained based on Timoshenko beam theory only, and for Euler-Bernoulli beam theory the same procedure can be applied. The kinetic energy equation of shaft element is similar to that of (kinetic energy equation of) the rigid disk, so the total kinetic energy for the shaft element may be written as [29,28]

$$T_{shaft} = \frac{1}{2} \int_0^L m_e (\dot{v}^2 + \dot{w}^2) dx + \int_0^L \frac{1}{2} I_d (\dot{\beta}_y^2 + \dot{\beta}_z^2) dx - \int_0^L I_{pe} \Omega \dot{\beta}_y \beta_z dx \quad (2.49)$$

where  $m_e, I_{de}, I_{pe}$  are the mass per unit length, diametral moment of inertia, and polar moment of inertia. The total potential energy of the shaft element, including the elastic bending energy, shear energy and the energy due to a constant axial load  $P$ , is [28,29]

$$\begin{aligned} U_{shaft} = & \frac{1}{2} \int_0^L EI \left[ \left( \frac{\partial \beta_z}{\partial x} \right)^2 + \left( \frac{\partial \beta_y}{\partial x} \right)^2 \right] dx \\ & + \frac{1}{2} \int_0^L k_s AG \left[ \left( \beta_y + \frac{\partial w}{\partial x} \right)^2 + \left( \beta_z - \frac{\partial v}{\partial x} \right)^2 \right] dx \\ & + \frac{1}{2} \int_0^L P \left[ \left( \frac{\partial v}{\partial x} \right)^2 + \left( \frac{\partial w}{\partial x} \right)^2 \right] dx \end{aligned} \quad (2.50)$$

Substituting Equation (2.48) in Equation (2.49) and Equation (2.50), one can obtain the kinetic and the potential energies as functions of the displacements of the end nodes and spatial shape function. The Lagrange's equation is utilized here to obtain the equation of motion for free vibration of the rotating shaft element [25,26].

$$([M_T] + [M_R])\{\ddot{q}\} + \Omega[G_{\text{shaft}}]\{\dot{q}\} + ([K_B] + [K_S] + [K_F])\{q\} = \{0\} \quad (2.51)$$

where

$\{q\}$  is the translational mass matrix :

$$\{q\} = \{v_1 \quad w_1 \quad \beta_{y1} \quad \beta_{z1} \quad v_2 \quad w_2 \quad \beta_{y2} \quad \beta_{z2}\}^T \quad (2.52)$$

$[M_T]$  is the translational mass matrix :

$$[M_T] = \int_0^L m_e [\Psi_{\text{Tim}}]^T [\Psi_{\text{Tim}}] dx = \int_0^L \rho A [\Psi_{\text{Tim}}]^T [\Psi_{\text{Tim}}] dx \quad (2.53)$$

$[M_R]$  is the rotational mass matrix :

$$[M_R] = \int_0^L I_{de} [\Phi_{\text{Tim}}]^T [\Phi_{\text{Tim}}] dx = \int_0^L \rho A [\Phi_{\text{Tim}}^T] [\Phi_{\text{Tim}}] dx \quad (2.54)$$

$[G_{\text{shaft}}]$  is the gyroscopic matrix :

$$[G_{\text{shaft}}] = \int_0^L I_{pe} [\Phi_{\text{Tim}}]^T \begin{bmatrix} 0 & 1 \\ -1 & 0 \end{bmatrix} [\Phi_{\text{Tim}}] dx \quad (2.55)$$

$[K_B]$  is the bending stiffness matrix :

$$[K_B] = \int_0^L EI [\Phi_{\text{Tim}}]^T [\Phi_{\text{Tim}}] dx \quad (2.56)$$

$[K_S]$  is the shear stiffness matrix:

$$[K_S] = \int_0^L k_s GA \left[ [\dot{\Psi}_{\text{Tim}}] + \begin{bmatrix} 0 & -1 \\ 1 & 0 \end{bmatrix} [\Phi_{\text{Tim}}] \right]^T \left[ [\dot{\Psi}_{\text{Tim}}] + \begin{bmatrix} 0 & -1 \\ 1 & 0 \end{bmatrix} [\Phi_{\text{Tim}}] \right] dx \quad (2.57)$$

$[K_F]$  is the geometric stiffness matrix due to axial load:

$$[K_F] = \int_0^L P [\dot{\Psi}_{\text{Tim}}]^T [\dot{\Psi}_{\text{Tim}}] dx \quad (2.58)$$

#### 2.5.4 Tapered driveshaft

There are two methods to model a tapered shaft. First method is to model the tapered shaft with a large number of uniform shaft elements with different diameters, and the second method is to incorporate the change in the cross-section of the tapered shaft into the element definition [10]. The later method is adapted here to obtain the element matrices based on Timoshenko beam theory. In fact, the procedure to construct the tapered or conical element is exactly same as producing the uniform shaft element, and the difference is in the kinetic and strain energy where the cross-section area and inertia terms must be integrated through the length of the element. Also, the shape functions are exactly the same as in uniform shaft element except that the shear deformation parameter  $\Gamma$  becomes [1]

$$\Gamma = \frac{12 E \bar{I}}{k_s G L^2 \bar{A}} \quad (2.59)$$

where  $\bar{I}$  and  $\bar{A}$  are the average moment of inertia and the average area of the cross-section. For rotating tapered shaft element, the element translational mass matrix, the rotational inertia matrix, the gyroscopic matrix, the bending stiffness matrix, the shear stiffness matrix and the geometric stiffness matrix due to axial force, respectively are [25,26].

$$[M_T]_{TP} = \int_0^L m_e(x) [\Psi_{Tim}]^T [\Psi_{Tim}] dx = \int_0^L \rho A(x) [\Psi_{Tim}]^T [\Psi_{Tim}] dx \quad (2.60)$$

$$[M_R]_{TP} = \int_0^L I_{de}(x) [\Phi_{Tim}]^T [\Phi_{Tim}] dx = \int_0^L \rho A(x) [\Phi_{Tim}]^T [\Phi_{Tim}] dx \quad (2.61)$$

$$[G_{shft}]_{TP} = \int_0^L I_{pe}(x) [\Phi_{Tim}]^T \begin{bmatrix} 0 & 1 \\ -1 & 0 \end{bmatrix} [\Phi_{Tim}] dx \quad (2.62)$$

$$[K_B]_{TP} = \int_0^L EI(x) [\dot{\Phi}_{Tim}]^T [\dot{\Phi}_{Tim}] dx \quad (2.63)$$

$$[K_B]_{TP} = \int_0^L EI(x) [\dot{\Phi}_{Tim}]^T [\dot{\Phi}_{Tim}] dx \quad (2.64)$$

$$[K_S]_{TP} = \int_0^L kGA(x) \left[ [\dot{\Psi}_{Tim}] + \begin{bmatrix} 0 & -1 \\ 1 & 0 \end{bmatrix} [\Phi_{Tim}] \right]^T \left[ [\dot{\Psi}_{Tim}] + \begin{bmatrix} 0 & -1 \\ 1 & 0 \end{bmatrix} [\Phi_{Tim}] \right] dx \quad (2.65)$$

$$[K_F]_{TP} = \int_0^L P [\dot{\Psi}_{Tim}]^T [\dot{\Psi}_{Tim}] dx \quad (2.66)$$

## 2.6 System equations of motion and analysis

The general equation of motion of rotor-bearing system is assembled using Equation (2.9), Equation (2.18) and Equation (2.51).

$$[M]\{\ddot{q}\} + \Omega[G]\{\dot{q}\} + [C]\{\dot{q}\} + [K]\{q\} = [Q] \quad (2.67)$$

where  $[M]$ ,  $[C]$ ,  $[G]$ ,  $[K]$ ,  $[Q]$  and  $\{q\}$  are the mass matrix, damping matrix, gyroscopic matrix, stiffness matrix, the forcing vector and the system displacement vector of the rotor-bearing system, respectively.

### 2.6.1 Whirl speeds analysis

The natural frequencies of the system are determined from the homogeneous form of the general equations of motion (2.67)

$$[M]\{\ddot{q}\} + [C]\{\dot{q}\} + \Omega[G]\{\dot{q}\} + [K]\{q\} = \{0\} \quad (2.68)$$

where  $[M]$ ,  $[C]$  and  $[K]$  are real and symmetric matrices and  $[G]$  is a real and skew-symmetric matrix; Equation (2.68) can be written in form [1,26]

$$[M^*]\{\dot{\tilde{x}}\} + [K^*]\{\tilde{x}\} = \{0\} \quad (2.69)$$

where the matrix  $[M^*]$  is a positive definite and real symmetric matrix and  $[K^*]$  is an arbitrary real matrix [1,26]

$$[M^*] = \begin{bmatrix} [M] & [0] \\ [0] & [I] \end{bmatrix}, \quad [K^*] = \begin{bmatrix} [G] + [C] & [K] \\ -[I] & [0] \end{bmatrix}, \quad \{\tilde{x}\} = \begin{bmatrix} \{\dot{q}\} \\ \{q\} \end{bmatrix} \quad (2.70)$$

The solution of Equation (2.69) can be assumed in the form

$$\{\tilde{x}\} = \{\tilde{X}\} e^{\lambda t} = \begin{bmatrix} \{\tilde{X}_1\} e^{\lambda_1 t} \\ \{\tilde{X}_2\} e^{\lambda_2 t} \\ \vdots \\ \{\tilde{X}_n\} e^{\lambda_n t} \end{bmatrix}_{2n \times 1} \quad (2.71)$$

Substituting Equation (2.71) into Equation (2.69) yields

$$(-[M^*]^{-1}[K^*])\{\tilde{X}\} = \lambda\{\tilde{X}\} \quad (2.72)$$

where

$$\begin{bmatrix} -[M]^{-1}[[C] + [G]] & -[M]^{-1}[K] \\ [I] & [0] \end{bmatrix}_{2n \times 2n} \begin{bmatrix} \{\tilde{X}_1\}e^{\lambda_1 t} \\ \{\tilde{X}_2\}e^{\lambda_2 t} \\ \vdots \\ \{\tilde{X}_n\}e^{\lambda_n t} \end{bmatrix}_{2n \times 1} = \begin{bmatrix} 0 \\ 0 \\ \vdots \\ 0 \end{bmatrix}_{2n \times 1} \quad (2.73)$$

$-[M^*]^{-1}[K^*]$  is an arbitrary real matrix that gives the eigenvalues and the eigenvectors of the system. The eigenvalues  $\lambda$  happen in pairs of complex conjugates as well as the eigenvectors  $\{\tilde{X}\}$  and they have the forms [1,26]

$$\lambda = \sigma \pm j\omega_d \quad (2.74)$$

$$\{\tilde{X}\} = \begin{Bmatrix} \lambda u \\ u \end{Bmatrix}, \quad \{\tilde{X}^*\} = \begin{Bmatrix} \lambda u^* \\ u^* \end{Bmatrix} \quad (2.75)$$

The real part of the eigenvalues,  $\sigma$ , represents the damping exponents that are used to determine the instability region of the driveshaft. The positive values of damping exponents refer to instability in the driveshaft. In addition, the imaginary parts of the eigenvalues,  $\omega_d$ , is the whirl speeds or the damped natural frequencies of the system.

### 2.6.2 Campbell Diagram and Critical Speeds

Campbell diagram is a map of natural frequencies of the driveshaft that shows the variation of the natural frequencies with the rotation speeds; the Campbell diagram is used to obtain the critical speeds. Figure 2.8 shows a typical Campbell diagram where the intersections of the natural frequency curve with the forcing frequency lines represent the critical speeds. In addition, beside the Campbell diagram, there are two other methods to obtain the critical speeds; one is called the direct method and the other is the iteration

method. The direct method can be used in case that the bearing coefficients are not function of the rotation speed, but if the bearing coefficients change with rotation speed the direct method must be replaced by the iteration method [1].

In the iteration method, the first critical speed is assumed as  $\Omega_1$  then  $[M(\Omega_1)]$ ,  $[K(\Omega_1)]$ ,  $[C(\Omega_1)]$  and  $[G(\Omega_1)]$  are determined and the first eigenvalue is calculated. A new guess of the first critical speed is obtained to calculate the first eigenvalue. The process will continue until acceptable convergence is obtained. In the direct method, the critical speeds are taken when one of the natural frequencies at a specific speed is equal to the forcing frequency [1]. The forcing frequency can be written in terms of rotational speed as

$$\omega_f = n\Omega \quad (2.76)$$

where  $n$  refers to the level of the lateral force on the shaft. For example, in out of balance  $n = 1$  and in a four bladed helicopter rotor  $n = 4$ . In Equation (2.67) the force is in form  $\{Q(t)\} = \{Q_0\}e^{j\omega_f t}$ , so the solutions of equation (2.67) will be in form  $\{q(t)\} = \{q_0\}e^{j\omega_f t}$  [1]

$$(-\Omega^2[n^2[M] + jn[G]] + j\Omega n [C] + [K]) \{q_0\} = \{Q_0\} \quad (2.77)$$

By putting  $\{Q_0\} = \{0\}$  in equation (2.77), one can get [1]

$$(-\Omega^2[n^2[M] + jn[G]] + j\Omega n [C] + [K]) \{q_0\} = \{0\} \quad (2.78)$$

The solution of eigenvalue problem  $\Omega$  is in complex form; the real part of  $\Omega$  gives the critical speed.

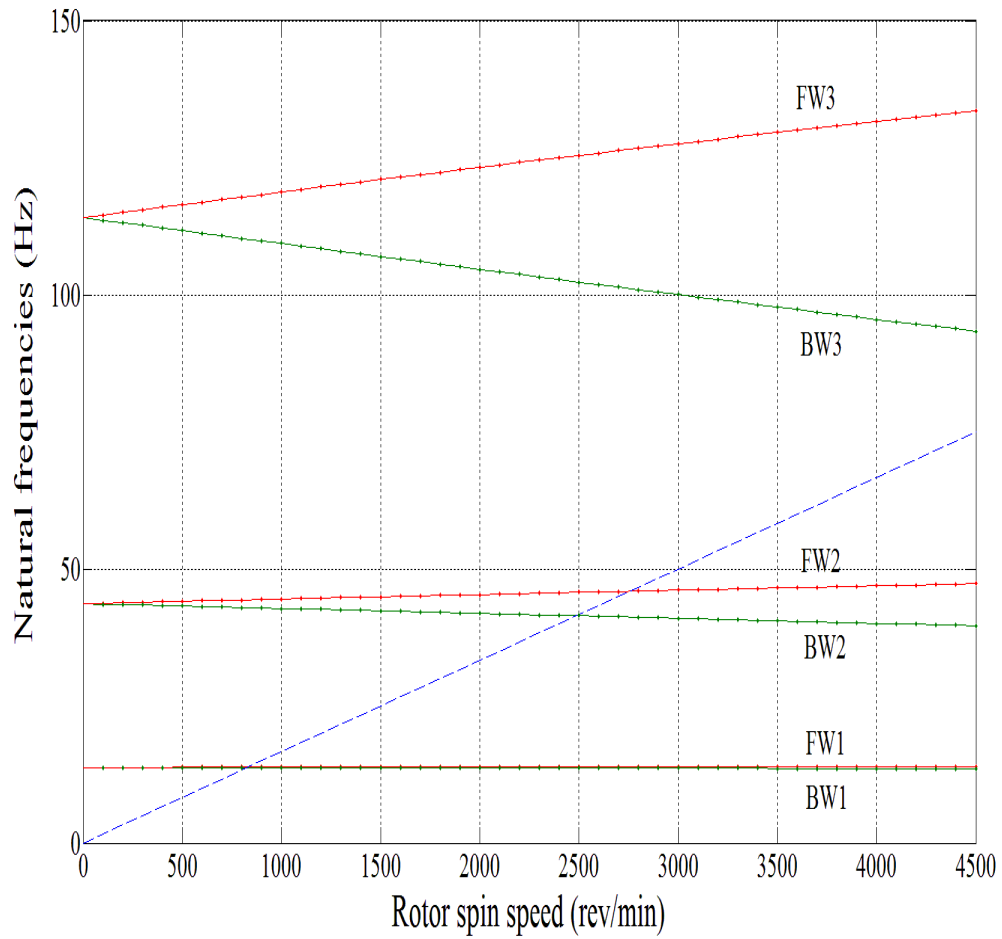


Figure 2.8 Typical Campbell diagram of rotor-bearing system.

### 2.6.3 Steady-State Synchronous Response

Synchronous force or excitation is defined as the force, whose frequency is similar to rotor speed. Mostly, the synchronous excitation happens because of the mass unbalance and disk skew. The equation of motion for the rotor-bearing system is

$$[M]\{\ddot{q}\} + \Omega[G]\{\dot{q}\} + [C]\{\dot{q}\} + [K]\{q\} = \{Q(t)\} \quad (2.79)$$

where  $\{Q(t)\}$  represents the resulting forces and moments of the mass unbalance and the disk skew [1]

$$\{Q(t)\} = \begin{Bmatrix} m_d e \Omega^2 \cos(\delta + \Omega t) \\ m_d e \Omega^2 \sin(\delta + \Omega t) \\ \tau(I_p - I_d) \Omega^2 \cos(\gamma + \Omega t) \\ \tau(I_p - I_d) \Omega^2 \sin(\gamma + \Omega t) \end{Bmatrix} \quad (2.80)$$

$$\{Q(t)\} = \Re \left( \Omega^2 \begin{Bmatrix} m_d e e^{j\delta} \\ -m_d e e^{j\delta} \\ j(I_{pk} - I_{dk}) \tau e^{j\gamma} \\ (I_{pk} - I_{dk}) \tau e^{j\gamma} \end{Bmatrix} e^{j\Omega t} \right) = \Re(\Omega^2 \{b_0\} e^{j\Omega t}) \quad (2.81)$$

where  $\Re$  represents the real solution part, and  $\Omega^2 \{b_0\}$  represents the force and moment vector that is acting at the node because of the mass unbalance and the disk skew. The steady-state solution can be assumed as [1]

$$\{q(t)\} = \Re(\Omega^2 \{q_0\} e^{j\Omega t}) \quad (2.82)$$

where  $\{q_0\}$  is a complex vector. Substituting Equation (2.82) and its derivatives into Equation (2.79), one can get [1]

$$\{q_0\} = [([K] - \Omega^2[M]) + j \Omega (\Omega[G] + [C])]^{-1} \Omega^2 \{b_0\} \quad (2.83)$$

## 2.7 Numerical Examples

In this section, examples on dynamic analysis of rotor-bearing system are provided. A MATLAB program was written to analyze a rotor-bearing system; the program is able to give the natural frequencies at any speed of the rotor, mode shapes, Campbell diagram, and critical speeds and unbalance response of the rotor-bearing system.

In Figure 2.9, a shaft, with 1.5 m long and 0.05 m diameter, is under study. Two disks are keyed to the shaft at 0.5 m and 1 m from the left end; the first disk from the left has diameter of 0.28 m and thickness of 0.07 m while the second disk has diameter of 0.35 m and thickness of 0.07 m. Also, there are two bearings at each end. The shaft is modeled be six elements with equal length. The meshing starts form the left side of the shaft, so the first disk from the left side coincides with node 3 while the second disk coincides with the node 5. Material properties of the rotor and the disk are:  $E = 211 \text{ GPa}$ ;  $G = 81.2 \text{ GPa}$ ; Density =  $7810 \text{ Kg/m}^3$ .

- a) Case 1 : Isotropic bearings :  $K_{yy} = K_{zz} = 1\text{MN/m}$
- b) Case 2: Anisotropic bearings:  $K_{yy} = 1\text{MN/m}$ ;  $K_{zz} = 0.8\text{MN/m}$



Figure 2.9 The rotor system configuration with two bearings and two disks.

In case 1, stiffness and inertia properties are identical in  $y$ - $x$  and  $z$ - $x$  planes. As a result, when the rotor does not rotate the natural frequencies of the rotor happen in pairs as it is shown in Table 2.1. However, when the rotor starts rotating, the pairs of the natural frequencies start to separate due to the gyroscopic effect. Figure 2.10 shows the Campbell

diagram of the case 1, and one can see the separation of the natural frequencies while the spinning speed increases.

Table 2.1 Eigenvalues and natural frequencies of the rotor supported by isotropic bearings at two different speeds (case 1).

0 (rpm)		4000 (rpm)	
Eigenvalues ( rad/s)	Natural frequency $\omega_n$ (Hz)	Eigenvalues ( rad/s)	Natural frequency $\omega_n$ (Hz)
$0 \pm 85.67 i$	13.64	$0 \pm 84.52 i$	13.46
$0 \pm 85.67 i$	13.64	$0 \pm 86.88 i$	13.83
$0 \pm 272 i$	43.31	$0 \pm 249.81 i$	39.78
$0 \pm 272 i$	43.31	$0 \pm 291.89 i$	46.48
$0 \pm 716.5 i$	114.09	$0 \pm 599.78 i$	95.51
$0 \pm 716.5 i$	114.09	$0 \pm 826.77 i$	131.65

Table 2.2 The first seven critical speeds of the rotor supported by isotropic bearings (case 1).

Critical speeds ( rpm)	816	821	2468	2729	5376	8835	9449
------------------------	-----	-----	------	------	------	------	------

In addition, Campbell diagram can be used to find the critical speeds; the first four critical speeds from the Campbell diagram are almost same as those were calculated using the direct method and they are shown in Table 2.2. Furthermore, the mode shapes of the rotor at 4000 rpm are illustrated in Figure 2.11 and because the stiffness and the

inertia are alike in y-x and z-x planes, the orbits in the mode shapes at any point along the rotor take circular shape.

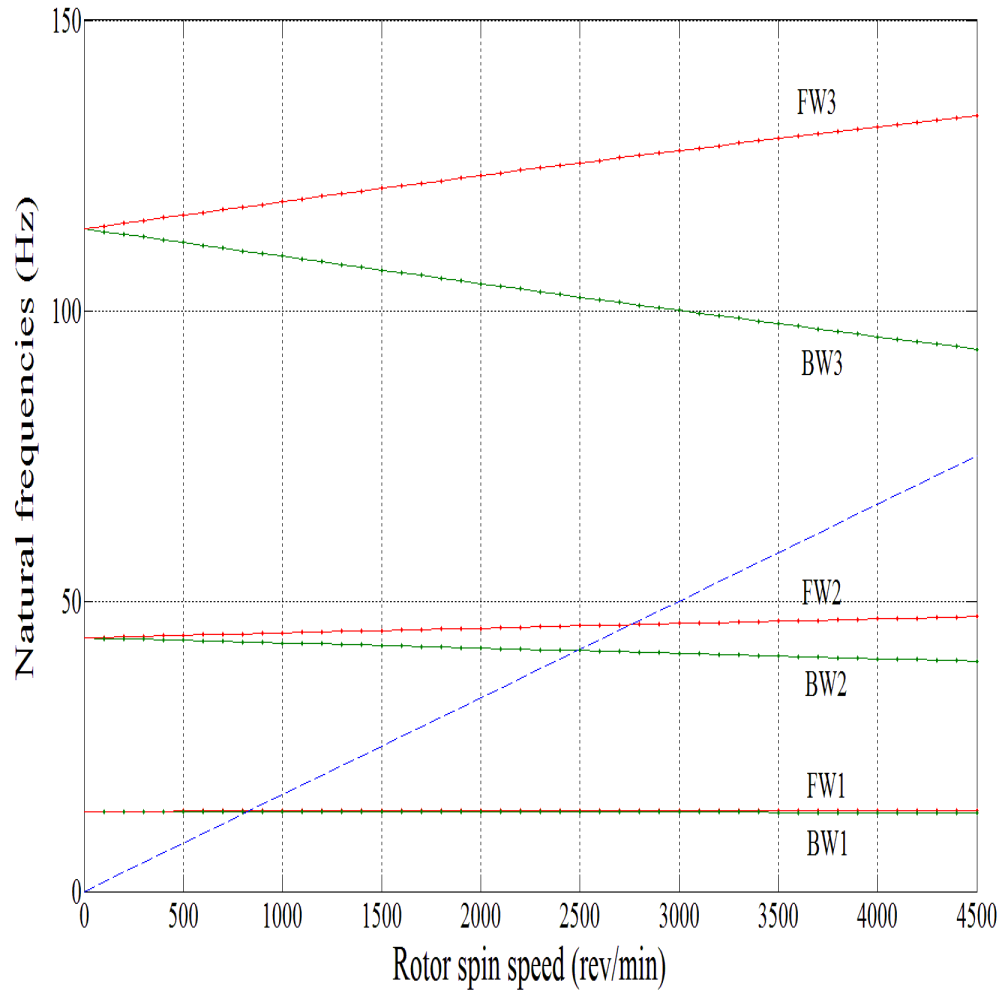


Figure 2.10 The Campbell diagram of the rotor system for isotropic bearings (case 1).

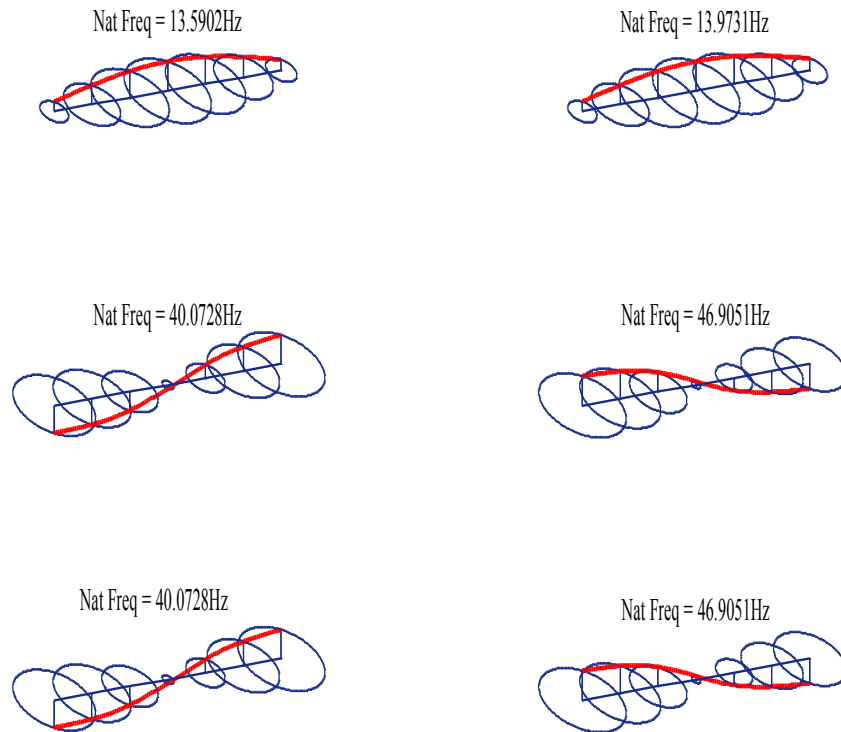


Figure 2.11 The mode shape of the rotor at 4000 rpm supported by isotropic bearings (case 1).

In case 2, the bearings on both the ends are anisotropic bearings. At 0 rpm the natural frequencies do not happen in pairs as in case 1 because stiffnesses in y and z directions are not identical any more. Table 2.3 shows the natural frequencies of case 2 at 0 rpm and 4000 rpm. Figure 2.12 illustrates the Campbell diagram of the case 2; even though that the natural frequencies at 0 rpm do not happen in pairs, one can see on the Campbell

diagram that the separation between the natural frequencies still happen as the rotation speed increases. In addition, under the effect of the anisotropic bearings, in Figure 2.13 the mode shapes form an elliptical orbit rather than a circular orbit as in case 1. Table 2.4 illustrates the critical speeds of the rotor system in case 2.

Table 2.3 Eigenvalues and natural frequencies of the rotor supported by anisotropic bearings at two different speeds (case 2).

0 (rpm)		4000 (rpm)	
Eigenvalues ( rad/s)	Natural frequency $\omega_n$ (Hz)	Eigenvalues ( rad/s)	Natural frequency $\omega_n$ (Hz)
$0 \pm 81.80 i$	13.03	$0 \pm 81.48 i$	12.97
$0 \pm 85.76 i$	13.66	$0 \pm 85.96 i$	13.83
$0 \pm 252.34 i$	40.18	$0 \pm 237.79 i$	37.86
$0 \pm 271.89 i$	43.29	$0 \pm 284.54$	45.31
$0 \pm 679.22 i$	108.16	$0 \pm 583.11 i$	92.85

Table 2.4 The first seven critical speeds of the rotor supported by anisotropic bearings (case 2).

Critical speeds ( rpm)	781	819	2348	2663	5258	8573	9325
------------------------	-----	-----	------	------	------	------	------

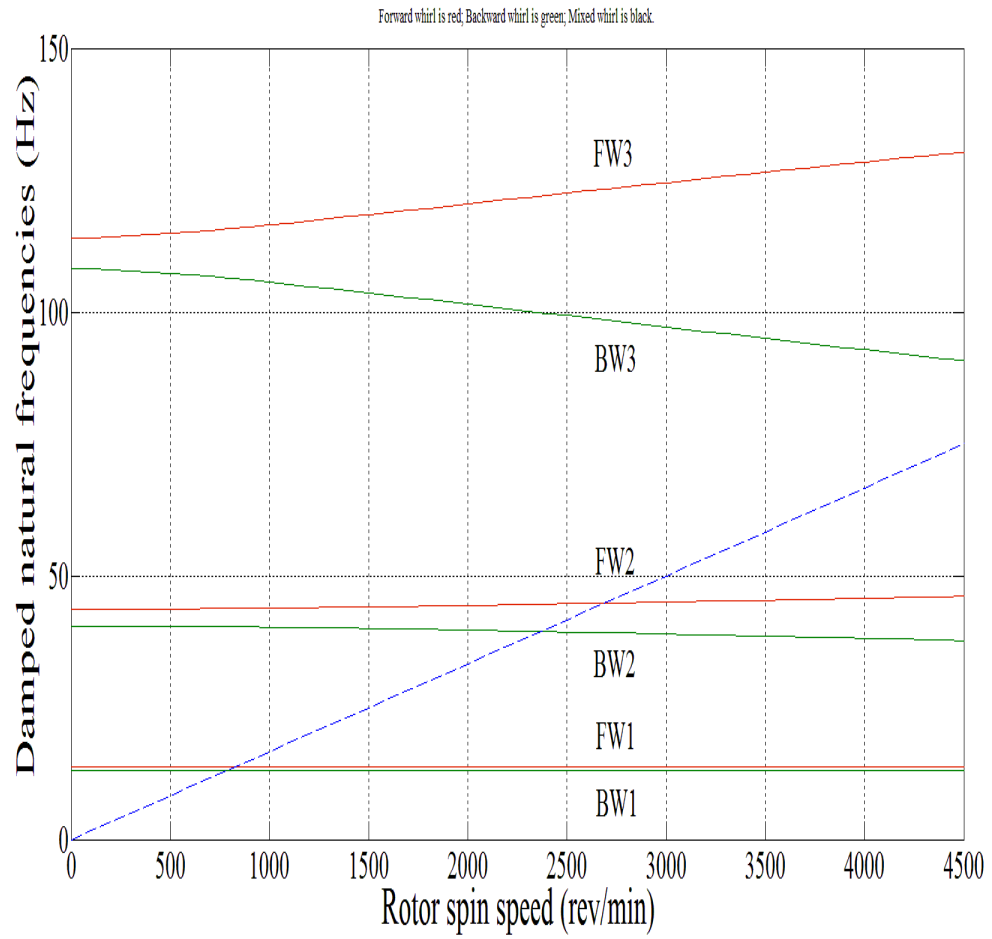


Figure 2.12 The Campbell diagram of the rotor system supported by anisotropic bearings (case 2).

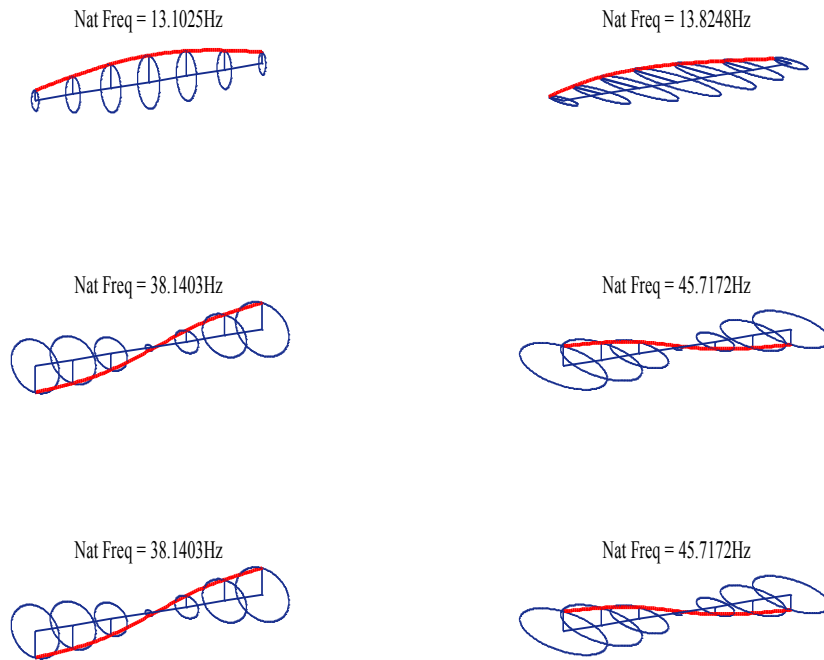


Figure 2.13: The mode shape of the rotor system supported by anisotropic bearings (case 2).

In the following example, the steady-state response of the rotor-bearing system of the previous example is presented. The bearing's properties are taken as  $K_{yy} = K_{zz} = 0.8\text{MN/m}$  and  $C_{yy} = C_{zz} = 80\text{Ns/m}$ , and the out of balance on the left disk is  $0.001\text{Kg.m}$ . The response in  $y$  and  $z$  directions of nodes 3 and 5 are shown in Figure 2.14 and Figure 2.15. The responses in  $y$  and  $z$  directions are coincident as it is shown on both the figures; this happens because of the equality of the stiffness in  $y$  and  $z$  directions. So, for any

nodes along the rotor the responses in y and z directions are equal. Also, the comparison between the responses at node 3 and node 5 in y direction is illustrated in Figure 2.16. The maximum values of the response of both the nodes happen at the same spinning speeds which are 792 rpm and 2561 rpm. And, by looking into the Campbell diagram in Figure 2.17, one can find that the previous spinning speeds are the second and the fourth critical speeds of the rotor.

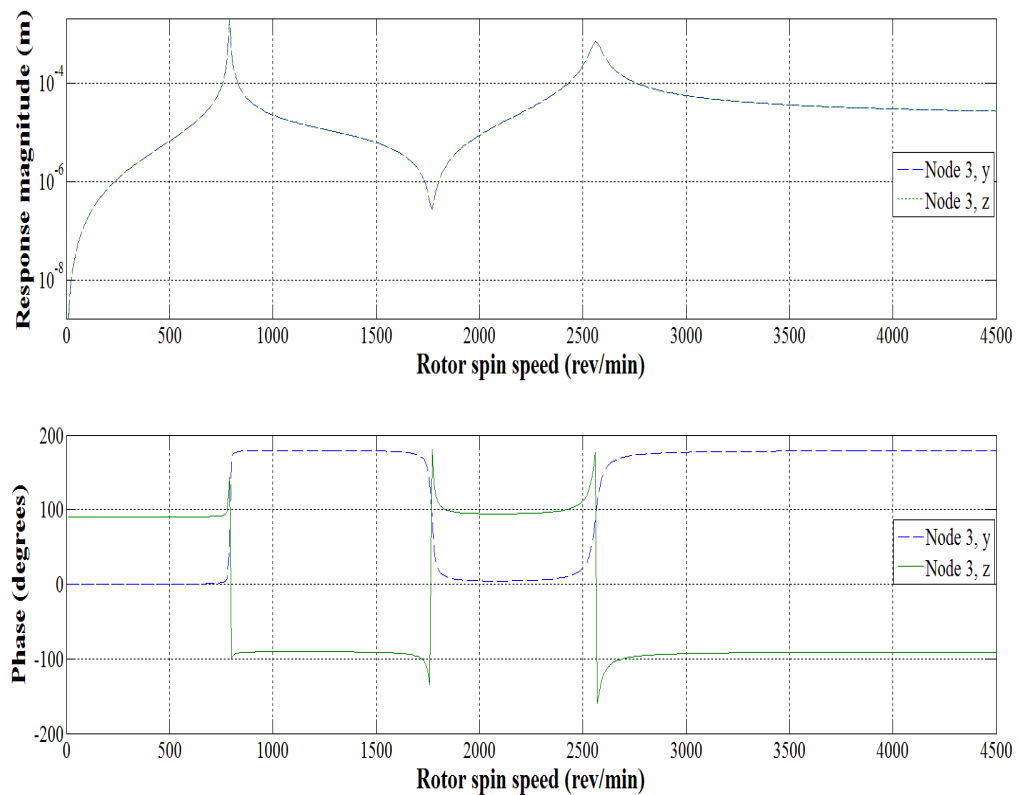


Figure 2.14: Steady-state response of the rotor-bearing system at node 3 in y and z directions case 1 (isotropic bearings)

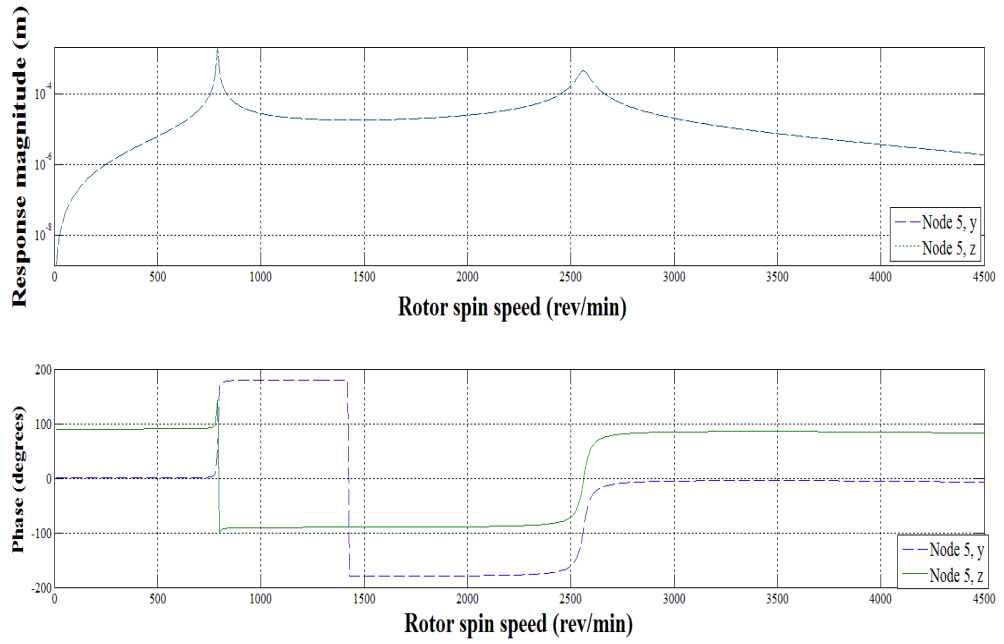


Figure 2.15: Steady-state response of the rotor-bearing system at node 5 in y and z directions for case 1 (isotropic bearings)

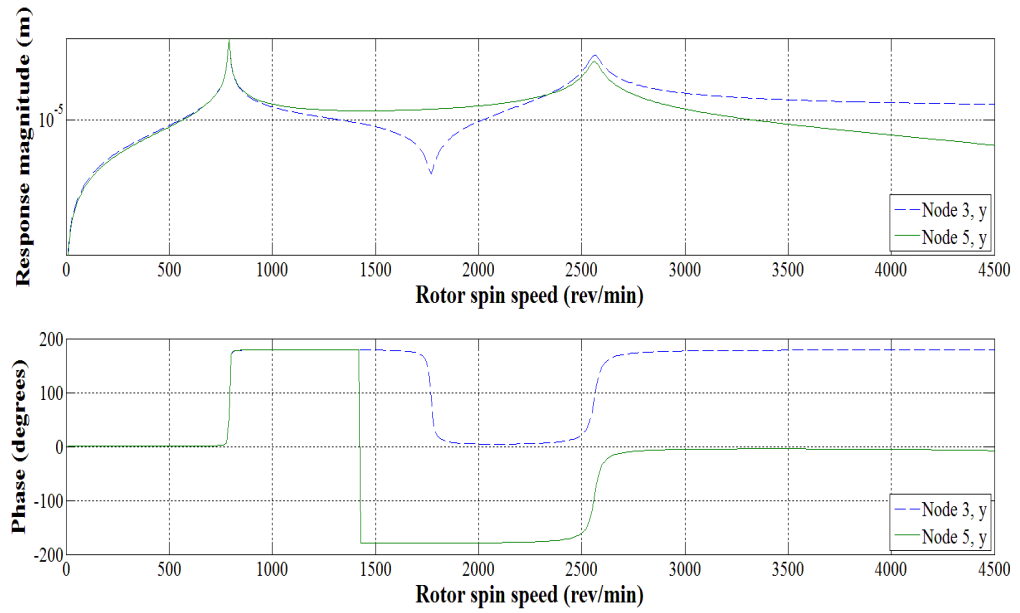


Figure 2.16: Steady-state response of the rotor-bearing system at node 3 and node 5 in y direction for case 1 (isotropic bearings)

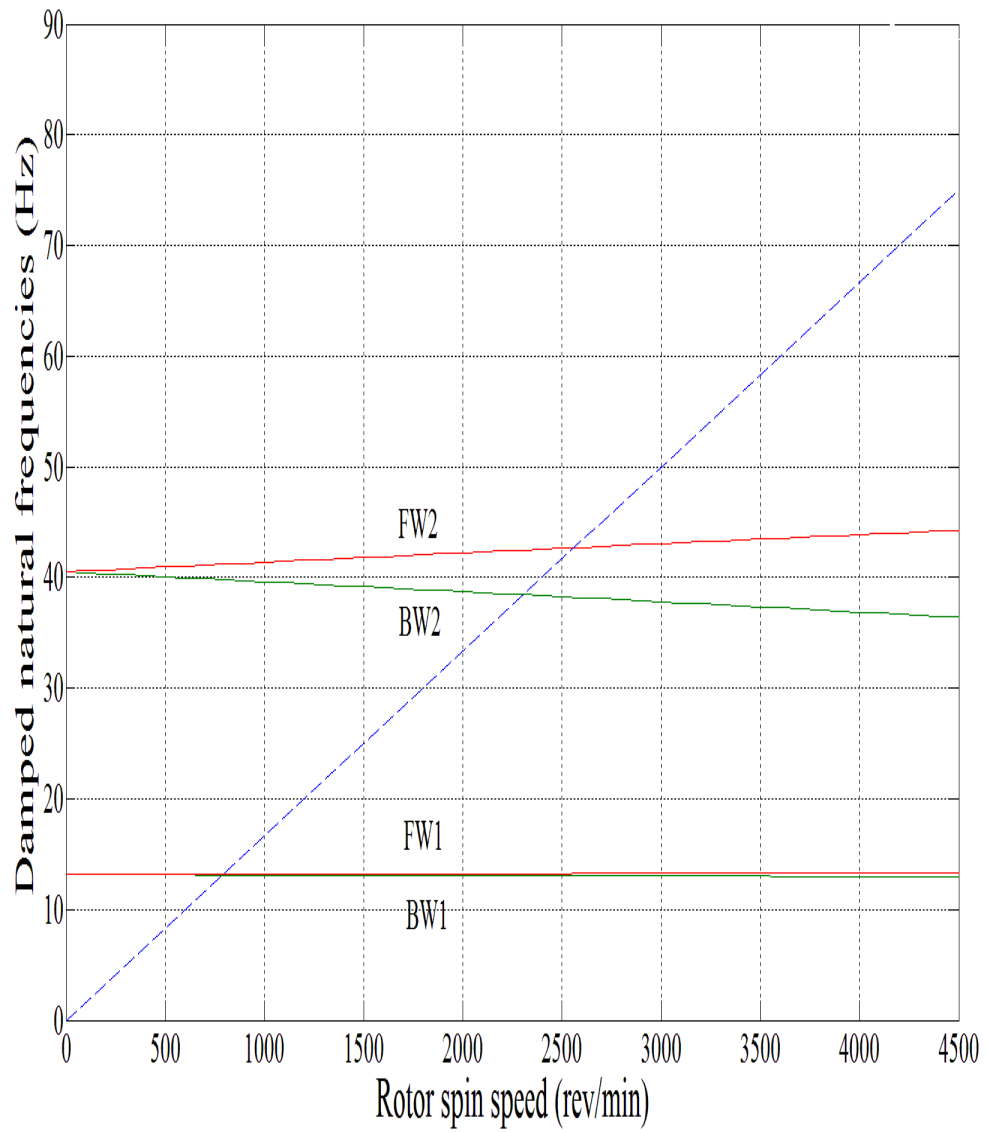


Figure 2.17 Campbell diagram of the rotor system supported by isotropic bearings

In the next example, an overhung rotor that is 1.5 m long and with 50 mm diameter is shown in Figure 2.18. The rotor has at its right end a disk with 350 mm diameter and 70 mm thickness. Also, there are two bearings; one is located at left end of the rotor and the other is located at 1 m from left end. Six Timoshenko shaft elements with equal lengths are used here. The natural frequencies of the rotor at 0 rpm and 4000 rpm under the effect of an axial load are determined. Bearing properties are:  $K_{yy} = K_{zz} = 10 \text{ MN/m}$ . Material properties of the rotor and the disk are :  $E = 211 \text{ GPa}$ ;  $G = 81.2 \text{ GPa}$ .

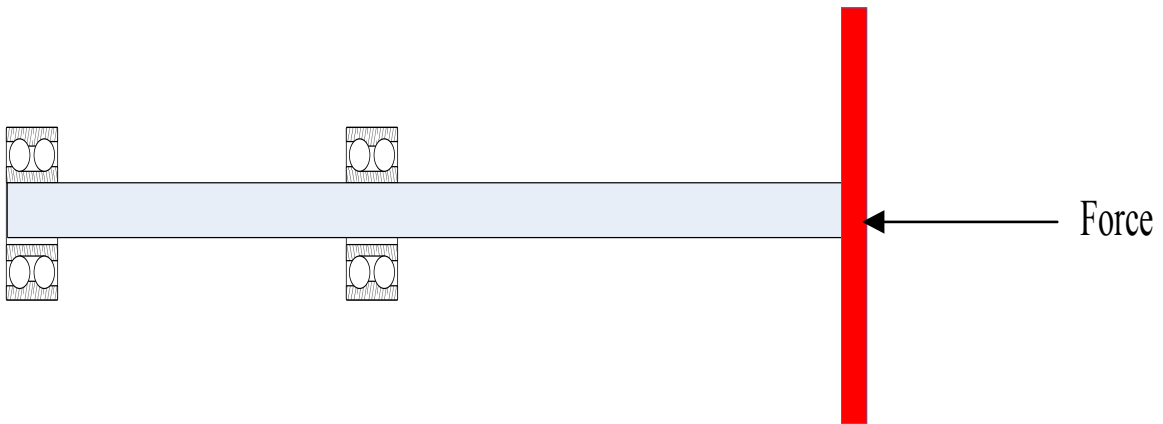


Figure 2.18 The configuration of the overhung rotor with one disk and two bearings

Table 2.5 illustrates the natural frequencies under the effect of the axial load. It is clear from Table 2.5 that the tensile force increases the natural frequencies while the compressive load decreases the natural frequencies.

Table 2.5 The natural frequencies in Hz under the effect of different tensile and compression axial loads

Speed (rpm)	Axial Load				
	0 KN	10 KN	-10 KN	100 KN	-100 KN
0	14.35	14.67	14.02	17.23	10.48
	14.35	14.67	14.02	17.23	10.48
	100.38	100.75	100.01	103.90	100.75
	100.38	100.75	100.01	103.90	100.75
	132.17	132.42	131.92	134.67	132.42
	132.17	132.42	131.92	134.67	132.42
4000	12.13	12.44	11.80	14.99	8.32
	16.54	16.84	16.22	19.28	12.85
	90.08	90.21	89.95	91.34	88.79
	100.94	101.34	100.54	104.75	96.76
	103.09	103.55	102.63	107.46	98.33
	186.88	187.14	186.61	189.48	184.19

In the last numerical example, a stepped shaft-disk system is shown in Figure 2.19. Two different cases are presented in this example to determine the natural frequencies. Table 2.6 gives the properties of the stepped shaft-disk system for the two cases. In the first case the length  $L_1$  and the diameters  $d_1$  and  $d_2$  are fixed, while the length  $L_2$  changes with

respect to the length  $L_1$ . Table 2.7 illustrates the natural frequencies of the stepped shaft with different  $L_2$ . Clearly, the natural frequencies increase with decreasing  $L_2$ . In the second case, the lengths  $L_1$  and  $L_2$  and the diameter  $d_2$  are fixed, while the diameter  $d_2$  changes with respect to the diameter  $d_1$ . The mass, the polar moment of inertia, and the diametral moment of inertia of the disk are calculated for the first  $d_2$  and then used for the other cases of  $d_2$ . Table 2.8 shows the natural frequencies when  $d_2$  is changed; reducing the diameter  $d_2$  decreases the natural frequencies.

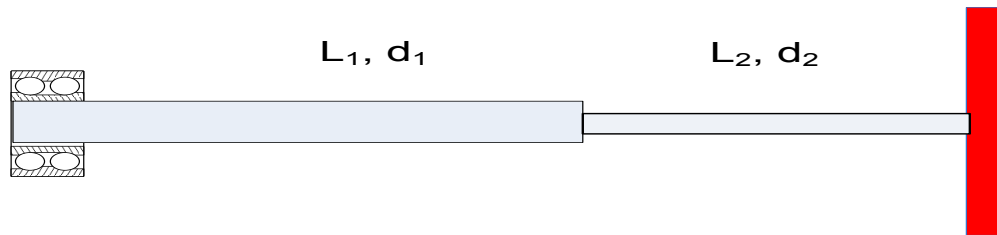


Figure 2.19 The stepped shaft-disk system

Table 2.6 The properties of the stepped shaft-disk system

Disk		
Thickness = 0.01 m		Outer Diameter = 0.1 m
Bearings		
$K_{yy} = 10^6$ N/m		$K_{zz} = 10^6$ N/m
Case 1		
Length, $L_1 = 0.06$ m	Diameter, $d_1 = 0.01$ m	Diameter, $d_2 = 0.005$ m
Case 2		
Diameter, $d_1 = 0.01$ m	Length, $L_1 = 0.06$ m	Length, $L_2 = 0.06$ m

Table 2.7 The natural frequencies in Hz of the stepped shaft with different lengths L2

Speed (rpm)	$L_2 = L_1$	$L_2 = 0.8 L_1$	$L_2 = 0.6 L_1$	$L_2 = 0.4 L_1$
0	592.5	714.4	882.6	1131.3
	592.5	714.4	882.6	1131.3
	1688.5	1978.4	2408.2	3018.9
	1688.5	1978.4	2408.2	3018.9
	4296	4654.8	5097.3	6016.4
	4296	4654.8	5097.3	6016.4
4000	571.2	686.8	846.6	1085.8
	613.8	742.5	919.5	1178.4
	1651	1945.9	2383.6	3004.4
	1729.1	2013.6	2434.8	3034.7
	4293.4	4652.5	5094.6	6012.8
	4298.8	4657.2	5100.1	6020.2

Table 2.8: The natural frequencies in Hz of the stepped shaft with different diameters  $d_2$ .

Speed (rpm)	$d_2 = 0.8d_1$	$d_2 = 0.6d_1$	$d_2 = 0.4d_1$	$d_2 = 0.2d_1$
0	1156.2	792.8	401.6	108
	1156.2	792.8	401.6	108
	3178.3	2248.6	1140.2	300.7
	3178.3	2248.6	1140.2	300.7
	5315	4491.8	4158	2598.4
	5315	4491.8	4158	2598.4
4000	1143.9	774.5	377.7	82.1
	1168.4	811	425.8	135.8
	3149.9	2211.6	1104.2	272.8
	3207	2287.6	1181.1	348.2
	5299.2	4486.6	4156.4	2597.8
	5331.4	4497.3	4159.8	2599

## 2.8 Summary

In this chapter, Euler-Bernoulli beam theory and Timoshenko beam theory were used to develop finite element models for a conventional metal driveshaft. The effect of axial load is included in both models. Also, tapered driveshaft is modeled based on Timoshenko beam theory. Numerical examples are given to perform rotordynamic analysis and to obtain the natural frequencies and critical speeds of conventional metal driveshaft.

## **Chapter 3**

# **Rotordynamic Analysis of Uniform Composite Shaft Using Finite Element Method**

### **3.1 Introduction**

Advanced composite materials are increasingly being utilized in a large scale in mechanical and aerospace applications such as automotive driveshaft and helicopter tail rotors. Advanced composite materials improve substantially the rotor-dynamic characteristics of a shaft in terms of critical speeds, bending natural frequencies and unbalance response. Hence, the composite shaft has all the potentials to replace the metallic shaft in such applications. In this chapter, the vibration analysis of composite shaft-disk system is conducted using the conventional finite element formulation. A composite finite element is developed for this purpose. The strain energy and the kinetic energy of the composite rotor system are determined to obtain the governing equations of motion of the system using the Lagrange's equations. The first-order shear deformable beam theory is used to establish the strain energy of the composite shaft system, while the kinetic energy is obtained by considering translational and rotational motions of a moving coordinate system that is attached to the cross-section of the shaft. In this model, the Timoshenko beam theory is adopted to include the effects of shear deformation and rotary inertia. In addition, the effects of gyroscopic forces, axial load, and coupling effect due to the lamination of composite layers are included. A conventional beam finite

element formulation with two end nodes and four degrees of freedom per each node is used to obtain the mass matrix, the gyroscopic matrix and the stiffness matrix of the composite rotor system in order to perform the vibration analysis. Using numerical examples the present model is validated in comparison with the results available in the literature. Rotor systems with stepped shafts are studied using the developed composite finite element. The critical speeds, natural frequencies, mode shapes, Campbell diagram and unbalance response of the stepped composite shaft-disk system are determined.

### 3.2 Stress - strain relations for a composite material layer

Figure 3.1 illustrates a single lamina deformed into a uniform cylinder where the angle  $\eta$  represents the angle between fiber orientation in the lamina and x-axis in cylindrical coordinate system  $(x, \theta, r)$ . The material coordinate of single lamina is depicted in Figure 3.2 where the axes 1 and 2 are the principal material directions. The stress-strain relations for a lamina in the principal material directions can be expressed as [20]:

$$\begin{bmatrix} \sigma_{11} \\ \sigma_{22} \\ \sigma_{33} \\ \tau_{23} \\ \tau_{13} \\ \tau_{12} \end{bmatrix} = \begin{bmatrix} Q_{11} & Q_{12} & Q_{13} & 0 & 0 & 0 \\ Q_{12} & Q_{22} & Q_{23} & 0 & 0 & 0 \\ Q_{13} & Q_{23} & Q_{33} & 0 & 0 & 0 \\ 0 & 0 & 0 & Q_{44} & 0 & 0 \\ 0 & 0 & 0 & 0 & Q_{55} & 0 \\ 0 & 0 & 0 & 0 & 0 & Q_{66} \end{bmatrix} \begin{bmatrix} \epsilon_{11} \\ \epsilon_{22} \\ \epsilon_{33} \\ \gamma_{23} \\ \gamma_{13} \\ \gamma_{12} \end{bmatrix} \quad (3.1)$$

The above equation may be written as:

$$[\sigma_{123}] = [Q][\epsilon_{123}] \quad (3.2)$$

where  $[Q]$  is the stiffness matrix of a single lamina, and it is a function of elastic moduli, shear moduli and the Poisson's ratio values of the lamina.

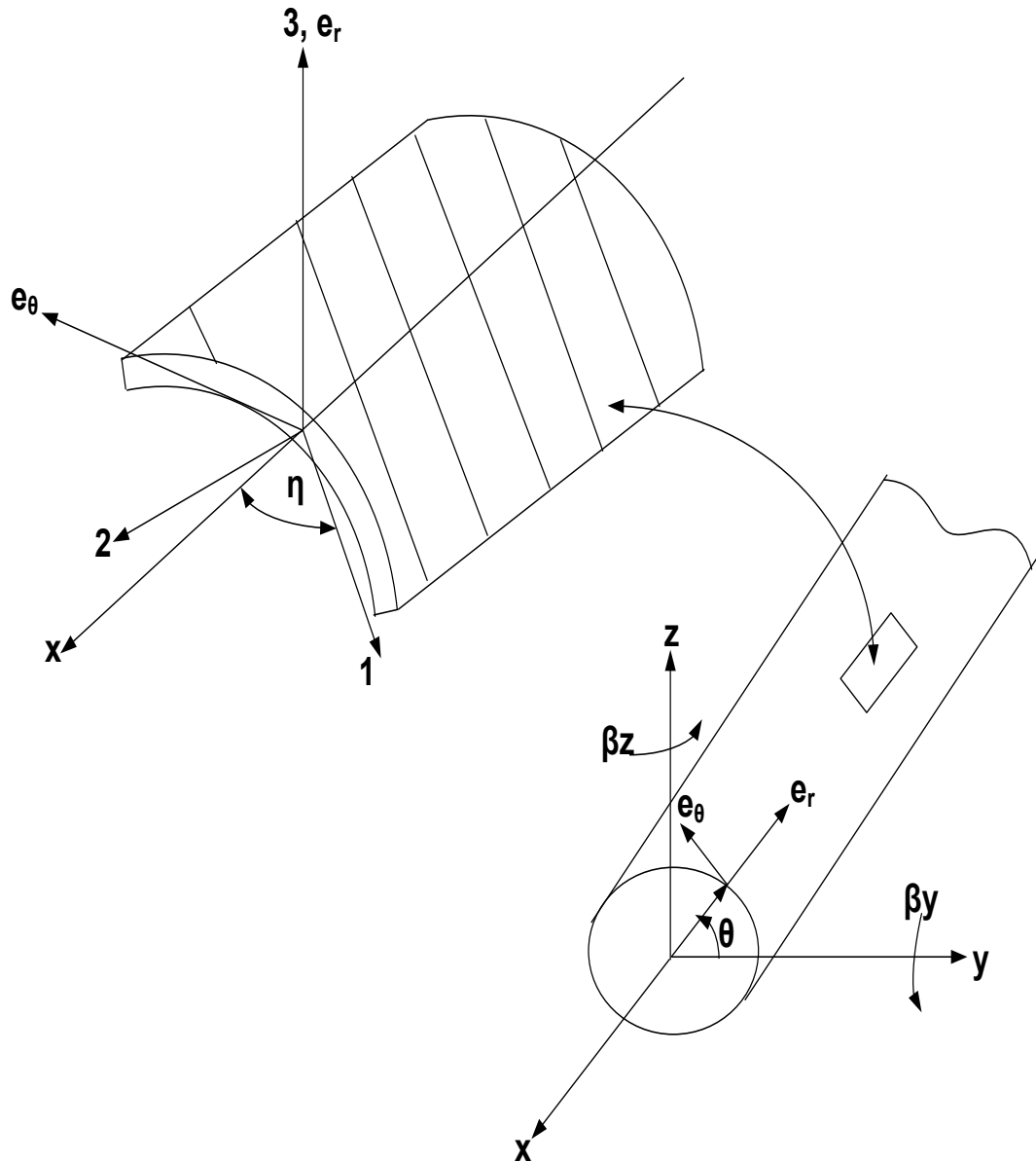


Figure 3.1 Single composite material lamina deformed into a uniform cylinder.

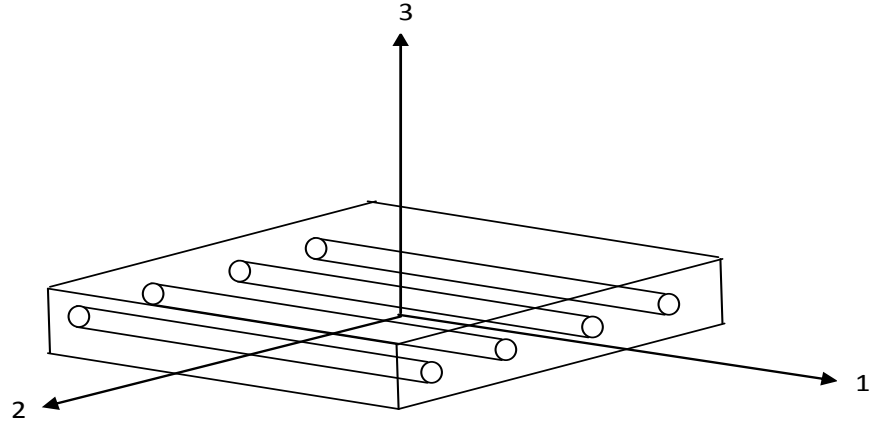


Figure 3.2 Single layer of composite material in the principal material coordinates.

To determine the stress-strain relations in cylindrical coordinate system, transformation from the principal material coordinate system (1, 2, 3) to cylindrical coordinate system (x,  $\theta$ , r) should be done. The relation between the stresses in cylindrical coordinate system (x,  $\theta$ , r) and principal material coordinate system (1, 2, 3) is [20]

$$\begin{bmatrix} \sigma_{xx} \\ \sigma_{\theta\theta} \\ \sigma_{rr} \\ \tau_{\theta r} \\ \tau_{xr} \\ \tau_{x\theta} \end{bmatrix} = \begin{bmatrix} m^2 & n^2 & 0 & 0 & 0 & 2mn \\ n^2 & m^2 & 0 & 0 & 0 & -2mn \\ 0 & 0 & 1 & 0 & 0 & 0 \\ 0 & 0 & 0 & m & -n & 0 \\ 0 & 0 & 0 & n & m & 0 \\ -mn & mn & 0 & 0 & 0 & m^2 - n^2 \end{bmatrix} \begin{bmatrix} \sigma_{11} \\ \sigma_{22} \\ \sigma_{33} \\ \tau_{23} \\ \tau_{13} \\ \tau_{12} \end{bmatrix} \quad (3.3)$$

where  $\eta$  is the fiber orientation angle,  $m = \cos \eta$ , and  $n = \sin \eta$ . Equation (3.3) can be abbreviated as

$$[\sigma_{x\theta r}] = [T_1][\sigma_{123}] \quad (3.4)$$

Similarly, one can get the relation between the strains in both the coordinate systems:

$$\begin{bmatrix} \epsilon_{xx} \\ \epsilon_{\theta\theta} \\ \epsilon_{rr} \\ \gamma_{\theta r} \\ \gamma_{xr} \\ \gamma_{x\theta} \end{bmatrix} = \begin{bmatrix} m^2 & n^2 & 0 & 0 & 0 & mn \\ n^2 & m^2 & 0 & 0 & 0 & -mn \\ 0 & 0 & 1 & 0 & 0 & 0 \\ 0 & 0 & 0 & m & -n & 0 \\ 0 & 0 & 0 & n & m & 0 \\ -2mn & 2mn & 0 & 0 & 0 & m^2 - n^2 \end{bmatrix} \begin{bmatrix} \epsilon_{11} \\ \epsilon_{22} \\ \epsilon_{33} \\ \gamma_{23} \\ \gamma_{13} \\ \gamma_{12} \end{bmatrix} \quad (3.5)$$

Equation (3.5) can be abbreviated as

$$[\epsilon_{x\theta r}] = [T_2][\epsilon_{123}] \quad (3.6)$$

Using Equations (3.1) - (3.6) with some mathematical manipulations, one can write the stress-strain relation in cylindrical coordinate system [20] as:

$$\begin{bmatrix} \sigma_{xx} \\ \sigma_{\theta\theta} \\ \sigma_{rr} \\ \tau_{\theta r} \\ \tau_{xr} \\ \tau_{x\theta} \end{bmatrix} = \begin{bmatrix} \bar{Q}_{11} & \bar{Q}_{12} & \bar{Q}_{13} & 0 & 0 & \bar{Q}_{16} \\ \bar{Q}_{12} & \bar{Q}_{22} & \bar{Q}_{23} & 0 & 0 & \bar{Q}_{26} \\ \bar{Q}_{13} & \bar{Q}_{23} & \bar{Q}_{33} & 0 & 0 & \bar{Q}_{36} \\ 0 & 0 & 0 & \bar{Q}_{44} & \bar{Q}_{45} & 0 \\ 0 & 0 & 0 & \bar{Q}_{45} & \bar{Q}_{55} & 0 \\ \bar{Q}_{16} & \bar{Q}_{26} & \bar{Q}_{36} & 0 & 0 & \bar{Q}_{66} \end{bmatrix} \begin{bmatrix} \epsilon_{xx} \\ \epsilon_{\theta\theta} \\ \epsilon_{rr} \\ \gamma_{\theta r} \\ \gamma_{xr} \\ \gamma_{x\theta} \end{bmatrix} \quad (3.7)$$

The above equation can be written in the following form

$$[\sigma_{x\theta r}] = [\bar{Q}][\epsilon_{x\theta r}] \quad (3.8)$$

where  $[\bar{Q}]$  is the transformed stiffness matrix of the layer and can be calculated by the following equation [20] :

$$[\bar{Q}] = [T_1][Q][T_2]^{-1} \quad (3.9)$$

### 3.1 Strain-displacement relations

Timoshenko beam theory is considered here to study the transverse vibration of the uniform composite shaft. So, the displacement fields of the composite shaft are assumed [20,22] as

$$u_x(x, y, z, t) = z\beta_y(x, t) - y\beta_z(x, t) = (r \sin \theta)\beta_y(x, t) - (r \cos \theta)\beta_z(x, t) \quad (3.10)$$

$$u_y(x, y, z, t) = v(x, t) \quad (3.11)$$

$$u_z(x, y, z, t) = w(x, t) \quad (3.12)$$

where  $y = r \cos \theta$  and  $z = r \sin \theta$ .  $u_x$ ,  $u_y$  and  $u_z$  are the displacements of any point of the composite shaft in x, y and z directions, and  $v$  and  $w$  are the displacements of a point on the reference axis of the shaft in y and z directions and  $\beta_y$  and  $\beta_z$  are the rotation angles of the cross-section about y-axis and z-axis. The strains can be determined using Equations (3.10) - (3.12) [20] as

$$\epsilon_{xx} = \frac{\partial u_x}{\partial x} = z \frac{\partial \beta_y}{\partial x} - y \frac{\partial \beta_z}{\partial x} \quad (3.13)$$

$$\epsilon_{yy} = \frac{\partial u_y}{\partial y} = 0 \quad (3.14)$$

$$\epsilon_{zz} = \frac{\partial u_z}{\partial z} = 0 \quad (3.15)$$

$$\gamma_{yz} = \frac{\partial u_z}{\partial y} + \frac{\partial u_y}{\partial z} = 0 \quad (3.16)$$

$$\gamma_{xz} = \frac{\partial u_x}{\partial z} + \frac{\partial u_z}{\partial x} = \beta_y + \frac{\partial w}{\partial x} \quad (3.17)$$

$$\gamma_{xy} = \frac{\partial u_x}{\partial y} + \frac{\partial u_y}{\partial x} = -\beta_z + \frac{\partial v}{\partial x} \quad (3.18)$$

The strain components in cylindrical coordinate system  $(x, \theta, r)$  can be written in terms of the strains in the Cartesian coordinate system  $(x, y, z)$  [20] as

$$\begin{bmatrix} \epsilon_{xx} \\ \epsilon_{\theta\theta} \\ \epsilon_{rr} \\ \gamma_{\theta r} \\ \gamma_{xr} \\ \gamma_{x\theta} \end{bmatrix} = \begin{bmatrix} 1 & 0 & 0 & 0 & 0 & 0 \\ 0 & h^2 & g^2 & -2gh & 0 & 0 \\ 0 & g^2 & h^2 & 2gh & 0 & 0 \\ 0 & -gh & gh & g^2 - h^2 & 0 & 0 \\ 0 & 0 & 0 & 0 & h & g \\ 0 & 0 & 0 & 0 & g & -h \end{bmatrix} \begin{bmatrix} \epsilon_{xx} \\ \epsilon_{yy} \\ \epsilon_{zz} \\ \gamma_{yz} \\ \gamma_{xz} \\ \gamma_{xy} \end{bmatrix} \quad (3.19)$$

where  $g = \cos \theta$  and  $h = \sin \theta$ . Substituting Equations (3.13) – (3.18) into Equation (3.19), one can get [20]

$$\epsilon_{xx} = r (\sin \theta) \frac{\partial \beta_y}{\partial x} - r (\cos \theta) \frac{\partial \beta_z}{\partial x} \quad (3.20)$$

$$\epsilon_{\theta\theta} = 0 \quad (3.21)$$

$$\epsilon_{rr} = 0 \quad (3.22)$$

$$\gamma_{\theta r} = 0 \quad (3.23)$$

$$\gamma_{xr} = (\sin \theta) \left( \frac{\partial w}{\partial x} + \beta_y \right) + (\cos \theta) \left( -\beta_z + \frac{\partial v}{\partial x} \right) \quad (3.24)$$

$$\gamma_{x\theta} = (\cos \theta) \left( \frac{\partial w}{\partial x} + \beta_y \right) - (\sin \theta) \left( -\beta_z + \frac{\partial v}{\partial x} \right) \quad (3.25)$$

Considering Equations (3.21)-(3.23), one can write Equation (3.7) as

$$\begin{bmatrix} \sigma_{xx} \\ \sigma_{\theta\theta} \\ \sigma_{rr} \\ \tau_{\theta r} \\ \tau_{xr} \\ \tau_{x\theta} \end{bmatrix} = \begin{bmatrix} \bar{Q}_{11} & 0 & \bar{Q}_{16} \\ \bar{Q}_{12} & 0 & \bar{Q}_{26} \\ \bar{Q}_{13} & 0 & \bar{Q}_{36} \\ 0 & \bar{Q}_{45} & 0 \\ 0 & \bar{Q}_{55} & 0 \\ \bar{Q}_{16} & 0 & \bar{Q}_{66} \end{bmatrix} \begin{bmatrix} \epsilon_{xx} \\ \gamma_{xr} \\ \gamma_{x\theta} \end{bmatrix} \quad (3.26)$$

In Timoshenko beam theory, the shear correction factor  $k_s$  is used to adjust the stress state. Introducing the shear correction factor  $k_s$  and choosing its value can be a complex issue especially for structure such as tapered composite shaft. And, because the objective of this thesis is to develop finite element models for tapered composite shaft, no attention is given for the shear correction factor  $k_s$ . However, the way that, the correction factor  $k_s$  is introduced and calculated in this thesis for uniform and tapered composite shafts, is based on [20,27]. Therefore, the Equation (3.26) can be written as

$$\begin{bmatrix} \sigma_{xx} \\ \sigma_{\theta\theta} \\ \sigma_{rr} \\ \tau_{\theta r} \\ \tau_{xr} \\ \tau_{x\theta} \end{bmatrix} = \begin{bmatrix} \bar{Q}_{11} & 0 & k_s \bar{Q}_{16} \\ \bar{Q}_{12} & 0 & k_s \bar{Q}_{26} \\ \bar{Q}_{13} & 0 & k_s \bar{Q}_{36} \\ 0 & k_s \bar{Q}_{45} & 0 \\ 0 & k_s \bar{Q}_{55} & 0 \\ k_s \bar{Q}_{16} & 0 & k_s \bar{Q}_{66} \end{bmatrix} \begin{bmatrix} \epsilon_{xx} \\ \gamma_{xr} \\ \gamma_{x\theta} \end{bmatrix} \quad (3.27)$$

### 3.2 Kinetic and strain energy expressions

The kinetic energy of the composite shaft is analogous to that of the isotropic shaft, so equation (2.49) is used to obtain:

$$T_{comp} = \frac{1}{2} \int_0^L m_c (\dot{v}^2 + \dot{w}^2) dx + \frac{1}{2} \int_0^L I_{dc} (\dot{\beta}_y^2 + \dot{\beta}_z^2) dx - \int_0^L I_{pc} \Omega \dot{\beta}_z \beta_y dx \quad (3.28)$$

where  $m_c, I_{dc},$  and  $I_{pc}$  are the mass per unit length, diametral mass moment of inertia, and polar mass moment of inertia.

$$m_c = \pi \sum_{s=1}^n \rho_s (r_{os}^2 - r_{is}^2) \quad (3.29)$$

$$I_{dc} = \frac{\pi}{4} \sum_{s=1}^n \rho_s (r_{os}^4 - r_{is}^4) \quad (3.30)$$

$$I_{pc} = \frac{\pi}{2} \sum_{s=1}^n \rho_s (r_{os}^4 - r_{is}^4) \quad (3.31)$$

where  $n$  is the number of the layers in the laminate, and  $r_{os}$  and  $r_{is}$  are the outer radius and inner radius of the  $s$ -th layer;  $\rho_s$  is the material density of the  $s$ -th layer. The strain energy of the composite shaft can be written as:

$$\begin{aligned} U_{BS} &= \frac{1}{2} \iiint_V [\sigma_{x\theta r}]^T [\epsilon_{x\theta r}] dV \\ &= \frac{1}{2} \iiint_V [\sigma_{xx}\epsilon_{xx} + \sigma_{\theta\theta}\epsilon_{\theta\theta} + \sigma_{rr}\epsilon_{rr} + \tau_{\theta r}\gamma_{\theta r} + \tau_{xr}\gamma_{xr} \\ &\quad + \tau_{x\theta}\gamma_{x\theta}] dV \end{aligned} \quad (3.32)$$

Considering Equation (3.20) – (3.25), Equation (3.32) can be reduced to

$$U_{BS} = \frac{1}{2} \int_0^L \left[ \int_A [\sigma_{xx}\epsilon_{xx} + \tau_{xr}\gamma_{xr} + \tau_{x\theta}\gamma_{x\theta}] dA \right] dx \quad (3.33)$$

Substituting Equation (3.20), Equation (3.24), and Equation (3.25) into Equation (3.33), one can obtain the strain energy [20] as

$$\begin{aligned}
U_{BS} = \frac{1}{2} \int_0^L \left[ \int_A \left[ \sigma_{xx} (r \sin \theta \frac{\partial \beta_y}{\partial x} \right. \right. \\
- r \cos \theta \frac{\partial \beta_z}{\partial x}) + \tau_{xr} (\beta_y \sin \theta \\
+ \frac{\partial w}{\partial x} \sin \theta + \frac{\partial v}{\partial x} \cos \theta - \beta_z \cos \theta) + \tau_{x\theta} (-\frac{\partial v}{\partial x} \sin \theta + \beta_z \sin \theta \\
+ \beta_y \cos \theta + \frac{\partial w}{\partial x} \cos \theta) \left. \right] dA \right] dx \tag{3.34}
\end{aligned}$$

From Equation (3.34), one can define the stress couples and the stress resultants [20] as:

$$M_y = \int_A \sigma_{xx} r \sin \theta dA \tag{3.35}$$

$$M_z = - \int_A \sigma_{xx} r \cos \theta dA \tag{3.36}$$

$$Q_{xr}^{(1)} = \int_A \tau_{xr} \sin \theta dA \tag{3.37}$$

$$Q_{xr}^{(2)} = \int_A \tau_{xr} \cos \theta dA \tag{3.38}$$

$$Q_{x\theta}^{(1)} = \int_A \tau_{x\theta} \sin \theta dA \tag{3.39}$$

$$Q_{x\theta}^{(2)} = \int_A \tau_{x\theta} \cos \theta \, dA \quad (3.40)$$

The forces and moments on the cross-section of the composite shaft are illustrated in Figure 3.3. Using Equations (3.35) – (3.40) in Equation (3.34), the strain energy can be written [20] as

$$U_{BS} = \frac{1}{2} \int_0^L \left[ M_y \frac{\partial \beta_y}{\partial x} + M_z \frac{\partial \beta_z}{\partial x} + Q_y \left( \frac{\partial v}{\partial x} - \beta_z \right) + Q_z \left( \beta_y + \frac{\partial w}{\partial x} \right) \right] dx \quad (3.41)$$

Where  $Q_y$  and  $Q_z$  are the shear force in  $y$  and  $z$  directions, respectively [20].

$$Q_y = Q_{xr}^{(2)} - Q_{x\theta}^{(1)} \quad (3.42)$$

$$Q_z = Q_{xr}^{(1)} + Q_{x\theta}^{(2)} \quad (3.43)$$

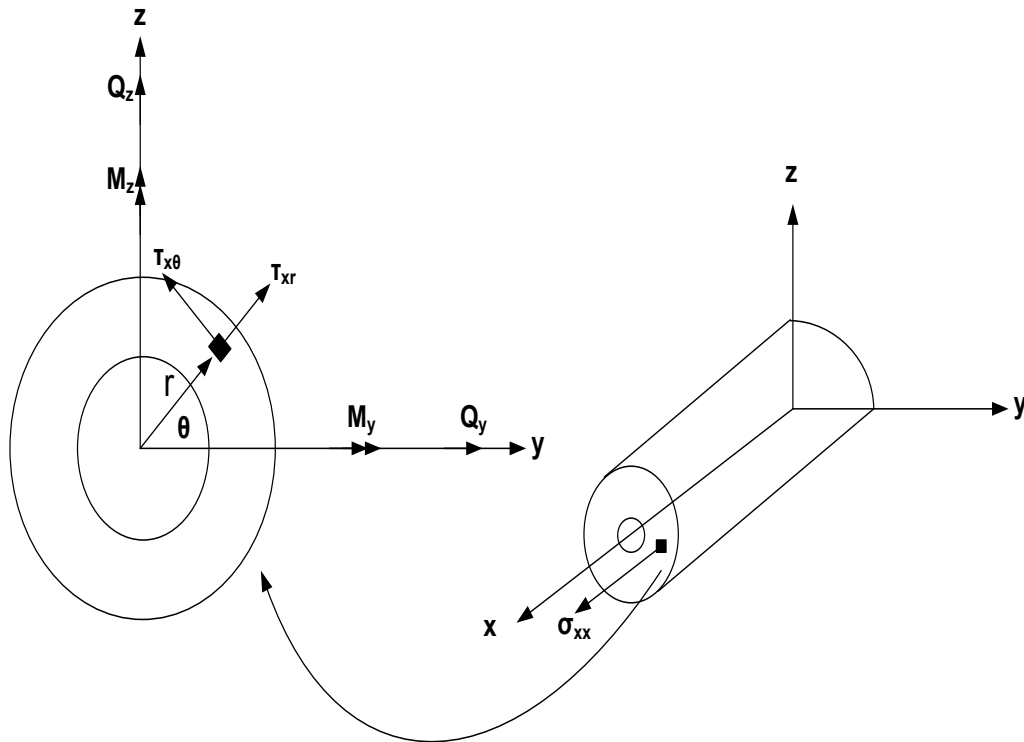


Figure 3.3 The forces and moments on the cross-section of the composite shaft

Considering Equation (3.27), Equation (3.20), Equation (3.24), and Equation (3.25), one can write the stress couples and the stress resultant in Equations (3.35) – (3.40) as

$$\begin{aligned}
M_y &= \int_0^{2\pi} \int_{r_i}^{r_o} (\bar{Q}_{11}\epsilon_{xx} + k_s\bar{Q}_{16}\gamma_{x\theta}) r^2 \sin\theta \, dr \, d\theta \\
&= \int_0^{2\pi} \int_{r_i}^{r_o} \left[ \bar{Q}_{11} \frac{\partial\beta_y}{\partial x} r^3 \sin\theta \right. \\
&\quad - \bar{Q}_{11} \frac{\partial\beta_z}{\partial x} r^3 \cos\theta - k_s\bar{Q}_{16}r^2 \frac{\partial v}{\partial x} \sin\theta \\
&\quad + k_s\bar{Q}_{16}r^2\beta_z \sin\theta + k_s\bar{Q}_{16}\beta_y r^2 \cos\theta \\
&\quad \left. + k_s\bar{Q}_{16}r^2 \frac{\partial w}{\partial x} \cos\theta \right] \sin\theta \, dr \, d\theta
\end{aligned} \tag{3.44}$$

$$\begin{aligned}
M_z &= - \int_0^{2\pi} \int_{r_i}^{r_o} (\bar{Q}_{11}\epsilon_{xx} + k_s\bar{Q}_{16}\gamma_{x\theta}) r^2 \cos\theta \, dr \, d\theta \\
&= - \int_0^{2\pi} \int_{r_i}^{r_o} \left[ \bar{Q}_{11} \frac{\partial\beta_y}{\partial x} r^3 \sin\theta \right. \\
&\quad - \bar{Q}_{11} \frac{\partial\beta_z}{\partial x} r^3 \cos\theta - k_s\bar{Q}_{16}r^2 \frac{\partial v}{\partial x} \sin\theta \\
&\quad + k_s\bar{Q}_{16}r^2\beta_z \sin\theta + k_s\bar{Q}_{16}\beta_y r^2 \cos\theta \\
&\quad \left. + k_s\bar{Q}_{16}r^2 \frac{\partial w}{\partial x} \cos\theta \right] \cos\theta \, dr \, d\theta
\end{aligned} \tag{3.45}$$

$$\begin{aligned}
Q_{x\theta}^{(1)} &= \int_0^{2\pi} \int_{r_i}^{r_o} k_s [\bar{Q}_{16} \epsilon_{xx} + \bar{Q}_{66} \gamma_{x\theta}] r \sin\theta \, dr \, d\theta \\
&= \int_0^{2\pi} \int_{r_i}^{r_o} k_s \left[ \bar{Q}_{16} (r^2 \sin\theta \frac{\partial \beta_y}{\partial x} - r^2 \cos\theta \frac{\partial \beta_z}{\partial x}) + \bar{Q}_{66} (-r \sin\theta \frac{\partial v}{\partial x} \right. \\
&\quad \left. + r \beta_z \sin\theta + r \beta_y \cos\theta + r \frac{\partial w}{\partial x} \cos\theta) \right] \sin\theta \, dr \, d\theta
\end{aligned} \tag{3.46}$$

$$\begin{aligned}
Q_{x\theta}^{(2)} &= \int_0^{2\pi} \int_{r_i}^{r_o} k_s [\bar{Q}_{16} \epsilon_{xx} + \bar{Q}_{66} \gamma_{x\theta}] r \cos\theta \, dr \, d\theta \\
&= \int_0^{2\pi} \int_{r_i}^{r_o} k_s \left[ \bar{Q}_{16} (r^2 \sin\theta \frac{\partial \beta_y}{\partial x} - r^2 \cos\theta \frac{\partial \beta_z}{\partial x}) + \bar{Q}_{66} (-r \sin\theta \frac{\partial v}{\partial x} \right. \\
&\quad \left. + r \beta_z \sin\theta + r \beta_y \cos\theta + r \frac{\partial w}{\partial x} \cos\theta) \right] \cos\theta \, dr \, d\theta
\end{aligned} \tag{3.47}$$

$$\begin{aligned}
Q_{xr}^{(1)} &= \int_0^{2\pi} \int_{r_i}^{r_o} k_s \bar{Q}_{55} \gamma_{xr} \sin\theta \, r \, dr \, d\theta \\
&= \int_0^{2\pi} \int_{r_i}^{r_o} k_s \bar{Q}_{55} \left[ r \cos\theta \frac{\partial v}{\partial x} \right. \\
&\quad \left. - r \beta_z \cos\theta + \beta_y r \sin\theta + r \frac{\partial w}{\partial x} \sin\theta \right] \sin\theta \, dr \, d\theta
\end{aligned} \tag{3.48}$$

$$\begin{aligned}
Q_{xr}^{(2)} &= \int_0^{2\pi} \int_{r_i}^{r_o} \bar{Q}_{55} \gamma_{zr} k_s \cos\theta r dr d\theta \\
&= \int_0^{2\pi} \int_{r_i}^{r_o} k_s \bar{Q}_{55} \left[ r \cos\theta \frac{\partial v}{\partial x} \right. \\
&\quad \left. - r \beta_z \cos\theta + \beta_y r \sin\theta + r \frac{\partial w}{\partial x} \sin\theta \right] \cos\theta dr d\theta \quad (3.49)
\end{aligned}$$

After performing the integration in Equations (3.44) – (3.49), the stress couples and the stress resultants can be written [20] as:

$$M_y = D_{11} \frac{\partial \beta_y}{\partial x} + \frac{1}{2} k_s B_{16} (\beta_z - \frac{\partial v}{\partial x}) \quad (3.50)$$

$$M_z = D_{11} \frac{\partial \beta_z}{\partial x} - \frac{1}{2} k_s B_{16} (\frac{\partial w}{\partial x} + \beta_y) \quad (3.51)$$

$$Q_{x\theta}^{(1)} = \frac{1}{2} B_{16} k_s \frac{\partial \beta_y}{\partial x} + k_s A_{66} \left( \beta_z - \frac{\partial v}{\partial x} \right) \quad (3.52)$$

$$Q_{x\theta}^{(2)} = -\frac{1}{2} k_s B_{16} \frac{\partial \beta_z}{\partial x} + k_s A_{66} (\beta_y + \frac{\partial w}{\partial x}) \quad (3.53)$$

$$Q_{xr}^{(1)} = A_{55} k_s (\beta_y + \frac{\partial w}{\partial x}) \quad (3.54)$$

$$Q_{xr}^{(2)} = A_{55} k_s (-\beta_z + \frac{\partial v}{\partial x}) \quad (3.55)$$

where

$$A_{66} = \frac{\pi}{2} \sum_{s=1}^n \bar{Q}_{66} (r_{os}^2 - r_{is}^2) \quad (3.56)$$

$$A_{55} = \frac{\pi}{2} \sum_{s=1}^n \bar{Q}_{55} (r_{os}^2 - r_{is}^2) \quad (3.57)$$

$$B_{16} = \frac{2}{3} \pi \sum_{s=1}^n \bar{Q}_{16} (r_{os}^3 - r_{is}^3) \quad (3.58)$$

$$D_{11} = \frac{\pi}{4} \sum_{s=1}^n \bar{Q}_{11} (r_{os}^4 - r_{is}^4) \quad (3.59)$$

The strain energy  $U_{BS}$  in Equation (3.41) represents the strain energy of the composite shaft that results from the bending moment and the shear force. In the case of the composite shaft under a constant axial force, the total strain energy of the composite shaft is

$$U_{comp} = U_{BS} + U_F \quad (3.60)$$

where  $U_F$  is the work done on the composite shaft due to a constant axial force  $P$  and can be written [9] as

$$U_F = \frac{1}{2} \int_0^L P \left[ \left( \frac{\partial v}{\partial x} \right)^2 + \left( \frac{\partial w}{\partial x} \right)^2 \right] dx \quad (3.61)$$

### 3.3 Conventional-Hermitian finite element formulation

In chapter 2, Hermitian finite element formulation was used to develop the equations of motion of the metal shaft. In this section, Hermitian finite element is used again but to develop a model for uniform composite shaft. The same procedure that was used to develop the finite element model for the metal shaft in chapter 2 is followed here to build up the finite element model for the uniform composite shaft. Timoshenko beam theory is considered to include the shear deformation; Figure 3.4 shows the relation between the rotation of cross-section and the shear deformation angle in y-x plane. The element that is used for the uniform composite shaft has two nodes located at its ends, and each node has four degrees of freedom: two translations ( $v$ ,  $w$ ) and two rotations ( $\beta_z$ ,  $\beta_y$ ). The relations between the rotations and the shear angles in y-x plane and z-x plane are

$$\beta_z = \frac{\partial v}{\partial x} - \gamma_{xy} = \frac{\partial v}{\partial x} - \phi_{xy} \quad (3.62)$$

$$\beta_y = -\frac{\partial w}{\partial x} + \gamma_{xz} = -\frac{\partial w}{\partial x} + \phi_{xz} \quad (3.63)$$

where  $\phi_{xz}$  and  $\phi_{xy}$  are the shear angles in z-x plane and y-x plane, respectively. To derive the shape functions, one can consider the y-x plane and represent the lateral displacement  $v(x, t)$  by a cubic polynomial with four parameters:

$$v(x, t) = a_0 + a_1x + a_2x^2 + a_3x^3 \quad (3.64)$$

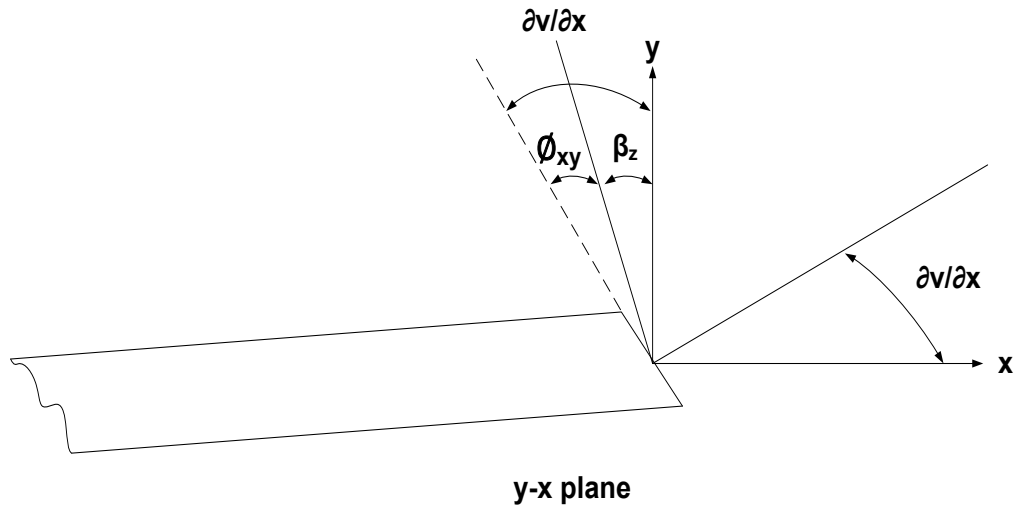


Figure 3.4 Deformed geometry of an edge of beam under the assumption of Timoshenko  
Beam theory

The rotation and translation boundary conditions in y-x plane are:

$$v(0, t) = v_1 \quad (3.65)$$

$$v(L, t) = v_2 \quad (3.66)$$

$$\beta_z(0, t) = \beta_{z1} = \frac{\partial v}{\partial x} \Big|_{x=0} - \phi_{xy}(0, t) \quad (3.67)$$

$$\beta_z(L, t) = \beta_{z2} = \frac{\partial v}{\partial x} \Big|_{x=L} - \phi_{xy}(L, t) \quad (3.68)$$

The shear angle  $\phi_{xy}$  and the lateral displacement  $v$  should be related together, and to obtain the relationship between them, the static equilibrium of the beam must be considered. The equilibrium of the beam in y-x plane can be written as:

$$\frac{\partial}{\partial x} [M_z] = -Q_y \quad (3.69)$$

$$\begin{aligned} & \frac{\partial}{\partial x} \left[ D_{11} \frac{\partial \beta_z}{\partial x} - \frac{1}{2} k_s B_{16} \left( \frac{\partial w}{\partial x} + \beta_y \right) \right] \\ &= - \left[ A_{55} k_s \left( -\beta_z + \frac{\partial v}{\partial x} \right) - \left( \frac{1}{2} B_{16} k_s \frac{\partial \beta_y}{\partial x} + k_s A_{66} \left( \beta_z - \frac{\partial v}{\partial x} \right) \right) \right] \end{aligned} \quad (3.70)$$

Using Equation (3.62) in Equation (3.70), one can get

$$\begin{aligned} & D_{11} \frac{\partial}{\partial x} \left( \frac{\partial}{\partial x} \left( \frac{\partial v}{\partial x} - \phi_{xy} \right) \right) - \left( \frac{1}{2} k_s B_{16} \right) \frac{\partial}{\partial x} \left( \frac{\partial w}{\partial x} \right) - B_{16} k_s \frac{\partial \beta_y}{\partial x} \\ &= -k_s (A_{66} + A_{55}) \phi_{xy} \end{aligned} \quad (3.71)$$

Now, using Equation (3.63) in Equation (3.71), one can get

$$\begin{aligned} & D_{11} \frac{\partial}{\partial x} \left( \frac{\partial}{\partial x} \left( \frac{\partial v}{\partial x} - \phi_{xy} \right) \right) - \left( \frac{1}{2} k_s B_{16} \right) \frac{\partial}{\partial x} \left( \frac{\partial w}{\partial x} \right) - B_{16} k_s \frac{\partial}{\partial x} \left( -\frac{\partial w}{\partial x} + \phi_{xz} \right) \\ &= -k_s (A_{66} + A_{55}) \phi_{xy} \end{aligned} \quad (3.72)$$

The shear angles in y-x plane and in z-x plane are constants with axial coordinate x, so

$$\frac{\partial^2 \phi_{xy}}{\partial x^2} = \frac{\partial \phi_{xz}}{\partial x} = 0 \quad (3.73)$$

Using Equation (3.73) into Equation (3.72), one can obtain the shear angle as:

$$\phi_{xy} = - \frac{D_{11}}{k_s (A_{55} + A_{66})} \left[ \frac{\partial^3 v}{\partial x^3} + \frac{1}{2} k_s B_{16} \frac{\partial^2 w}{\partial x^2} \right] \quad (3.74)$$

$\frac{\partial^2 w}{\partial x^2}$  has a small influence on the shear angle  $\phi_{xy}$  and can be neglected for simplification,

so the shear angle can be written as

$$\phi_{xy} = -\frac{D_{11}}{k_s(A_{55} + A_{66})} \frac{\partial^3 v}{\partial x^3} = -\frac{L^2 \Gamma_{\text{comp}}}{2} a_3 \quad (3.75)$$

where

$$\Gamma_{\text{comp}} = \frac{12D_{11}}{k_s(A_{55} + A_{66})L^2} \quad (3.76)$$

$\Gamma_{\text{comp}}$  is the shear deformation parameter for composite shaft, and it represents the ratio between bending stiffness and shear stiffness. Applying the lateral and rotational boundary conditions gives

$$v_1 = a_0 \quad (3.77)$$

$$v_2 - v_1 = a_1 L + a_2 L^2 + a_3 L^3 \quad (3.78)$$

$$a_1 = \beta_{z1} + \phi_{xy} = \beta_{z1} - \frac{L^2 \Gamma_{\text{comp}}}{2} a_3 \quad (3.79)$$

$$\beta_{z2} - \beta_{z1} = 2a_2 L + 3a_3 L^2 \quad (3.80)$$

Substituting Equation (3.79) in Equation (3.78), one can get

$$v_2 - v_1 = L\beta_{z1} + a_2 L^2 + \left(1 - \frac{\Gamma_{\text{comp}}}{2}\right) a_3 L^3 \quad (3.81)$$

From Equation (3.80)

$$a_2 = \frac{\beta_{z2} - \beta_{z1} - 3a_3 L^2}{2L} \quad (3.82)$$

Substituting Equation (3.82) in Equation (3.81) gives

$$a_3 = -\frac{1}{L^3(1 + \Gamma_{\text{comp}})} [2(v_2 - v_1) - L(\beta_{z1} + \beta_{z2})] \quad (3.83)$$

Then, substituting Equation (3.83) in Equation (3.79) and Equation (3.82) to obtain  $a_1$  and  $a_2$  as

$$a_1 = \beta_{z1} + \frac{\Gamma_{\text{comp}}}{2L(1 + \Gamma_{\text{comp}})} [2(v_2 - v_1) - L(\beta_{z1} + \beta_{z2})] \quad (3.84)$$

$$a_2 = \frac{1}{2L}(\beta_{z2} - \beta_{z1}) + \frac{3}{2L^2(1 + \Gamma_{\text{comp}})} [2(v_2 - v_1) - L(\beta_{z1} + \beta_{z2})] \quad (3.85)$$

Substituting Equations (3.83)-(3.85) and Equation (3.77) in Equation (3.64) to obtain the lateral displacement  $v(x, t)$  as:

$$v(x, t) = N_{t1}(x)v_1(t) + N_{t2}(x)\beta_{z1}(t) + N_{t3}(x)v_2(t) + N_{t4}(x)\beta_{z2}(t) \quad (3.86)$$

where

$$N_{t1} = \frac{1}{1 + \Gamma_{\text{comp}}} [1 + \Gamma_{\text{comp}} - \Gamma_{\text{comp}}\xi - 3\xi^2 + 2\xi^3] \quad (3.87)$$

$$N_{t2} = \frac{L}{1 + \Gamma_{\text{comp}}} \left[ \frac{(2 + \Gamma_{\text{comp}})\xi}{2} - \frac{(4 + \Gamma_{\text{comp}})\xi^2}{2} + \xi^3 \right] \quad (3.88)$$

$$N_{t3} = \frac{1}{1 + \Gamma_{\text{comp}}} [\Gamma_{\text{comp}}\xi + 3\xi^2 - 2\xi^3] \quad (3.89)$$

$$N_{t4} = \frac{L}{1 + \Gamma_{\text{comp}}} \left[ -\frac{\Gamma_{\text{comp}}\xi}{2} + \frac{(\Gamma_{\text{comp}} - 2)\xi^2}{2} + \xi^3 \right] \quad (3.90)$$

$$\xi = \frac{x}{L} \quad (3.91)$$

Substituting Equation (3.83) in Equation (3.75), then substituting Equation (3.75) and Equation (3.86) into Equation (3.62), one can obtain  $\beta_z(x, t)$  as:

$$\beta_z(x, t) = N_{r1}(x)v_1(t) + N_{r2}(x)\beta_{z1}(t) + N_{r3}(x)v_2(t) + N_{r4}(x)\beta_{z2}(t) \quad (3.92)$$

where

$$N_{r1} = \frac{6}{L(1 + \Gamma_{\text{comp}})} [\xi^2 - \xi] \quad (3.93)$$

$$N_{r2} = \frac{1}{1 + \Gamma_{\text{comp}}} [1 - 4\xi + 3\xi^2 + \Gamma_{\text{comp}}(1 - \xi)] \quad (3.94)$$

$$N_{r3} = \frac{6}{L(1 + \Gamma_{\text{comp}})} [-\xi^2 + \xi] \quad (3.95)$$

$$N_{r4} = \frac{1}{1 + \Gamma_{\text{comp}}} [3\xi^2 - 2\xi + \Gamma_{\text{comp}}\xi] \quad (3.96)$$

$$\xi = \frac{x}{L} \quad (3.97)$$

To obtain  $w(x, t)$  and  $\beta_y(x, t)$ , the previous procedure for obtaining  $v(x, t)$  and  $\beta_z(x, t)$  can be repeated again. Consequently, the internal displacements and rotations of the composite element can be expressed in terms of the displacements and rotations of the end points and the shape functions as

$$\begin{bmatrix} v \\ w \\ \beta_y \\ \beta_z \end{bmatrix} = \begin{bmatrix} N_{t1} & 0 & 0 & N_{t2} & N_{t3} & 0 & 0 & N_{t4} \\ 0 & N_{t1} & -N_{t2} & 0 & 0 & N_{t3} & -N_{t4} & 0 \\ 0 & -N_{r1} & N_{r2} & 0 & 0 & -N_{r3} & N_{r4} & 0 \\ N_{r1} & 0 & 0 & N_{r2} & N_{r3} & 0 & 0 & N_{r4} \end{bmatrix} \begin{bmatrix} v_1 \\ w_1 \\ \beta_{y1} \\ \beta_{z1} \\ v_2 \\ w_2 \\ \beta_{y2} \\ \beta_{z2} \end{bmatrix} \quad (3.98)$$

Substituting Equation (3.98) into Equation (3.28) the kinetic energy expression and into Equation (3.60) the strain energy expression and then applying the Lagrange's equations the equations of motion of the composite shaft element can be obtained.

Lagrange's equation :

$$\frac{d}{dt} \left( \frac{\partial L}{\partial \dot{q}} \right) - \frac{\partial L}{\partial q} = Q \quad (3.99)$$

where

$$L = T_{comp} - (U_{BS} + U_F) \quad (3.100)$$

$q$  is the vector of generalized coordinates, and  $Q$  is the vector of generalized forces. Since the composite shaft element has two nodes and each node has four degrees of freedom, there are eight generalized co-ordinates. And, the generalized co-ordinates for the shaft element are

$$\{q\} = \{v_1 \quad w_1 \quad \beta_{y1} \quad \beta_{z1} \quad v_2 \quad w_2 \quad \beta_{y2} \quad \beta_{z2}\}^T \quad (3.101)$$

After applying Lagrange's equation, the equations of motion can be written as

$$\begin{aligned} & ([M_{Tc}] + [M_{Rc}])\{\ddot{q}\} + \Omega[G_{shaft\_c}]\{\dot{q}\} + ([K_{Bc}] + [K_{Shc}] + [K_{Fc}] + [K_c])\{q\} \\ & = \{0\} \end{aligned} \quad (3.102)$$

where

$$[M_{Tc}] = \int_0^L m [N_t]^T [N_t] dx \quad (3.103)$$

$$[M_{Rc}] = \int_0^L I_d [N_r]^T [N_r] dx \quad (3.104)$$

$$[G_{Shaft_c}] = \int_0^L I_p [N_r]^T \begin{bmatrix} 0 & 1 \\ -1 & 0 \end{bmatrix} [N_r] dx \quad (3.105)$$

$$[K_{Bc}] = \int_0^L D_{11} [N_r']^T [N_r'] dx \quad (3.106)$$

$$[K_{Shc}] = \int_0^L \frac{L^4}{144} \Gamma_{comp}^2 k_s (A_{55} + A_{66}) [N_t''']^T [N_t'''] dx \quad (3.107)$$

$$[K_c] = \int_0^L \frac{L^2}{24} \Gamma_{comp} k_s B_{16} ([N_t''']^T [N_r'] + [N_r''']^T [N_t']) dx \quad (3.108)$$

$$[K_{Fc}] = \int_0^L P [N_t']^T [N_t'] dx \quad (3.109)$$

$$[N_t] = \begin{bmatrix} N_{t1} & 0 & 0 & N_{t2} & N_{t3} & 0 & 0 & N_{t4} \\ 0 & N_{t1} & -N_{t2} & 0 & 0 & N_{t3} & -N_{t4} & 0 \end{bmatrix} \quad (3.110)$$

$$[N_r] = \begin{bmatrix} 0 & -N_{r1} & N_{r2} & 0 & 0 & -N_{r3} & N_{r4} & 0 \\ N_{r1} & 0 & 0 & N_{r2} & N_{r3} & 0 & 0 & N_{r4} \end{bmatrix} \quad (3.111)$$

More details on how to obtain Equations (3.103)-(3.111) are given in Appendix A.

### 3.4 Numerical examples

To validate the conventional-Hermitian finite element model of the uniform composite shaft, a composite hollow shaft made of boron/epoxy lamina is considered for the vibration analysis. The configuration geometry and the properties of the composite

material are given in Table 3.1 and Table 3.2. A MATLAB<sup>®</sup> program has been written to perform the vibration analysis of the composite shaft. The first critical speed of the boron/epoxy shaft is calculated and compared with those given in the reference papers. The results of the first critical speed are presented in Table 3.3 and from this table a good agreement between the results that are based on the present model and that were predicted using beam theories is observed. In this example, the shaft is modeled by nine elements of equal length using the conventional-Hermitian finite element model while in the model of Ref. [20] the shaft was modeled using Lagrangian finite element model by 20 finite elements of equal length. In addition, in Ref. [22] the composite shaft was modeled using a hierarchical composite finite element and one element with ten hierarchical terms was enough for convergence.

Moreover, in this example the wall thickness of the composite shaft is relatively small, so the composite shaft can be considered as a shell structure which is advanced than a beam structure. Therefore, it can be observed from Table 3.3 that the first critical speed obtained using Sander's shell theory [16] is near to the first critical speed obtained experimentally [12] than those first critical speeds that were calculated using models based on beam theories. The first five critical speeds of the composite shaft are given in Table 3.4. The Campbell diagram of the boron/epoxy shaft is presented in Figure 3.5, and it is clear that the natural frequencies are almost constant for all the rotor spin speeds and the difference between the frequencies of the forward whirl and the backward whirl is very small. Figure 3.6 shows the mode shapes of the composite shaft at 5000 rpm, and

one can see that the first and second modes are similar and the third and fourth are similar modes and the fifth and sixth modes also are similar; this indicates that the gyroscopic effect in this example is not effective even for high frequencies.

Table 3.1 The dimensions of the composite shaft and the properties of the bearing [20].

Composite Shaft				
Length, L= 2.47 m	Mean Diameter, D = 12.69 cm	Wall thickness, t = 1.321 mm	Lay-up from inside [90/45/-45/0 <sub>6</sub> /90]	Shear correction factor, $k_s = 0.503$
Bearing				
$K_{yy} = 1740 \text{ GN/m}$			$K_{zz} = 1740 \text{ GN/m}$	

Table 3.2 Properties of the composite materials [20]

Properties	Boron-epoxy	Graphite-epoxy
$E_{11}$ (GPa)	211	139
$E_{22}$ (GPa)	24	11
$G_{12}=G_{13}$ (GPa)	6.9	6.05
$G_{23}$ (GPa)	6.9	3.78
$\nu_{12}$	0.36	0.313
Density ( $\text{Kg/m}^3$ )	1967	1578

Table 3.3 The first critical speed of the boron-epoxy composite shaft.

	Theory or Method	First critical speed (rpm)
Zinberg and Symonds [12]	Measured experimentally	6000
	Equivalent Modulus Beam Theory	5780
Dos Reis et al.[29]	Bernoulli-Euler beam theory with stiffness determined by shell finite elements	4942
Kim and Bert [16]	Sander's shell theory	5872
	Donnell's shallow shell theory	6399
Bert and Kim [28]	Bresse-Timoshenko beam theory	5788
Gupta and Singh [14]	Equivalent Modulus Beam Theory	5747
	Layerwise beam theory (LBT)	5620
Chang et al. [20]	Continuum-based Timoshenko beam theory	5762
Boukhalifa et al. [22,23]	Timoshenko beam theory with the p and hp versions of the finite element method	5760
The present model	Timoshenko beam theory with conventional finite element method	5747

Table 3.4 The first five critical speeds of the boron-epoxy composite shaft.

Critical speed (rpm)	5747	5773	20679	20930	40944
----------------------	------	------	-------	-------	-------

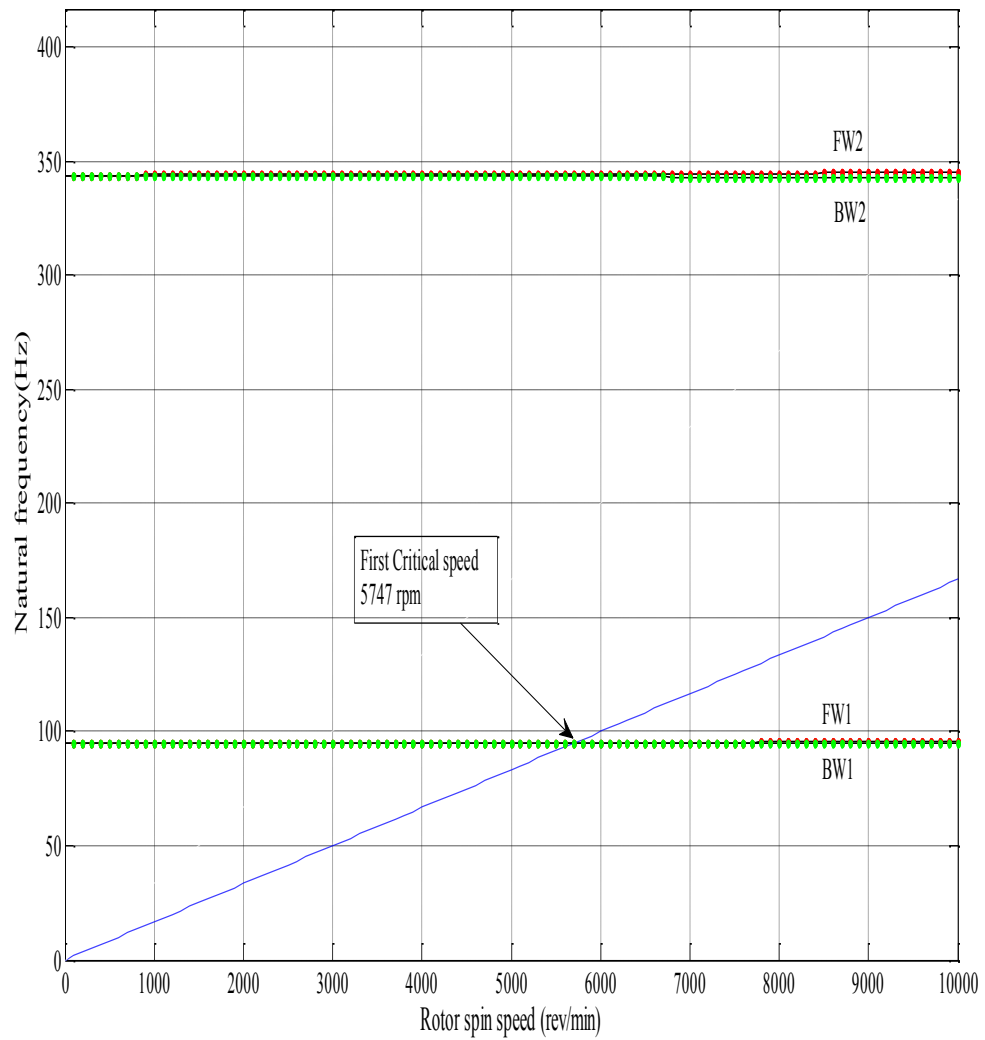


Figure 3.5 Campbell diagram of boron/epoxy composite shaft.

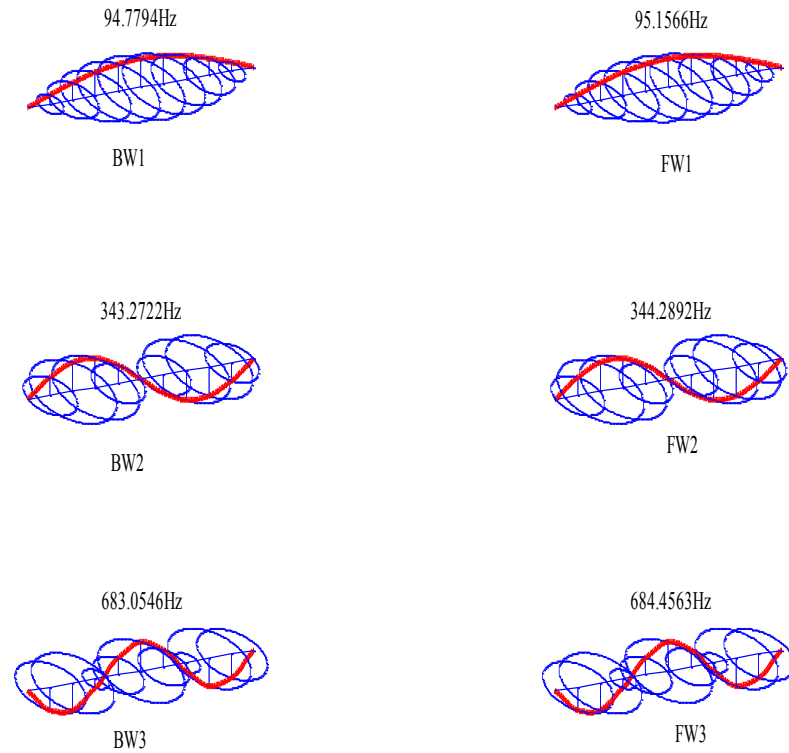


Figure 3.6 Mode shapes of the boron/epoxy composite shaft at 5000 rpm.

In the following example, the frequencies, mode shapes, Campbell diagram and critical speeds of a graphite/epoxy shaft-disk system are determined. The laminate lay-up of the shaft is  $[90/45/-45/0_6/90]$  starting from inside; the composite shaft is attached at its center to a uniform-thickness rigid disk and it is supported at the ends by two identical bearings. The geometric properties of the composite shaft and the disk are in Table 3.5 as well as bearing properties. This example is given in References [20,22], and it is given here for further validation of the conventional-Hermitian finite element model.

Table 3.5 The dimensions and properties of the composite shaft-disk system [20]

Composite Shaft				
Length, $L = 0.72$ m	Inner diameter $ID = 0.028$ m	Outer diameter $OD = 0.048$ m	Lay-up from inside [90/45/-45/0 <sub>6</sub> /90]	Shear correction factor, $k_s =$ 0.503
Disk				
Mass, $m = 2.4364$ Kg	Diametral mass moment of inertia, $I_d = 0.1901$ Kg.m <sup>2</sup>		Polar mass moment of inertia, $I_p = 0.3778$ Kg.m <sup>2</sup>	
Bearing				
$K_{yy} = 17.5$ MN/m		$K_{zz} = 17.5$ MN/m		
$C_{yy} = 500$ N.s/m		$C_{zz} = 500$ N.s/m		
The mass eccentricity of the disk, $e = 5 \times 10^{-5}$ m.				

Figure 3.7 shows the Campbell diagram containing the frequencies of the first two pairs of bending whirling modes. The intersection points of the line  $R = 1$  ( $R$  is a ratio between the whirling bending frequency and the rotation speed) with the whirling frequency curves represent the critical speeds of the composite shaft-disk system. In this example, the shaft is modeled by ten elements of equal length using the conventional-Hermitian finite element model, but in Ref. [22] the composite shaft was modeled by two elements and ten hierarchical terms for each element. Unfortunately, no results on this example are

given in Ref. [22] except the Campbell diagram. Since the critical speeds can be obtained from the Campbell diagram, the author of this thesis used the Campbell diagram in Ref. [22] to obtain the first critical speed which is 7400 rpm. The first five critical speeds of the composite shaft-disk system determined using the conventional-Hermitian finite element model are illustrated in Table 3.6.

Table 3.6 The first five critical speeds of the graphite/epoxy composite shaft-disk system.

Critical speed (rpm)	7294	8685	8700	73033	73702
----------------------	------	------	------	-------	-------

Moreover, the eigenvalues of the composite shaft running at 6000 rpm and 0 rpm are listed in Table 3.7, and the agreement in the results can be observed between the conventional-Hermitian finite element model and Lagrangian finite element model [20]. There is no information given about the meshing in Ref. [20]. The mode shapes of the composite shaft running at 6000 rpm are illustrated in Figure 3.8. The unbalance response and phase angle of the shaft at the disk location which is the center of the composite shaft are shown in Figure 3.9, and it is shown that the response is at its peak at the third critical speed and this means that the unbalance force excites the forward frequencies. Also, since the properties of the bearings are identical in  $z$  and  $y$  directions, the orbits in the mode shapes at any point along the rotor take circular form and the response in  $z$ - $x$  and  $y$ - $x$  planes are same.

Table 3.7 The lowest five eigenvalues in rad/s of the graphite/epoxy composite shaft-disk system running at 6000 rpm and 0 rpm.

Modes	The Present Modal		Chang et al. [20] Lagrangian finit element
	0 rpm	6000 rpm	6000 rpm
1BW	909	909	902.9
1FW	909	910	903.6
2BW	1311	835	826.7
2FW	1311	2057	2048.1
3BW	7779	7767	7841.5
3FW	7779	7794	7868.1
4BW	8149	8148	8215.4
4FW	8149	8151	8218.7
5BW	16205	16192	16305.4
5FW	16205	16217	16332.1

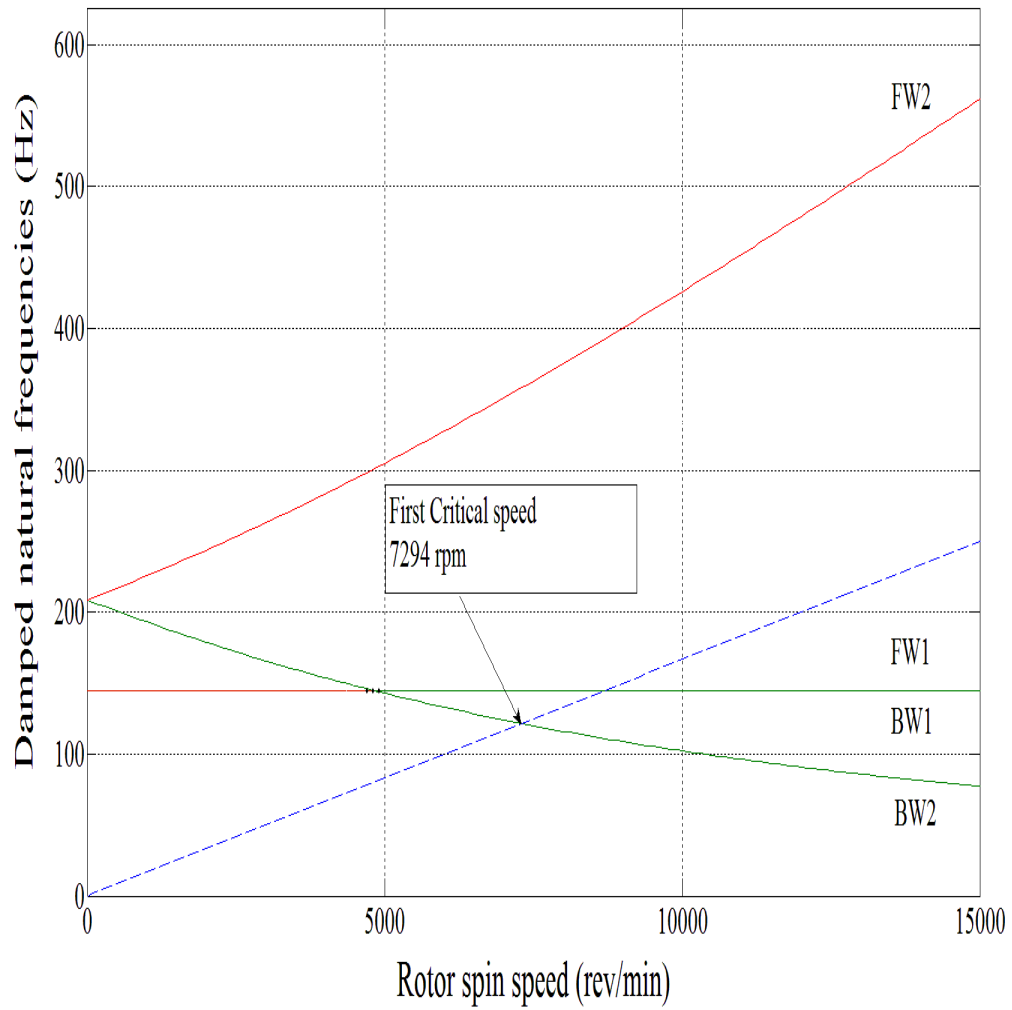


Figure 3.7 The Campbell diagram of the graphite/epoxy composite shaft-disk system.

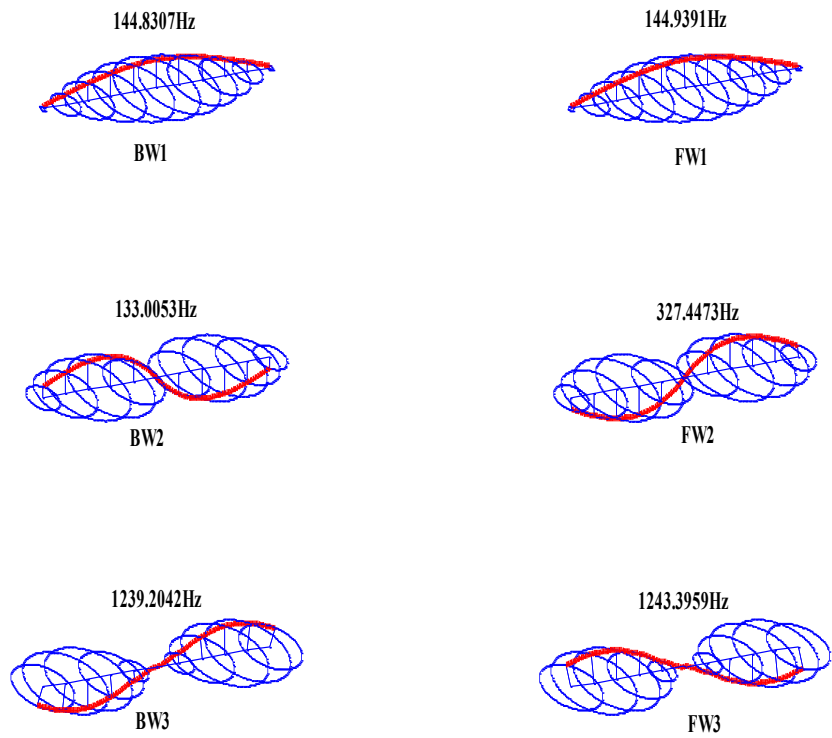


Figure 3.8 The mode shapes of the graphite/epoxy composite shaft-disk system at 6000 rpm.

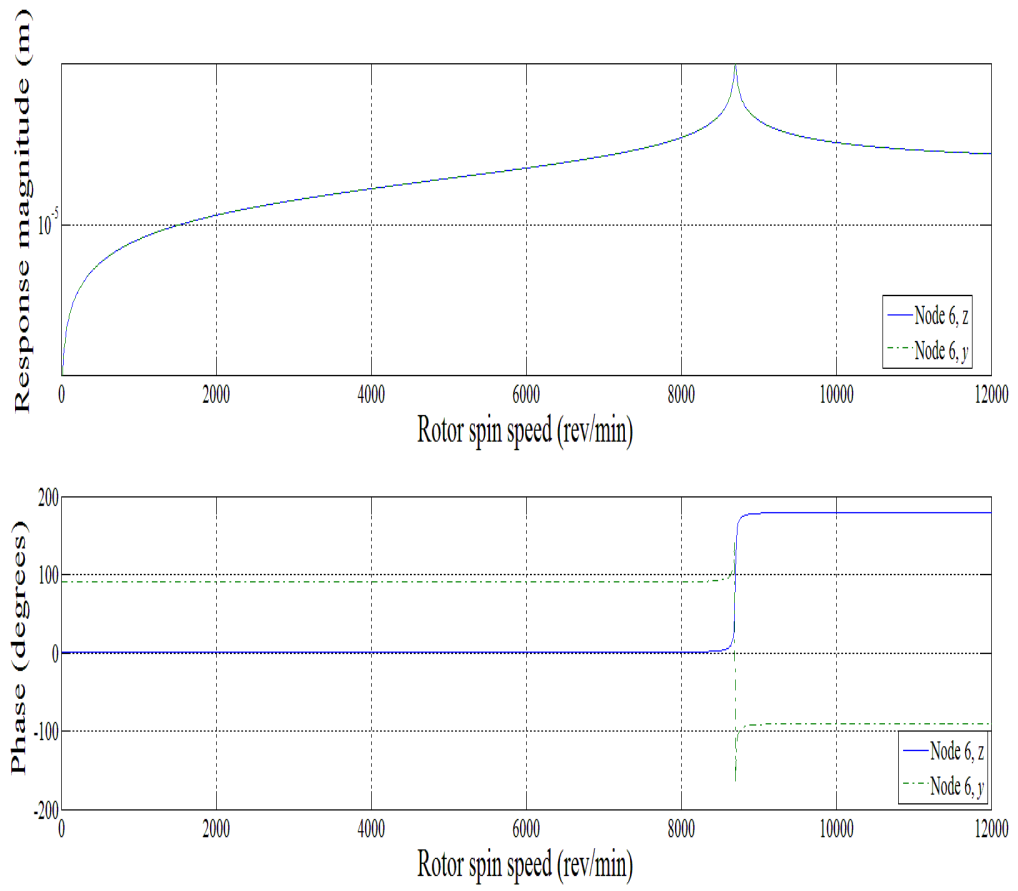


Figure 3.9 Unbalance response and phase angle of the graphite/epoxy composite shaft at the disk position in y and z directions

In the next example, a stepped composite shaft-disk system is studied. The effects of the fiber orientation angle and the shaft's length on the natural frequencies are studied. The stepped composite shaft-disk system consists of two segments with different diameters, a disk of steel at the right end and a bearing at the left end; Figure 3.10 illustrates the stepped composite shaft-disk system. The shaft is made of boron/epoxy material, and the geometric properties of the stepped shaft are listed in Table 3.8. The thickness of each layer is 0.5 mm and length of the first segment  $L_1$  is 0.05 m. The properties of the composite material were already given in Table 3.2.

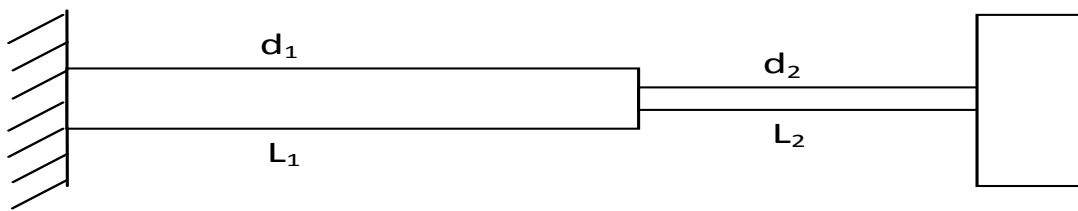


Figure 3.10 The stepped composite shaft-disk system.

Table 3.9 shows the natural frequencies of the stepped composite shaft with different lengths at different rotational speeds. The length of the segment 1 is fixed while the length of the segment 2 changes by 20 percent every time. The segment 1 and the segment 2 of the stepped composite shaft are divided into five elements for each. The elements of the segment 1 have equal length and the same thing can be said about the elements of the segment 2. The length of the elements in the segment 2 changes with changing the length of the segment 2 while the length of the elements of the segment 1 is always fixed. From Table 3.9, one can see that the natural frequency increases when the length decreases.

Table 3.8 The geometric dimensions and properties of the composite shaft-disk system

The Stepped Composite Shaft Properties			
Segment	Outer Diameter	Inner Diameter	Lay-up
1	0.015 m	0.005 m	[0/90/0/90/0/90/0/90/0/90]
2	0.011 m	0.005 m	[0/90/0/90/0/90]
Steel Disk			
Density	Outer Diameter	Inner Diameter	Thickness
7810 Kg/m <sup>3</sup>	0.035 m	0.011 m	0.005 m
Bearing			
$K_{zz} = 17.5 \text{ MN/m}$		$K_{yy} = 17.5 \text{ MN/m}$	

Furthermore, the natural frequencies of the stepped composite shaft with different fiber orientation angles are presented in Table 3.10. The lengths of the segment 1 and the segment 2 are each 0.05 m, and the number of layers for segment 1 and segment 2 are 10 and 6, respectively. The fiber orientation angle changes from 0° to 90° by increment of 30° for all the layers; the natural frequency is maximum when the fiber angle  $\eta$  is 0° and then it reduces until it reaches the minimum value when the fiber orientation angle  $\eta$  is 90°.

Table 3.9 Natural frequencies in Hz of stepped composite rotor with different lengths

Rotational Speed (rpm)	Mode	$L_2 = L_1$	$L_2 = 0.8 L_1$	$L_2 = 0.6 L_1$	$L_2 = 0.4 L_1$	$L_2 = 0.2 L_1$
0	BW1	3145.2	3694.6	4399.8	5338.4	6680.7
	FW1	3145.2	3694.6	4399.8	5338.4	6680.7
	BW2	6461.2	6862.9	7354.8	8080.6	9487.4
	FW2	6461.2	6862.9	7354.8	8080.6	9487.4
5000	BW1	3122.1	3665.9	4363.7	5292.3	6623.3
	FW1	3168.1	3722.9	4435.4	5384.1	6737.9
	BW2	6409.5	6814.2	7312.1	8047.1	9465.3
	FW2	6514.2	6913	7399.2	8115.5	9510.6

In the following example, three cases are considered to study the natural frequency of the stepped composite shaft-disk system. In the first case, the length of segment 1 is increased and the length of segment 2 is decreased while the total length of the stepped composite shaft remains the same. In the second case, the diameter of segment 2 reduces by 20 percent each time. In the last case, the effect of the mass of the disk on the natural frequencies is determined. The boron/epoxy composite material is used in all the three cases, and the thickness of each layer is 0.5 mm.

Table 3.10 Natural frequencies in Hz of stepped composite rotor with different fiber orientation angles

Rotational Speed (rpm)	Mode	$\eta = 0^\circ$	$\eta = 30^\circ$	$\eta = 60^\circ$	$\eta = 90^\circ$
0	BW1	3978.7	2909.8	2234.3	2132.5
	FW1	3978.7	2911.2	2234.5	2132.5
	BW2	7515	6505.4	5484.5	4947.1
	FW2	7515	6511.3	5485.2	4947.1
5000	BW1	3962.2	2882.2	2203.5	2104
	FW1	3994.8	2938.7	2265.3	2160.8
	BW2	7456.7	6461.3	5441.1	4901.3
	FW2	7574.5	6556.7	5530.1	4994.7

#### Case 1

The dimensions of the composite shaft-disk system were already given in Table 3.8, and the total length  $L$  of the stepped composite shaft is 10 cm. Five elements of equal length are used for the segment 1 and the segment 2, and the length of the element in both the segments changes with changing the segment length. Table 3.11 presents the natural frequencies of the stepped composite shaft; one can see that when  $L_1$  starts to increase and  $L_2$  starts to decrease the natural frequency decreases for all the speeds.

Table 3.11 The natural frequencies of the stepped composite shaft-disk system with different lengths of segment 1 and segment 2

Rotational Speed (rpm)	Mode	$L_1 = 0.5 L$	$L_1 = 0.6 L$	$L_1 = 0.7 L$	$L_1 = 0.8 L$	$L_1 = 0.9 L$
		$L_2 = 0.5 L$	$L_2 = 0.4 L$	$L_2 = 0.3 L$	$L_2 = 0.2 L$	$L_2 = 0.1 L$
0	BW1	3145.2	3267.4	3454.8	3696.5	3944.8
	FW1	3145.2	3267.4	3454.8	3696.5	3944.8
	BW2	6461.2	6520	6667.8	7004.0	7838.2
	FW2	6461.2	6520	6667.8	7004.0	7838.2
5000	BW1	3122.1	3245.6	3434.7	3679.2	3931.1
	FW1	3168.1	3288.9	3474.5	3713.5	3958.2
	BW2	6409.5	6465.9	6610.9	6943.9	7775.4
	FW2	6514.2	6575.6	6725.9	7065.3	7902.1

## Case 2

Here, the effect of the diameter of segment 2 on the natural frequency is studied. Table 3.12 lists the properties of segment 2 of the stepped shaft; the properties of segment 1, the disk and the bearing are same as in case 1. The total length of the stepped shaft is 10 cm and  $L_1$  and  $L_2$  are equal. The stepped composite shaft is divided into ten elements with equal length for all the cases in Table 3.12. The polar mass moment of inertia  $I_p$ , the diametral mass moment of inertia  $I_d$ , and the mass  $m_d$  of the disk are calculated for the first case in Table 3.12 then they are used for the other cases in the table. Table 3.13 shows the natural frequencies of the shaft with different diameters of segment 2 at different rotation speeds. It is clear from Table 3.13 that the natural frequency decreases when the diameter of segment 2 decreases.

Table 3.12 The geometric dimensions of segment 2 of the stepped shaft

Outer Diameter	Inner Diameter	Lay-up from inside
$d_2 = d_1$	0.005 m	[0/90/0/90/0/90/0/90/0/90]
$d_2 = 0.8 d_1$	0.005 m	[0/90/0/90/0/90/0/90]
$d_2 = 0.6 d_1$	0.005 m	[0/90/0/90/0/90]
$d_2 = 0.4 d_1$	0.005 m	[0/90/0/90]
$d_2 = 0.2 d_1$	0.005 m	[0/90]

Table 3.13 The natural frequencies of the stepped composite shaft-disk system with different diameters of the segment 2

Speed (rpm)	Mode	$d_2 = d_1$	$d_2 = 0.8 d_1$	$d_2 = 0.6 d_1$	$d_2 = 0.4 d_1$	$d_2 = 0.2 d_1$
0	BW1	4147.2	3752.2	3145.2	2330.7	1387
	FW1	4147.2	3752.2	3145.2	2330.7	1387
	BW2	9890	8221.8	6461.2	4742.1	2961.6
	FW2	9890	8221.8	6461.2	4742.1	2961.6
5000	BW1	4136.3	3736.8	3122.1	2296.9	1342.9
	FW1	4158.1	3767.4	3168.1	2364.2	1431.3
	BW2	9847.6	8168.6	6409.5	4698.1	2926.8
	FW2	9932.2	8275.5	6514.2	4788.1	2999.5

### Case 3

In this case the effect of the mass of the disk on the natural frequency is studied; the information about the composite shaft system in Table 3.8 is used here. The total length of the stepped shaft is 10 cm; the segment 1 and the segment 2 have the same length. The stepped composite shaft is divided into ten elements of equal length. The results of the natural frequencies of the stepped shaft are given in Table 3.14; increasing the disk mass reduces the natural frequency of the stepped composite shaft for all rotation speeds.

Table 3.14 The natural frequencies of the stepped composite shaft-disk system with different densities of the disk

Speed (rpm)	Mode	Density (Kg / m <sup>3</sup> )				
		1000	4000	7000	10000	13000
0	BW1	4165.8	3456.2	3199.9	3011.7	2850.8
	FW1	4165.8	3456.2	3199.9	3011.7	2850.8
	BW2	10732	80970	6704.2	5964.5	5522.5
	FW2	10732	80970	6704.2	5964.5	5522.5
5000	BW1	4161.0	3443.5	3179	2982.6	2814.2
	FW1	4170.7	3468.7	3220.5	3040.5	2887.1
	BW2	10717	80452	6651.2	5917.1	5481.5
	FW2	10747	81492	6758.3	6013.4	5565.3

In the last example, the effect of the axial load on the natural frequency of a composite shaft is considered. Figure 3.11 shows a stepped composite shaft with two bearings and one disk, and the required information of the composite shaft system is listed in Table 3.15. The axial force (compressive or tensile) starts from 100 N and then increases by 100 N until it reaches 500 N. The segment 1 of the stepped composite shaft is divided into five elements of equal length and the same thing applies for the segment 2.

Figures 3.12 – 3.14 illustrate the natural frequencies at 0 and 5000 rpm, and it can be observed that the increase in the tensile force leads to increase in the natural frequencies for all rotating speeds while increasing the compressive force reduces the natural frequencies. This is so because the axial tensile force makes the shaft more stiffer thereby increasing the natural frequencies while the compressive force reduces the shaft stiffness and results in lower natural frequencies.

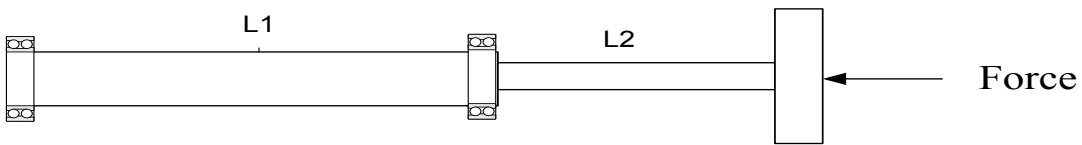


Figure 3.11 The stepped composite shaft under the axial load

Table 3.15 The geometric dimensions of the composite shaft-disk system

The Stepped Composite Shaft Properties				
Segment	Length	Outer Diameter	Inner Diameter	Lay-up
1	$L_1 = 1 \text{ m}$	0.015 m	0.005 m	[0/90/0/90/0/90/0/90/0/90]
2	$L_2 = 0.5 \text{ m}$	0.011 m	0.005 m	[0/90/0/90/0/90]
Disk				
Density	Outer Diameter	Inner Diameter	Thickness	
$7810 \text{ Kg/m}^3$	0.105 m	0.011 m	0.005 m	
Bearing				
$K_{yy} = 30 \text{ MN/m}$			$K_{zz} = 30 \text{ MN/m}$	

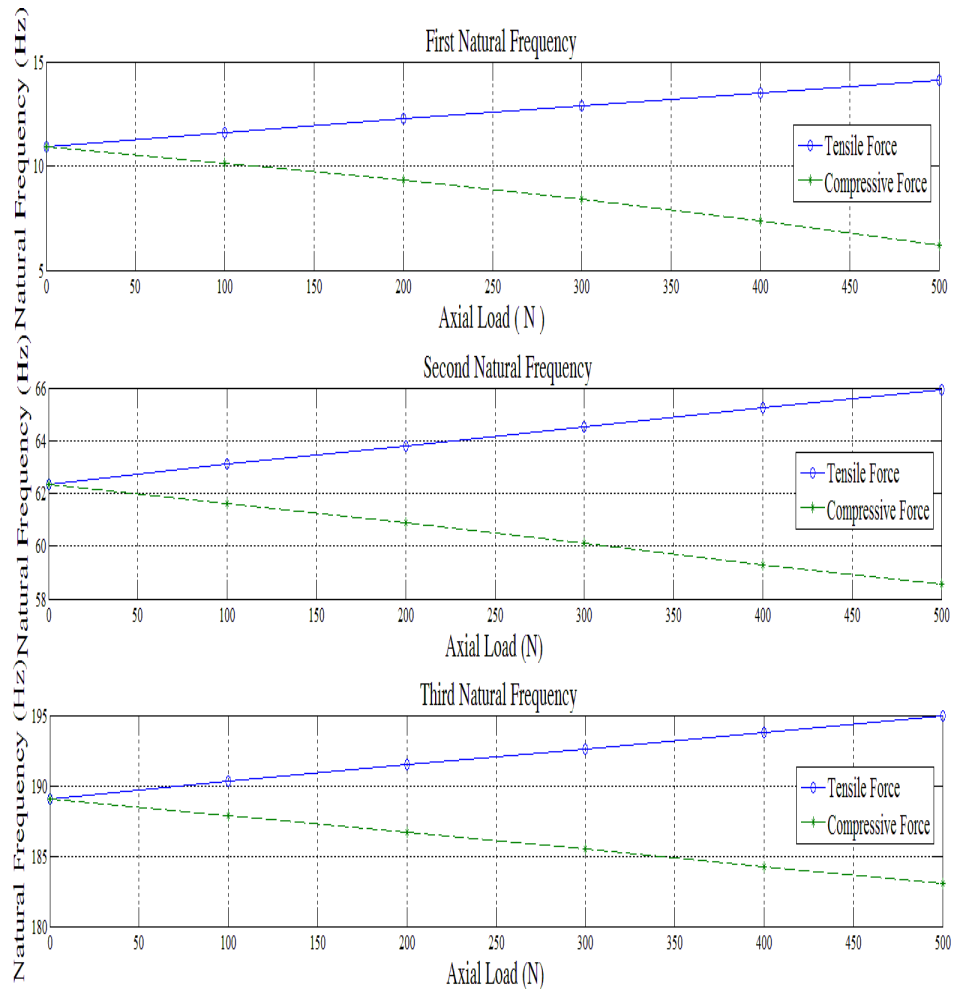


Figure 3.12 The natural frequencies of the stepped composite shaft at 0 rpm under different axial loads

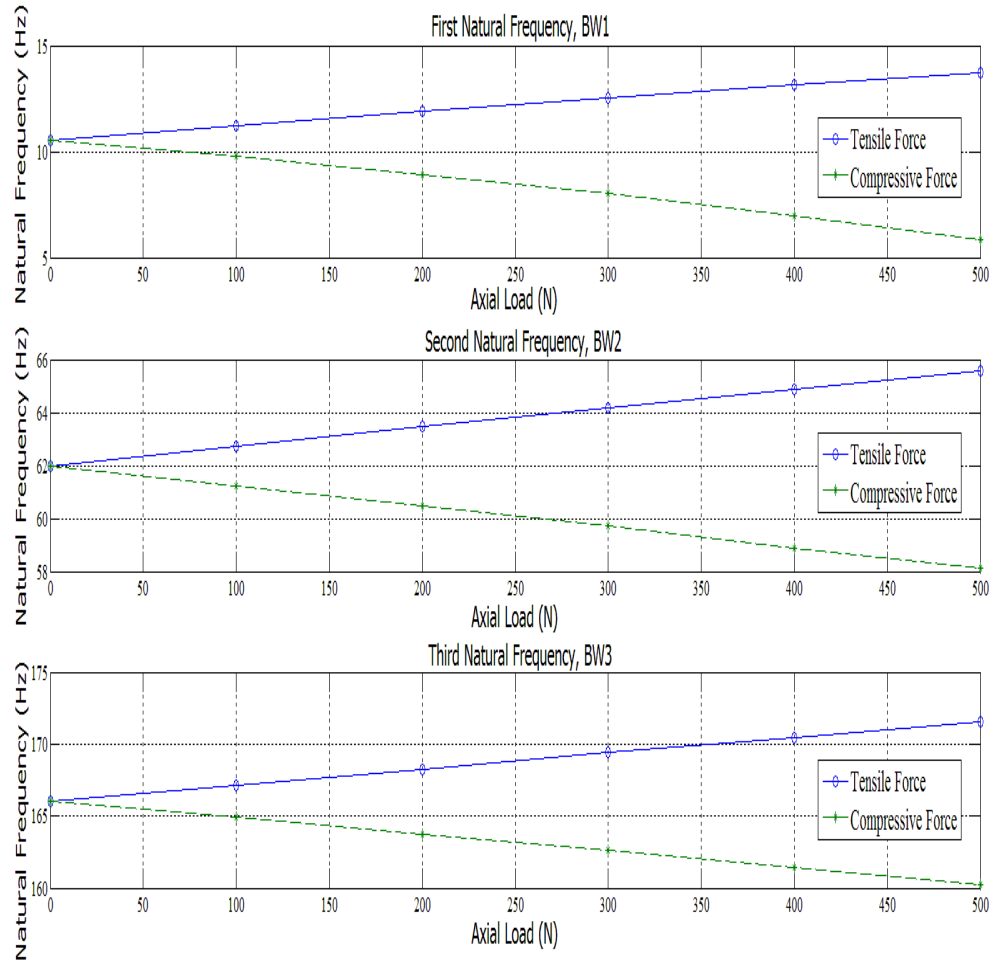


Figure 3.13 The backward natural frequencies of the stepped composite shaft at 5000 rpm under different axial loads

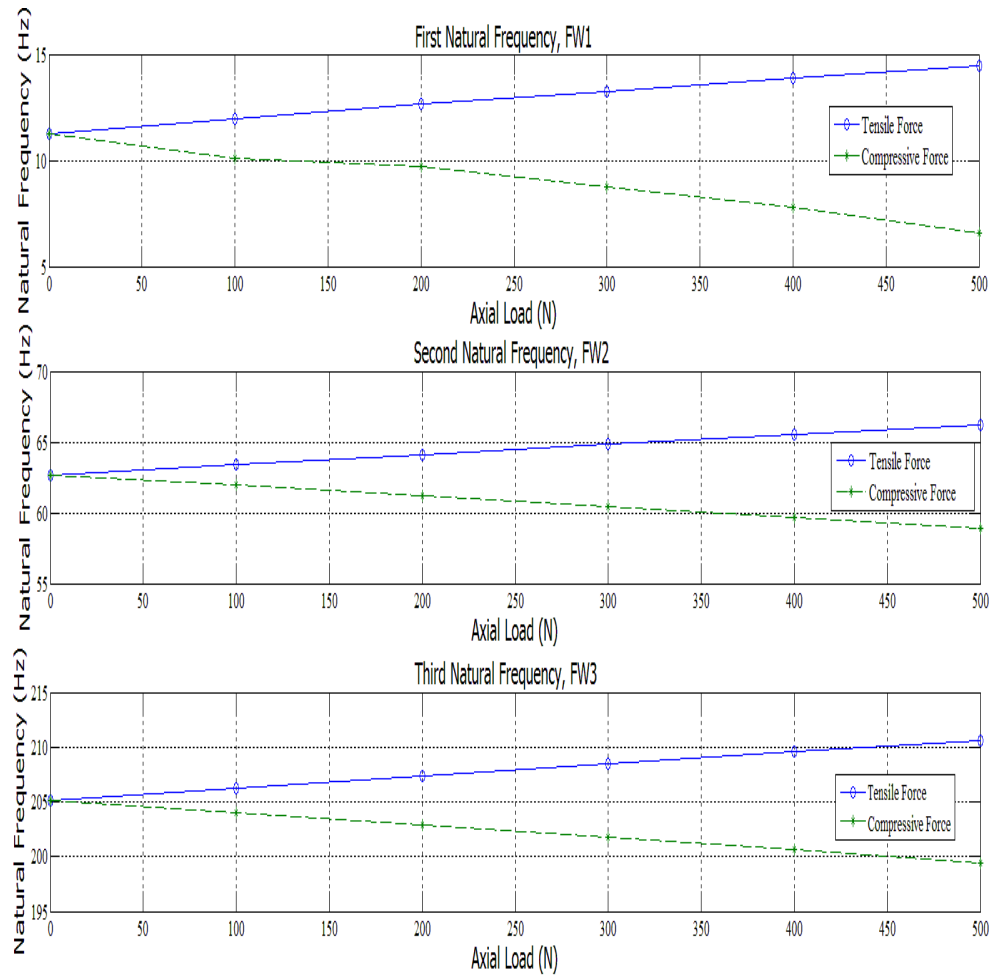


Figure 3.14 The forward natural frequencies at 5000 rpm under different axial loads.

### 3.5 Summary

This chapter presents the vibration analysis of composite shaft using conventional-Hermitian finite element method. Timoshenko beam theory is adopted, and the effects of the rotary inertia, shear deformation, gyroscopic forces, axial load, and the coupling effects due to the lamination of composite layers were considered. The results obtained using the conventional finite element model were validated with the results available in the literature and a good agreement has been observed. In addition, a parametric study on stepped composite shaft with a disk at the end has been carried out. The main conclusions of this chapter are listed in the following:

- 1) The natural frequency of the composite shaft is affected significantly by changing fiber orientation, the rotor's length, the rotating speed and the axial load.
- 2) Element with four degrees of freedom per node is good enough to obtain results that match those given in References [20, 22, 23] which used six degrees of freedom per node.
- 3) In stepped composite shaft, when the length of the segment 1 that is thicker and closer to the bearing is fixed, the natural frequencies of the stepped composite shaft increase with decreasing the length and increasing the diameter of the segment 2 that is thinner and connected to the disk.

## Chapter 4

# Rotordynamic Analysis of Tapered Composite Shaft Using Finite Element Method

### 4.1 Introduction

One method to improve the dynamic characteristics of a structure is tapering the structure. For example, tapered beam and tapered plate have better dynamic characteristics than those of non-tapered beam and plate [24]. Same thing can be said about the rotating shaft, tapering the shaft can increase the bending stiffness, and this can lead to an improvement of the dynamic characteristics of the shaft and reduction in vibration. This chapter provides four computational models for free vibration analysis of tapered shaft using finite element method and Rayleigh – Ritz method.

In this chapter, a hierarchical composite finite element, a conventional-Lagrangian composite finite element, a conventional-Hermitian composite finite element, and Rayleigh-Ritz method are used to model tapered Timoshenko rotating driveshaft; the effects of taper angle, rotary inertia, gyroscopic forces, axial load, and coupling effect due to the lamination of composite layers are taken into account.

### 4.2 Stress-strain relations for tapered cylinder layer

Figure 4.1 shows a single lamina deformed into a conical tube with taper angle  $\alpha$  that can change functionally in  $x$  direction. The principal material directions are denoted by 1, 2, and 3. The axis 1' extends along the tapered tube surface while 3'-axis is perpendicular to

the same surface. The fiber angle  $\eta$  is the angle between 1-axis and 1'-axis and the angle between 2-axis and 2'-axis.

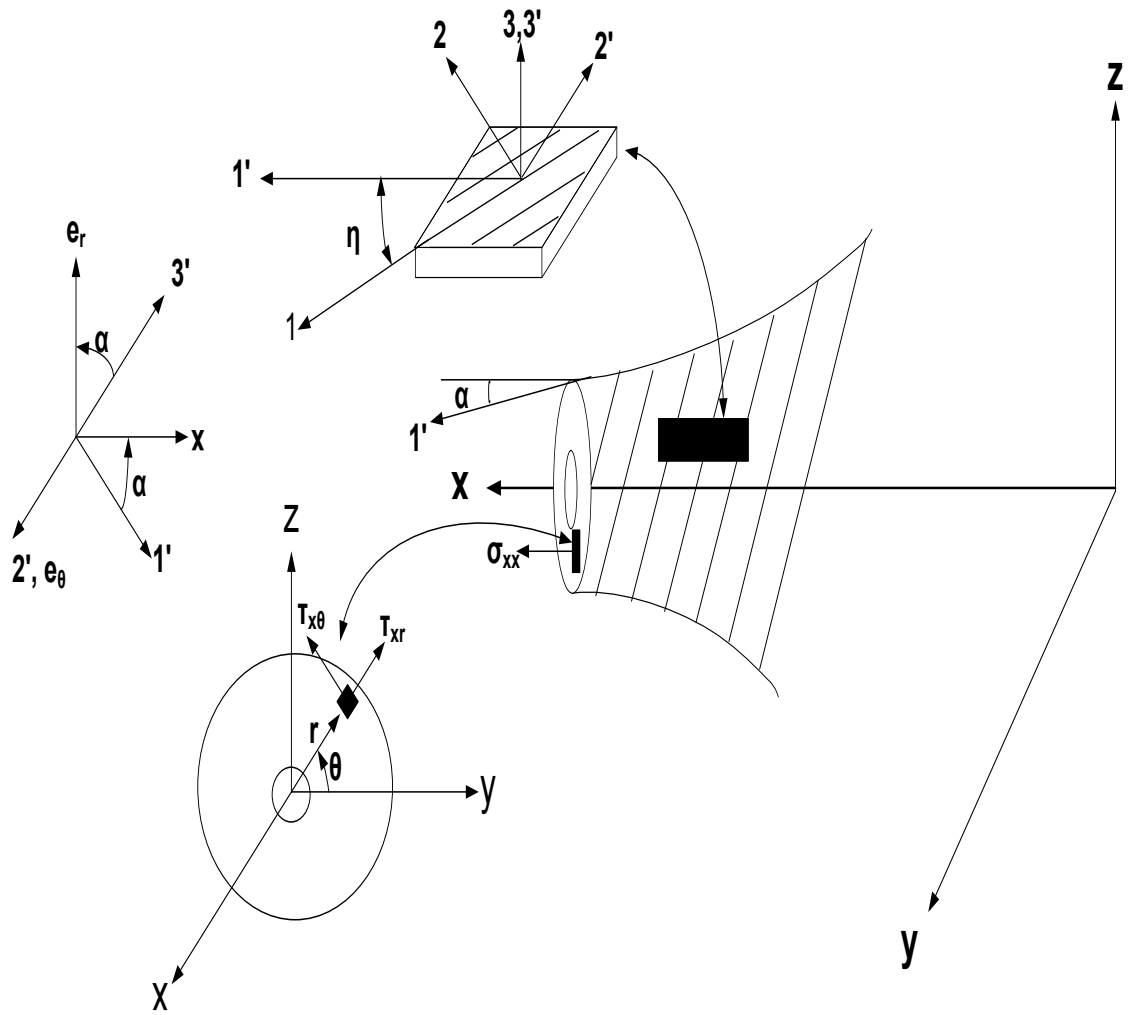


Figure 4.1 Single composite lamina deformed into tapered cylinder

To determine the stress-strain relations of tapered tube lamina in cylindrical coordinate system, transformation from the principal material coordinate system (1, 2, 3) to cylindrical coordinate system (x,  $\theta$ , r) must be done. To do this, it is necessary to apply sequence of transformations as following:

- 1)  $\eta$  about 3-axis in principal material coordinate system (1, 2, 3).
- 2)  $\alpha$  about 2'-axis in primed coordinate system (1', 2', 3').

The stress – strain relations for lamina with respect to the principal material coordinate system were shown in Chapter 3 and they are repeated here again. So, the stress-strain relations for a lamina in the principal material directions are

$$\begin{bmatrix} \sigma_{11} \\ \sigma_{22} \\ \sigma_{33} \\ \tau_{23} \\ \tau_{13} \\ \tau_{12} \end{bmatrix} = \begin{bmatrix} Q_{11} & Q_{12} & Q_{13} & 0 & 0 & 0 \\ Q_{12} & Q_{22} & Q_{23} & 0 & 0 & 0 \\ Q_{13} & Q_{23} & Q_{33} & 0 & 0 & 0 \\ 0 & 0 & 0 & Q_{44} & 0 & 0 \\ 0 & 0 & 0 & 0 & Q_{55} & 0 \\ 0 & 0 & 0 & 0 & 0 & Q_{66} \end{bmatrix} \begin{bmatrix} \epsilon_{11} \\ \epsilon_{22} \\ \epsilon_{33} \\ \gamma_{23} \\ \gamma_{13} \\ \gamma_{12} \end{bmatrix} \quad (4.1)$$

That is

$$[\sigma_{123}] = [Q][\epsilon_{123}] \quad (4.2)$$

where [Q] is the stiffness matrix of a single lamina, and it is a function of elastic moduli, shear moduli and the Poisson's ratio of the lamina. The stresses in primed coordinate system (1', 2', 3') are related to the stresses in principal material coordinate system (1, 2, 3) as [24]

$$\begin{bmatrix} \sigma_{1'1'} \\ \sigma_{2'2'} \\ \sigma_{3'3'} \\ \tau_{2'3'} \\ \tau_{1'3'} \\ \tau_{1'2'} \end{bmatrix} = \begin{bmatrix} m^2 & n^2 & 0 & 0 & 0 & 2mn \\ n^2 & m^2 & 0 & 0 & 0 & -2mn \\ 0 & 0 & 1 & 0 & 0 & 0 \\ 0 & 0 & 0 & m & -n & 0 \\ 0 & 0 & 0 & n & m & 0 \\ -mn & mn & 0 & 0 & 0 & m^2 - n^2 \end{bmatrix} \begin{bmatrix} \sigma_{11} \\ \sigma_{22} \\ \sigma_{33} \\ \tau_{23} \\ \tau_{13} \\ \tau_{12} \end{bmatrix} \quad (4.3)$$

where  $m = \cos \eta$  and  $n = \sin \eta$ . Equation (4.3) can be abbreviated as

$$[\sigma_{1'2'3'}] = [T_1][\sigma_{123}] \quad (4.4)$$

Similarly, one can get the relation between the strains in both coordinate systems as:

$$\begin{bmatrix} \varepsilon_{1'1'} \\ \varepsilon_{2'2'} \\ \varepsilon_{3'3'} \\ \gamma_{2'3'} \\ \gamma_{1'3'} \\ \gamma_{1'2'} \end{bmatrix} = \begin{bmatrix} m^2 & n^2 & 0 & 0 & 0 & mn \\ n^2 & m^2 & 0 & 0 & 0 & -mn \\ 0 & 0 & 1 & 0 & 0 & 0 \\ 0 & 0 & 0 & m & -n & 0 \\ 0 & 0 & 0 & n & m & 0 \\ -2mn & 2mn & 0 & 0 & 0 & m^2 - n^2 \end{bmatrix} \begin{bmatrix} \varepsilon_{11} \\ \varepsilon_{22} \\ \varepsilon_{33} \\ \gamma_{23} \\ \gamma_{13} \\ \gamma_{12} \end{bmatrix} \quad (4.5)$$

Equation (4.5) can be abbreviated as

$$[\varepsilon_{1'2'3'}] = [T_2][\varepsilon_{123}] \quad (4.6)$$

Using Equations (4.4) and (4.6) into Equation (4.2), one can get the relation between stresses and strains in primed coordinate system ( $1', 2', 3'$ ) as [24]:

$$\begin{bmatrix} \sigma_{1'1'} \\ \sigma_{2'2'} \\ \sigma_{3'3'} \\ \tau_{2'3'} \\ \tau_{1'3'} \\ \tau_{1'2'} \end{bmatrix} = \begin{bmatrix} \bar{Q}_{11} & \bar{Q}_{12} & \bar{Q}_{13} & 0 & 0 & \bar{Q}_{16} \\ \bar{Q}_{12} & \bar{Q}_{22} & \bar{Q}_{23} & 0 & 0 & \bar{Q}_{26} \\ \bar{Q}_{13} & \bar{Q}_{23} & \bar{Q}_{33} & 0 & 0 & \bar{Q}_{36} \\ 0 & 0 & 0 & \bar{Q}_{44} & \bar{Q}_{45} & 0 \\ 0 & 0 & 0 & \bar{Q}_{45} & \bar{Q}_{55} & 0 \\ \bar{Q}_{16} & \bar{Q}_{26} & \bar{Q}_{36} & 0 & 0 & \bar{Q}_{66} \end{bmatrix} \begin{bmatrix} \varepsilon_{1'1'} \\ \varepsilon_{2'2'} \\ \varepsilon_{3'3'} \\ \gamma_{2'3'} \\ \gamma_{1'3'} \\ \gamma_{1'2'} \end{bmatrix} \quad (4.7)$$

The above equation can be written in the following form

$$[\sigma_{1'2'3'}] = [\bar{Q}][\varepsilon_{1'2'3'}] \quad (4.8)$$

where  $[\bar{Q}]$  is the transformed stiffness of the layer and can be calculated by the following equation

$$[\bar{Q}] = [T_1][Q][T_2]^{-1} \quad (4.9)$$

Now, the stresses in primed coordinate system (1', 2', 3') are related to the stresses in cylindrical coordinate system (x,  $\theta$ , r) as in the following [24]:

$$\begin{bmatrix} \sigma_{xx} \\ \sigma_{\theta\theta} \\ \sigma_{rr} \\ \tau_{\theta r} \\ \tau_{xr} \\ \tau_{x\theta} \end{bmatrix} = \begin{bmatrix} c^2 & 0 & s^2 & 0 & 2sc & 0 \\ 0 & 1 & 0 & 0 & 0 & 0 \\ s^2 & 0 & c^2 & 0 & -2sc & 0 \\ 0 & 0 & 0 & c & 0 & -s \\ -sc & 0 & sc & 0 & c^2 - s^2 & 0 \\ 0 & 0 & 0 & s & 0 & c \end{bmatrix} \begin{bmatrix} \sigma_{1'1'} \\ \sigma_{2'2'} \\ \sigma_{3'3'} \\ \tau_{2'3'} \\ \tau_{1'3'} \\ \tau_{1'2'} \end{bmatrix} \quad (4.10)$$

where  $c = \cos \alpha$  and  $s = \sin \alpha$ . Equation (4.10) can be abbreviated as

$$[\sigma_{x\theta r}] = [T_3][\sigma_{1'2'3'}] \quad (4.11)$$

Similarly, one can get the relation between the strains in primed coordinate system (1', 2', 3') and cylindrical coordinate system (x,  $\theta$ , r) as:

$$\begin{bmatrix} \varepsilon_{xx} \\ \varepsilon_{\theta\theta} \\ \varepsilon_{rr} \\ \gamma_{\theta r} \\ \gamma_{xr} \\ \gamma_{x\theta} \end{bmatrix} = \begin{bmatrix} c^2 & 0 & s^2 & 0 & sc & 0 \\ 0 & 1 & 0 & 0 & 0 & 0 \\ s^2 & 0 & c^2 & 0 & -sc & 0 \\ 0 & 0 & 0 & c & 0 & -s \\ -2sc & 0 & 2sc & 0 & c^2 - s^2 & 0 \\ 0 & 0 & 0 & s & 0 & c \end{bmatrix} \begin{bmatrix} \varepsilon_{1'1'} \\ \varepsilon_{2'2'} \\ \varepsilon_{3'3'} \\ \gamma_{2'3'} \\ \gamma_{1'3'} \\ \gamma_{1'2'} \end{bmatrix} \quad (4.12)$$

Equation (4.12) can be abbreviated as

$$[\varepsilon_{x\theta r}] = [T_4][\varepsilon_{1'2'3'}] \quad (4.13)$$

Using Equations (4.11) and (4.13) into Equation (4.8), one can write the stress-strain relation in cylindrical coordinate system  $(x, \theta, r)$  as in the following [24]:

$$\begin{bmatrix} \sigma_{xx} \\ \sigma_{\theta\theta} \\ \sigma_{rr} \\ \tau_{\theta r} \\ \tau_{xr} \\ \tau_{x\theta} \end{bmatrix} = \begin{bmatrix} \bar{Q}_{11} & \bar{Q}_{12} & \bar{Q}_{13} & \bar{Q}_{14} & \bar{Q}_{15} & \bar{Q}_{16} \\ \bar{Q}_{21} & \bar{Q}_{22} & \bar{Q}_{23} & \bar{Q}_{24} & \bar{Q}_{25} & \bar{Q}_{26} \\ \bar{Q}_{31} & \bar{Q}_{32} & \bar{Q}_{33} & \bar{Q}_{34} & \bar{Q}_{35} & \bar{Q}_{36} \\ \bar{Q}_{41} & \bar{Q}_{42} & \bar{Q}_{43} & \bar{Q}_{44} & \bar{Q}_{45} & \bar{Q}_{46} \\ \bar{Q}_{51} & \bar{Q}_{52} & \bar{Q}_{53} & \bar{Q}_{54} & \bar{Q}_{55} & \bar{Q}_{56} \\ \bar{Q}_{61} & \bar{Q}_{62} & \bar{Q}_{63} & \bar{Q}_{64} & \bar{Q}_{65} & \bar{Q}_{66} \end{bmatrix} \begin{bmatrix} \varepsilon_{xx} \\ \varepsilon_{\theta\theta} \\ \varepsilon_{rr} \\ \gamma_{\theta r} \\ \gamma_{xr} \\ \gamma_{x\theta} \end{bmatrix} \quad (4.14)$$

The above equation can be written as

$$[\sigma_{x\theta r}] = [\bar{Q}][\varepsilon_{x\theta r}] \quad (4.15)$$

where  $[\bar{Q}]$  is the transformed stiffness of the layer and can be calculated by the following equation :

$$[\bar{Q}] = [T_3][\bar{Q}][T_4]^{-1} = [T_3][T_1][Q][T_2]^{-1}[T_4]^{-1} \quad (4.16)$$

Considering Equations (3.21)-(3.23) and introducing the shear correction factor  $k_s$  in the same way as in Equation (3.27), one can write Equation (4.14) as

$$\begin{bmatrix} \sigma_{xx} \\ \sigma_{\theta\theta} \\ \sigma_{rr} \\ \tau_{\theta r} \\ \tau_{xr} \\ \tau_{x\theta} \end{bmatrix} = \begin{bmatrix} \bar{Q}_{11} & k_s \bar{Q}_{15} & k_s \bar{Q}_{16} \\ \bar{Q}_{21} & k_s \bar{Q}_{25} & k_s \bar{Q}_{26} \\ \bar{Q}_{31} & k_s \bar{Q}_{35} & k_s \bar{Q}_{36} \\ k_s \bar{Q}_{41} & k_s \bar{Q}_{45} & k_s \bar{Q}_{46} \\ k_s \bar{Q}_{51} & k_s \bar{Q}_{55} & k_s \bar{Q}_{56} \\ k_s \bar{Q}_{61} & k_s \bar{Q}_{65} & k_s \bar{Q}_{66} \end{bmatrix} \begin{bmatrix} \varepsilon_{xx} \\ \gamma_{xr} \\ \gamma_{x\theta} \end{bmatrix} \quad (4.17)$$

### 4.3 Kinetic and potential energy expressions

Since the mass, the diametral mass moment of inertia and the polar mass moment of inertia of a tapered composite shaft change with respect to the axial coordinate of the shaft, the kinetic energy for tapered composite shaft is

$$T_{comp} = \frac{1}{2} \int_0^L m_c(x) (\dot{v}^2 + \dot{w}^2) dx + \frac{1}{2} \int_0^L I_{dc}(x) (\dot{\beta}_y^2 + \dot{\beta}_z^2) dx - \int_0^L I_{pc}(x) \Omega \dot{\beta}_z \beta_y dx \quad (4.18)$$

where  $m_c$ ,  $I_{dc}$ ,  $I_{pc}$  are the mass per unit length, diametral mass moment of inertia, and polar mass moment of inertia.

$$m_c(x) = \pi \sum_{s=1}^n \rho_s (r_{os}^2(x) - r_{is}^2(x)) \quad (4.19)$$

$$I_{dc}(x) = \frac{\pi}{4} \sum_{s=1}^n \rho_s (r_{os}^4(x) - r_{is}^4(x)) \quad (4.20)$$

$$I_{pc}(x) = \frac{\pi}{2} \sum_{s=1}^n \rho_s (r_{os}^4(x) - r_{is}^4(x)) \quad (4.21)$$

where  $n$  is the number of the layers in the laminate, and  $\rho_s$  is the density of the layer.  $r_{os}$  and  $r_{is}$  are the outer radius and inner radius of the  $s$ -th layer. For conical shape, the inner radius and outer radius are

$$r_{os}(x) = \left(1 - \frac{x}{L}\right) r_{o1} + \frac{x}{L} r_{o2} \quad (4.22)$$

$$r_{is}(x) = \left(1 - \frac{x}{L}\right) r_{i1} + \frac{x}{L} r_{i2} \quad (4.23)$$

where  $r_{i1}$ ,  $r_{i2}$ ,  $r_{o1}$ , and  $r_{o2}$  are defined in Figure 4.2.

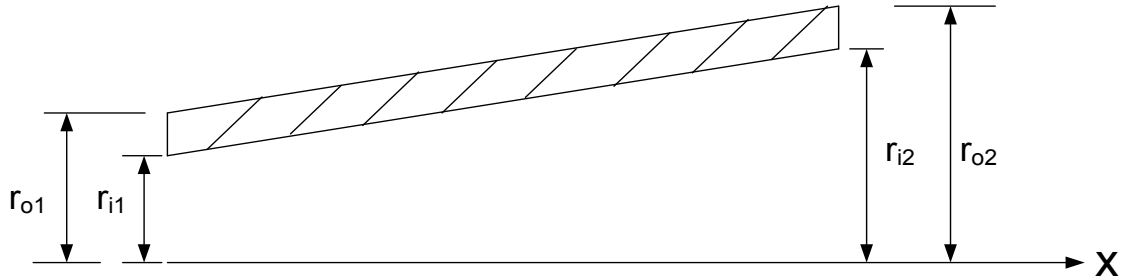


Figure 4.2 Typical tapered shaft element

From Equation (3.41), the strain energy of tapered composite shaft can be written as

$$U_{BS} = \frac{1}{2} \int_0^L \left[ M_y \frac{\partial \beta_y}{\partial x} + M_z \frac{\partial \beta_z}{\partial x} + Q_y \left( \frac{\partial v}{\partial x} - \beta_z \right) + Q_z \left( \beta_y + \frac{\partial w}{\partial x} \right) \right] dx \quad (4.24)$$

In chapter 3, the stress couples and the stress resultants were defined as

$$M_y = \int_A \sigma_{xx} r \sin \theta dA \quad (4.25)$$

$$M_z = - \int_A \sigma_{xx} r \cos \theta dA \quad (4.26)$$

$$Q_{xr}^{(1)} = \int_A \tau_{xr} \sin \theta dA \quad (4.27)$$

$$Q_{xr}^{(2)} = \int_A \tau_{xr} \cos \theta \, dA \quad (4.28)$$

$$Q_{x\theta}^{(1)} = \int_A \tau_{x\theta} \sin \theta \, dA \quad (4.29)$$

$$Q_{x\theta}^{(2)} = \int_A \tau_{x\theta} \cos \theta \, dA \quad (4.30)$$

Substituting Equation (3.20), Equation (3.24), and Equation (3.25) into Equation (4.17), and then considering Equation (4.17) for Equations (4.25) - (4.30), one can write the stress couples and the stress resultants of the tapered composite shaft as

$$\begin{aligned} M_y = \int_0^{2\pi} \int_{r_i}^{r_o} r^2 \sin \theta \left[ \bar{Q}_{11} \left( \frac{\partial \beta_y}{\partial x} r \sin \theta - \frac{\partial \beta_z}{\partial x} r \cos \theta \right) \right. \\ \left. + k_s \bar{Q}_{15} \left( \left( \frac{\partial w}{\partial x} + \beta_y \right) \sin \theta + \left( \frac{\partial v}{\partial x} - \beta_z \right) \cos \theta \right) \right. \\ \left. + k_s \bar{Q}_{16} \left( \left( \frac{\partial w}{\partial x} + \beta_y \right) \cos \theta - \left( \frac{\partial v}{\partial x} - \beta_z \right) \sin \theta \right) \right] dr \, d\theta \quad (4.31) \end{aligned}$$

$$\begin{aligned} M_z = - \int_0^{2\pi} \int_{r_i}^{r_o} r^2 \cos \theta \left[ \bar{Q}_{11} \left( \frac{\partial \beta_y}{\partial x} r \sin \theta - \frac{\partial \beta_z}{\partial x} r \cos \theta \right) \right. \\ \left. + k_s \bar{Q}_{15} \left( \left( \frac{\partial w}{\partial x} + \beta_y \right) \sin \theta + \left( \frac{\partial v}{\partial x} - \beta_z \right) \cos \theta \right) \right. \\ \left. + k_s \bar{Q}_{16} \left( \left( \frac{\partial w}{\partial x} + \beta_y \right) \cos \theta - \left( \frac{\partial v}{\partial x} - \beta_z \right) \sin \theta \right) \right] dr \, d\theta \quad (4.32) \end{aligned}$$

$$\begin{aligned}
Q_{xr}^{(1)} = & \int_0^{2\pi} \int_{r_i}^{r_o} r \sin \theta \left[ k_s \bar{Q}_{51} \left( \frac{\partial \beta_y}{\partial x} r \sin \theta - \frac{\partial \beta_z}{\partial x} r \cos \theta \right) \right. \\
& + k_s \bar{Q}_{55} \left( \left( \frac{\partial w}{\partial x} + \beta_y \right) \sin \theta + \left( \frac{\partial v}{\partial x} - \beta_z \right) \cos \theta \right) \\
& \left. + k_s \bar{Q}_{56} \left( \left( \frac{\partial w}{\partial x} + \beta_y \right) \cos \theta - \left( \frac{\partial v}{\partial x} - \beta_z \right) \sin \theta \right) \right] dr d\theta \quad (4.33)
\end{aligned}$$

$$\begin{aligned}
Q_{xr}^{(2)} = & \int_0^{2\pi} \int_{r_i}^{r_o} r \cos \theta \left[ k_s \bar{Q}_{51} \left( \frac{\partial \beta_y}{\partial x} r \sin \theta - \frac{\partial \beta_z}{\partial x} r \cos \theta \right) \right. \\
& + k_s \bar{Q}_{55} \left( \left( \frac{\partial w}{\partial x} + \beta_y \right) \sin \theta + \left( \frac{\partial v}{\partial x} - \beta_z \right) \cos \theta \right) \\
& \left. + k_s \bar{Q}_{56} \left( \left( \frac{\partial w}{\partial x} + \beta_y \right) \cos \theta - \left( \frac{\partial v}{\partial x} - \beta_z \right) \sin \theta \right) \right] dr d\theta \quad (4.34)
\end{aligned}$$

$$\begin{aligned}
Q_{x\theta}^{(1)} = & \int_0^{2\pi} \int_{r_i}^{r_o} r \sin \theta \left[ k_s \bar{Q}_{61} \left( \frac{\partial \beta_y}{\partial x} r \sin \theta - \frac{\partial \beta_z}{\partial x} r \cos \theta \right) \right. \\
& + k_s \bar{Q}_{65} \left( \left( \frac{\partial w}{\partial x} + \beta_y \right) \sin \theta + \left( \frac{\partial v}{\partial x} - \beta_z \right) \cos \theta \right) \\
& \left. + k_s \bar{Q}_{66} \left( \left( \frac{\partial w}{\partial x} + \beta_y \right) \cos \theta - \left( \frac{\partial v}{\partial x} - \beta_z \right) \sin \theta \right) \right] dr d\theta \quad (4.35)
\end{aligned}$$

$$\begin{aligned}
Q_{x\theta}^{(2)} = \int_0^{2\pi} \int_{r_i}^{r_o} r \cos \theta \left[ k_s \bar{Q}_{61} \left( \frac{\partial \beta_y}{\partial x} r \sin \theta - \frac{\partial \beta_z}{\partial x} r \cos \theta \right) \right. \\
+ k_s \bar{Q}_{65} \left( \left( \frac{\partial w}{\partial x} + \beta_y \right) \sin \theta + \left( \frac{\partial v}{\partial x} - \beta_z \right) \cos \theta \right) \\
\left. + k_s \bar{Q}_{66} \left( \left( \frac{\partial w}{\partial x} + \beta_y \right) \cos \theta - \left( \frac{\partial v}{\partial x} - \beta_z \right) \sin \theta \right) \right] dr d\theta \quad (4.36)
\end{aligned}$$

After applying the integrations in Equations (4.31) – (4.36), the stress resultants and stress couples of the tapered composite shaft are

$$M_y = \bar{D}_{11} \frac{\partial \beta_y}{\partial x} + \bar{B}_{15} k_s \left( \beta_y + \frac{\partial w}{\partial x} \right) + \frac{1}{2} \bar{B}_{16} k_s \left( \beta_z - \frac{\partial v}{\partial x} \right) \quad (4.37)$$

$$M_z = \bar{D}_{11} \frac{\partial \beta_z}{\partial x} - \bar{B}_{15} k_s \left( \frac{\partial v}{\partial x} - \beta_z \right) - \frac{1}{2} \bar{B}_{16} k_s \left( \beta_y + \frac{\partial w}{\partial x} \right) \quad (4.38)$$

$$Q_{xr}^{(1)} = \bar{B}_{51} k_s \frac{\partial \beta_y}{\partial x} + k_s \bar{A}_{55} \left( \beta_y + \frac{\partial w}{\partial x} \right) + k_s \bar{A}_{56} \left( \beta_z - \frac{\partial v}{\partial x} \right) \quad (4.39)$$

$$Q_{xr}^{(2)} = -\bar{B}_{51} k_s \frac{\partial \beta_z}{\partial x} + k_s \bar{A}_{55} \left( \frac{\partial v}{\partial x} - \beta_z \right) + k_s \bar{A}_{56} \left( \beta_y + \frac{\partial w}{\partial x} \right) \quad (4.40)$$

$$Q_{x\theta}^{(1)} = \frac{1}{2} \bar{B}_{61} k_s \frac{\partial \beta_y}{\partial x} + k_s \bar{A}_{65} \left( \beta_y + \frac{\partial w}{\partial x} \right) + k_s \bar{A}_{66} \left( \beta_z - \frac{\partial v}{\partial x} \right) \quad (4.41)$$

$$Q_{x\theta}^{(2)} = -\frac{1}{2} \bar{B}_{61} k_s \frac{\partial \beta_z}{\partial x} + k_s \bar{A}_{65} \left( \frac{\partial v}{\partial x} - \beta_z \right) + k_s \bar{A}_{66} \left( \beta_y + \frac{\partial w}{\partial x} \right) \quad (4.42)$$

where

$$\bar{A}_{66}(x) = \frac{\pi}{2} \sum_{s=1}^n \bar{Q}_{66} (r_{os}^2(x) - r_{is}^2(x)) \quad (4.43)$$

$$\bar{A}_{65}(x) = \frac{\pi}{2} \sum_{s=1}^n \bar{Q}_{65} (r_{os}^2(x) - r_{is}^2(x)) \quad (4.44)$$

$$\bar{A}_{55}(x) = \frac{\pi}{2} \sum_{s=1}^n \bar{Q}_{55} (r_{os}^2(x) - r_{is}^2(x)) \quad (4.45)$$

$$\bar{A}_{56}(x) = \frac{\pi}{2} \sum_{s=1}^n \bar{Q}_{56} (r_{os}^2(x) - r_{is}^2(x)) \quad (4.46)$$

$$\bar{B}_{16}(x) = \frac{2}{3} \pi \sum_{s=1}^n \bar{Q}_{16} (r_{os}^3(x) - r_{is}^3(x)) \quad (4.47)$$

$$\bar{B}_{15}(x) = \frac{\pi}{3} \sum_{s=1}^n \bar{Q}_{15} (r_{os}^3(x) - r_{is}^3(x)) \quad (4.48)$$

$$\bar{B}_{51}(x) = \frac{\pi}{3} \sum_{s=1}^n \bar{Q}_{51} (r_{os}^3(x) - r_{is}^3(x)) \quad (4.49)$$

$$\bar{B}_{61}(x) = \frac{2}{3} \pi \sum_{s=1}^n \bar{Q}_{61} (r_{os}^3(x) - r_{is}^3(x)) \quad (4.50)$$

$$\bar{D}_{11}(x) = \frac{\pi}{4} \sum_{s=1}^n \bar{Q}_{11} (r_{os}^4(x) - r_{is}^4(x)) \quad (4.51)$$

Equations (4.43) - (4.51) represent  $\bar{A}\bar{B}\bar{D}$  matrix of the tapered composite shaft. For zero taper angle  $\bar{B}_{51}$  and  $\bar{A}_{56}$  will vanish because  $\bar{Q}_{15} = \bar{Q}_{56} = 0$ . Increasing the taper angle leads to increasing in  $\bar{B}_{51}$  and  $\bar{A}_{56}$ , so the effect of  $\bar{B}_{51}$  and  $\bar{A}_{56}$  will be significant at high taper angle. Substituting Equations (4.37) – (4.42) into Equation (4.24) gives the strain energy in terms of  $\bar{A}\bar{B}\bar{D}$  matrix as:

$$\begin{aligned}
U_{BS} = \frac{1}{2} \int_0^L & \left[ \left( \frac{\partial \beta_y}{\partial x} \right) \left( \bar{D}_{11} \frac{\partial \beta_y}{\partial x} + \bar{B}_{15} k_s \left( \beta_y + \frac{\partial w}{\partial x} \right) + \frac{1}{2} \bar{B}_{16} k_s \left( \beta_z - \frac{\partial v}{\partial x} \right) \right) \right. \\
& + \left( \frac{\partial \beta_z}{\partial x} \right) \left( \bar{D}_{11} \frac{\partial \beta_z}{\partial x} - \bar{B}_{15} k_s \left( \frac{\partial v}{\partial x} - \beta_z \right) - \frac{1}{2} \bar{B}_{16} k_s \left( \beta_y + \frac{\partial w}{\partial x} \right) \right) \\
& + \left( \frac{\partial v}{\partial x} \right. \\
& \left. - \beta_z \right) k_s \left( \left( -\bar{B}_{51} \frac{\partial \beta_z}{\partial x} + \bar{A}_{55} \left( \frac{\partial v}{\partial x} - \beta_z \right) + \bar{A}_{56} \left( \beta_y + \frac{\partial w}{\partial x} \right) \right) \right. \\
& \left. - \left( \frac{1}{2} \bar{B}_{61} \frac{\partial \beta_y}{\partial x} + \bar{A}_{65} \left( \beta_y + \frac{\partial w}{\partial x} \right) + \bar{A}_{66} \left( \beta_z - \frac{\partial v}{\partial x} \right) \right) \right) \\
& + \left( \beta_y \right. \\
& \left. + \frac{\partial w}{\partial x} \right) k_s \left( \left( \bar{B}_{51} \frac{\partial \beta_y}{\partial x} + \bar{A}_{55} \left( \beta_y + \frac{\partial w}{\partial x} \right) + \bar{A}_{56} \left( \beta_z - \frac{\partial v}{\partial x} \right) \right) \right. \\
& \left. + \left( -\frac{1}{2} \bar{B}_{61} \frac{\partial \beta_z}{\partial x} + \bar{A}_{65} \left( \frac{\partial v}{\partial x} - \beta_z \right) + \bar{A}_{66} \left( \beta_y + \frac{\partial w}{\partial x} \right) \right) \right) \right] dx \quad (4.52)
\end{aligned}$$

The strain energy  $U_{BS}$  Equation (4.52) represents the strain energy of the composite shaft that results from the bending moment and the shear force, but when the composite shaft is under a constant axial force, the total strain energy of the composite shaft is

$$U_{comp} = U_{BS} + U_F \quad (4.53)$$

where  $U_F$  is the external work done on the shaft due to a constant axial force  $P$  and can be written as

$$U_F = \frac{1}{2} \int_0^L P \left[ \left( \frac{\partial v}{\partial x} \right)^2 + \left( \frac{\partial w}{\partial x} \right)^2 \right] dx \quad (4.54)$$

#### 4.4 Finite element formulation

##### 4.4.1 Hierarchical composite shaft element formulation

The shape functions in hierarchical finite element can be established from polynomial or trigonometric functions. In this work the trigonometric function is chosen to build the model. Figure 4.3 illustrates a hierarchical beam finite element for tapered composite shaft. The element has two nodes and each of them have four degrees of freedom (two translational and two rotational). In hierarchical finite element method, the transverse displacement field of the beam element in y-direction can be expressed as

$$v = c_1 + c_2 \frac{x}{L} + \sum_{n=1}^N c_{n+2} \sin \frac{n\pi x}{L} \quad (4.55)$$

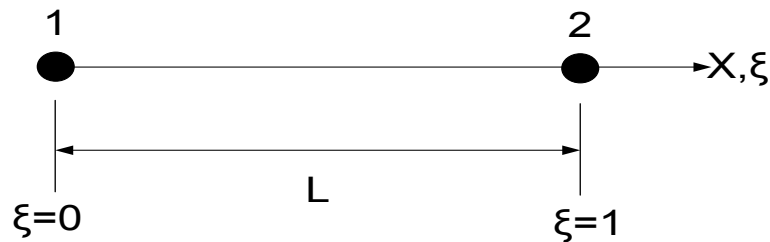


Figure 4.3 Hierarchical beam finite element with two nodes

The local coordinate  $x$  and non-dimensional coordinate  $\xi$  are related by

$$\xi = \frac{x}{L}, \quad (0 \leq \xi \leq 1) \quad (4.56)$$

So, Equation (4.55) can be written as

$$v = c_1 + c_2\xi + \sum_{n=1}^N c_{n+2} \sin(n\pi\xi) \quad (4.57)$$

$$v = [1 \quad \xi \quad \sin \pi\xi \quad \dots \quad \sin N\pi\xi] \begin{bmatrix} c_1 \\ c_2 \\ c_3 \\ c_4 \\ \vdots \\ c_{N+2} \end{bmatrix} \quad (4.58)$$

$$v = [K^v]\{c\} \quad (4.59)$$

where  $N$  is the number of the hierarchical terms of displacement. In local coordinate system, the nodal displacements in  $y$ -direction are

$$\{q_v\} = \begin{bmatrix} v_1 \\ v_2 \\ v_3 \\ v_4 \\ \vdots \\ v_{N+2} \end{bmatrix} = \begin{bmatrix} 1 & 0 & 0 & 0 & & 0 \\ 1 & L & 0 & 0 & & 0 \\ 0 & 0 & 1 & 0 & & 0 \\ 0 & 0 & 0 & 1 & & 0 \\ \vdots & \vdots & \vdots & \vdots & \ddots & \vdots \\ 0 & 0 & 0 & 0 & & 1 \end{bmatrix} \begin{bmatrix} c_1 \\ c_2 \\ c_3 \\ c_4 \\ \vdots \\ c_{N+2} \end{bmatrix} \quad (4.60)$$

$$\{q_v\} = [K^{qv}]\{c\} \quad (4.61)$$

The displacement in y-direction can be expressed as

$$v = [f_1 \quad f_2 \quad f_3 \quad f_4 \quad \dots \dots \quad f_{N+2}] \begin{bmatrix} v_1 \\ v_2 \\ v_3 \\ v_4 \\ \vdots \\ \vdots \\ v_{N+2} \end{bmatrix} \quad (4.62)$$

$$v = [N_v]\{q_v\} = f_1 v_1 + f_2 v_2 + \sum_{n=1}^N f_{n+2} v_{n+2} \quad (4.63)$$

Substituting Equations (4.59) and (4.61) into Equation (4.63)

$$[N_v]\{q_v\} = [N_v][K^{qv}]\{c\} = [K^v]\{c\} \quad (4.64)$$

The shape functions of the displacement  $v$  can be written as

$$[N_v] = [1 - \xi \quad \xi \quad \sin \pi \xi \quad \sin 2\pi \xi \quad \sin 3\pi \xi \quad \dots \dots \quad \sin N\pi \xi] \quad (4.65)$$

where

$$f_1 = 1 - \xi \quad (4.66)$$

$$f_2 = \xi \quad (4.67)$$

$$f_{n+2} = \sin(n \pi \xi) \quad (4.68)$$

where  $N$  is the number of the hierarchical terms,  $n = 1, 2, 3, \dots, N$ .

The functions  $f_1$  and  $f_2$  are polynomial functions and they correspond to the nodal displacements of the hierarchical element, whilst  $f_{n+2}$  function is trigonometric function and it corresponds to the hierarchical terms and contributes only to the internal field of

the displacement and does not affect the nodal displacement [22]. Repeating the previous procedure, one can obtain the shape functions for  $w$ ,  $\beta_y$  and  $\beta_z$ . As a result, the displacement vector formed by the variables  $v$ ,  $w$ ,  $\beta_y$  and  $\beta_z$  can be written as [22]:

$$\begin{bmatrix} v \\ w \\ \beta_y \\ \beta_z \end{bmatrix} = \begin{bmatrix} [N_v] & [0] & [0] & [0] \\ [0] & [N_w] & [0] & [0] \\ [0] & [0] & [N_{\beta_y}] & [0] \\ [0] & [0] & [0] & [N_{\beta_z}] \end{bmatrix} \begin{bmatrix} \{q_v\} \\ \{q_w\} \\ \{q_{\beta_y}\} \\ \{q_{\beta_z}\} \end{bmatrix} \quad (4.69)$$

$$[N_{v,w,\beta_y,\beta_z}] = [f_1 \ f_2 \ f_3 \ \dots \ \dots \ f_{N+2}] \quad (4.70)$$

$$\{q_v\} = \{v_1, v_2, v_3, \dots \dots \dots, v_{N+2}\}^T \quad (4.71)$$

$$\{q_w\} = \{w_1, w_2, w_3, \dots \dots \dots, w_{N+2}\}^T \quad (4.72)$$

$$\{q_{\beta_y}\} = \{\beta_{y1}, \beta_{y2}, \beta_{y3}, \dots \dots \dots, \beta_{y(N+2)}\}^T \quad (4.73)$$

$$\{q_{\beta_z}\} = \{\beta_{z1}, \beta_{z2}, \beta_{z3}, \dots \dots \dots, \beta_{z(N+2)}\}^T \quad (4.74)$$

Substituting Equation (4.69) into Equation (4.18), Equation (4.52), and Equation (4.54) and then applying the Lagrange's equations, one can get the equations of motion of free vibration of spinning tapered composite driveshaft. In addition to the number of the nodes, the number of the generalized co-ordinates depends on the number of the hierarchical terms. So, the generalized co-ordinates are

$$\begin{aligned}
q_1 = v_1 & \quad q_2 = v_2 & \quad q_3 = v_3 & \quad \dots\dots & \quad q_b = v_{N+2} \\
q_{b+1} = w_1 & \quad q_{b+2} = w_2 & \quad q_{b+3} = w_3 & \quad \dots\dots & \quad q_{2b} = w_{N+2} \\
q_{2b+1} = \beta_{y1} & \quad q_{2b+2} = \beta_{y2} & \quad q_{2b+3} = \beta_{y3} & \quad \dots\dots & \quad q_{3b} = \beta_{y(N+2)} \\
q_{3b+1} = \beta_{z1} & \quad q_{3b+2} = \beta_{z2} & \quad q_{3b+3} = \beta_{z3} & \quad \dots\dots & \quad q_{4b} = \beta_{z(N+2)}
\end{aligned} \tag{4.75}$$

where  $b = N + 2$ . Also, the generalized co-ordinates can be expressed as

$$\{q\} = \begin{bmatrix} \{q_v\} \\ \{q_w\} \\ \{q_{\beta_y}\} \\ \{q_{\beta_z}\} \end{bmatrix} \tag{4.76}$$

After applying Lagrange's equations, the equations of motion of free vibration of rotating tapered composite driveshaft can be written as

$$[M]\{\ddot{q}\} + [G]\{\dot{q}\} + ([K] + [K_p])\{q\} = \{0\} \tag{4.77}$$

where

$$[M] = \begin{bmatrix} [M_{11}] & [0] & [0] & [0] \\ [0] & [M_{22}] & [0] & [0] \\ [0] & [0] & [M_{33}] & [0] \\ [0] & [0] & [0] & [M_{44}] \end{bmatrix} \tag{4.78}$$

$$[G] = \begin{bmatrix} [0] & [0] & [0] & [0] \\ [0] & [0] & [0] & [0] \\ [0] & [0] & [0] & [G_{34}] \\ [0] & [0] & [G_{43}] & [0] \end{bmatrix} \tag{4.79}$$

$$[K] = \begin{bmatrix} [K_{11}] & 0 & [K_{13}] & [K_{14}] \\ [0] & [K_{22}] & [K_{23}] & [K_{24}] \\ [K_{31}] & [K_{32}] & [K_{33}] & [K_{34}] \\ [K_{41}] & [K_{42}] & [K_{43}] & [K_{44}] \end{bmatrix} \quad (4.80)$$

$$[K_p] = \begin{bmatrix} [K_{pv}] & [0] & [0] & [0] \\ [0] & [K_{pw}] & [0] & [0] \\ [0] & [0] & [0] & [0] \\ [0] & [0] & [0] & [0] \end{bmatrix} \quad (4.81)$$

$$[M_{11}] = L \int_0^1 m(\xi) [N_v]^T [N_v] d\xi \quad (4.82)$$

$$[M_{22}] = L \int_0^1 m(\xi) [N_w]^T [N_w] d\xi \quad (4.83)$$

$$[M_{33}] = L \int_0^1 m(\xi) [N_{\beta_y}]^T [N_{\beta_y}] d\xi \quad (4.84)$$

$$[M_{44}] = L \int_0^1 m(\xi) [N_{\beta_z}]^T [N_{\beta_z}] d\xi \quad (4.85)$$

$$[G_{34}] = -L\Omega \int_0^1 I_p(\xi) [N_{\beta_y}]^T [N_{\beta_y}] d\xi \quad (4.86)$$

$$[G_{43}] = L\Omega \int_0^1 I_p(\xi) [N_{\beta_z}]^T [N_{\beta_z}] d\xi \quad (4.87)$$

$$[K_{11}] = \frac{1}{L} \int_0^1 k_s (\bar{A}_{55}(\xi) + \bar{A}_{66}(\xi)) [N'_v]^T [N'_v] d\xi \quad (4.88)$$

$$[K_{13}] = -\frac{1}{2L} \int_0^1 k_s \bar{B}_{16}(\xi) [N'_v]^T [N'_{\beta_y}] d\xi \quad (4.89)$$

$$[K_{14}] = \int_0^1 \left[ -\frac{1}{L} k_s \bar{B}_{15}(\xi) [N'_v]^T [N'_{\beta_z}] - k_s (\bar{A}_{55}(\xi) + \bar{A}_{66}(\xi)) [N'_v]^T [N_{\beta_z}] \right] d\xi \quad (4.90)$$

$$[K_{22}] = \frac{1}{L} \int_0^1 k_s (\bar{A}_{55}(\xi) + \bar{A}_{66}(\xi)) [N'_w]^T [N'_w] d\xi \quad (4.91)$$

$$[K_{23}] = \int_0^1 \left[ \frac{1}{L} k_s \bar{B}_{15}(\xi) [N'_w]^T [N'_{\beta_y}] + k_s (\bar{A}_{55}(\xi) + \bar{A}_{66}(\xi)) [N'_w]^T [N_{\beta_y}] \right] d\xi \quad (4.92)$$

$$[K_{24}] = -\frac{1}{2L} \int_0^1 k_s \bar{B}_{16}(\xi) [N'_w]^T [N'_{\beta_z}] d\xi \quad (4.93)$$

$$[K_{31}] = -\frac{1}{2L} \int_0^1 k_s \bar{B}_{16}(\xi) [N'_{\beta_y}]^T [N'_v] d\xi \quad (4.94)$$

$$[K_{32}] = \int_0^1 \left[ \frac{1}{L} k_s \bar{B}_{15}(\xi) [N'_{\beta_y}]^T [N'_w] + k_s (\bar{A}_{55}(\xi) + \bar{A}_{66}(\xi)) [N_{\beta_y}]^T [N'_v] \right] d\xi \quad (4.95)$$

$$\begin{aligned}
[K_{33}] = & \int_0^1 \left[ \frac{1}{L} \bar{D}_{11}(\xi) [N'_{\beta_y}]^T [N'_{\beta_y}] \right. \\
& + k_s \bar{B}_{15}(\xi) \left( [N'_{\beta_y}]^T [N_{\beta_y}] + [N_{\beta_y}]^T [N'_{\beta_y}] \right) + k_s L (\bar{A}_{55}(\xi) \\
& \left. + \bar{A}_{66}(\xi)) [N_{\beta_y}] [N_{\beta_y}] \right] d\xi
\end{aligned} \tag{4.96}$$

$$[K_{34}] = \int_0^1 \left[ \frac{1}{2} k_s \bar{B}_{16}(\xi) [N'_{\beta_y}]^T [N_{\beta_z}] - \frac{1}{2} k_s \bar{B}_{16}(\xi) [N_{\beta_y}]^T [N'_{\beta_z}] \right] d\xi \tag{4.97}$$

$$[K_{41}] = \int_0^1 \left[ -\frac{1}{L} k_s \bar{B}_{15}(\xi) [N'_{\beta_z}]^T [N'_v] - k_s (\bar{A}_{55}(\xi) + \bar{A}_{66}(\xi)) [N'_{\beta_z}]^T [N'_v] \right] d\xi \tag{4.98}$$

$$[K_{42}] = -\frac{1}{2L} \int_0^1 \left[ k_s \bar{B}_{16}(\xi) [N'_{\beta_z}]^T [N'_w] \right] d\xi \tag{4.99}$$

$$[K_{43}] = \int_0^1 \left[ \frac{1}{2} k_s \bar{B}_{16}(\xi) [N_{\beta_z}]^T [N'_{\beta_y}] - \frac{1}{2} k_s \bar{B}_{16}(\xi) [N'_{\beta_z}]^T [N_{\beta_y}] \right] d\xi \tag{4.100}$$

$$\begin{aligned}
[K_{44}] = & \int_0^1 \left[ \frac{1}{L} \bar{D}_{11}(\xi) [N'_{\beta_z}]^T [N'_{\beta_z}] + k_s \bar{B}_{15}(\xi) \left( [N'_{\beta_z}]^T [N_{\beta_z}] + [N_{\beta_z}]^T [N'_{\beta_z}] \right) \right. \\
& \left. + k_s L (\bar{A}_{55}(\xi) + \bar{A}_{66}(\xi)) [N_{\beta_z}] [N_{\beta_z}] \right] d\xi
\end{aligned} \tag{4.101}$$

$$[K_{pv}] = \int_0^1 P [N'_v]^T [N'_v] d\xi \quad (4.102)$$

$$[K_{pw}] = \int_0^1 P [N'_w]^T [N'_w] d\xi \quad (4.103)$$

Appendix B shows in details how to obtain the mass sub-matrices, gyroscopic sub-matrices and stiffness sub-matrices for tapered composite driveshaft using hierarchical finite element method.

#### 4.4.2 Lagrangian composite shaft element formulation

The Lagrangian interpolation functions are used here to approximate the displacement fields of the tapered composite rotor. Figure 4.4 shows an element with three nodes; two nodes are at the ends of the element and one node is at the center of the element. Each node has four degrees of freedom, two translational in y and z directions and two rotational about y and z axes. The displacement fields are approximated by a quadratic approximation.

$$v(x) = a + bx + cx^2 \quad (4.104)$$

$$w(x) = d + ex + fx^2 \quad (4.105)$$

$$\beta_y(x) = \tilde{a} + \tilde{b}x + \tilde{c}x^2 \quad (4.106)$$

$$\beta_z(x) = \tilde{d} + \tilde{e}x + \tilde{f}x^2 \quad (4.107)$$

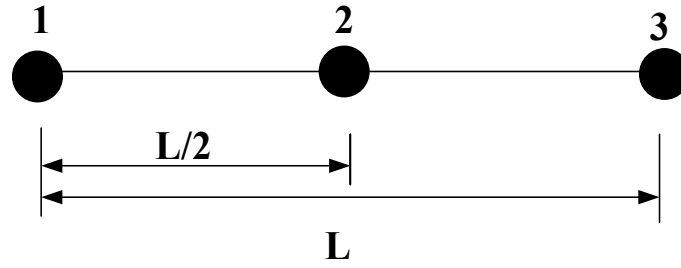


Figure 4.4 Beam element with three nodes

By considering the displacement in y-direction, one can write the displacements of the three nodes in y-direction as [31]

$$v_1 = a + bx_1 + cx_1^2 \quad (4.108)$$

$$v_2 = a + bx_2 + cx_2^2 \quad (4.109)$$

$$v_3 = a + bx_3 + cx_3^2 \quad (4.110)$$

Equations (4.108) – (4.110) can be written in matrix form as

$$\begin{bmatrix} v_1 \\ v_2 \\ v_3 \end{bmatrix} = \begin{bmatrix} 1 & x_1 & x_1^2 \\ 1 & x_2 & x_2^2 \\ 1 & x_3 & x_3^2 \end{bmatrix} \begin{bmatrix} a \\ b \\ c \end{bmatrix}, \{v\} = [A]\{\lambda\} \quad (4.111)$$

$$\begin{bmatrix} a \\ b \\ c \end{bmatrix} = \begin{bmatrix} 1 & x_1 & x_1^2 \\ 1 & x_2 & x_2^2 \\ 1 & x_3 & x_3^2 \end{bmatrix}^{-1} \begin{bmatrix} v_1 \\ v_2 \\ v_3 \end{bmatrix}, \{\lambda\} = [A]^{-1}\{v\} \quad (4.112)$$

where

$$\begin{bmatrix} a \\ b \\ c \end{bmatrix} = \frac{1}{\det [A]} \begin{bmatrix} \delta_1 & \delta_2 & \delta_3 \\ \epsilon_1 & \epsilon_2 & \epsilon_3 \\ \mu_1 & \mu_2 & \mu_3 \end{bmatrix} \begin{bmatrix} v_1 \\ v_2 \\ v_3 \end{bmatrix} \quad (4.113)$$

$$\delta_1 = x_2x_3^2 - x_3x_2^2 \quad \epsilon_1 = x_2^2 - x_3^2 \quad \mu_1 = x_3 - x_2 \quad (4.114)$$

$$\delta_2 = x_3 x_1^2 - x_1 x_3^2 \quad \varepsilon_2 = x_3^2 - x_1^2 \quad \mu_2 = x_1 - x_3 \quad (4.115)$$

$$\delta_3 = x_1 x_2^2 - x_2 x_1^2 \quad \varepsilon_3 = x_1^2 - x_2^2 \quad \mu_3 = x_2 - x_1 \quad (4.116)$$

Substituting Equation (4.112) into Equation (4.104) for  $v(x)$ , one can get

$$v(x) = N_{11}v_1 + N_{22}v_2 + N_{33}v_3 \quad (4.117)$$

where

$$N_{11} = \left(1 - \frac{2x}{L}\right) \left(1 - \frac{x}{L}\right) \quad (4.118)$$

$$N_{22} = \frac{4x}{L} \left(1 - \frac{x}{L}\right) \quad (4.119)$$

$$N_{33} = \left(\frac{2x}{L} - 1\right) \left(\frac{x}{L}\right) \quad (4.120)$$

$N_{11}$ ,  $N_{22}$ , and  $N_{33}$  are the shape functions that are used to approximate field solution of  $v(x)$ . Repeating the previous procedure for  $w(x)$ ,  $\beta_y(x)$ , and  $\beta_z(x)$ , one can get same shape functions as those of  $v(x)$ . So, the displacement field variables can be written as

$$v(x) = \sum_{i=1}^3 v_i(t) N_{ii}(x) \quad (4.121)$$

$$w(x) = \sum_{i=1}^3 w_i(t) N_{ii}(x) \quad (4.122)$$

$$\beta_y(x) = \sum_{i=1}^3 \beta_{yi}(t) N_{ii}(x) \quad (4.123)$$

$$\beta_z(x) = \sum_{i=1}^3 \beta_{zi}(t) N_{ii}(x) \quad (4.124)$$

Substituting Equations (4.121) - (4.124) into Equation (4.18), Equation (4.52), and Equation (4.54) and then applying the Lagrange's equations, one can get the equations of motion of free vibration of tapered composite driveshaft. After applying Lagrange's equations, the equations of motion of the tapered composite shaft based on Lagrangian composite shaft element formulation can be written as:

$$[M]\{\ddot{q}\} + [G]\{\dot{q}\} + ([K] + [K_P])\{q\} = \{0\} \quad (4.125)$$

where

$$\{q\} = \{\{q_1\} \quad \{q_2\} \quad \{q_3\} \quad \{q_4\}\}^T \quad (4.126)$$

$$\{q_1\} = \{v_1 \quad v_2 \quad v_3\} \quad (4.127)$$

$$\{q_2\} = \{w_1 \quad w_2 \quad w_3\} \quad (4.128)$$

$$\{q_3\} = \{\beta_{y1} \quad \beta_{y2} \quad \beta_{y3}\} \quad (4.129)$$

$$\{q_4\} = \{\beta_{z1} \quad \beta_{z2} \quad \beta_{z3}\} \quad (4.130)$$

$$[M] = \begin{bmatrix} [M_{11}]_{3 \times 3} & [0]_{3 \times 3} & [0]_{3 \times 3} & [0]_{3 \times 3} \\ [0]_{3 \times 3} & [M_{22}]_{3 \times 3} & [0]_{3 \times 3} & [0]_{3 \times 3} \\ [0]_{3 \times 3} & [0]_{3 \times 3} & [M_{33}]_{3 \times 3} & [0]_{3 \times 3} \\ [0]_{3 \times 3} & [0]_{3 \times 3} & [0]_{3 \times 3} & [M_{44}]_{3 \times 3} \end{bmatrix}_{12 \times 12} \quad (4.131)$$

$$[G] = \begin{bmatrix} [0]_{3 \times 3} & [0]_{3 \times 3} & [0]_{3 \times 3} & [0]_{3 \times 3} \\ [0]_{3 \times 3} & [0]_{3 \times 3} & [0]_{3 \times 3} & [0]_{3 \times 3} \\ [0]_{3 \times 3} & [0]_{3 \times 3} & [0]_{3 \times 3} & [G_{34}]_{3 \times 3} \\ [0]_{3 \times 3} & [0]_{3 \times 3} & [G_{43}]_{3 \times 3} & [0]_{3 \times 3} \end{bmatrix}_{12 \times 12} \quad (4.132)$$

$$[K] = \begin{bmatrix} [K_{11}]_{3 \times 3} & [0]_{3 \times 3} & [K_{13}]_{3 \times 3} & [K_{14}]_{3 \times 3} \\ [0]_{3 \times 3} & [K_{22}]_{3 \times 3} & [K_{23}]_{3 \times 3} & [K_{24}]_{3 \times 3} \\ [K_{31}]_{3 \times 3} & [K_{32}]_{3 \times 3} & [K_{33}]_{3 \times 3} & [K_{34}]_{3 \times 3} \\ [K_{41}]_{3 \times 3} & [K_{42}]_{3 \times 3} & [K_{43}]_{3 \times 3} & [K_{44}]_{3 \times 3} \end{bmatrix}_{12 \times 12} \quad (4.133)$$

$$[K_p] = \begin{bmatrix} [K_{pv}]_{3 \times 3} & [0]_{3 \times 3} & [0]_{3 \times 3} & [0]_{3 \times 3} \\ [0]_{3 \times 3} & [K_{pw}]_{3 \times 3} & [0]_{3 \times 3} & [0]_{3 \times 3} \\ [0]_{3 \times 3} & [0]_{3 \times 3} & [0]_{3 \times 3} & [0]_{3 \times 3} \\ [0]_{3 \times 3} & [0]_{3 \times 3} & [0]_{3 \times 3} & [0]_{3 \times 3} \end{bmatrix}_{12 \times 12} \quad (4.134)$$

$$[N_i] = [N_{11} \quad N_{22} \quad N_{33}] \quad (4.135)$$

$$[N'_i] = [N'_{11} \quad N'_{22} \quad N'_{33}] \quad (4.136)$$

$$[M_{11}]_{3 \times 3} = \int_0^L m(x) [N_i]^T [N_i] dx \quad (4.137)$$

$$[M_{22}]_{3 \times 3} = \int_0^L m(x) [N_i]^T [N_i] dx \quad (4.138)$$

$$[M_{33}]_{3 \times 3} = \int_0^L m(x) [N_i]^T [N_i] dx \quad (4.139)$$

$$[M_{44}]_{3 \times 3} = \int_0^L m(x) [N_i]^T [N_i] dx \quad (4.140)$$

$$[G_{34}]_{3 \times 3} = -\Omega \int_0^L I_p(x) [N_i]^T [N_i] dx \quad (4.141)$$

$$[G_{43}]_{3 \times 3} = \Omega \int_0^L I_p(x) [N_i]^T [N_i] dx \quad (4.142)$$

$$[K_{11}]_{3 \times 3} = \int_0^L k_s (\bar{A}_{55}(x) + \bar{A}_{66}(x)) [N'_i]^T [N'_i] dx \quad (4.143)$$

$$[K_{13}]_{3 \times 3} = -\frac{1}{2} \int_0^L k_s \bar{B}_{16}(x) [N'_i]^T [N'_i] dx \quad (4.144)$$

$$[K_{14}]_{3 \times 3} = \int_0^L [-k_s \bar{B}_{15}(x) [N'_i]^T [N'_i] - k_s (\bar{A}_{55}(x) + \bar{A}_{66}(x)) [N'_i]^T [N_i]] dx \quad (4.145)$$

$$[K_{22}]_{3 \times 3} = \int_0^L k_s (\bar{A}_{55}(x) + \bar{A}_{66}(x)) [N'_i]^T [N'_i] dx \quad (4.146)$$

$$[K_{23}]_{3 \times 3} = \int_0^L [k_s \bar{B}_{15}(x) [N'_i]^T [N'_i] + k_s (\bar{A}_{55}(x) + \bar{A}_{66}(x)) [N'_i]^T [N_i]] dx \quad (4.147)$$

$$[K_{24}]_{3 \times 3} = -\frac{1}{2} \int_0^L [k_s \bar{B}_{16}(x) [N'_i]^T [N'_i]] dx \quad (4.148)$$

$$[K_{31}]_{3 \times 3} = -\frac{1}{2} \int_0^L [k_s \bar{B}_{16}(x) [N'_i]^T [N'_i]] dx \quad (4.149)$$

$$[K_{32}]_{3 \times 3} = \int_0^L [k_s \bar{B}_{15}(x) [N'_i]^T [N'_i] + k_s (\bar{A}_{55}(x) + \bar{A}_{66}(x)) [N_i]^T [N'_i]] dx \quad (4.150)$$

$$[K_{33}]_{3 \times 3} = \int_0^L [\bar{D}_{11}(x) [N'_i]^T [N'_i] + k_s \bar{B}_{15}(x) ([N'_i]^T [N_i] + [N_i]^T [N'_i]) + k_s (\bar{A}_{55}(x) + \bar{A}_{66}(x)) [N_i]^T [N_i]] dx \quad (4.151)$$

$$[K_{34}]_{3 \times 3} = \int_0^L \left[ \frac{1}{2} k_s \bar{B}_{16}(x) [N'_i]^T [N_i] - \frac{1}{2} k_s \bar{B}_{16}(x) [N_i]^T [N'_i] \right] dx \quad (4.152)$$

$$[K_{41}]_{3 \times 3} = \int_0^L [-k_s \bar{B}_{15}(x) [N'_i]^T [N'_i] - k_s (\bar{A}_{55}(x) + \bar{A}_{66}(\xi)) [N_i]^T [N'_i]] dx \quad (4.153)$$

$$[K_{42}]_{3 \times 3} = -\frac{1}{2} \int_0^L [k_s \bar{B}_{16}(x) [N'_i]^T [N'_i]] dx \quad (4.154)$$

$$[K_{43}]_{3 \times 3} = \frac{1}{2} \int_0^L [k_s \bar{B}_{16}(x) [N_i]^T [N'_i] - k_s \bar{B}_{16}(x) [N'_i]^T [N_i]] dx \quad (4.155)$$

$$[K_{44}]_{3 \times 3} = \int_0^L [\bar{D}_{11}(x) [N'_i]^T [N'_i] + k_s \bar{B}_{15}(x) ([N'_i]^T [N_i] + [N_i]^T [N'_i]) + k_s (\bar{A}_{55}(x) + \bar{A}_{66}(x)) [N_i]^T [N_i]] dx \quad (4.156)$$

$$[K_{pv}]_{3 \times 3} = \int_0^L P [N'_i]^T [N'_i] dx \quad (4.157)$$

$$[K_{pw}]_{3 \times 3} = \int_0^L P [N_i']^T [N_i'] dx \quad (4.158)$$

Appendix C shows in details how to obtain the mass sub-matrices, gyroscopic sub-matrices and stiffness sub-matrices for tapered composite driveshaft using Lagrangian composite shaft element formulation

#### 4.4.3 Conventional-Hermitian composite shaft element formulation

In chapter 3, conventional-Hermitian composite shaft element was used to build up uniform composite shaft element and then to develop the equations of motion of the uniform composite shaft. The same procedure that was used in section 3.5, to develop the equations of motion of the uniform composite shaft, is followed here to obtain shaft element for the tapered composite shaft and then to develop the equations of motion of the tapered composite shaft. Herein, the tapered composite shaft element has two nodes at its ends, and each node has four degrees of freedom, two translations ( $v$  and  $w$ ) and two rotations ( $\beta_y$  and  $\beta_z$ ). From section 3.5,  $\beta_z$  and  $\beta_y$  are related to the shear angles in y-x plane and z-x plane, respectively as:

$$\beta_z = \frac{\partial v}{\partial x} - \gamma_{xy} = \frac{\partial v}{\partial x} - \phi_{xy} \quad (4.159)$$

$$\beta_y = -\frac{\partial w}{\partial x} + \gamma_{xz} = -\frac{\partial w}{\partial x} + \phi_{xz} \quad (4.160)$$

To derive the shape functions for the tapered composite shaft element, one can consider the y-x plane and represent the lateral displacement  $v(x, t)$  by a cubic polynomial with four parameters as:

$$v(x, t) = a_0 + a_1x + a_2x^2 + a_3x^3 \quad (4.161)$$

The translational and rotational boundary conditions in y-x plane of the tapered shaft element are

$$v(0, t) = v_1 \quad (4.162)$$

$$v(L, t) = v_2 \quad (4.163)$$

$$\beta_z(0, t) = \beta_{z1} = \left. \frac{\partial v}{\partial x} \right|_{x=0} - \phi_{xy} \quad (4.164)$$

$$\beta_z(L, t) = \beta_{z2} = \left. \frac{\partial v}{\partial x} \right|_{x=L} - \phi_{xy} \quad (4.165)$$

The shear angle  $\phi_{xy}$  and the lateral displacement  $v$  should be related together. To obtain the relationship between them, the static equilibrium of the beam must be considered. Thus, the equilibrium of the beam in y-x plane can be written as

$$\frac{\partial}{\partial x} [M_z] = -Q_y \quad (4.166)$$

$$\begin{aligned} & \frac{\partial}{\partial x} \left[ \bar{D}_{11} \frac{\partial \beta_z}{\partial x} - \bar{B}_{15} k_s \left( \frac{\partial v}{\partial x} - \beta_z \right) - \frac{1}{2} \bar{B}_{16} k_s \left( \beta_y + \frac{\partial w}{\partial x} \right) \right] \\ &= - \left[ \left( -k_s \bar{B}_{51} \frac{\partial \beta_z}{\partial x} + k_s \bar{A}_{55} \left( \frac{\partial v}{\partial x} - \beta_z \right) + k_s \bar{A}_{56} \left( \beta_y + \frac{\partial w}{\partial x} \right) \right) \right. \\ & \quad \left. - \left( \frac{1}{2} k_s \bar{B}_{61} \frac{\partial \beta_y}{\partial x} + k_s \bar{A}_{65} \left( \beta_y + \frac{\partial w}{\partial x} \right) + k_s \bar{A}_{66} \left( \beta_z - \frac{\partial v}{\partial x} \right) \right) \right] \quad (4.167) \end{aligned}$$

Using Equation (4.159) in Equation (4.167), one can get

$$\begin{aligned}
& \bar{D}_{11} \frac{\partial}{\partial x} \left( \frac{\partial}{\partial x} \left( \frac{\partial v}{\partial x} - \phi_{xy} \right) \right) - \bar{B}_{15} k_s \frac{\partial}{\partial x} \left( \frac{\partial v}{\partial x} \right) + \bar{B}_{15} k_s \frac{\partial}{\partial x} \left( \frac{\partial v}{\partial x} - \phi_{xy} \right) \\
& \quad - \frac{1}{2} \bar{B}_{16} k_s \frac{\partial \beta_y}{\partial x} - \frac{1}{2} k_s \bar{B}_{16} \frac{\partial}{\partial x} \left( \frac{\partial w}{\partial x} \right) \\
& = \bar{B}_{15} k_s \frac{\partial}{\partial x} \left( \frac{\partial v}{\partial x} - \phi_{xy} \right) - k_s (\bar{A}_{55} + \bar{A}_{66}) \phi_{xy} + \frac{1}{2} k_s \bar{B}_{61} \frac{\partial \beta_y}{\partial x}
\end{aligned} \tag{4.168}$$

where  $\bar{D}_{11}$ ,  $\bar{B}_{15}$ ,  $\bar{B}_{16}$ ,  $\bar{A}_{55}$ , and  $\bar{A}_{66}$  are the averages of  $D_{11}$ ,  $B_{15}$ ,  $B_{16}$ ,  $A_{55}$ , and  $A_{66}$ , respectively. Since  $\bar{A}\bar{B}\bar{D}$  matrix changes with axial coordinate  $x$ , it is easier to use the average of  $\bar{A}\bar{B}\bar{D}$  matrix in Equation (4.167) to obtain  $\phi_{xy}$ . Now, using Equation (4.160) in Equation (4.168), one can get

$$\begin{aligned}
& \bar{D}_{11} \frac{\partial}{\partial x} \left( \frac{\partial}{\partial x} \left( \frac{\partial v}{\partial x} - \phi_{xy} \right) \right) - \bar{B}_{15} k_s \frac{\partial}{\partial x} \left( \frac{\partial v}{\partial x} \right) - \bar{B}_{16} k_s \frac{\partial}{\partial x} \left( -\frac{\partial w}{\partial x} + \phi_{xz} \right) \\
& \quad - \frac{1}{2} k_s \bar{B}_{16} \frac{\partial}{\partial x} \left( \frac{\partial w}{\partial x} \right) = -k_s (\bar{A}_{55} + \bar{A}_{66}) \phi_{xy}
\end{aligned} \tag{4.169}$$

The change of the shear angles  $\phi_{xy}$  and  $\phi_{xz}$  along the axial coordinate  $x$  of the tapered composite shaft is assumed to be small, thus

$$\frac{\partial^2 \phi_{xy}}{\partial x^2} \approx \frac{\partial \phi_{xz}}{\partial x} \approx 0 \tag{4.170}$$

Considering Equation (4.170), one can write the shear angle as

$$\phi_{xy} = -\frac{1}{k_s(\bar{A}_{55} + \bar{A}_{66})} \left[ \bar{D}_{11} \frac{\partial^3 v}{\partial x^3} - k_s \bar{B}_{51} \frac{\partial^2 v}{\partial x^2} + \frac{1}{2} k_s \bar{B}_{61} \frac{\partial^2 w}{\partial x^2} \right] \quad (4.171)$$

The coupling term is neglected for simplification, so the shear angle can be written as

$$\phi_{xy} = -\frac{1}{k_s(\bar{A}_{55} + \bar{A}_{66})} \left[ \bar{D}_{11} \frac{\partial^3 v}{\partial x^3} - \bar{B}_{51} k_s \frac{\partial^2 v}{\partial x^2} \right] \quad (4.172)$$

If one considered the z-x plane, the shear angle  $\phi_{xz}$  is

$$\phi_{xz} = -\frac{1}{k_s(\bar{A}_{55} + \bar{A}_{66})} \left[ \bar{D}_{11} \frac{\partial^3 w}{\partial x^3} - \bar{B}_{51} k_s \frac{\partial^2 w}{\partial x^2} \right] \quad (4.173)$$

Substituting Equation (4.161) into Equation (4.172), the shear angle  $\phi_{xy}$  can be written as

$$\phi_{xy} = -[\Gamma_1 a_3 + \Gamma_2 a_2 + 3\Gamma_2 a_3 x] \quad (4.174)$$

where

$$\Gamma_1 = \frac{6 \bar{D}_{11}}{k_s(\bar{A}_{55} + \bar{A}_{66})} \quad (4.175)$$

$$\Gamma_2 = \frac{-2 \bar{B}_{15}}{(\bar{A}_{55} + \bar{A}_{66})} \quad (4.176)$$

Since the shear angle is assumed to be constant along the axial coordinate x of the tapered composite shaft, one can put  $3\Gamma_2 a_3 x \approx 0$ . So, the shear angle in Equation (4.174) can be written as:

$$\phi_{xy} = -\Gamma_1 a_3 - \Gamma_2 a_2 \quad (4.177)$$

Applying the lateral and rotational boundary conditions gives

$$v_1 = a_o \quad (4.178)$$

$$v_2 - v_1 = a_1 L + a_2 L^2 + a_3 L^3 \quad (4.179)$$

$$a_1 = \beta_{z1} + \Phi_{xy} = \beta_{z1} - \Gamma_1 a_3 - \Gamma_2 a_2 \quad (4.180)$$

$$\beta_{z2} - \beta_{z1} = 2a_2 L + 3a_3 L^2 \quad (4.181)$$

From Equation (4.181)

$$a_2 = \frac{1}{2L} [\beta_{z2} - \beta_{z1} - 3a_3 L^2] \quad (4.182)$$

Substituting Equation (4.182) into Equation (4.180) gives

$$a_1 = \beta_{z1} - \frac{\Gamma_2}{2L} (\beta_{z2} - \beta_{z1}) - a_3 \left( \frac{2\Gamma_1 - 3L\Gamma_2}{2} \right) \quad (4.183)$$

To obtain  $a_3$ , one can Substitute Equation (4.183) and Equation (4.182) into Equation (4.179).

$$a_3 = \frac{1}{\Gamma_3} [-2(v_2 - v_1) + (L + \Gamma_2)\beta_{z1} + (L - \Gamma_2)\beta_{z2}] \quad (4.184)$$

where

$$\Gamma_3 = \frac{L^3 - 3\Gamma_2 L^2 + 2\Gamma_1 L}{2} \quad (4.185)$$

Substituting Equation (4.184) into Equation (4.183) and Equation (4.182), gives  $a_1$  and  $a_2$ , respectively.

$$a_1 = \beta_{z1} - \frac{\Gamma_2}{2L} (\beta_{z2} - \beta_{z1}) - \Gamma_4 [-2(v_2 - v_1) + (L + \Gamma_2)\beta_{z1} + (L - \Gamma_2)\beta_{z2}] \quad (4.186)$$

$$a_2 = \frac{1}{2L} (\beta_{z2} - \beta_{z1}) - \Gamma_5 [-2(v_2 - v_1) + (L + \Gamma_2)\beta_{z1} + (L - \Gamma_2)\beta_{z2}] \quad (4.187)$$

where

$$\Gamma_4 = \frac{2\Gamma_1 - 3L\Gamma_2}{2\Gamma_3} \quad (4.188)$$

$$\Gamma_5 = \frac{3L^2}{2L\Gamma_3} \quad (4.189)$$

Now, substituting  $a_0$ ,  $a_1$ ,  $a_2$  and  $a_3$  into Equation (4.161), one can obtain the lateral displacement  $v(x, t)$  as :

$$v(x, t) = N_{t1}(x)v_1(t) + N_{t2}(x)\beta_{z1}(t) + N_{t3}(x)v_2(t) + N_{t4}(x)\beta_{z2}(t) \quad (4.190)$$

where

$$N_{t1} = \left[ 1 - 2L\Gamma_4\xi - 2L^2\Gamma_5\xi^2 + \frac{2L^3}{\Gamma_3}\xi^3 \right] \quad (4.191)$$

$$N_{t2} = \left[ \left( 1 + \frac{\Gamma_2}{2L} - \Gamma_4(L + \Gamma_2) \right) L \xi - \left( \frac{1}{2L} + \Gamma_5(L + \Gamma_2) \right) L^2 \xi^2 + \frac{L^3}{\Gamma_3}(L + \Gamma_2)\xi^3 \right] \quad (4.192)$$

$$N_{t3} = \left[ 2\Gamma_4L\xi + 2\Gamma_5L^2\xi^2 - \frac{2}{\Gamma_3}L^3\xi^3 \right] \quad (4.193)$$

$$N_{t4} = \left[ \left( -\frac{\Gamma_2}{2L} - \Gamma_4(L - \Gamma_2) \right) L \xi + \left( \frac{1}{2L} - \Gamma_5(L - \Gamma_2) \right) L^2 \xi^2 + \frac{1}{\Gamma_3}(L - \Gamma_2)L^3\xi^3 \right] \quad (4.194)$$

$$\xi = \frac{x}{L} \quad (4.195)$$

Substituting Equation (4.190) and Equation (4.172) into Equation (4.159) gives the rotation  $\beta_z$  as:

$$\beta_z(x, t) = N_{r1}(x)v_1(t) + N_{r2}(x)\beta_{z1}(t) + N_{r3}(x)v_2(t) + N_{r4}(x)\beta_{z2}(t) \quad (4.196)$$

where

$$N_{r1} = \left( \frac{2\Gamma_1}{\Gamma_3} - 2\Gamma_4 - 2\Gamma_2\Gamma_5 + \left( \frac{6\Gamma_2}{\Gamma_3} - 4\Gamma_5 \right) L \xi + \frac{6}{\Gamma_3} L^2 \xi^2 \right) \quad (4.197)$$

$$\begin{aligned} N_{r2} = & \left( 1 + \frac{\Gamma_2}{2L} - \Gamma_4(L + \Gamma_2) - \frac{\Gamma_2}{2} \left( \frac{1}{L} + 2\Gamma_5(L + \Gamma_2) \right) + \frac{\Gamma_1}{\Gamma_3} (L + \Gamma_2) \right. \\ & + \left. \left( \frac{3\Gamma_2}{\Gamma_3} (L + \Gamma_2) - \left( \frac{1}{L} + 2\Gamma_5(L + \Gamma_2) \right) \right) L \xi \right. \\ & \left. + \frac{3}{\Gamma_3} (L + \Gamma_2) L^2 \xi^2 \right) \end{aligned} \quad (4.198)$$

$$N_{r3} = 2\Gamma_4 + 2\Gamma_5\Gamma_2 - 2\frac{\Gamma_1}{\Gamma_3} + \left( 4\Gamma_5 - 6\frac{\Gamma_2}{\Gamma_3} \right) L \xi - \frac{6}{\Gamma_3} L^2 \xi^2 \quad (4.199)$$

$$\begin{aligned} N_{r4} = & \left( -\Gamma_4 + \Gamma_2\Gamma_5 + \frac{\Gamma_1}{\Gamma_3} \right) (L - \Gamma_2) + \left( \frac{1}{L(L - \Gamma_2)} - 2\Gamma_5 + 3\frac{\Gamma_2}{\Gamma_3} \right) (L - \Gamma_2) L \xi \\ & + \frac{3}{\Gamma_3} (L - \Gamma_2) L^2 \xi^2 \end{aligned} \quad (4.200)$$

If the z-x plane is considered and the previous procedure followed, the internal displacements and rotations of the tapered element can be expressed in terms of the displacements and rotations of the end points and the shape functions as:

$$\begin{bmatrix} v \\ w \\ \beta_y \\ \beta_z \end{bmatrix} = \begin{bmatrix} N_{t1} & 0 & 0 & N_{t2} & N_{t3} & 0 & 0 & N_{t4} \\ 0 & N_{t1} & -N_{t2} & 0 & 0 & N_{t3} & -N_{t4} & 0 \\ 0 & -N_{r1} & N_{r2} & 0 & 0 & -N_{r3} & N_{r4} & 0 \\ N_{r1} & 0 & 0 & N_{r2} & N_{r3} & 0 & 0 & N_{r4} \end{bmatrix} \begin{bmatrix} v_1 \\ w_1 \\ \beta_{y1} \\ \beta_{z1} \\ v_2 \\ w_2 \\ \beta_{y2} \\ \beta_{z2} \end{bmatrix} \quad (4.201)$$

Equation (4.172) and Equation (4.173) can be written as:

$$\phi_{xy} = \frac{\partial v}{\partial x} - \beta_z = - \left[ \frac{\Gamma_1}{6} \frac{\partial^3 v}{\partial x^3} + \frac{\Gamma_2}{2} \frac{\partial^2 v}{\partial x^2} \right] \quad (4.202)$$

$$\phi_{xz} = \beta_y + \frac{\partial w}{\partial x} = - \left[ \frac{\Gamma_1}{6} \frac{\partial^3 w}{\partial x^3} + \frac{\Gamma_2}{2} \frac{\partial^2 w}{\partial x^2} \right] \quad (4.203)$$

Substituting Equation (4.202) and Equation (4.203) into Equation (4.52), the strain energy  $U_{BS}$  can be written as

$$\begin{aligned}
U_{BS} = \frac{1}{2} \int_0^L & \left[ \left( \frac{\partial \beta_y}{\partial x} \right) \left( \bar{D}_{11} \frac{\partial \beta_y}{\partial x} - \bar{B}_{15} k_s \left( \frac{\Gamma_1}{6} \frac{\partial^3 w}{\partial x^3} + \frac{\Gamma_2}{2} \frac{\partial^2 w}{\partial x^2} \right) \right. \right. \\
& + \frac{1}{2} \bar{B}_{16} k_s \left( \frac{\Gamma_1}{6} \frac{\partial^3 v}{\partial x^3} + \frac{\Gamma_2}{2} \frac{\partial^2 v}{\partial x^2} \right) \\
& + \left( \frac{\partial \beta_z}{\partial x} \right) \left( \bar{D}_{11} \frac{\partial \beta_z}{\partial x} + \bar{B}_{15} k_s \left( \frac{\Gamma_1}{6} \frac{\partial^3 v}{\partial x^3} + \frac{\Gamma_2}{2} \frac{\partial^2 v}{\partial x^2} \right) \right. \\
& + \frac{1}{2} \bar{B}_{16} k_s \left( \frac{\Gamma_1}{6} \frac{\partial^3 w}{\partial x^3} + \frac{\Gamma_2}{2} \frac{\partial^2 w}{\partial x^2} \right) \\
& - \left( \frac{\Gamma_1}{6} \frac{\partial^3 v}{\partial x^3} + \frac{\Gamma_2}{2} \frac{\partial^2 v}{\partial x^2} \right) k_s \left( \left( -\bar{B}_{51} \frac{\partial \beta_z}{\partial x} - \bar{A}_{55} \left( \frac{\Gamma_1}{6} \frac{\partial^3 v}{\partial x^3} + \frac{\Gamma_2}{2} \frac{\partial^2 v}{\partial x^2} \right) \right) \right. \\
& - \left. \left. \left( \frac{1}{2} \bar{B}_{61} \frac{\partial \beta_y}{\partial x} + \bar{A}_{66} \left( \frac{\Gamma_1}{6} \frac{\partial^3 v}{\partial x^3} + \frac{\Gamma_2}{2} \frac{\partial^2 v}{\partial x^2} \right) \right) \right) \right) \\
& - \left( \frac{\Gamma_1}{6} \frac{\partial^3 w}{\partial x^3} \right. \\
& + \left. \frac{\Gamma_2}{2} \frac{\partial^2 w}{\partial x^2} \right) k_s \left( \left( \bar{B}_{51} \frac{\partial \beta_y}{\partial x} - \bar{A}_{55} \left( \frac{\Gamma_1}{6} \frac{\partial^3 w}{\partial x^3} + \frac{\Gamma_2}{2} \frac{\partial^2 w}{\partial x^2} \right) \right) \right. \\
& \left. \left. + \left( -\frac{1}{2} \bar{B}_{61} \frac{\partial \beta_z}{\partial x} - \bar{A}_{66} \left( \frac{\Gamma_1}{6} \frac{\partial^3 w}{\partial x^3} + \frac{\Gamma_2}{2} \frac{\partial^2 w}{\partial x^2} \right) \right) \right) \right] dx
\end{aligned} \tag{4.204}$$

Using Equation (4.201) in Equation (4.204) and Equation (4.54), one can obtain the total strain energy in Equation (4.53) in terms of the nodal displacements the shape functions, and the derivatives of the shape functions. Moreover, to obtain the kinetic energy in terms of the nodal displacements and the shape functions, one needs to substitute Equation (4.201) into the kinetic energy equation of the tapered composite shaft, Equation (4.18). Since the total strain energy and the kinetic energy are expressed in terms of the nodal displacements and the shape functions, one can apply Lagrange's equations to obtain the equations of motion. Herein, the generalized co-ordinates for the tapered composite shaft element are

$$\{q\} = \{v_1 \quad w_1 \quad \beta_{y1} \quad \beta_{z1} \quad v_2 \quad w_2 \quad \beta_{y2} \quad \beta_{z2}\}^T \quad (4.205)$$

After applying Lagrange's equations, the equations of motion of the tapered composite driveshaft can be written as:

$$([M_{Tc}] + [M_{Rc}])\{\ddot{q}\} + \Omega G_{\text{shaft}_{c,T}}\{\dot{q}\} + ([K_{TP} + K_{FT}])\{q\} = 0 \quad (4.206)$$

where

$$[M_{TC}] = \int_0^L m(x) [N_t]^T [N_t] dx \quad (4.207)$$

$$[M_{RC}] = \int_0^L I_d(x) [N_r]^T [N_r] dx \quad (4.208)$$

$$[G_{\text{Shaft}_{c-T}}] = \int_0^L I_p(x) [N_r]^T \begin{bmatrix} 0 & 1 \\ -1 & 0 \end{bmatrix} [N_r] dx \quad (4.209)$$

$$[K_{FT}] = \int_0^L P [N_t']^T [N_t'] dx \quad (4.210)$$

$$[K_{TP}] = [K_1] + [K_2] + [K_3] + [K_4] + [K_5] + [K_6] + [K_7] + [K_8] \quad (4.211)$$

$$[K_1] = \int_0^L \bar{D}_{11} [N_r']^T [N_r'] dx \quad (4.212)$$

$$[K_2] = \int_0^L \frac{\Gamma_1^2}{36} k_s (\bar{A}_{55} + \bar{A}_{66}) [N_t''']^T [N_t'''] dx \quad (4.213)$$

$$[K_3] = \int_0^L \frac{\Gamma_1 \Gamma_2}{12} k_s (\bar{A}_{55} + \bar{A}_{66}) ([N_t''']^T [N_t''] + [N_t'']^T [N_t''']) dx \quad (4.214)$$

$$[K_4] = \int_0^L \frac{\Gamma_2^2}{4} k_s (\bar{A}_{55} + \bar{A}_{66}) [N_t'']^T [N_t''] dx \quad (4.215)$$

$$[K_5] = \int_0^L \frac{\Gamma_1}{12} k_s \bar{B}_{16} ([N_t''']^T [N_r'] + [N_r']^T [N_t''']) dx \quad (4.216)$$

$$[K_6] = \int_0^L \frac{\Gamma_2}{4} k_s \bar{B}_{16} ([N_t'']^T [N_r'] + [N_r']^T [N_t'']) dx \quad (4.217)$$

$$[K_7] = \int_0^L \frac{\Gamma_1}{6} k_s \bar{B}_{15} ( [N_t''']^T \begin{bmatrix} 0 & -1 \\ 1 & 0 \end{bmatrix} [N_r'] + [N_r']^T \begin{bmatrix} 0 & -1 \\ 1 & 0 \end{bmatrix} [N_t'''] ) dx \quad (4.218)$$

$$[K_8] = \int_0^L \frac{\Gamma_2}{2} k_s \bar{B}_{15} ( [N_t'']^T \begin{bmatrix} 0 & -1 \\ 1 & 0 \end{bmatrix} [N_r'] + [N_r']^T \begin{bmatrix} 0 & -1 \\ 1 & 0 \end{bmatrix} [N_t''] ) dx \quad (4.219)$$

#### 4.5 Rayleigh – Ritz solution

In this section, Rayleigh – Ritz method is utilized to obtain an approximate solution for the tapered composite shaft. The reason behind using Rayleigh – Ritz method is to validate the models in section 4.4 which were established using finite element method. The simply supported condition at the ends of the tapered composite shaft is used to obtain the model, and the series solution functions are assumed for  $v, w, \beta_y$  and  $\beta_z$  in the form [16]

$$v = \bar{v} e^{i\omega t} \quad (4.220)$$

$$w = \bar{w} e^{i\omega t} \quad (4.221)$$

$$\beta_y = \bar{\beta}_y e^{i\omega t} \quad (4.222)$$

$$\beta_z = \bar{\beta}_z e^{i\omega t} \quad (4.223)$$

where

$$\bar{v}(x) = \sum_{j=1}^n V_j \sin \frac{j\pi x}{L} \quad (4.224)$$

$$\bar{w}(x) = \sum_{j=1}^n W_j \sin \frac{j\pi x}{L} \quad (4.225)$$

$$\bar{\beta}_y(x) = \sum_{j=1}^n B_{yj} \cos \frac{j\pi x}{L} \quad (4.226)$$

$$\bar{\beta}_z(x) = \sum_{j=1}^n B_{zj} \cos \frac{j\pi x}{L} \quad (4.227)$$

Here,  $n$  is the number of Ritz terms and  $\omega$  is whirl frequency. To obtain the equations of motion, Equations (4.220) - (4.223) must be substituted in Equation (4.18) and Equation (4.52) which represent the kinetic energy of the tapered composite shaft and the strain energy of the tapered composite shaft, respectively. After obtaining the energy expressions in terms of the series solution of  $v, w, \beta_y$  and  $\beta_z$ , Lagrange's equations can be used to establish the equations of motion of the tapered composite shaft. The equations of motion of free vibration of the rotating tapered composite shaft are

$$[M_r]\{\ddot{q}\} + [G_r]\{\dot{q}\} + [K_r]\{q\} = \{0\} \quad (4.228)$$

where

$$[M_r] = \begin{bmatrix} [M_V]_{n \times n} & [0]_{n \times n} & [0]_{n \times n} & [0]_{n \times n} \\ [0]_{n \times n} & [M_W]_{n \times n} & [0]_{n \times n} & [0]_{n \times n} \\ [0]_{n \times n} & [0]_{n \times n} & [M_{B_y}]_{n \times n} & [0]_{n \times n} \\ [0]_{n \times n} & [0]_{n \times n} & [0]_{n \times n} & [M_{B_z}]_{n \times n} \end{bmatrix}_{4n \times 4n} \quad (4.229)$$

$$[G_r] = \begin{bmatrix} [0]_{n \times n} & [0]_{n \times n} & [0]_{n \times n} & [0]_{n \times n} \\ [0]_{n \times n} & [0]_{n \times n} & [0]_{n \times n} & [0]_{n \times n} \\ [0]_{n \times n} & [0]_{n \times n} & [0]_{n \times n} & [G_{B_z}]_{n \times n} \\ [0]_{n \times n} & [0]_{n \times n} & [G_{B_y}]_{n \times n} & [0]_{n \times n} \end{bmatrix}_{4n \times 4n} \quad (4.230)$$

$$[K_r] = \begin{bmatrix} [K_{V1}]_{n \times n} & [0]_{n \times n} & [K_{V3}]_{n \times n} & [K_{V4}]_{n \times n} \\ [0]_{n \times n} & [K_{W2}]_{n \times n} & [K_{W3}]_{n \times n} & [K_{W4}]_{n \times n} \\ [K_{B_y1}]_{n \times n} & [K_{B_y2}]_{n \times n} & [K_{B_y3}]_{n \times n} & [K_{B_y4}]_{n \times n} \\ [K_{B_z1}]_{n \times n} & [K_{B_z2}]_{n \times n} & [K_{B_z3}]_{n \times n} & [K_{B_z4}]_{n \times n} \end{bmatrix}_{4n \times 4n} \quad (4.231)$$

$$\{q\} = \{V_1, V_2, \dots, V_n \quad W_1, W_2, \dots, W_n \quad B_{y1}, B_{y2}, \dots, B_{yn} \quad B_{z1}, B_{z2}, \dots, B_{zn}\}^T \quad (4.232)$$

$$[H] = [H_1 \quad H_2 \quad \dots \quad H_n]_{1 \times n} = \left[ \sin \frac{1\pi x}{L} \quad \sin \frac{2\pi x}{L} \quad \dots \quad \sin \frac{n\pi x}{L} \right]_{1 \times n} \quad (4.233)$$

$$[F] = [F_1 \quad F_2 \quad \dots \quad F_n]_{1 \times n} = \left[ \cos \frac{1\pi x}{L} \quad \cos \frac{2\pi x}{L} \quad \dots \quad \cos \frac{n\pi x}{L} \right]_{1 \times n} \quad (4.234)$$

$$[M_V]_{n \times n} = \int_0^L m(x) [H]^T [H] dx \quad (4.235)$$

$$[M_W]_{n \times n} = \int_0^L m(x) [H]^T [H] dx \quad (4.236)$$

$$[M_{B_y}]_{n \times n} = \int_0^L m(x) [F]^T [F] dx \quad (4.237)$$

$$[M_{B_z}]_{n \times n} = \int_0^L m(x) [F]^T [F] dx \quad (4.238)$$

$$[G_{B_z}]_{n \times n} = -\Omega \int_0^L I_p(x) [F]^T [F] dx \quad (4.239)$$

$$[G_{B_y}]_{n \times n} = \Omega \int_0^L I_p(x) [F]^T [F] dx \quad (4.240)$$

$$[K_{V1}]_{n \times n} = \int_0^L k_s (\bar{A}_{55}(x) + \bar{A}_{66}(x)) [H']^T [H'] dx \quad (4.241)$$

$$[K_{V3}]_{n \times n} = -\frac{1}{2} \int_0^L k_s \bar{B}_{16}(x) [H']^T [F'] dx \quad (4.242)$$

$$[K_{V4}]_{n \times n} = \int_0^L [-k_s \bar{B}_{15}(x) [H']^T [F'] - k_s (\bar{A}_{55}(x) + \bar{A}_{66}(x)) [H']^T [F]] dx \quad (4.243)$$

$$[K_{W2}]_{n \times n} = \int_0^L k_s (\bar{A}_{55}(x) + \bar{A}_{66}(x)) [H']^T [H'] dx \quad (4.244)$$

$$[K_{W3}]_{n \times n} = \int_0^L [k_s \bar{B}_{16}(x) [H']^T [F'] + k_s (\bar{A}_{55}(x) + \bar{A}_{66}(x)) [H']^T [F]] dx \quad (4.245)$$

$$[K_{W4}]_{n \times n} = -\frac{1}{2} \int_0^L [k_s \bar{B}_{16}(x) [H']^T [F']] dx \quad (4.246)$$

$$[K_{By1}]_{n \times n} = -\frac{1}{2} \int_0^L [k_s \bar{B}_{16}(x) [F']^T [H']] dx \quad (4.247)$$

$$[K_{By2}]_{n \times n} = \int_0^L [k_s \bar{B}_{15}(x) [F']^T [H'] + k_s (\bar{A}_{55}(x) + \bar{A}_{66}(x)) [F]^T [H']] dx \quad (4.248)$$

$$\begin{aligned} [K_{By3}]_{n \times n} = & \int_0^L [\bar{D}_{11}(x) [F']^T [F'] + k_s \bar{B}_{15}(x) ([F']^T [F] + [F]^T [F']) \\ & + k_s (\bar{A}_{55}(x) + \bar{A}_{66}(x)) [F]^T [F]] dx \end{aligned} \quad (4.249)$$

$$[K_{By4}]_{n \times n} = \int_0^L \left[ \frac{1}{2} k_s \bar{B}_{16}(x) [F']^T [F] - \frac{1}{2} k_s \bar{B}_{16}(x) [F]^T [F'] \right] dx \quad (4.250)$$

$$[K_{Bz1}]_{n \times n} = \int_0^L [-k_s \bar{B}_{15}(x) [F']^T [H'] - k_s (\bar{A}_{55}(x) + \bar{A}_{66}(\xi)) [F]^T [H']] dx \quad (4.251)$$

$$[K_{Bz2}]_{n \times n} = -\frac{1}{2} \int_0^L [k_s \bar{B}_{16}(x) [F']^T [H']] dx \quad (4.252)$$

$$[K_{Bz3}]_{n \times n} = \frac{1}{2} \int_0^L [k_s \bar{B}_{16}(x) [F]^T [H'] - k_s \bar{B}_{16}(x) [F']^T [H]] dx \quad (4.253)$$

$$[K_{Bz4}]_{n \times n} = \int_0^L [\bar{D}_{11}(x) [F']^T [F'] + k_s \bar{B}_{15}(x) ([F']^T [F] + [F]^T [F']) + k_s (\bar{A}_{55}(x) + \bar{A}_{66}(x)) [F]^T [F]] dx \quad (4.254)$$

#### 4.6 Validation

In the following example, the fundamental natural frequency and first critical speed of the tapered composite shaft are studied using finite element method and the Rayleigh-Ritz method. In this analysis, a hollow tapered composite shaft made of graphite-epoxy lamina is considered. The shaft is simply supported at the ends; the outer diameter of the composite shaft at the left end is 12.69 cm while the outer diameter at the right end increases with changing the taper angle. The outer diameter of the composite shaft at the left end is constant for all the taper angles. Figure 4.5 shows the configuration of the tapered graphite - epoxy composite shaft. The properties of the graphite-epoxy composite material are listed in Table 4.1. The wall thickness of the tapered composite shaft is 1.321 mm, and the composite shaft is made of ten layers, each with the same thickness. In addition, the configuration of the composite shaft is  $[90^\circ/45^\circ/-45^\circ/0^\circ_6/90^\circ]$  and the lay-up starts from the inside. The total length of the composite shaft is 2.47 m. The correction factor  $k_s$  for the composite shaft at the zero taper angle is 0.503 [20], yet this value is considered for all taper angles in this example.

Table 4.1 Properties of the composite materials [20]

Properties	Boron-epoxy	Graphite-epoxy
$E_{11}$ (GPa)	211	139
$E_{22}$ (GPa)	24	11
$G_{12} = G_{13}$ (GPa)	6.9	6.05
$G_{23}$ (GPa)	6.9	3.78
$\nu_{12}$	0.36	0.313
Density ( $\text{Kg/m}^3$ )	1967	1578

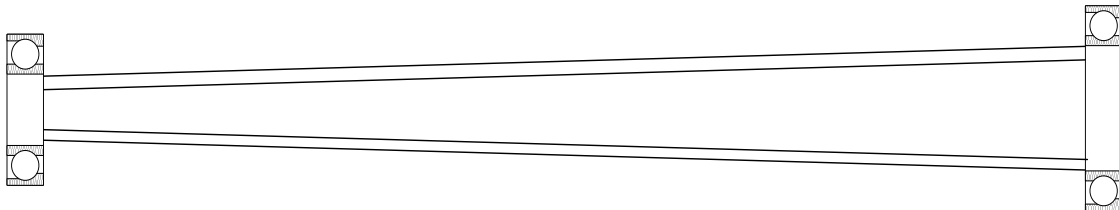


Figure 4.5 The configuration of the tapered graphite - epoxy composite shaft

Six elements, twenty elements, nine elements with equal length are used for hierarchical finite element, Lagrangian finite element, and Hermitian finite element, respectively; the same number of the elements was used for all the taper angles in the three models. Also, in Rayleigh-Ritz method five Ritz terms were used. The first critical speeds of the tapered composite shaft calculated using finite element method are illustrated in Table 4.2 beside the speeds obtained using the Rayleigh-Ritz method. It can be seen from Table 4.2 that

the difference is small between finite element method and the Rayleigh-Ritz method in obtaining the first critical speed. And the difference does not exceed 4 percent between Rayleigh-Ritz method and Lagrangian finite element method in obtaining the first critical speed when the taper angle is 4°.

Table 4.2 First critical speed in rpm of the tapered composite shaft with different taper angles using finite element method and Rayleigh-Ritz method

Taper angle, degrees	Finite element method			Rayleigh-Ritz method
	Hierarchical finite element	Lagrangian finite element	Hermitian finite element	
0	5220	5219	5220	5220
1	6647	6645	6650	6667
2	7721	7718	7730	7820
3	8531	8525	8548	8772
4	9126	9121	9155	9510

Another observation from Table 4.2 is that the critical speed of the composite shaft increases when increasing the taper angle, because the circumference of the cross-section increases through the length of the shaft from the left end to the right end when increasing the taper angle. This means the amount of composite material increases through the length of the shaft when increasing the taper angle, which makes the tapered composite shaft stiffer than the uniform composite shaft. The natural frequencies of the

tapered composite shaft are shown in Table 4.3; the results were obtained at 10,000 rpm and the results obtained by finite element models are comparable with the results predicted using the Rayleigh-Ritz method.

Table 4.3 The natural frequencies in Hz of the tapered composite shaft at 10000 rpm with different taper angles obtained using finite element method and Rayleigh-Ritz method.

Taper angle, degrees	Mode	Hierarchical finite element	Lagrangian finite element	Hermitian finite element	Rayleigh-Ritz method
0	BW1	87	86	86	87
	FW1	88	87	87	88
	BW2	317	316	317	316
	FW2	319	319	320	319
1	BW1	111	110	110	110
	FW1	112	112	112	112
	BW2	387	386	388	386
	FW2	390	390	391	389
2	BW1	128	128	128	130
	FW1	131	131	131	132
	BW2	437	436	439	436
	FW2	441	440	443	441

3	BW1	142	142	142	146
	FW1	146	145	145	149
	BW2	473	472	476	473
	FW2	477	476	480	477
4	BW1	152	152	152	159
	FW1	157	157	157	163
	BW2	499	499	504	500
	FW2	504	502	508	504

#### 4.7 Summary

Herein, hierarchical finite element, Lagrangian finite element, Hermitian finite element are used to develop three different finite element models of tapered composite driveshaft for rotordynamic analysis. These models are based on Timoshenko beam theory, so rotary inertia and shear deformation are accounted for in these models. In addition, the effect of axial load, gyroscopic force, coupling due to the lamination of composite layers, and taper angle are incorporated in the three finite element models. The kinetic energy and the strain energy of the tapered composite driveshaft were determined and then Lagrange's equation was used to obtain the equations of motion. For the purpose of comparing with the finite element models, Rayleigh-Ritz method was used to develop a model of tapered composite driveshaft. A numerical example was given to validate the finite element models, and a good agreement was found between the results of the finite element models and Rayleigh-Ritz solution.

## Chapter 5

### Parametric Study of Tapered Composite Shaft

#### 5.1 Introduction

In the previous chapter, different mathematical models were established for vibration analysis of the tapered composite shaft; these mathematical models are the conventional-Hermitian finite element model, the hierarchical finite element model, and the Lagrangian finite element model. It is important to assess these models in terms of their ability to predict the natural frequencies and the critical speeds of the tapered composite shaft, so in chapter 4 the finite element models were validated using Rayleigh-Ritz formulation and a good agreement between these models was observed.

Therefore, the conventional-Hermitian finite element model, the hierarchical finite element model, and the Lagrangian finite element model are credible enough to perform rotordynamic analysis and to study the effects of different parameters, such as the taper angle, fiber orientation, and axial load, on the natural frequencies and the critical speeds of the tapered composite shaft. Two cases of the tapered composite shaft are considered to perform rotordynamic analysis; the effects of different parameters, such as the taper angle, fiber orientation, and axial load, on the natural frequencies and the critical speeds of these two tapered composite shafts are studied in this chapter. In addition, in this chapter in the analysis of the tapered composite shafts it is assumed that torque buckling does not happen.

## 5.2 Tapered composite shaft case A

In this section, rotordynamic analysis of the tapered composite shaft is performed using the conventional-Hermitian finite element model, the hierarchical finite element model, and the Lagrangian finite element model. The tapered composite shaft has a disk at its middle and two bearings at the ends; the configuration of the tapered composite shaft is illustrated in Figure 5.1. The shaft is made of a graphite-epoxy composite material, and the geometric properties of the composite shaft are given in Table 5.1. Different taper angles are considered in the analysis. The inner and outer diameters at the left end of the shaft do not change with changing the taper angle, while at the right end they increase when increasing the taper angle. The tapered composite shaft is modeled by ten elements, twenty elements, eight elements of equal length using the conventional-Hermitian finite element model, the Lagrangian finite element model, and the hierarchical finite element model, respectively.

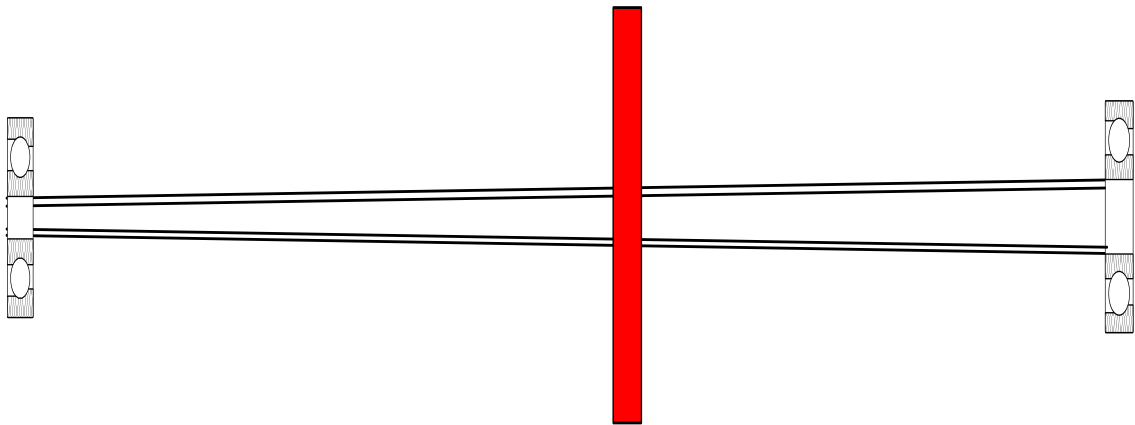


Figure 5.1 The configuration of the tapered composite shaft with disk in the middle

Table 5.1 The geometric dimensions and properties of the tapered composite shaft

<b>Composite Shaft</b>				
Length, $L = 0.72$ m	Inner diameter , ID = 0.028 m	Outer diameter , OD = 0.048 m	Lay-up from inside [90/45/-45/0 <sub>6</sub> /90]	Shear correction factor, $k_s =$ 0.56
<b>Disk</b>				
Mass, $m = 2.4364$ Kg	Diametral mass moment of inertia, $I_d =$ 0.1901 Kg.m <sup>2</sup>		Polar mass moment of inertia, $I_p = 0.3778$ Kg.m <sup>2</sup>	
<b>Bearing</b>				
$K_{yy} = K_{zz} = 17.5$ MN/m			$C_{zz} = C_{yy} = 500$ N.s/m	

Table 5.2 shows the first critical speeds of the tapered composite shaft for different taper angles, and it can be seen from the table that the first critical speed increases when increasing the taper angle. However, Figure 5.2 - Figure 5.4 show that the increase in the first critical speed when increasing the taper angle does not continue because the first critical speed reaches its maximum at 10° taper angle and then starts to drop off when increasing the taper angle; to understand why this happens, one needs to return to Equations (4.43) – (4.51) and to look at Figure 5.5 – Figure 5.8. The equations represent the  $\bar{A}\bar{B}\bar{D}$  matrix that depends on the stiffness and the radius of the layer. Whereas, Figure

5.5 – Figure 5.8 represent the material stiffnesses for each single layer of the tapered composite shaft; from the figures it is clear that  $\bar{Q}_{11}$  is much higher than  $\bar{Q}_{15}$ ,  $\bar{Q}_{16}$ ,  $\bar{Q}_{55}$  and  $\bar{Q}_{66}$  for all the layers and the taper angles, and  $\bar{Q}_{11}$  decreases with increasing the taper angle except for the layer with fiber orientation of  $90^\circ$ . Consequently, in Figure 5.2 - Figure 5.4, the inner and the outer radii of the layer control the first critical speed for taper angle of  $0^\circ \leq \alpha \leq 10^\circ$  while  $\bar{Q}_{11}$  controls the first critical speed for taper angle of  $10^\circ < \alpha \leq 20^\circ$ .

Table 5.2 The first critical speed in rpm of the tapered composite shaft for different taper angles.

Taper angle	Hierarchical finite element	Lagrangian finite element	Hermitian finite element
$0^\circ$	7295	7328	7328
$1^\circ$	9710	9772	9760
$2^\circ$	11467	11551	11537
$3^\circ$	12820	12912	12903
$4^\circ$	13855	13935	13935

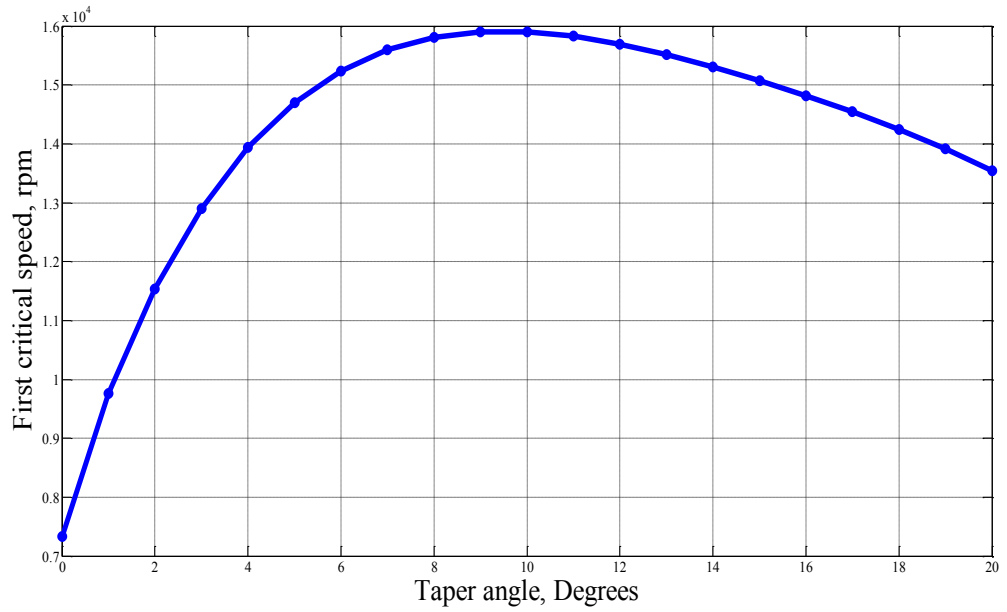


Figure 5.2 The first critical speeds of the tapered composite shaft for different taper angles obtained using Hermitian finite element model

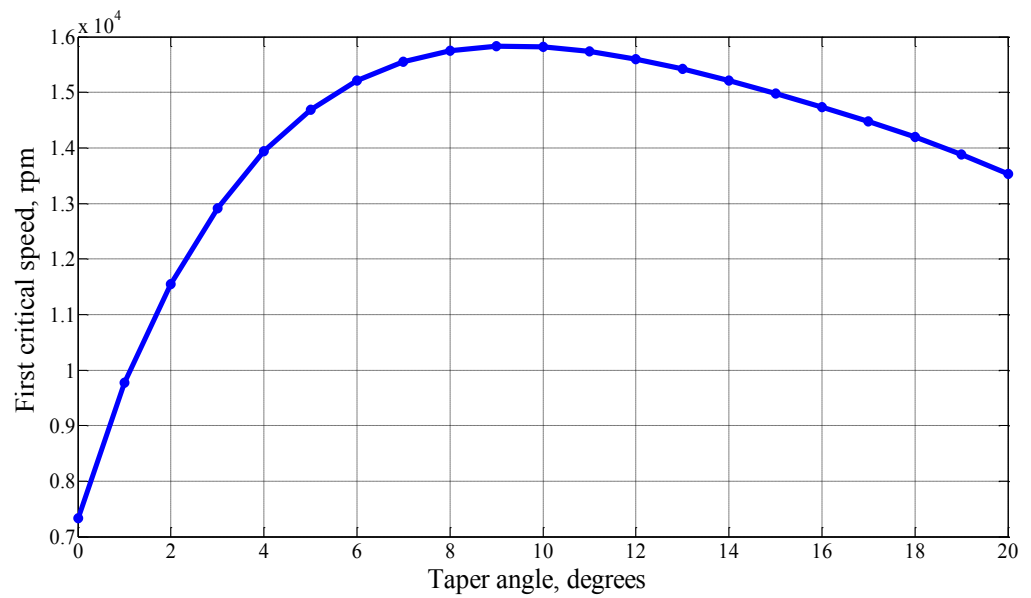


Figure 5.3 The first critical speeds of the tapered composite shaft for different taper angles determined using Lagrangian finite element model

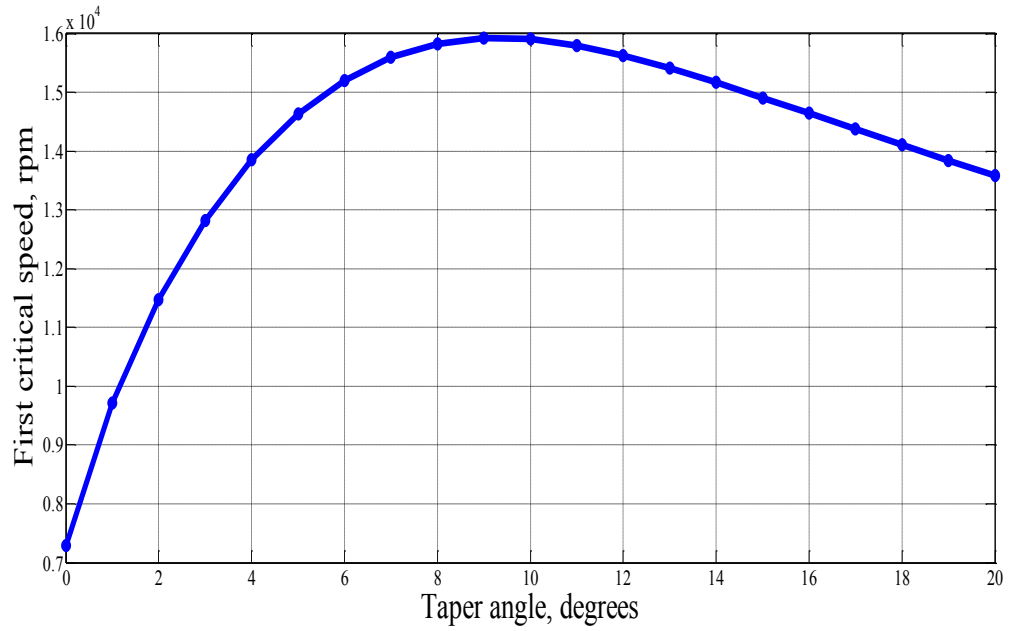


Figure 5.4 The first critical speeds of the tapered composite shaft for different taper angles determined using Hierarchical finite element model

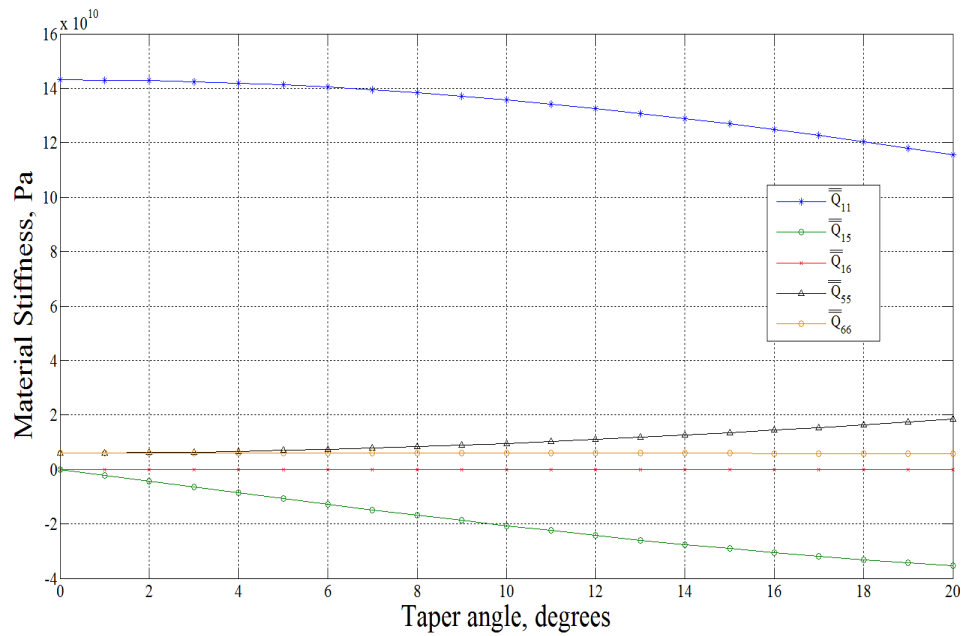


Figure 5.5  $\bar{Q}_{11}$ ,  $\bar{Q}_{15}$ ,  $\bar{Q}_{16}$ ,  $\bar{Q}_{55}$ , and  $\bar{Q}_{66}$  for the layer of graphite-epoxy with fiber orientation angle of  $0^\circ$

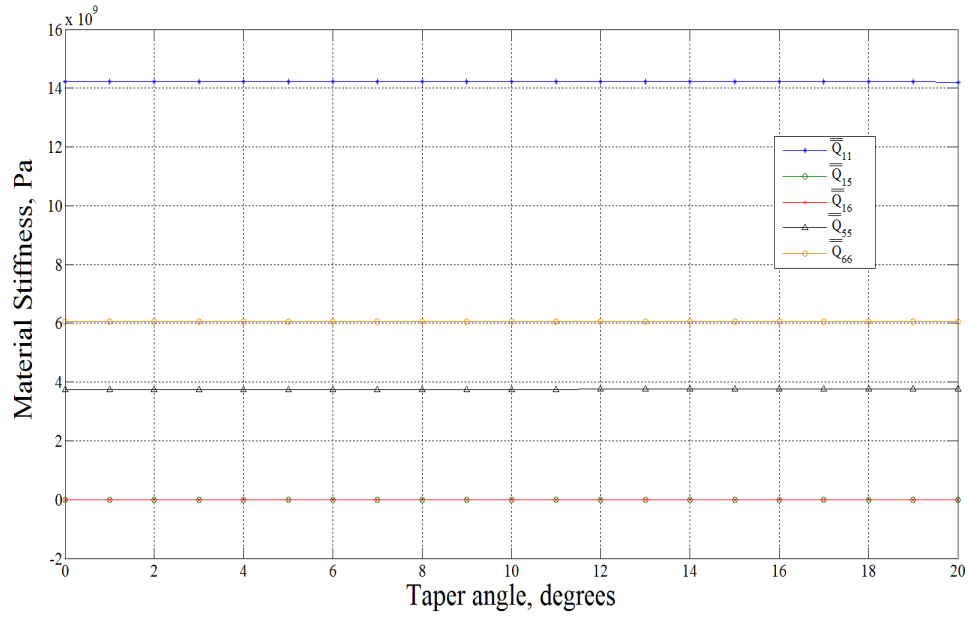


Figure 5.6  $\bar{Q}_{11}$ ,  $\bar{Q}_{15}$ ,  $\bar{Q}_{16}$ ,  $\bar{Q}_{55}$ , and  $\bar{Q}_{66}$  for the layer of graphite-epoxy with fiber orientation angle of  $90^\circ$

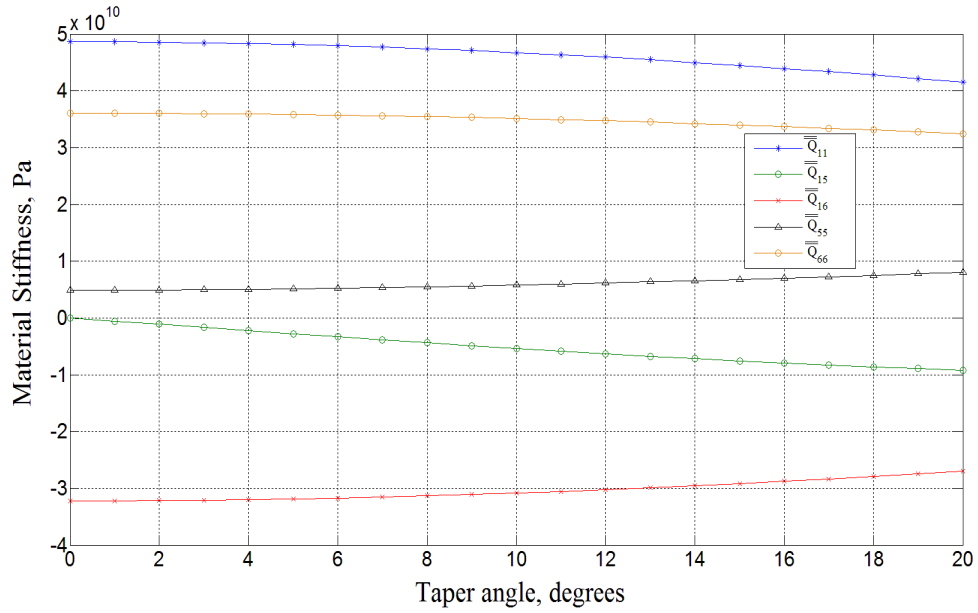


Figure 5.7  $\bar{Q}_{11}$ ,  $\bar{Q}_{15}$ ,  $\bar{Q}_{16}$ ,  $\bar{Q}_{55}$ , and  $\bar{Q}_{66}$  for the layer of graphite-epoxy with fiber orientation angle of  $45^\circ$

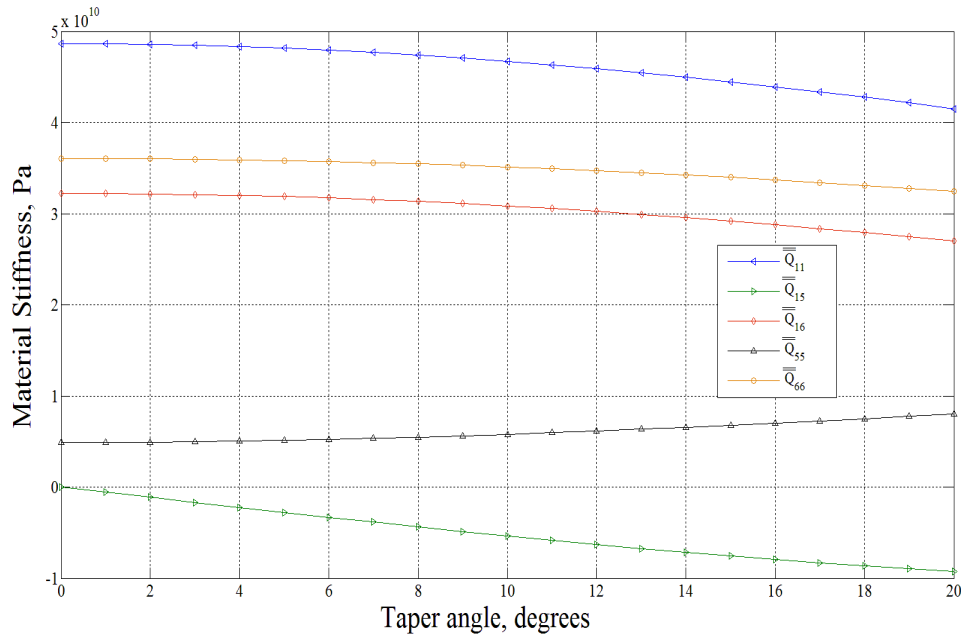


Figure 5.8  $\bar{Q}_{11}$ ,  $\bar{Q}_{15}$ ,  $\bar{Q}_{16}$ ,  $\bar{Q}_{55}$ , and  $\bar{Q}_{66}$  for the layer of graphite-epoxy with fiber orientation angle of  $-45^\circ$

Moreover, the effect of the disk position on the first critical speed is studied. Figure 5.9 shows the tapered composite shaft with different disk positions. Table 5.3 illustrates the first critical speed of the tapered composite shaft for different disk positions and taper angles. For taper angles of  $0^\circ$  and  $1^\circ$  the maximum value of the first critical speed happens when the position of the disk is located at the center, while for taper angles between  $2^\circ$  and  $4^\circ$  the maximum value of the critical speed happens when the disk is located at a distance of  $4L/10$  from the left end. It can be said for high taper angles that the critical speed reaches its maximum as the disk approaches the left bearing where the inner and outer diameters are smaller than that at the right end. The results in Table 5.3 are determined using only the conventional-Hermitian finite element model.

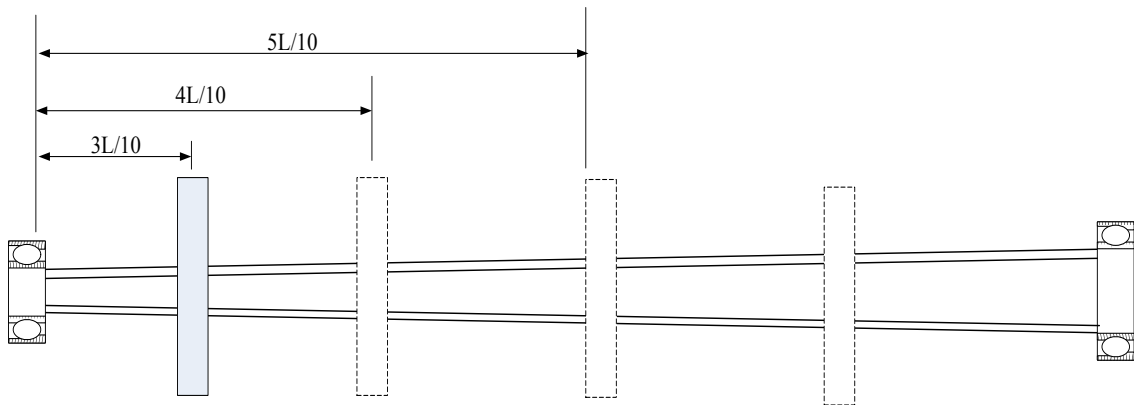


Figure 5.9 Tapered composite shaft with different positions of the disk.

Table 5.3 First critical speed in rpm of the tapered composite shaft for different taper angles and positions of the disk

Taper angle, degrees	The position of the disk				
	3L/10	4L/10	5L/10	6L/10	7L/10
0	5748	6602	7328	6602	5748
1	8144	9570	9760	8889	8159
2	10448	12011	11537	10829	10273
3	12532	13511	12903	12405	12033
4	14224	14408	13935	13639	13440
5	15285	15002	14699	14573	14527

Furthermore, the effect of the stacking sequence of the layers on the first critical speed of the tapered composite shaft is analyzed. Table 5.4 – Table 5.6 illustrate the first critical

speed for different stacking sequences and taper angles. The lay-up for the layers starts from inside, and there are ten layers with four different fiber orientation angles.

The layers near the outer surface have larger circumferences and volumes than those near the inner surface of the shaft, and they resist more bending moment than those layers that near form the inner surface; as a result, the outer surface layers control the stiffness of the shaft. Consequently, it can be observed from Table 5.4 – Table 5.6 that laying up the layers that have high stiffness near the outer side of the shaft increases the critical speed. For example, at a taper angle of  $4^\circ$ , the first critical speed of the configuration  $[0_6^\circ / 90^\circ / 45^\circ / -45^\circ / 90^\circ]$  is 13474 rpm, and in this configuration the layers that have fiber orientation of  $0^\circ$  are laid up on the inner side of the shaft. The layers with fiber orientation of  $0^\circ$  have higher stiffness than other layers, so laying up them near the outer surface increases the critical speed. Thus, the configuration  $[90^\circ / 45^\circ / -45^\circ / 90^\circ / 0_6^\circ]$ , where the layers with  $0^\circ$  fiber orientation are laid-up on the outer side of the shaft, has higher first critical speed than the other configurations in Table 5.4 – Table 5.5. Moreover, it can be observed from the Table 5.4 that the difference between the first critical speeds of the configurations A and E decreases when increasing the taper angle; for example, at  $0^\circ$ ,  $2^\circ$ , and  $4^\circ$  the differences in first critical speeds between the configurations A and E are 19%, 9.4%, and 5.1%, respectively. This is an indication that increasing the taper angle eliminates to some extent the effect of stacking sequence on the first critical speed and the natural frequencies.

Table 5.4 The first critical speed in rpm of the tapered composite shaft for different taper angles and stacking sequences obtained using Hermitian finite element model

Configuration	Stacking sequence	Taper angle, degrees				
		0°	1°	2°	3°	4°
A	[0 <sub>6</sub> <sup>0</sup> /90°/45°/-45°/90°]	6475	8949	10832	12324	13474
B	[90°/0 <sub>6</sub> <sup>0</sup> /45°/-45°/90°]	6821	9296	11151	12604	13713
C	[90°/45°/0 <sub>6</sub> <sup>0</sup> /-45°/90°]	7056	9514	11333	12744	13818
D	[90°/45°/-45°/0 <sub>6</sub> <sup>0</sup> /90°]	7328	9760	11537	12903	13931
E	[90°/45°/-45°/90°/0 <sub>6</sub> <sup>0</sup> ]	7707	10117	11853	13174	14164

Table 5.5 The first critical speed in rpm of the tapered composite shaft for different taper angles and stacking sequences determined using Lagrangian finite element model

Configuration	Stacking sequence	Taper angle, degrees				
		0°	1°	2°	3°	4°
A	[0 <sub>6</sub> <sup>0</sup> /90°/45°/-45°/90°]	6475	8962	10848	12333	13478
B	[90°/0 <sub>6</sub> <sup>0</sup> /45°/-45°/90°]	6821	9308	11166	12613	13718
C	[90°/45°/0 <sub>6</sub> <sup>0</sup> /-45°/90°]	7060	9530	11354	12758	13823
D	[90°/45°/-45°/0 <sub>6</sub> <sup>0</sup> /90°]	7328	9772	11551	12912	13935
E	[90°/45°/-45°/90°/0 <sub>6</sub> <sup>0</sup> ]	7707	10129	11868	13184	14167

Table 5.6 The first critical speed in rpm of the tapered composite shaft for different taper angles and stacking sequences determined using Hierarchical finite element model

Configuration	Stacking sequence	Taper angle, degrees				
		0°	1°	2°	3°	4°
A	$[0_6^{\circ}/90^{\circ}/45^{\circ}/-45^{\circ}/90^{\circ}]$	6456	8920	10787	12265	13418
B	$[90^{\circ}/0_6^{\circ}/45^{\circ}/-45^{\circ}/90^{\circ}]$	6798	9260	11099	12538	13653
C	$[90^{\circ}/45^{\circ}/0_6^{\circ}/-45^{\circ}/90^{\circ}]$	7032	9477	11278	12676	13751
D	$[90^{\circ}/45^{\circ}/-45^{\circ}/0_6^{\circ}/90^{\circ}]$	7295	9710	11467	12820	13855
E	$[90^{\circ}/45^{\circ}/-45^{\circ}/90^{\circ}/0_6^{\circ}]$	7668	10059	11776	13084	14078

In addition, Figure 5.10 – Figure 5.15 illustrate the mode shapes and Campbell diagrams for the tapered composite shaft with configuration of  $[90^{\circ}/45^{\circ}/-45^{\circ}/0_6^{\circ}/90^{\circ}]$  for three different taper angles. It can be observed that increasing the taper angle increases the natural frequency and affects the mode shape. These figures were obtained using the conventional-Hermitian finite element model

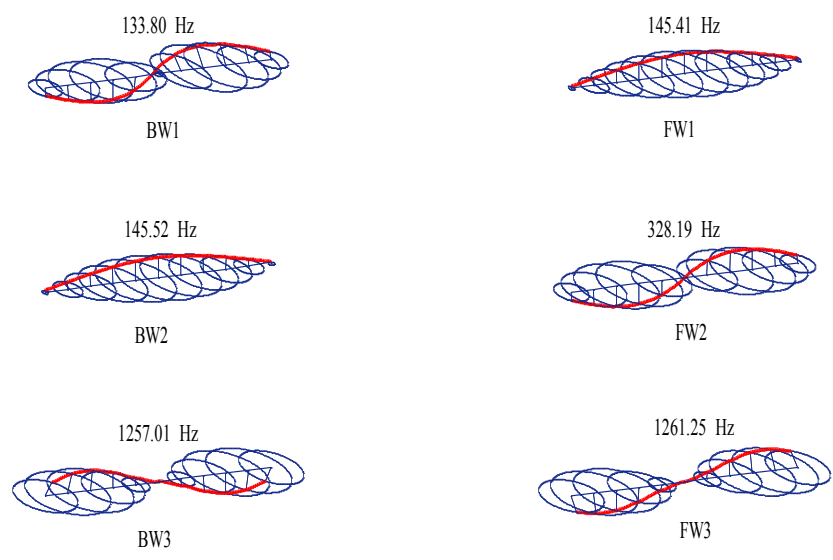


Figure 5.10 The mode shapes of the tapered composite shaft with taper angle of  $0^\circ$  at 6000 rpm

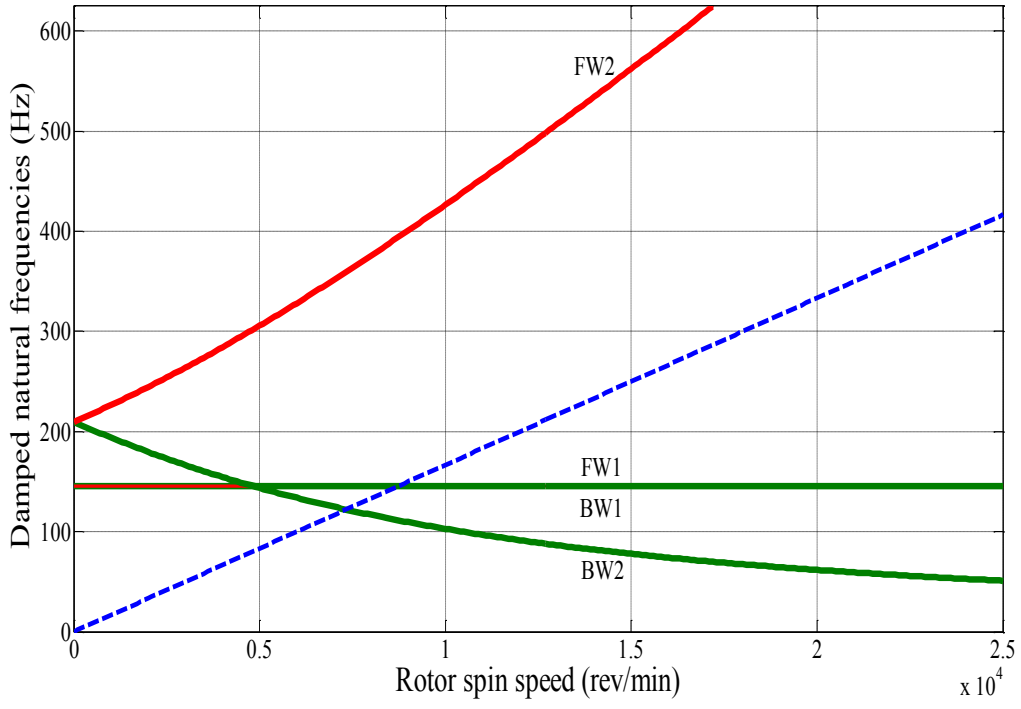


Figure 5.11 Campbell diagram of the tapered composite shaft with taper angle of  $0^\circ$ .

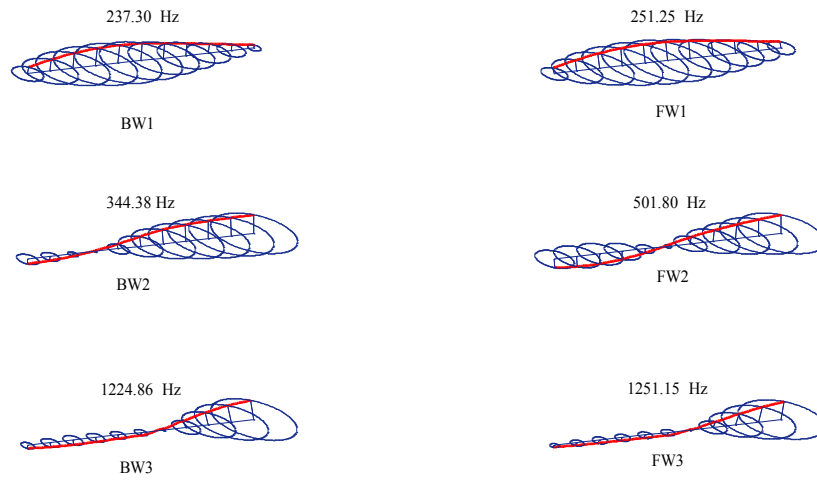


Figure 5.12 The mode shapes of the tapered composite shaft with taper angle of  $3^\circ$  at 6000 rpm

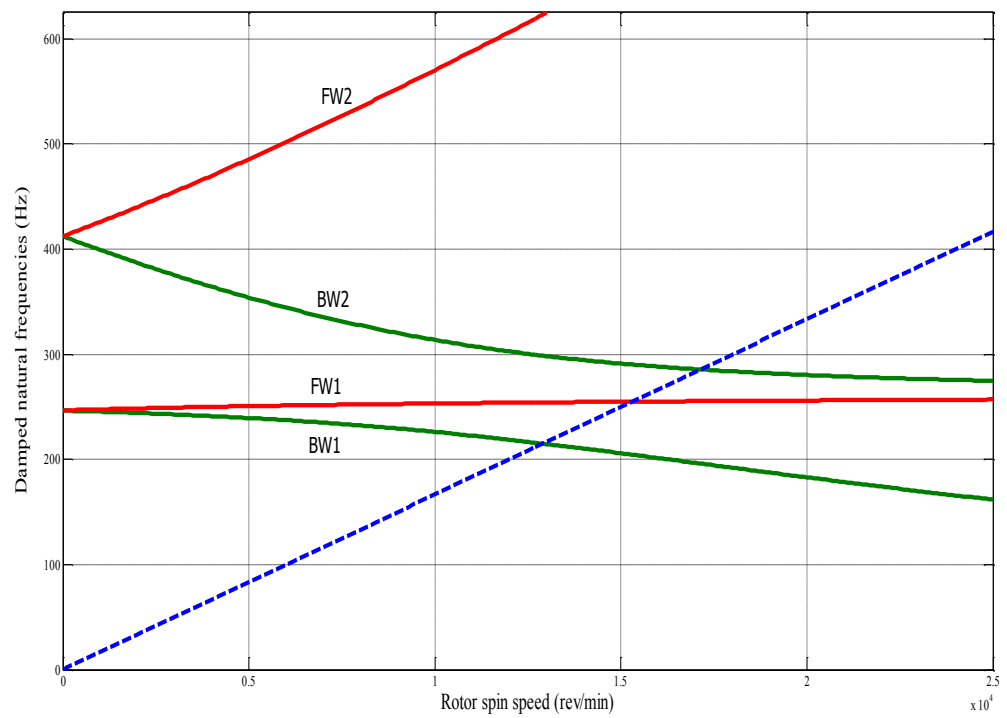


Figure 5.13 Campbell diagram of the tapered composite shaft with taper angle of  $3^\circ$ .

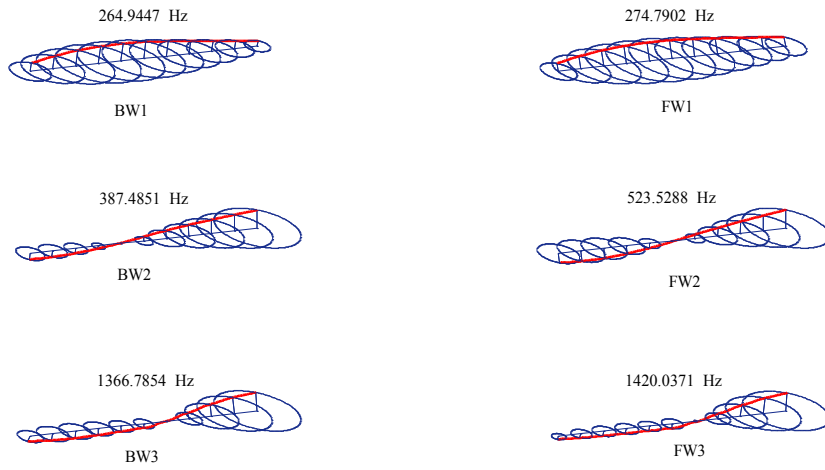


Figure 5.14 The mode shapes of the tapered composite shaft with taper angle of  $5^\circ$  at 6000 rpm

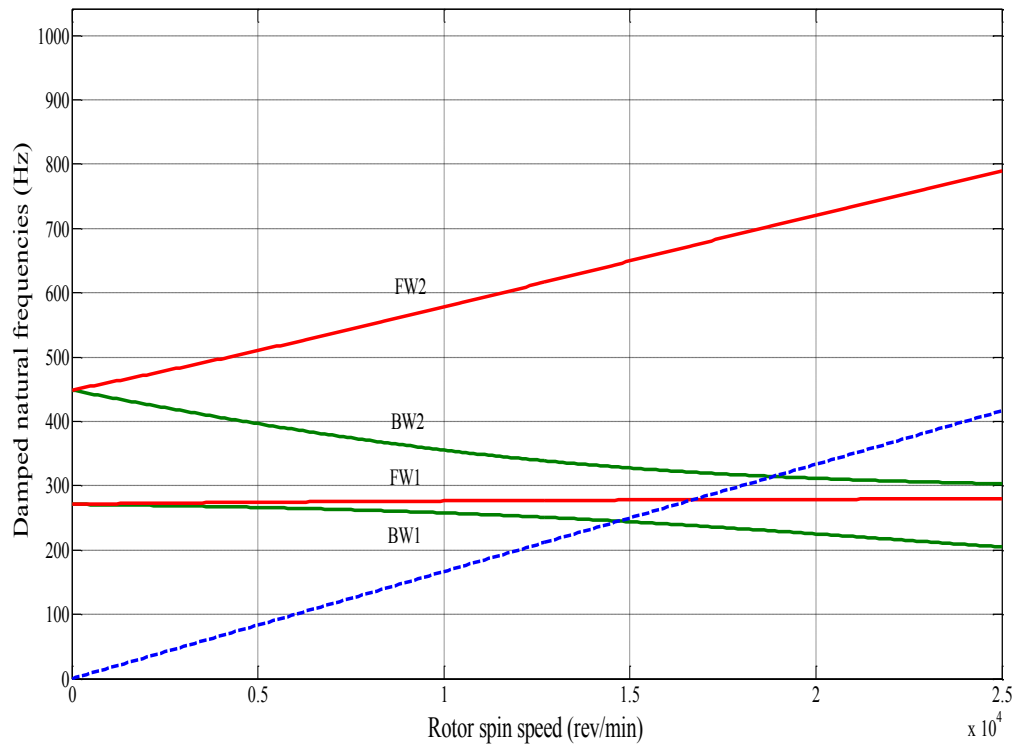


Figure 5.15 Campbell diagram of the tapered composite shaft with taper angle of  $5^\circ$ .

### 5.3 Tapered composite shaft Case B

In the following example, vibration of a tapered composite shaft subjected to different effects is studied. The tapered composite shaft is fixed by a bearing at one end and is free at the other end. The shaft is made of boron-epoxy composite material, and the properties of the composite material are listed in Table 4.1. The tapered composite shaft is made of ten layers, and the thickness of each layer is 0.25 mm. Also, the length of the shaft  $L$  is 0.5 m and the inner diameter  $d_i$  at the free end is 1 cm. The hierarchical finite element model only is used here, and seven elements of equal length are considered for the analysis.

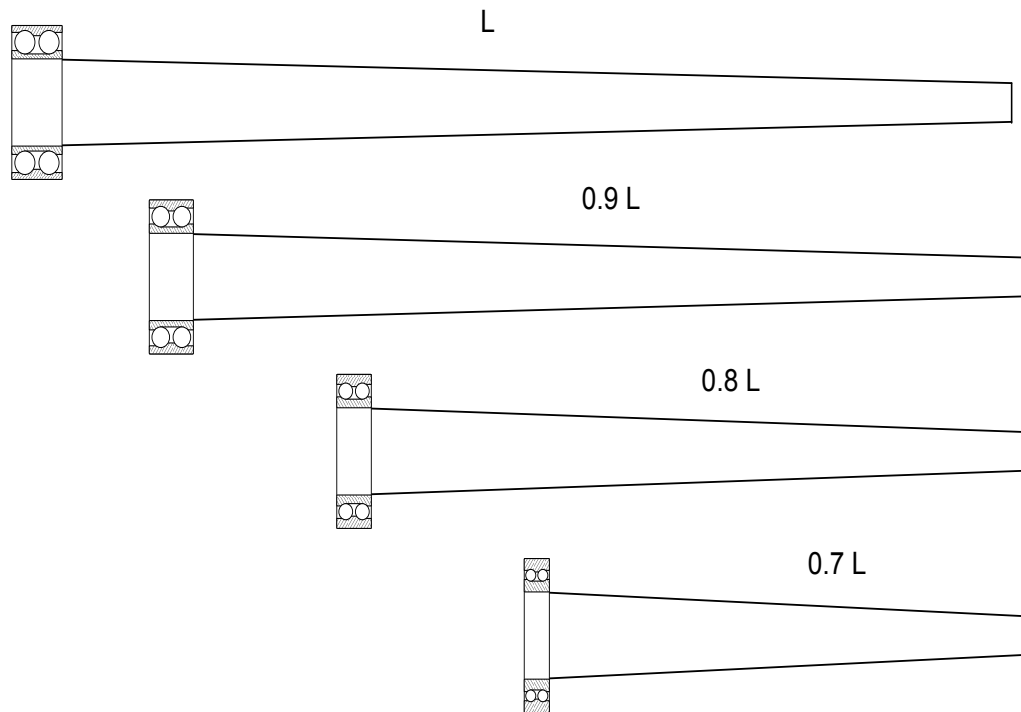


Figure 5.16 Different lengths of the tapered composite shaft.

### 5.3.1 Effect of length on natural frequencies and first critical speed

In this section, the effect of the length on the natural frequencies and first critical speed of the tapered composite shaft is discussed. Figure 5.16 shows the configuration of the tapered composite shaft with different lengths. The length of the tapered composite shaft changes from  $L$  to  $0.7L$  by 10 percent every time, and the natural frequencies and critical speeds were obtained for different taper angles for each length. The inner diameter at the free end of the tapered composite shaft is kept at 1 cm, whereas the inner diameter of the other end changes with the changing taper angle and length. The stiffness of the bearings  $K_{yy}$  and  $K_{zz}$  are 10 GN/m. The configuration of the tapered composite shaft is  $[90^\circ/45^\circ/-45^\circ/0_6^\circ/90^\circ]$  and the lay-up starts from inside. Table 5.7 and Table 5.8 show the natural frequencies and critical speeds, respectively, of the tapered composite shaft with different lengths and taper angles. Two rotational speeds, 0 rpm and 5,000 rpm, are considered to calculate the natural frequencies. One can observe from the tables that the natural frequencies and first critical speed increase either when the length decreases or when the taper angle increases.

Furthermore, Table 5.7 shows that, in this example, the gyroscopic effect does not influence the natural frequency. For instance, the first backward natural frequency at 0 rpm and 5,000 rpm are almost the same for all taper angles. The natural frequencies in Table 5.7 are obtained using the hierarchical finite element. Moreover, Figure 5.17 shows the first critical speeds obtained using the hierarchical finite elements. From the figures, the difference between the first critical speeds increases with an increasing taper angle.

Table 5.7 Natural frequencies in Hz of the tapered composite shaft with different lengths

Length, m	Rotational speed (rpm)	Mode	Taper angle, degrees					
			0°	1°	2°	3°	4°	5°
L = 0.5	0	BW1	416	737	1235	1272	1483	1658
		FW1	416	737	1235	1272	1483	1658
		BW2	1297	2001	2508	2876	3146	3348
		FW2	1297	2001	2508	2876	3146	3348
	5000	BW1	415	737	1022	1271	1482	1657
		FW1	416	738	1024	1273	1484	1660
		BW2	1297	2001	2507	2875	3145	3347
		FW2	1298	2002	2509	2876	3147	3349
0.9 L	0	BW1	511	864	1175	1444	1672	1860
		FW1	511	864	1175	1444	1672	1860
		BW2	1582	2335	2871	3258	3542	3754
		FW2	1582	2335	2871	3258	3542	3754
	5000	BW1	511	864	1175	1444	1671	1859
		FW1	512	865	1177	1446	1673	1862
		BW2	1582	2335	2870	3257	3541	3753
		FW2	1583	2336	2873	3260	3543	3755

0.8 L	0	BW1	644	1035	1376	1669	1914	2118
		FW1	644	1035	1376	1669	1914	2118
		BW2	1970	2774	3342	3748	4045	4269
		FW2	1970	2774	3341	3748	4045	4269
	5000	BW1	644	1034	1375	1667	1913	2117
		FW1	644	1036	1377	1669	1915	2120
		BW2	1969	2774	3341	3747	4045	4268
		FW2	1971	2775	3343	3750	4047	4270
0.7 L	0	BW1	835	1272	1648	1968	2236	2458
		FW1	835	1272	1648	1968	2236	2458
		BW2	2514	3371	3969	4395	4707	4941
		FW2	2514	3371	3969	4395	4707	4941
	5000	BW1	835	1271	1647	1968	2235	2457
		FW1	836	1273	1649	1970	2237	2459
		BW2	2514	3370	3968	4396	4706	4940
		FW2	2516	3372	3970	4397	4708	4942

Table 5.8 First critical speed in rpm of the tapered composite shaft with different lengths and taper angles

Length, m	Taper angle	First critical speed based on Hierarchical finite element, rpm
L = 0.5	0°	24952
	1°	44130
	2°	61079
	3°	75764
	4°	88166
	5°	98457
0.9 L	0°	30682
	1°	51702
	2°	70124
	3°	85987
	4°	99340
	5°	110410
0.8 L	0°	38613
	1°	61839
	2°	82001
	3°	99239
	4°	113690

	5°	125650
0.7 L	0°	50021
	1°	75917
	2°	98155
	3°	117100
	4°	132740
	5°	145730

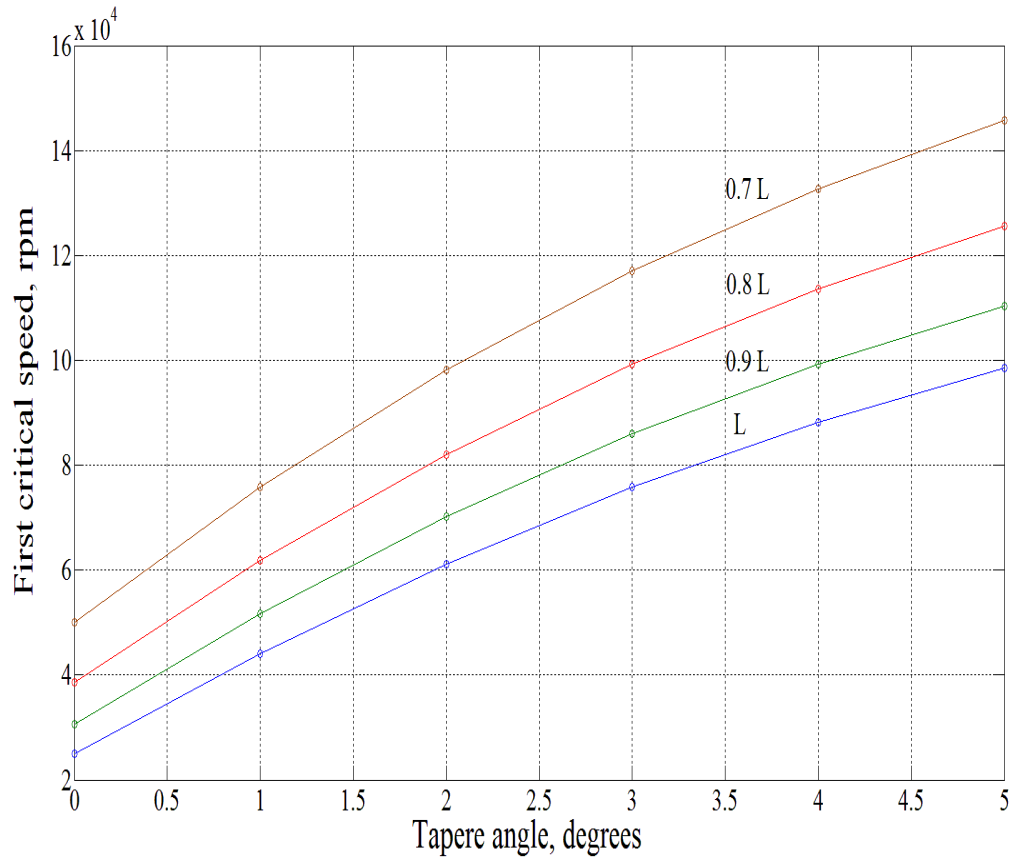


Figure 5.17 First critical speeds for different lengths determined using hierarchical finite

element

### **5.3.2 Effect of shaft diameter on natural frequencies and first critical speed**

In this section, the effect of the inner diameter on the natural frequencies and first critical speed is analyzed. The length of the tapered composite shaft  $L$  is fixed at 0.5 m and the configuration of the tapered composite shaft and the stiffness of the bearing are the same as in section 5.3.1. To see its influence on the natural frequencies and first critical speed of the rotating tapered composite shaft, the inner diameter  $d_i$  at the free end is 1 cm and it is varied from  $d_i$  to  $0.7d_i$ . The natural frequency results are illustrated in Table 5.9, and it can be observed that the natural frequency decreases when the inner diameter at the free end decreases.

In addition, the first critical speeds of the tapered composite shaft are represented in Table 5.10, and Figure 5.18. These show that reducing the inner diameter at the free end reduces the critical speed. Also, when the taper angle increases, the difference between first critical speeds decreases. For instance, when the taper angle is  $0^\circ$  the first critical speeds of the tapered composite shaft obtained using the hierarchical finite element are 24,952 rpm and 19,427 rpm for inner diameters  $d_i$  and  $0.7 d_i$ , respectively. But, when the taper angle is  $5^\circ$  the first critical speeds become 98,457 rpm and 96,671 rpm for  $d_i$  and  $0.7 d_i$ , respectively. The difference between first critical speed values for  $5^\circ$  is less than the difference for  $0^\circ$ .

Table 5.9 Natural frequencies in Hz of the tapered composite shaft at 5000 rpm for different diameters obtained using hierarchical finite element.

Diameter, cm	Mode	Taper angle, degrees					
		0°	1°	2°	3°	4°	5°
$d_i = 1$ cm	BW1	415	737	1022	1271	1482	1657
	FW1	416	738	1024	1273	1484	1660
	BW2	1297	2001	2507	2875	3145	3347
	FW2	1298	2002	2509	2876	3147	3349
0.9 $d_i$	BW1	385	709	998	1252	1467	1647
	FW1	386	710	1000	1254	1469	1649
	BW2	1208	1928	2451	2833	3114	3324
	FW2	1209	1930	2453	2835	3116	3327
0.8 $d_i$	BW1	354	680	9744	1232	1452	1636
	FW1	355	681	975	1234	1455	1639
	BW2	1117	1853	2393	2789	3082	3301
	FW2	1118	1855	2395	2791	3084	3303
0.7 $d_i$	BW1	323	651	950	1213	1438	1624
	FW1	323	653	951	1210	1440	1629
	BW2	1025	1776	2333	2744	3049	3277
	FW2	1026	1778	2335	2746	3051	3280

Table 5.10 First critical speed in rpm of the tapered composite shaft for different diameters.

Diameter, cm	Taper angle	First critical speed based on Hierarchical finite element, rpm
$d_i = 1 \text{ cm}$	$0^\circ$	24952
	$1^\circ$	44130
	$2^\circ$	61079
	$3^\circ$	75764
	$4^\circ$	88166
	$5^\circ$	98457
$0.9 d_i$	$0^\circ$	23118
	$1^\circ$	42453
	$2^\circ$	59661
	$3^\circ$	74636
	$4^\circ$	87313
	$5^\circ$	97597
$0.8 d_i$	$0^\circ$	21275
	$1^\circ$	40697
	$2^\circ$	58234
	$3^\circ$	73511
	$4^\circ$	86471

	5°	97242
0.7 d <sub>i</sub>	0°	19427
	1°	39054
	2°	56846
	3°	72394
	4°	85650
	5°	96671

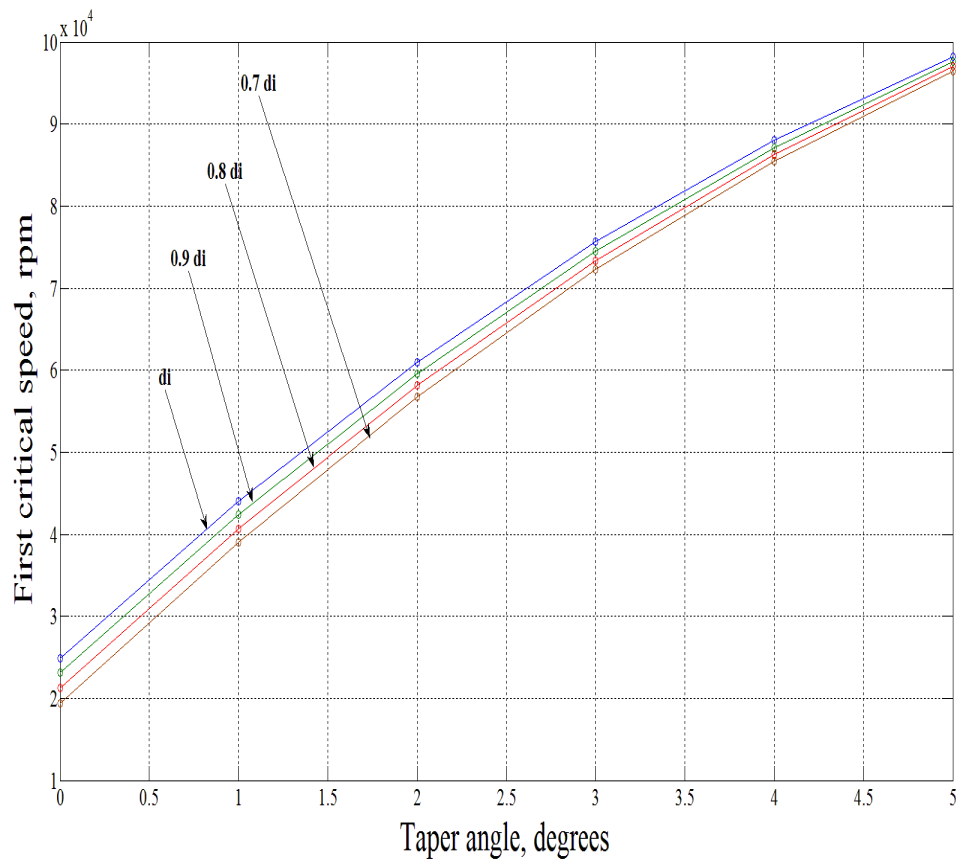


Figure 5.18 First critical speeds for different diameters obtained using hierarchical finite

element

### 5.3.3 Effect of fiber orientation on the natural frequencies and first critical speed

In the following example, the influences of ply orientation angle on natural frequencies and first critical speed of the tapered composite shaft are studied. The configuration and material properties of the tapered composite shaft from section 5.3.1 are considered. The ten layers have the same fiber orientation, and the lamination angles vary from  $0^\circ$  to  $90^\circ$  to investigate their effects on the natural frequencies and the first critical speed.

Table 5.11 – Table 5.13 present the natural frequency and first critical speed of the tapered composite shaft with different lamination angles. According to the results in the tables, the natural frequencies and first critical speed of the tapered composite shaft decrease with increasing fiber orientation angles of the layers and vice versa. Moreover, Figure 5.19 shows the first critical speeds that were obtained using hierarchical finite element. According to the results in Figure 5.19, at  $0^\circ$  taper angle, the first critical speeds of the tapered composite shaft are close to each other for fiber orientation angle  $45^\circ \leq \eta \leq 90^\circ$ , for example the first critical speed for  $45^\circ$  and  $90^\circ$  are 14796 rpm and 13934, respectively, and the difference between the two first critical speeds is 5.8 %. However when the taper angle is  $5^\circ$ , the variation between the first critical speeds for fiber orientation angle  $45^\circ \leq \eta \leq 90^\circ$  is clearly noticeable where the first critical speed for  $45^\circ$  is 70189 rpm and for  $90^\circ$  is 63428 rpm and the difference between the two critical speeds is 9.8 %.

Table 5.11 Natural frequencies in Hz of the tapered composite shaft at 5000 rpm with different fiber orientation angles obtained using hierarchical finite element - I

Fiber orientation angle	Mode	Taper angle, degrees					
		0°	1°	2°	3°	4°	5°
0°	BW1	469	810	1078	1281	1431	1542
	FW1	469	811	1079	1282	1432	1543
	BW2	1409	2039	2405	2629	2775	2878
	FW2	1410	2039	2405	2629	2776	2879
20°	BW1	316	563	788	988	1162	1312
	FW1	316	564	789	990	1165	1315
	BW2	1001	1581	2028	2374	2641	2848
	FW2	1002	1583	2031	2377	2644	2852
30°	BW1	270	487	692	886	1065	1228
	FW1	270	488	694	888	1068	1232
	BW2	866	1401	1850	2228	2547	2814
	FW2	867	1403	1853	2232	2552	2820
45°	BW1	244	445	640	831	1016	1192
	FW1	245	446	642	832	1019	1196
	BW2	790	1299	1749	2153	251	2839
	FW2	792	1300	1752	2158	2521	2847

Table 5.12 Natural frequencies in Hz of the tapered composite shaft at 5000 rpm with different fiber orientation angles obtained using hierarchical finite element - II

Fiber orientation angle	Mode	Taper angle, degrees					
		0°	1°	2°	3°	4°	5°
60°	BW1	236	432	624	813	999	1179
	FW1	237	433	626	816	1002	1183
	BW2	764	126	1707	2112	2480	2815
	FW2	765	126	1711	2117	2486	2822
70°	BW1	233	426	615	800	980	1154
	FW1	234	428	617	803	984	1158
	BW2	752	1238	1666	2049	2392	2698
	FW2	754	1240	1670	2053	2398	2704
80°	BW1	232	4223	605	782	951	1109
	FW1	233	4232	607	785	954	1113
	BW2	742	1208	1601	193	2225	2470
	FW2	744	1209	1604	194	2229	2475
90°	BW1	232	420	599	769	928	1073
	FW1	232	421	601	771	930	1076
	BW2	738	1186	1551	1851	2097	2299
	FW2	739	1188	1553	1854	2100	2302

Table 5.13 First critical speed in rpm of the tapered composite shaft with different fiber orientation angles

Fiber Orientation angle	Taper angle	First critical speed based on Hierarchical finite element, rpm
0°	0°	28140
	1°	48605
	2°	64648
	3°	76758
	4°	85717
	5°	92115
20°	0°	19208
	1°	34108
	2°	47642
	3°	59622
	4°	69956
	5°	78717
30°	0°	16403
	1°	29367
	2°	41612
	3°	52866
	4°	63147

	5°	72900
45°	0°	14796
	1°	26863
	2°	38558
	3°	49687
	4°	60886
	5°	70189
60°	0°	14242
	1°	25948
	2°	37432
	3°	48621
	4°	59429
	5°	69748
70°	0°	14036
	1°	25592
	2°	36784
	3°	47651
	4°	58095
	5°	68029

80°	0°	13938
	1°	25300
	2°	36138
	3°	46493
	4°	56269
	5°	65390
90°	0°	13934
	1°	25188
	2°	35785
	3°	45749
	4°	54983
	5°	63428

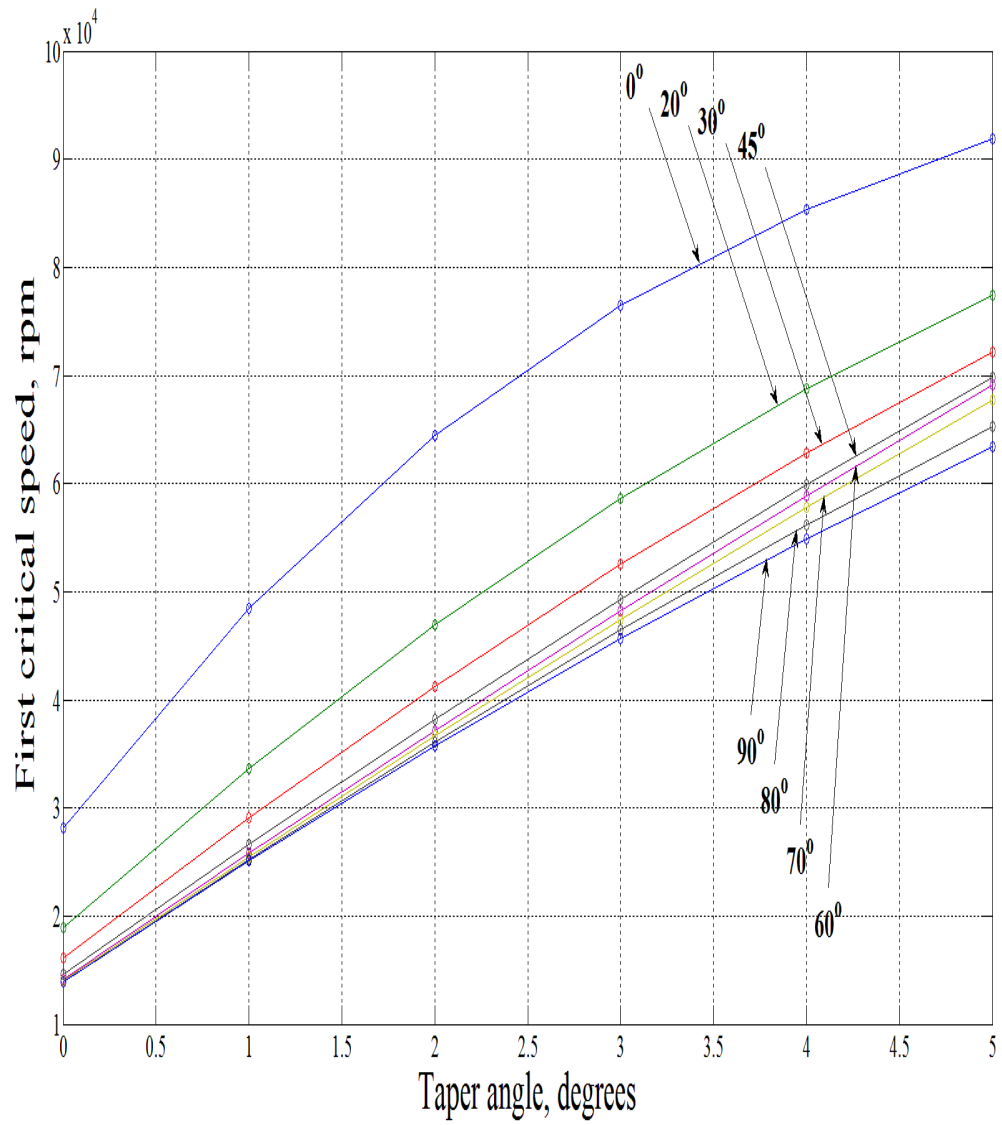


Figure 5.19 First critical speeds for different fiber orientation angles based on hierarchical finite element

#### **5.3.4 Effect of the stiffness of the bearing on the first critical speed**

This section shows how a bearing's stiffness can influence the first critical speed of the tapered composite shaft. This analysis is conducted using the tapered composite shaft from section 5.3.1. The stiffness of the bearing varies from 0.01 MN/m to 10 GN/m. Figure 5.20 presents the variation of the first critical speed of the tapered composite shaft for various levels of bearing stiffness.

The figure shows that, at low bearing stiffness, increasing the taper angle decreases the first critical speed; despite the fact that, at high bearing stiffness, increasing the taper angle increases the first critical speed. In addition, it can be observed from the figure that at a small taper angle the required stiffness for the bearing to be considered as simply supported condition, which is the condition that increasing the stiffness of the bearing does not affect the first critical speed and the natural frequencies any more, is lower than the stiffness required for the bearing at large taper angle.

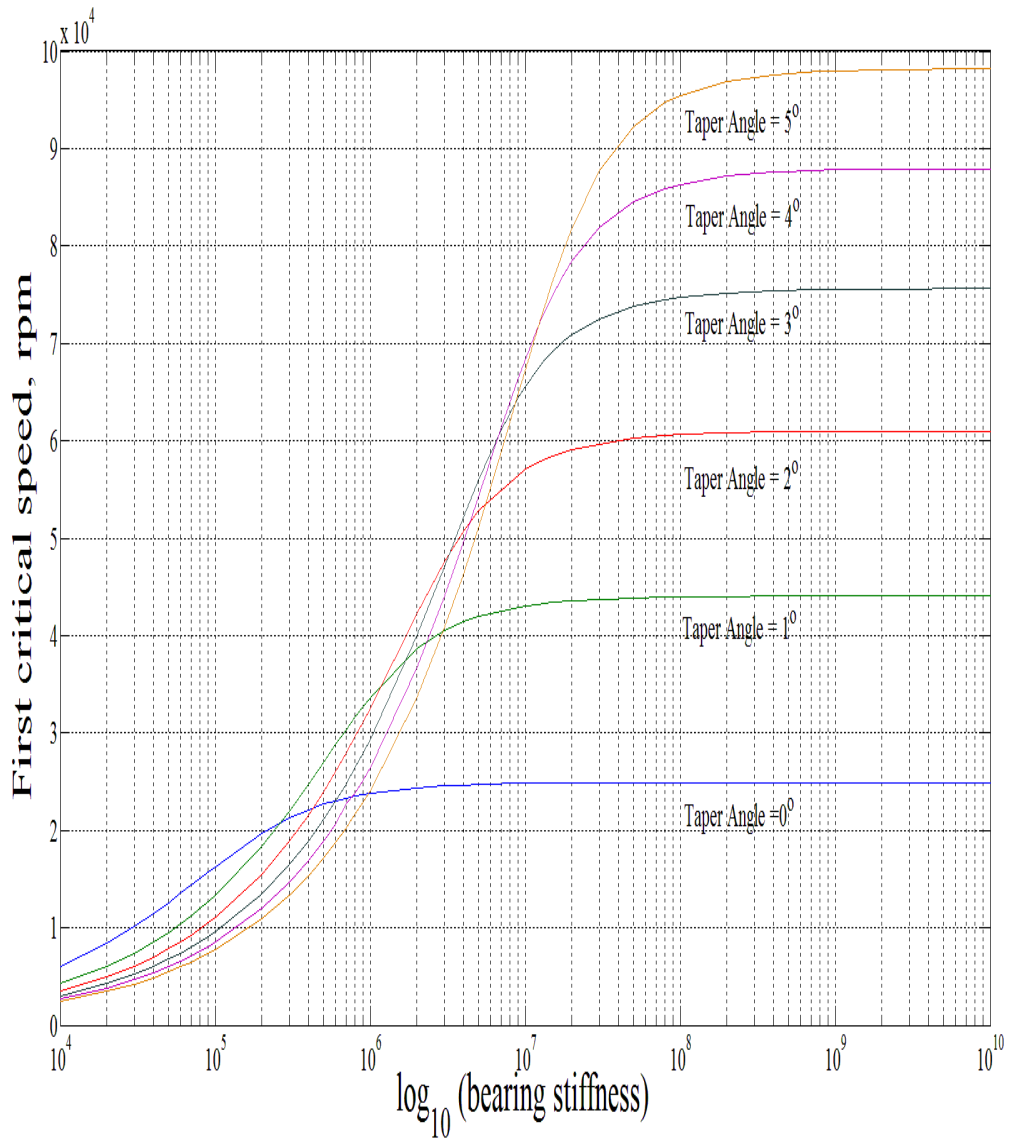


Figure 5.20 First critical speed for different bearing stiffness values determined using hierarchical finite element.

### **5.3.5 Effect of axial load on natural frequencies and first critical speed**

To study the consequence, on the natural frequencies and first critical speed, of applying axial load, the tapered composite shaft in section 5.3.1 is considered. The tensile and compressive loads are applied at the free end of the tapered composite shaft, and the compressive loads are less than the buckling loads. The results of the natural frequencies and first critical speed of applying the tensile and compressive loads on the tapered composite shaft are illustrated in Table 5.14, Table 5.15 and Figure 5.21 – Figure 5.26. The natural frequencies and critical speeds are obtained using the hierarchical finite element.

According to the results in the tables and figures, the tensile load increases and the compressive load decreases the natural frequency and critical speed. This is because the tensile load increases the stiffness of the tapered composite shaft, while the compressive load decreases it. In addition, increasing the taper angle increases the natural frequency and the first critical speed for both the tensile and compressive loads.

Table 5.14 Natural frequencies in Hz of the tapered composite shaft at 5000 rpm with different tensile loads using the hierarchical finite element

Tensile Load (KN)	Mode	Taper angle, degrees					
		0°	1°	2°	3°	4°	5°
1	BW1	433	744	1027	1274	1484	1659
	FW1	434	746	1029	1276	1486	1662
	BW2	1311	2008	2512	2878	3148	3349
	FW2	1312	2010	2514	2880	3149	3351
3	BW1	463	759	1037	1281	1489	1664
	FW1	464	760	1038	1283	1491	1665
	BW2	1339	2022	2522	2886	3154	3354
	FW2	1334	2024	2524	2888	3156	3357
6	BW1	506	781	1051	1291	1497	1669
	FW1	507	782	1052	1293	1499	1672
	BW2	1379	2043	2536	2897	3162	3361
	FW2	1380	2045	2538	2899	3166	3364
9	BW1	545	802	1064	1301	1504	1675
	FW1	546	803	1066	1303	1507	1677
	BW2	1418	2064	2550	2908	3171	3369
	FW2	1418	2066	2553	2910	3173	3371

Table 5.15 Natural frequencies in Hz of the tapered composite shaft at 5000 rpm with different compressive loads using hierarchical finite element

Compressive Load (KN)	Mode	Taper angle, degrees					
		0°	1°	2°	3°	4°	5°
1	BW1	398	729	1018	1268	1479	1655
	FW1	398	731	1019	1270	1481	1658
	BW2	1283	1993	2502	2871	3142	3345
	FW2	1284	1996	2504	2873	3144	3346
3	BW1	361	713	1008	1261	1474	1651
	FW1	362	715	1006	1263	1477	1654
	BW2	1254	1979	2492	2864	3136	3340
	FW2	1255	1981	2494	2866	3138	3342
6	BW1	295	688	993	1250	1466	1645
	FW1	296	690	995	1253	1468	1648
	BW2	1210	1957	2477	2852	3127	3332
	FW2	1211	1958	2479	2855	3129	3335
9	BW1	214	662	977	1240	1459	1639
	FW1	214	663	979	1242	1461	1641
	BW2	1163	1934	2463	2841	3118	3325
	FW2	1165	1936	2464	2843	3120	3327

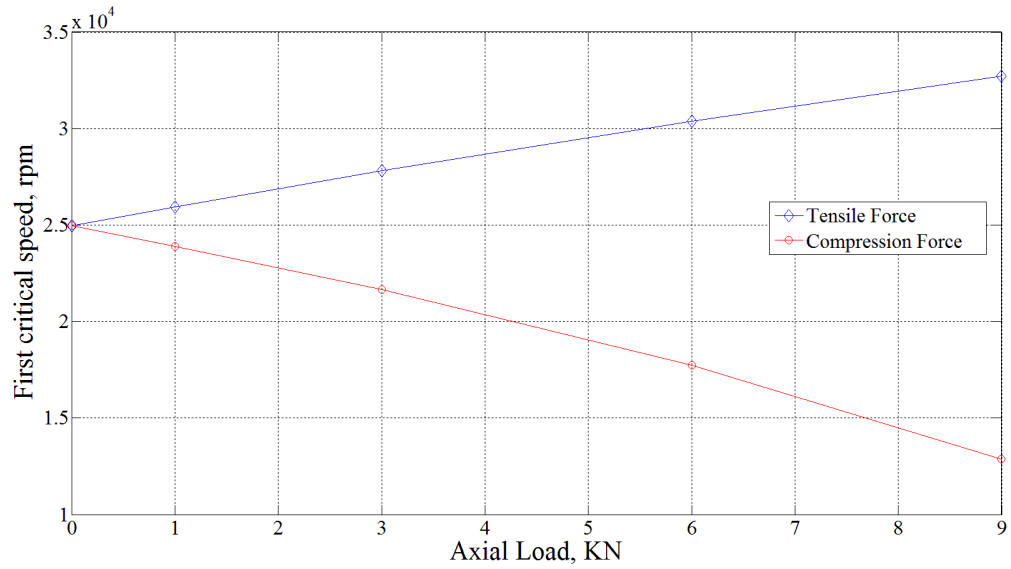


Figure 5.21 First critical speed of the tapered composite shaft with taper angle of  $0^\circ$  for different axial loads obtained using hierarchical finite element

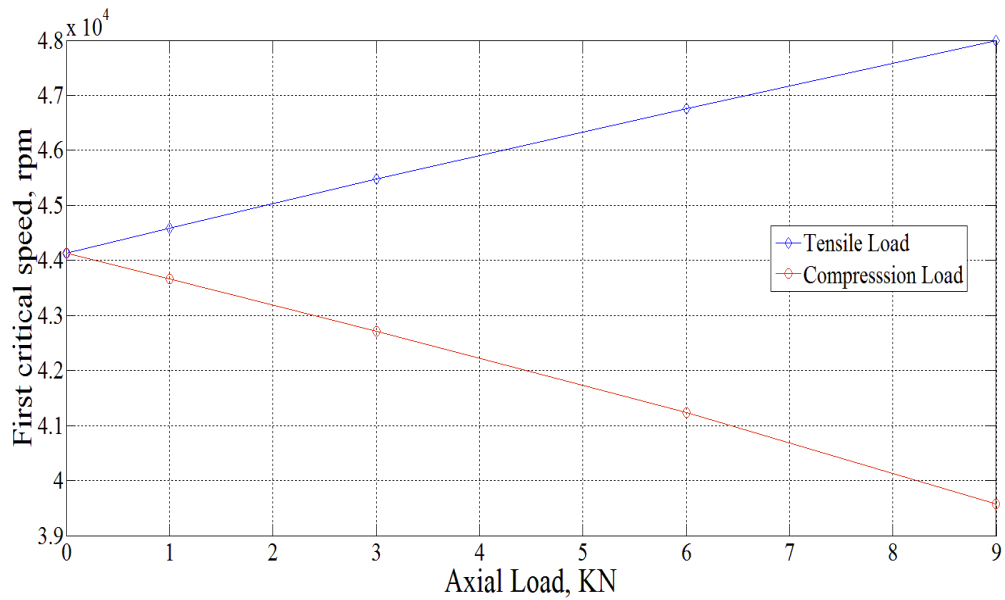


Figure 5.22 First critical speed of the tapered composite shaft with taper angle of  $1^\circ$  for different axial loads obtained using hierarchical finite element

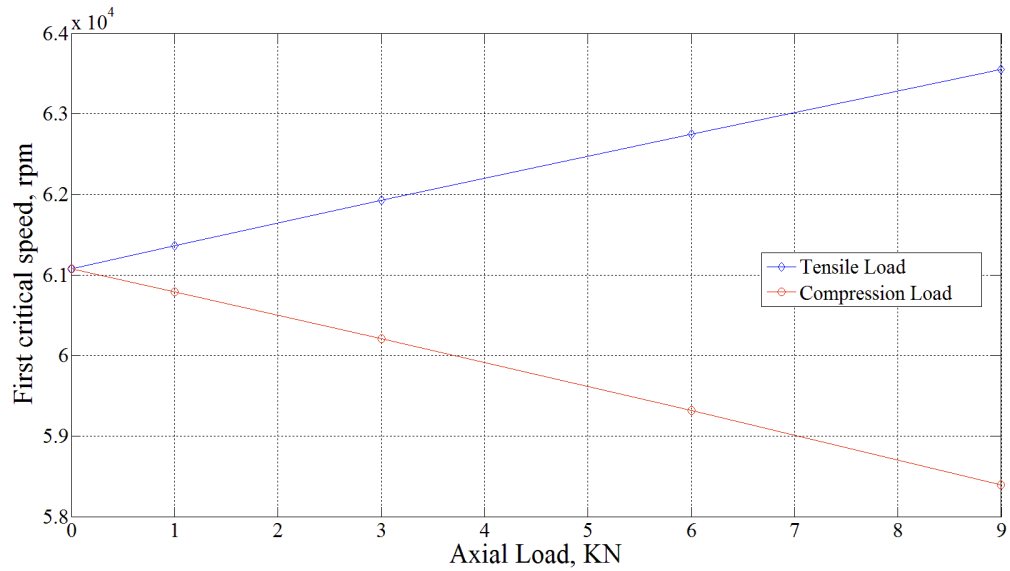


Figure 5.23 First critical speed of the tapered composite shaft with taper angle of  $2^\circ$  for different axial loads obtained using hierarchical finite element

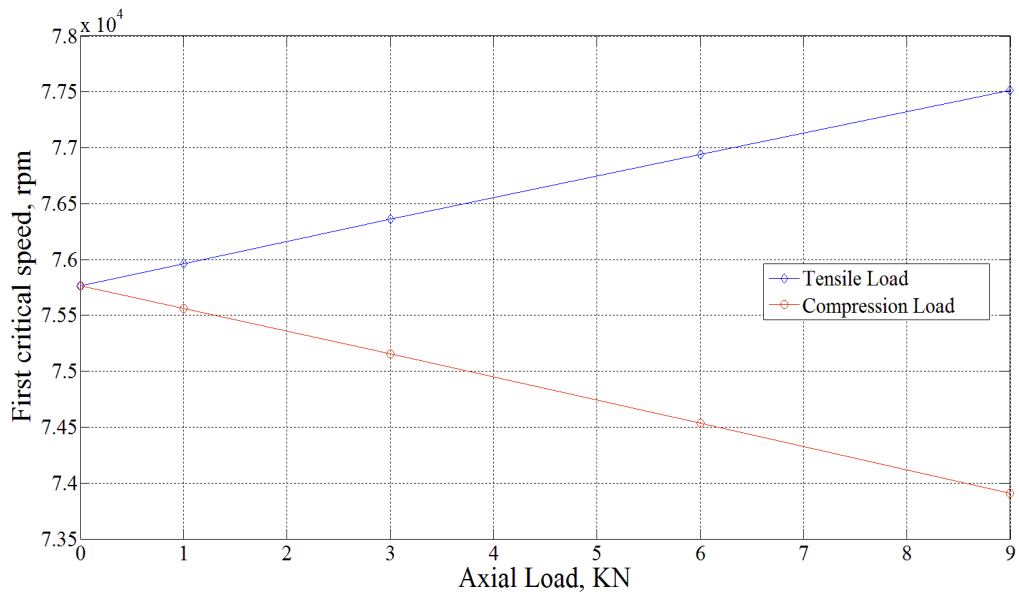


Figure 5.24 First critical speed of the tapered composite shaft with taper angle of  $3^\circ$  for different axial loads obtained using hierarchical finite element

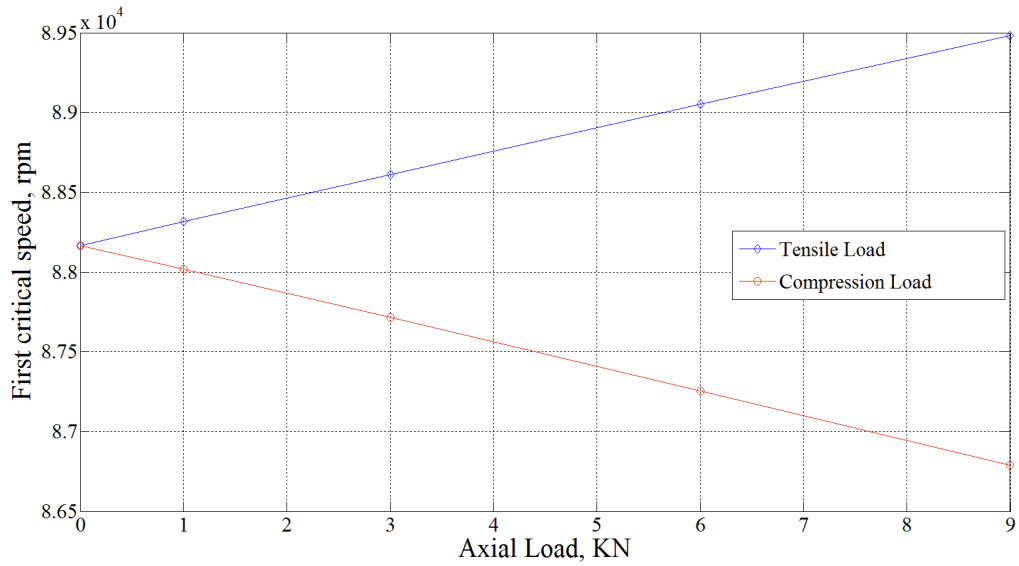


Figure 5.25 First critical speed of the tapered composite shaft with taper angle of  $4^\circ$  for different axial loads obtained using hierarchical finite element

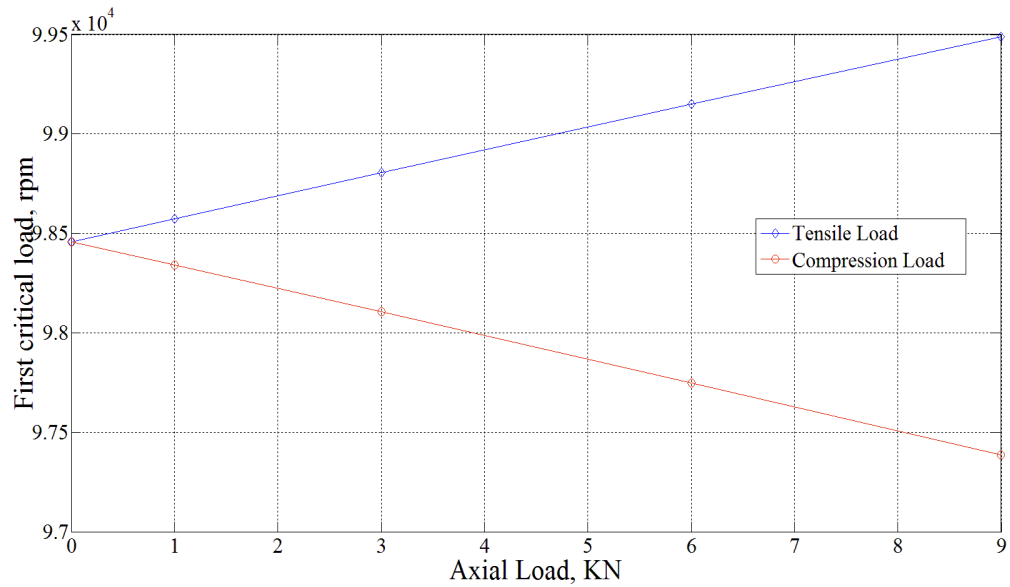


Figure 5.26 First critical speed of the tapered composite shaft with taper angle of  $5^\circ$  for different axial loads obtained using hierarchical finite element

### 5.3.6 Effect of the disk on the natural frequencies and first critical speed

Another factor that can influence the natural frequencies and critical speeds of the tapered composite shaft is the attached disk. Therefore, this section discusses the influence of the disk's mass on the natural frequencies and first critical speeds. The tapered composite shaft in section 5.3.1 is considered for the analysis, and Figure 5.27 shows the tapered composite shaft with the attached disk. The disk is attached at the free end of the shaft, the thickness of the disk is 0.02 m, and the outer and inner diameters of the disk are 0.06 m and 0.015 m, respectively. Table 5.16 and Table 5.17 illustrate the natural frequencies and first critical speed of the tapered composite shaft for different disk masses, and the results in Table 5.16 were obtained using the hierarchical finite element. From the tables, one can observe that increasing the density reduces the natural frequencies and first critical speed; thus, to eliminate the effect of the disk's density, increasing the taper angle can be helpful because increasing the taper angle can increase the natural frequencies and first critical speed.

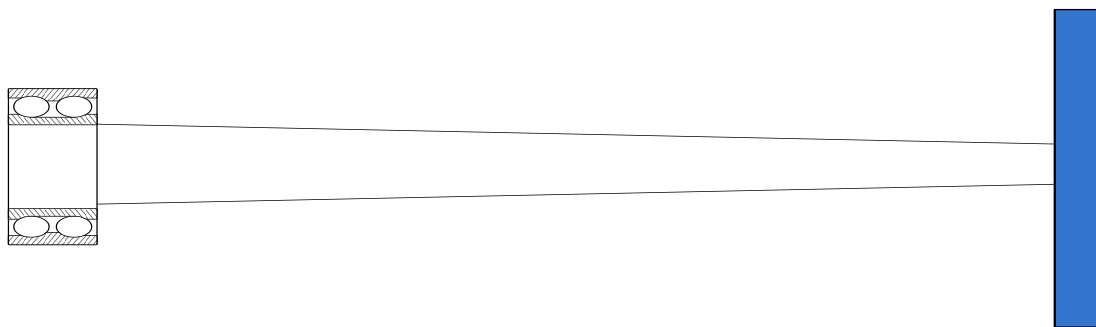


Figure 5.27 The tapered composite shaft with the attached disk

Table 5.16 Natural frequencies in Hz of the tapered composite shaft at 5000 rpm with different material densities of the disk

Density Kg/m <sup>3</sup>	Mode	Taper angle, degrees					
		0°	1°	2°	3°	4°	5°
1000	BW1	300	491	653	796	920	1029
	FW1	302	494	657	800	925	1033
	BW2	1039	1555	1931	2209	2418	2575
	FW2	1047	1566	1942	2221	2428	2585
4000	BW1	267	421	543	645	729	798
	FW1	275	429	552	653	738	807
	BW2	928	1347	1650	188	2074	2229
	FW2	960	1393	1705	1944	2133	2286
8000	BW1	252	395	507	5978	671	731
	FW1	267	411	522	613	686	746
	BW2	820	1136	1359	1534	1680	1808
	FW2	878	1218	1452	1633	1782	1911
12000	BW1	241	378	484	570	640	696
	FW1	262	401	507	593	662	718
	BW2	738	997	1177	1319	1439	1545
	FW2	812	1090	1278	1425	1548	1656

Table 5.17 The first critical speed in rpm of the tapered composite shaft for different material densities of the disk

Density, Kg/m <sup>3</sup>	Taper angle, degrees	First critical speed based on Hierarchical finite element, rpm
1000	0	17840
	1	29160
	2	38847
	3	47394
	4	54942
	5	61590
4000	0	15556
	1	24369
	2	31422
	3	37359
	4	42416
	5	46746
8000	0	14318
	1	22091
	2	28189
	3	33273
	4	37588

	5	41278
12000	0	13385
	1	20435
	2	25915
	3	30484
	4	34385
	5	37754

#### 5.4 Summary

In this chapter a comprehensive parametric study of the tapered composite shaft is carry out. Two cases are considered. In case A the tapered composite shaft with a disk at the center and with two bearings at the ends, is considered; the hierarchical, the Lagrangian, and the conventional-Hermitian finite element models are used to study the effects of the taper angle and stacking sequence on the natural frequencies and first critical speeds. Furthermore, in case B the effects of the length, diameter, fiber orientation angle, bearing stiffness, axial load and disk's mass on the natural frequencies and first critical speeds are studied; the tapered composite shaft is fixed by bearing at one end and is free at the other end. In case B the results of the natural frequencies and first critical speeds are determined using the hierarchical finite element model.

## Chapter 6

### Conclusions, contributions, and future work

#### 6.1 Conclusions

In the present dissertation three finite element models have been developed for rotordynamic analysis of the tapered composite shaft. These models were developed using the hierarchical finite element formulation, Lagrangian finite element formulation, and conventional-Hermitian finite element formulation. The three finite element models are based on Timoshenko beam theory, and the effects of rotary inertia, transverse shear deformation, gyroscopic force, axial load, coupling due to the lamination of composite layers, and taper angle are incorporated in the three finite element models of the tapered composite shaft.

In order to validate the three finite element models, Rayleigh - Ritz method is used to obtain an approximate solution for simply supported tapered composite shaft. In chapter 4 a numerical example is given, and it is found that the bending natural frequencies and first critical speeds, for different taper angles of the tapered composite shaft, determined using Rayleigh-Ritz method are in agreement with those obtained using the hierarchical, the Lagrangian, and the conventional-Hermitian finite element models.

In this thesis, the tapered composite shaft means that the inner and outer diameters of one end are constant while the inner and outer diameters of the other end increase with increasing the taper angle. Consequently, it is found that increasing the taper angle

increases the bending natural frequencies and first critical speed of the tapered composite shaft. However, it is seen from the numerical results of Case A in chapter 5 that this direct relationship between the first critical speed and the taper angle does not sustain because the first critical speed reaches its maximum value at  $10^\circ$  and then starts to drop off with increasing the taper angle.

In chapter 5 an extensive parametric study of the rotordynamic response of tapered composite shaft is presented, and the effects of stacking sequence, fiber orientation angles, taper angle, axial load, bearing stiffness, disk's position, the inner diameter, and the length of the tapered composite shaft are studied. The important points that can be said about the results in chapter 5 are the following:

- ✓ Stacking the layers that have high stiffness near the outer surface of the shaft increases the natural frequencies and first critical speed; because the layers near the outer surface have higher volume and circumference than those near the inner surface of the shaft.
- ✓ Increasing the taper angle when using low stiffness bearing decreases the first critical speed; whereas, increasing the taper angle when using high stiffness bearing increases the first critical speed.
- ✓ The natural frequencies and first critical speed of the tapered composite shaft increase with applying tensile load and decrease with applying compressive load along the axial coordinate of the tapered composite shaft.

- ✓ Decreasing the length of the tapered composite shaft and increasing the diameter increase the natural frequencies and the first critical speed and vice versa.

## **6.2 Contributions**

Using the conventional – Hermitian finite element formulation and following the same procedure as in References [8,25] to obtain the finite element model for uniform metal driveshaft, the author of this thesis develops in chapter 3 a finite element model for uniform composite driveshaft based on Timoshenko beam theory and uses this model to carry out rotordynamic analysis of the stepped composite shaft.

Three finite element models for tapered composite shaft are developed. These models are developed using:

- 1) The hierarchical finite element formulation.
- 2) The Lagrangian finite element formulation.
- 3) The conventional-Hermitian finite element formulation.

## **6.3 Future work**

Rotordynamic analysis of the tapered and the uniform composite shafts can be continued, and the following recommendations can be considered:

- ✓ Using any one of the three finite element models, dynamic stability of the tapered composite shaft can be studied.

- ✓ The effect of damping on the response of the tapered composite shaft can be considered.
- ✓ The Rayleigh-Ritz model of the tapered composite shaft can be extended to include the effect of the rigid disk and the bearings rather than considering only the simply supported condition as it has been done in this thesis.
- ✓ Manufacturing the tapered composite shaft using the advanced fiber placement machine and performing experimental rotordynamic analysis.
- ✓ One of the new applications of the composite material in oil and gas industries is manufacturing the drill pipe using the composite materials; the drill pipe is part of the drillstring which is considered as driveshaft. The present work can be extended to develop a finite element model for drillstring made of composite materials and to perform the rotordynamic analysis.

## References

- [1] M. Friswell, J. Penny, S. Garvey, and A. Lees, *Dynamics of Rotating Machines*, First edition, Cambridge University Press, 2010.
- [2] I. Daniel, and O. Ishai, *Engineering of Mechanics of Composite Materials*, Second edition, Oxford University Press, 2006.
- [3] S.V. Hoa, *Principles of the Manufacturing of Composite Materials*, DEStech Publications, 2009.
- [4] R.L Ruhl, "Dynamics of Distributed Parameter Turbo-rotor Systems: Transfer Matrix and Finite Element Techniques," Ph.D. Thesis, Cornell University, Ithaca, New York, 1970.
- [5] H.D. Nelson, and J. N. McVaugh, "The Dynamics of Rotor-Bearing Systems Using Finite Elements," ASME, Journal of Engineering for Industry, Vol. 98, No. 2, pp. 593-600, 1976.
- [6] E.S. Zorzi, and H.D. Nelson, "The dynamics of rotor-bearing systems with axial torque," ASME, Journal of Mechanical Design, Vol. 102, pp. 158–161, 1980.
- [7] E.S. Zorzi, and H.D. Nelson, "Finite element simulation of rotor-bearing systems with internal damping," ASME, Journal of Engineering for Power, Vol. 99, pp. 71-76, 1977.
- [8] H. D. Nelson, "A Finite Rotating Shaft Element Using Timoshenko Beam Theory," ASME, Journal of Mechanical Design, Vol.102, pp. 793-804, 1980.

- [9] L.W. Chen and D.M. Ku, "Dynamic stability analysis of a rotating shaft by the finite element method," *Journal of Sound and Vibration*, Vol.143, pp. 143–151, 1999.
- [10] L.M. Greenhill, W.B. Bickford, and H.D. Nelson, "A conical beam finite element for rotor dynamics analysis," *Journal of Vibration and Acoustics*, Vol. 107, pp. 421-430, 1985.
- [11] G. Genta, and A. Gugliotta, "A conical element for finite element rotor dynamics," *Journal of Sound and Vibration*, Vol. 120, pp.175-182, 1988.
- [12] M. A. Mohiuddin, and Y.A. Khulief, "Modal characteristics of rotors using a conical shaft finite element," *Journal of Computer Methods in Applied Mechanics and Engineering*, Vol. 115, pp. 125-144, 1994.
- [13] H. Zinberg, and M.F. Symonds, "The Development of an Advanced Composite Tail Rotor Driveshaft," *The 26th Annual Forum of the American Helicopter Society*, Washington, DC, 1970.
- [14] L. Hetherington, R. Kraus, and M. Darlow, "Demonstration of a supercritical composite helicopter power transmission shaft," *Journal of American Helicopter Society*, Vol.40, pp. 50-56, 1995.
- [15] S.P. Singh, and K. Gupta, "Composite shaft rotordynamic analysis using a layerwise theory," *Journal of Sound and Vibration*, Vol. 191 (5), pp. 739–756, 1996.

- [16] H.B.H. Gubran, and K. Gupta, "The effect of stacking sequence and coupling mechanisms on the natural frequencies of composite shafts," *Journal of Sound and Vibration*, Vol.282, pp. 231–248, 2005.
- [17] C.D. Kim, and C.W. Bert, "Critical speed analysis of laminated composite, hollow drive shafts," *Composites Engineering*, Vol.3, pp. 633-643, 1993.
- [18] H.-T. Hu and Wang K.-L, "Vibration Analysis of Rotating Laminated Cylindrical Shells," *AIAA Journal*, Vol. 45(8), pp. 2051–2061, 2007.
- [19] Chen L.-W. and Peng W.-K., "Dynamic stability of rotating composite shaft under periodical axial compressive loads," *Journal of Sound and Vibration*, Vol.212 (2), pp. 215–230, 1998.
- [20] M.-Y. Chang, J.-K. Chen and C.-Y. Chang, "A simple spinning laminated composite shaft model," *International Journal of Solids and Structures*, Vol.41, pp.637–662, 2004.
- [21] M.-Y. Chang, J. H. Huang, and C.-Y. Chang, "Vibration analysis of rotating composite shafts containing randomly oriented reinforcements," *Composite structures*, Vol.63 (1), pp. 21–32, 2004.
- [22] A. Boukhalfa, and A. Hadjoui, "Free vibration analysis of a rotating composite shaft using the p-version of the finite element method," *International Journal of Rotating Machinery*, Vol.2008, Article ID 752062, pp. 10, 2008.

- [23] A. Boukhalifa, and A. Hadjoui, "Free vibration analysis of an embarked rotating composite shaft using the hp-version of the FEM," *Latin American Journal of Solids and Structures*, Vol. 7, pp.105–141, 2010.
- [24] W. Kim, "Vibration of rotating tapered composite shaft and applications to high speed cutting," PhD Thesis, Michigan University, USA, 1999.
- [25] S.L. Edney, C.H.J. Fox, and E.J. Williams, "Tapered Timoshenko finite elements for rotordynamics analysis," *Journal of Sound and Vibration*, Vol.137 (3), pp. 463-481, 1990.
- [26] W.J. Chen and E.J. Gunter, *Introduction to Dynamics of Rotor-Bearing Systems*, First edition, Trafford Publishing, 2007.
- [27] S. Dharmarajan and H. McCutchen, " *Journal of Composite Materials*, Vol.7, pp530–535, 1973.
- [28] C.W. Bert, "The effect of bending-twisting coupling on the critical speed of driveshaft," In *Proceedings, 6th Japan-US conference on Composite Materials*, pp.29-36, Orlando, FL. Technomic, Lancaster, 1992.
- [29] C.W. Bert, and C.D. Kim, "Whirling of composite-material driveshaft including bending-twisting coupling and transverse shear deformation," *Journal of Vibration and Acoustics*, Vol.117, pp. 17-21, 1995.
- [30] H. L. M. Dos Reis, R. B. Goldman, and P. H. Verstrate, "Thin-walled laminated composite cylindrical tubes - part III: critical speed analysis," *Journal of composites Technology and Research*, Vol. 9(2), pp. 58-62, 1987.

- [31] R. Ganesan, *Finite Element Method in Machine Design*, Class notes, Mechanical and Industrial Engineering Department, Concordia University.

## Appendix A

### Uniform Composite shaft-Conventional finite element

The displacement field of the shaft element in terms of nodal displacements and shape functions is

$$\begin{bmatrix} v \\ w \\ \beta_y \\ \beta_z \end{bmatrix} = \begin{bmatrix} N_{t1} & 0 & 0 & N_{t2} & N_{t3} & 0 & 0 & N_{t4} \\ 0 & N_{t1} & -N_{t2} & 0 & 0 & N_{t3} & -N_{t4} & 0 \\ 0 & -N_{r1} & N_{r2} & 0 & 0 & -N_{r3} & N_{r4} & 0 \\ N_{r1} & 0 & 0 & N_{r2} & N_{r3} & 0 & 0 & N_{r4} \end{bmatrix} \begin{bmatrix} v_1 \\ w_1 \\ \beta_{y1} \\ \beta_{z1} \\ v_2 \\ w_2 \\ \beta_{y2} \\ \beta_{z2} \end{bmatrix} \quad (\text{A.1})$$

The kinetic energy of the uniform composite shaft is

$$T_{comp} = \frac{1}{2} \int_0^L m_c (\dot{v}^2 + \dot{w}^2) dx + \frac{1}{2} \int_0^L I_{dc} (\dot{\beta}_y^2 + \dot{\beta}_z^2) dx - \int_0^L I_{pc} \Omega \dot{\beta}_z \beta_y dx \quad (\text{A.2})$$

The strain energy of the uniform composite shaft due to axial load is

$$U_F = \frac{1}{2} \int_0^L P \left[ \left( \frac{\partial v}{\partial x} \right)^2 + \left( \frac{\partial w}{\partial x} \right)^2 \right] dx \quad (\text{A.3})$$

The strain energy of the uniform composite shaft due to bending moments and shear forces is

$$\begin{aligned}
U_{BS} = \frac{1}{2} \int_0^L & \left[ \left( D_{11} \frac{\partial \beta_y}{\partial x} + \frac{1}{2} k_s B_{16} \left( \beta_z - \frac{\partial v}{\partial x} \right) \right) \frac{\partial \beta_y}{\partial x} \right. \\
& + \left( D_{11} \frac{\partial \beta_z}{\partial x} - \frac{1}{2} k_s B_{16} \left( \frac{\partial w}{\partial x} + \beta_y \right) \right) \frac{\partial \beta_z}{\partial x} \\
& + \left( A_{55} k_s \left( -\beta_z + \frac{\partial v}{\partial x} \right) \right) \left( \frac{\partial v}{\partial x} - \beta_z \right) \\
& - \left( \frac{1}{2} B_{16} k_s \frac{\partial \beta_y}{\partial x} + k_s A_{66} \left( \beta_z - \frac{\partial v}{\partial x} \right) \right) \left( \frac{\partial v}{\partial x} - \beta_z \right) \\
& + \left( \left( A_{55} k_s \left( \beta_y + \frac{\partial w}{\partial x} \right) \right) \right) \left( \beta_y + \frac{\partial w}{\partial x} \right) \\
& \left. + \left( -\frac{1}{2} k_s B_{16} \frac{\partial \beta_z}{\partial x} + k_s A_{66} \left( \beta_y + \frac{\partial w}{\partial x} \right) \right) \left( \beta_y + \frac{\partial w}{\partial x} \right) \right] dx \tag{A.4}
\end{aligned}$$

From chapter 3, the shear angles in y-x plane and z-x plane are

$$\phi_{xy} = \frac{\partial v}{\partial x} - \beta_z \tag{A.5}$$

$$\phi_{xz} = \frac{\partial w}{\partial x} + \beta_y \tag{A.6}$$

Substituting Equations (A.5) and (A.6) into Equation (A.4), one can obtain the following

$$\begin{aligned}
U_{BS} = \frac{1}{2} \int_0^L \left[ \left( D_{11} \frac{\partial \beta_y}{\partial x} + \frac{1}{2} k_s B_{16} (-\phi_{xy}) \right) \frac{\partial \beta_y}{\partial x} \right. \\
+ \left( D_{11} \frac{\partial \beta_z}{\partial x} - \frac{1}{2} k_s B_{16} (\phi_{xz}) \right) \frac{\partial \beta_z}{\partial x} \\
+ k_s (A_{55} + A_{66}) (\phi_{xy}^2 + \phi_{xz}^2) - \frac{1}{2} k_s B_{16} \phi_{xy} \frac{\partial \beta_y}{\partial x} \\
\left. - \frac{1}{2} k_s B_{16} \phi_{xz} \frac{\partial \beta_z}{\partial x} \right] dx
\end{aligned} \tag{A.7}$$

Also, from chapter 3, the shear angles can be expressed as

$$\phi_{xy} = -\frac{D_{11}}{k_s(A_{55} + A_{66})} \frac{\partial^3 v}{\partial x^3} = -\frac{L^2}{12} \frac{\Gamma_{\text{comp}}}{L^2} \frac{\partial^3 v}{\partial x^3} \tag{A.8}$$

$$\phi_{xz} = -\frac{D_{11}}{k_s(A_{55} + A_{66})} \frac{\partial^3 w}{\partial x^3} = -\frac{L^2}{12} \frac{\Gamma_{\text{comp}}}{L^2} \frac{\partial^3 w}{\partial x^3} \tag{A.9}$$

where

$$\Gamma_{\text{comp}} = \frac{12D_{1111}}{k_s(A_{55} + A_{66})L^2} \tag{A.10}$$

Substituting Equations (A.8) and (A.9) into Equation (A.7), one can obtain

$$\begin{aligned}
U_{BS} = & \frac{1}{2} \int_0^L \left[ \left( D_{11} \frac{\partial \beta_y}{\partial x} + \frac{1}{2} k_s B_{16} \left( \frac{L^2 \Gamma_{\text{comp}}}{12} \frac{\partial^3 v}{\partial x^3} \right) \right) \frac{\partial \beta_y}{\partial x} \right. \\
& + \left( D_{11} \frac{\partial \beta_z}{\partial x} - \frac{1}{2} k_s B_{16} \left( -\frac{L^2 \Gamma_{\text{comp}}}{12} \frac{\partial^3 w}{\partial x^3} \right) \right) \frac{\partial \beta_z}{\partial x} \\
& + k_s (A_{55} + A_{66}) \left( \left( -\frac{L^2 \Gamma_{\text{comp}}}{12} \frac{\partial^3 v}{\partial x^3} \right)^2 + \left( -\frac{L^2 \Gamma_{\text{comp}}}{12} \frac{\partial^3 w}{\partial x^3} \right)^2 \right) \\
& - \frac{1}{2} k_s B_{16} \left( -\frac{L^2 \Gamma_{\text{comp}}}{12} \frac{\partial^3 v}{\partial x^3} \right) \frac{\partial \beta_y}{\partial x} \\
& \left. - \frac{1}{2} k_s B_{16} \left( -\frac{L^2 \Gamma_{\text{comp}}}{12} \frac{\partial^3 w}{\partial x^3} \right) \frac{\partial \beta_z}{\partial x} \right] dx \tag{A.11}
\end{aligned}$$

Substituting Equation (A.1) into Equation (A.2), Equation (A.3), and Equation (A.11), and then applying Lagrange's equations, one can obtain the equations of motion of the uniform composite shaft. The generalized co-ordinates for the shaft element are

$$\{q\} = \{v_1 \quad w_1 \quad \beta_{y1} \quad \beta_{z1} \quad v_2 \quad w_2 \quad \beta_{y2} \quad \beta_{z2}\}^T \tag{A.12}$$

Using Lagrange's equations

$$\frac{d}{dt} \left( \frac{\partial L}{\partial \dot{q}_i} \right) - \frac{\partial L}{\partial q_i} = 0 \tag{A.13}$$

where

$$L = T_{\text{comp}} - (U_{BS} + U_F)$$

Applying Lagrange's equation gives

$$\begin{aligned}
& \frac{d}{dt} \left[ \frac{\partial T_{comp}}{\partial \dot{q}_1} \right] - \frac{\partial T_{comp}}{\partial q_1} \\
&= \int_0^L [m_c (\dot{v}_1 N_{t1} N_{t1} + \ddot{\beta}_{z1} N_{t1} N_{t2} + \dot{v}_2 N_{t1} N_{t3} \\
&+ \ddot{\beta}_{z2} N_{t1} N_{t4}) \\
&+ I_d (\dot{v}_1 N_{r1} N_{r1} + \ddot{\beta}_{z1} N_{r1} N_{r2} + \dot{v}_2 N_{r1} N_{r3} + \ddot{\beta}_{z2} N_{r1} N_{r4}) \\
&- I_p (-\dot{w}_1 N_{r1} N_{r1} + \dot{\beta}_{y1} N_{r1} N_{r2} - \dot{w}_2 N_{r1} N_{r3} \\
&+ \dot{\beta}_{y2} N_{r1} N_{r4})] dx \tag{A.14}
\end{aligned}$$

$$\begin{aligned}
& \frac{d}{dt} \left[ \frac{\partial T_{comp}}{\partial \dot{q}_2} \right] - \frac{\partial T_{comp}}{\partial q_2} \\
&= \int_0^L [m_c (\ddot{w}_1 N_{t1} N_{t1} - \ddot{\beta}_{y1} N_{t1} N_{t2} + \ddot{w}_2 N_{t1} N_{t3} - \ddot{\beta}_{y2} N_{t1} N_{t4}) \\
&+ I_d (\ddot{w}_1 N_{r1} N_{r1} - \ddot{\beta}_{y1} N_{r1} N_{r2} + \ddot{w}_2 N_{r1} N_{r3} - \ddot{\beta}_{y2} N_{r1} N_{r4}) \\
&- I_p (\dot{v}_1 N_{r1} N_{r1} + \dot{\beta}_{z1} N_{r1} N_{r2} + \dot{v}_2 N_{r1} N_{r3} + \dot{\beta}_{z2} N_{r1} N_{r4})] dx \tag{A.15}
\end{aligned}$$

$$\begin{aligned}
& \frac{d}{dt} \left[ \frac{\partial T_{comp}}{\partial \dot{q}_3} \right] - \frac{\partial T_{comp}}{\partial q_3} \\
&= \int_0^L [m_c (-\ddot{w}_1 N_{t2} N_{t1} + \ddot{\beta}_{y1} N_{t2} N_{t2} - \ddot{w}_2 N_{t2} N_{t3} + \ddot{\beta}_{y2} N_{t2} N_{t4}) \\
&+ I_d (-\ddot{w}_1 N_{r2} N_{r1} + \ddot{\beta}_{y1} N_{r2} N_{r2} - \ddot{w}_2 N_{r2} N_{r3} + \ddot{\beta}_{y2} N_{r2} N_{r4}) \\
&+ I_p (\dot{v}_1 N_{r2} N_{r1} + \dot{\beta}_{z1} N_{r2} N_{r2} + \dot{v}_2 N_{r2} N_{r3} + \dot{\beta}_{z2} N_{r2} N_{r4})] dx \tag{A.16}
\end{aligned}$$

$$\begin{aligned}
& \frac{d}{dt} \left[ \frac{\partial T_{comp}}{\partial \dot{q}_4} \right] - \frac{\partial T_{comp}}{\partial q_4} \\
&= \int_0^L \left[ m_c (\ddot{v}_1 N_{t2} N_{t1} + \ddot{\beta}_{z1} N_{t2} N_{t2} + \ddot{v}_2 N_{t2} N_{t3} + \ddot{\beta}_{z2} N_{t2} N_{t4}) \right. \\
&\quad + I_d (\ddot{v}_1 N_{r2} N_{r1} + \ddot{\beta}_{z1} N_{r2} N_{r2} + \ddot{v}_2 N_{r2} N_{r3} + \ddot{\beta}_{z2} N_{r2} N_{r4}) \\
&\quad \left. - I_p (-\dot{w}_1 N_{r2} N_{r1} + \dot{\beta}_{y1} N_{r2} N_{r2} - \dot{w}_2 N_{r2} N_{r3} + \dot{\beta}_{y2} N_{r2} N_{r4}) \right] dx \quad (A.17)
\end{aligned}$$

$$\begin{aligned}
& \frac{d}{dt} \left[ \frac{\partial T_{comp}}{\partial \dot{q}_5} \right] - \frac{\partial T_{comp}}{\partial q_5} \\
&= \int_0^L \left[ m_c (\ddot{v}_1 N_{t3} N_{t1} + \ddot{\beta}_{z1} N_{t3} N_{t2} + \ddot{v}_2 N_{t3} N_{t3} + \ddot{\beta}_{z2} N_{t3} N_{t4}) \right. \\
&\quad + I_d (\ddot{v}_1 N_{r3} N_{r1} + \ddot{\beta}_{z1} N_{r3} N_{r2} + \ddot{v}_2 N_{r3} N_{r3} + \ddot{\beta}_{z2} N_{r3} N_{r4}) \\
&\quad \left. - I_p (-\dot{w}_1 N_{r3} N_{r1} + \dot{\beta}_{y1} N_{r3} N_{r2} - \dot{w}_2 N_{r3} N_{r3} \right. \\
&\quad \left. + \dot{\beta}_{y2} N_{r3} N_{r4}) \right] dx \quad (A.18)
\end{aligned}$$

$$\begin{aligned}
& \frac{d}{dt} \left[ \frac{\partial T_{comp}}{\partial \dot{q}_6} \right] - \frac{\partial T_{comp}}{\partial q_6} \\
&= \int_0^L \left[ m_c (\ddot{w}_1 N_{t3} N_{t1} - \ddot{\beta}_{y1} N_{t3} N_{t2} + \ddot{w}_2 N_{t3} N_{t3} - \ddot{\beta}_{y2} N_{t3} N_{t4}) \right. \\
&\quad + I_d (\ddot{w}_1 N_{r3} N_{r1} - \ddot{\beta}_{y1} N_{r3} N_{r2} + \ddot{w}_2 N_{r3} N_{r3} - \ddot{\beta}_{y2} N_{r3} N_{r4}) \\
&\quad \left. - I_p (\dot{v}_1 N_{r3} N_{r1} + \dot{\beta}_{z1} N_{r3} N_{r2} + \dot{v}_2 N_{r3} N_{r3} + \dot{\beta}_{z2} N_{r3} N_{r4}) \right] dx \quad (A.19)
\end{aligned}$$

$$\begin{aligned}
& \frac{d}{dt} \left[ \frac{\partial T_{comp}}{\partial \dot{q}_7} \right] - \frac{\partial T_{comp}}{\partial q_7} \\
&= \int_0^L [m_c (-\ddot{w}_1 N_{t4} N_{t1} + \ddot{\beta}_{y1} N_{t4} N_{t2} - \ddot{w}_2 N_{t4} N_{t3} + \ddot{\beta}_{y2} N_{t4} N_{t4}) \\
&+ I_d (-\ddot{w}_1 N_{r4} N_{r1} + \ddot{\beta}_{y1} N_{r4} N_{r2} - \ddot{w}_2 N_{r4} N_{r3} + \ddot{\beta}_{y2} N_{r4} N_{r4}) \\
&+ I_p (\dot{v}_1 N_{r4} N_{r1} + \dot{\beta}_{z1} N_{r4} N_{r2} + \dot{v}_2 N_{r4} N_{r3} + \dot{\beta}_{z2} N_{r4} N_{r4})] dx \quad (A.20)
\end{aligned}$$

$$\begin{aligned}
& \frac{d}{dt} \left[ \frac{\partial T_{comp}}{\partial \dot{q}_8} \right] - \frac{\partial T_{comp}}{\partial q_8} \\
&= \int_0^L [m_c (\dot{v}_1 N_{t4} N_{t1} + \dot{\beta}_{z1} N_{t4} N_{t2} + \dot{v}_2 N_{t4} N_{t3} + \dot{\beta}_{z2} N_{t4} N_{t3}) \\
&+ I_d (\dot{v}_1 N_{r4} N_{r1} + \dot{\beta}_{z1} N_{r4} N_{r2} + \dot{v}_2 N_{r4} N_{r3} + \dot{\beta}_{z2} N_{r4} N_{r4}) \\
&- I_p (-\dot{w}_1 N_{r4} N_{r1} + \dot{\beta}_{y1} N_{r4} N_{r2} - \dot{w}_2 N_{r4} N_{r3} + \dot{\beta}_{y2} N_{r4} N_{r4})] dx \quad (A.21)
\end{aligned}$$

$$\begin{aligned}
\frac{\partial U_{BS}}{\partial q_1} &= \int_0^L \left[ \frac{L^2}{24} \Gamma_{comp} B_{16} k_s \left( -w_1 \dot{\dot{N}}_{t1} \dot{N}_{r1} + \beta_{y1} \dot{\dot{N}}_{t1} \dot{N}_{r2} - w_2 \dot{\dot{N}}_{t1} \dot{N}_{r3} \right. \right. \\
&+ \left. \beta_{y2} \dot{\dot{N}}_{t1} \dot{N}_{r4} \right) \\
&+ D_{11} (v_1 \dot{N}_{r1} \dot{N}_{r1} + \beta_{z1} \dot{N}_{r1} \dot{N}_{r2} + v_2 \dot{N}_{r1} \dot{N}_{r3} + \beta_{z2} \dot{N}_{r1} \dot{N}_{r4}) \\
&+ \frac{L^2}{24} \Gamma_{comp} B_{16} k_s \left( w_1 \dot{N}_{r1} \dot{\dot{N}}_{t1} - \beta_{y1} \dot{N}_{r1} \dot{\dot{N}}_{t2} + w_2 \dot{N}_{r1} \dot{\dot{N}}_{t3} \right. \\
&- \left. \beta_{y2} \dot{N}_{r1} \dot{\dot{N}}_{t4} \right) + \frac{L^4}{144} \Gamma_{comp}^2 k_s (A_{66} + A_{55}) \left( v_1 \dot{\dot{N}}_{t1} \dot{\dot{N}}_{t1} \right. \\
&+ \left. \beta_{z1} \dot{\dot{N}}_{t1} \dot{\dot{N}}_{t2} + v_2 \dot{\dot{N}}_{t1} \dot{\dot{N}}_{t3} + \beta_{z2} \dot{\dot{N}}_{t1} \dot{\dot{N}}_{t4} \right) \Big] dx \quad (A.22)
\end{aligned}$$

$$\begin{aligned}
\frac{\partial U_{BS}}{\partial q_2} = \int_0^L & \left[ D_{11} (w_1 \dot{N}_{r1} \dot{N}_{r1} - \beta_{y1} \dot{N}_{r1} \dot{N}_{r2} + w_2 \dot{N}_{r1} \dot{N}_{r3} - \beta_{y2} \dot{N}_{r1} \dot{N}_{r4}) \right. \\
& - \frac{L^2}{24} \Gamma_{\text{comp}} B_{16} k_s \left( v_1 \dot{N}_{r1} \ddot{N}_{t1} + \beta_{z1} \dot{N}_{r1} \ddot{N}_{t2} + v_2 \dot{N}_{r1} \ddot{N}_{t3} \right. \\
& \left. \left. + \beta_{z2} \dot{N}_{r1} \ddot{N}_{t4} \right) + \frac{L^2}{24} \Gamma_{\text{comp}} B_{16} k_s \left( v_1 \ddot{N}_{t1} \dot{N}_{r1} + \beta_{z1} \ddot{N}_{t1} \dot{N}_{r2} \right. \right. \\
& \left. \left. + v_2 \ddot{N}_{t1} \dot{N}_{r3} + \beta_{z2} \ddot{N}_{t1} \dot{N}_{r4} \right) \right. \\
& \left. + \frac{L^4}{144} \Gamma_{\text{comp}}^2 k_s (A_{66} + A_{55}) \left( w_1 \ddot{N}_{t1} \ddot{N}_{t1} - \beta_{y1} \ddot{N}_{t1} \ddot{N}_{t2} \right. \right. \\
& \left. \left. + w_2 \ddot{N}_{t1} \ddot{N}_{t3} - \beta_{y2} \ddot{N}_{t1} \ddot{N}_{t4} \right) \right] dx
\end{aligned} \tag{A.23}$$

$$\begin{aligned}
\frac{\partial U_{BS}}{\partial q_3} = \int_0^L & \left[ D_{11} (-w_1 \dot{N}_{r2} \dot{N}_{r1} + \beta_{y1} \dot{N}_{r2} \dot{N}_{r2} - w_2 \dot{N}_{r2} \dot{N}_{r3} + \beta_{y2} \dot{N}_{r2} \dot{N}_{r4}) \right. \\
& + \frac{L^2}{24} \Gamma_{\text{comp}} B_{16} k_s \left( v_1 \dot{N}_{r2} \ddot{N}_{t1} + \beta_{z1} \dot{N}_{r2} \ddot{N}_{t2} + v_2 \dot{N}_{r2} \ddot{N}_{t3} \right. \\
& \left. \left. + \beta_{z2} \dot{N}_{r2} \ddot{N}_{t4} \right) \right. \\
& - \frac{L^2}{24} \Gamma_{\text{comp}} B_{16} k_s \left( v_1 \ddot{N}_{t2} \dot{N}_{r1} + \beta_{z1} \ddot{N}_{t2} \dot{N}_{r2} + v_2 \ddot{N}_{t2} \dot{N}_{r3} \right. \\
& \left. \left. + \beta_{z2} \ddot{N}_{t2} \dot{N}_{r4} \right) \right. \\
& \left. + \frac{L^4}{144} \Gamma_{\text{comp}}^2 k_s (A_{66} + A_{55}) \left( -w_1 \ddot{N}_{t2} \ddot{N}_{t1} + \beta_{y1} \ddot{N}_{t2} \ddot{N}_{t2} \right. \right. \\
& \left. \left. - w_2 \ddot{N}_{t2} \ddot{N}_{t3} + \beta_{y2} \ddot{N}_{t2} \ddot{N}_{t4} \right) \right] dx
\end{aligned} \tag{A.24}$$

$$\begin{aligned}
\frac{\partial U_{BS}}{\partial q_4} = \int_0^L \left[ \frac{L^2}{24} \Gamma_{\text{comp}} B_{16} k_s \left( -w_1 \dot{\dot{N}}_{t2} \dot{N}_{r1} + \beta_{y1} \dot{\dot{N}}_{t2} \dot{N}_{r2} - w_2 \dot{\dot{N}}_{t2} \dot{N}_{r3} \right. \right. \\
+ \beta_{y2} \dot{\dot{N}}_{t2} \dot{N}_{r4} \left. \right) \\
+ D_{11} (v_1 \dot{N}_{r2} \dot{N}_{r1} + \beta_{z1} \dot{N}_{r2} \dot{N}_{r2} + v_2 \dot{N}_{r2} \dot{N}_{r3} \\
+ \beta_{z2} \dot{N}_{r2} \dot{N}_{r4}) + \frac{L^2}{24} \Gamma_{\text{comp}} B_{16} k_s \left( w_1 \dot{N}_{r2} \dot{\dot{N}}_{t1} - \beta_{y1} \dot{N}_{r2} \dot{\dot{N}}_{t2} \right. \\
+ w_2 \dot{N}_{r2} \dot{\dot{N}}_{t3} - \beta_{y2} \dot{N}_{r2} \dot{\dot{N}}_{t4} \left. \right) \\
+ \frac{L^4}{144} \Gamma_{\text{comp}}^2 k_s (A_{66} + A_{55}) \left( v_1 \dot{\dot{N}}_{t2} \dot{\dot{N}}_{t1} + \beta_{z1} \dot{\dot{N}}_{t2} \dot{\dot{N}}_{t2} \right. \\
\left. + v_2 \dot{\dot{N}}_{t2} \dot{\dot{N}}_{t3} + \beta_{z2} \dot{\dot{N}}_{t2} \dot{\dot{N}}_{t4} \right) \Big] dx
\end{aligned} \tag{A.25}$$

$$\begin{aligned}
\frac{\partial U_{BS}}{\partial q_5} = \int_0^L \left[ \frac{L^2}{24} \Gamma_{\text{comp}} B_{16} k_s \left( -w_1 \dot{\dot{N}}_{t3} \dot{N}_{r1} + \beta_{y1} \dot{\dot{N}}_{t3} \dot{N}_{r2} - w_2 \dot{\dot{N}}_{t3} \dot{N}_{r3} \right. \right. \\
+ \beta_{y2} \dot{\dot{N}}_{t3} \dot{N}_{r4} \left. \right) \\
+ D_{11} (v_1 \dot{N}_{r3} \dot{N}_{r1} + \beta_{z1} \dot{N}_{r3} \dot{N}_{r2} + v_2 \dot{N}_{r3} \dot{N}_{r3} + \beta_{z2} \dot{N}_{r3} \dot{N}_{r4}) \\
+ \frac{L^2}{24} \Gamma_{\text{comp}} B_{16} k_s \left( w_1 \dot{N}_{r3} \dot{\dot{N}}_{t1} - \beta_{y1} \dot{N}_{r3} \dot{\dot{N}}_{t2} + w_2 \dot{N}_{r3} \dot{\dot{N}}_{t3} \right. \\
- \beta_{y2} \dot{N}_{r3} \dot{\dot{N}}_{t4} \left. \right) + \frac{L^4}{144} \Gamma_{\text{comp}}^2 k_s (A_{66} + A_{55}) \left( v_1 \dot{\dot{N}}_{t3} \dot{\dot{N}}_{t1} \right. \\
\left. + \beta_{z1} \dot{\dot{N}}_{t3} \dot{\dot{N}}_{t2} + v_2 \dot{\dot{N}}_{t3} \dot{\dot{N}}_{t3} + \beta_{z2} \dot{\dot{N}}_{t3} \dot{\dot{N}}_{t4} \right) \Big] dx
\end{aligned} \tag{A.26}$$

$$\begin{aligned}
\frac{\partial U_{BS}}{\partial q_6} = \int_0^L & \left[ D_{11} (w_1 \dot{N}_{r3} \dot{N}_{r1} - \beta_{y1} \dot{N}_{r3} \dot{N}_{r2} + w_2 \dot{N}_{r3} \dot{N}_{r3} - \beta_{y2} \dot{N}_{r3} \dot{N}_{r4}) \right. \\
& - \frac{L^2}{24} \Gamma_{\text{comp}} B_{16} k_s \left( v_1 \dot{N}_{r3} \ddot{N}_{t1} + \beta_{z1} \dot{N}_{r3} \ddot{N}_{t2} + v_2 \dot{N}_{r3} \ddot{N}_{t3} \right. \\
& \left. \left. + \beta_{z2} \dot{N}_{r3} \ddot{N}_{t4} \right) + \frac{L^2}{24} \Gamma_{\text{comp}} B_{16} k_s \left( v_1 \ddot{N}_{t3} \dot{N}_{r1} + \beta_{z1} \ddot{N}_{t3} \dot{N}_{r2} \right. \right. \\
& \left. \left. + v_2 \ddot{N}_{t3} \dot{N}_{r3} + \beta_{z2} \ddot{N}_{t3} \dot{N}_{r4} \right) \right. \\
& \left. + \frac{L^4}{144} \Gamma_{\text{comp}}^2 k_s (A_{66} + A_{55}) \left( w_1 \ddot{N}_{t3} \ddot{N}_{t1} - \beta_{y1} \ddot{N}_{t3} \ddot{N}_{t2} \right. \right. \\
& \left. \left. + w_2 \ddot{N}_{t3} \ddot{N}_{t3} - \beta_{y2} \ddot{N}_{t3} \ddot{N}_{t4} \right) \right] dx
\end{aligned} \tag{A.27}$$

$$\begin{aligned}
\frac{\partial U_{BS}}{\partial q_7} = \int_0^L & \left[ D_{11} (-w_1 \dot{N}_{r4} \dot{N}_{r1} + \beta_{y1} \dot{N}_{r4} \dot{N}_{r2} - w_2 \dot{N}_{r4} \dot{N}_{r3} + \beta_{y2} \dot{N}_{r4} \dot{N}_{r4}) \right. \\
& + \frac{L^2}{24} \Gamma_{\text{comp}} B_{16} k_s \left( v_1 \dot{N}_{r4} \ddot{N}_{t1} + \beta_{z1} \dot{N}_{r4} \ddot{N}_{t2} + v_2 \dot{N}_{r4} \ddot{N}_{t3} \right. \\
& \left. \left. + \beta_{z2} \dot{N}_{r4} \ddot{N}_{t4} \right) \right. \\
& - \frac{L^2}{24} \Gamma_{\text{comp}} B_{16} k_s \left( v_1 \ddot{N}_{t4} \dot{N}_{r1} + \beta_{z1} \ddot{N}_{t4} \dot{N}_{r2} + v_2 \ddot{N}_{t4} \dot{N}_{r3} \right. \\
& \left. \left. + \beta_{z2} \ddot{N}_{t4} \dot{N}_{r4} \right) \right. \\
& \left. + \frac{L^4}{144} \Gamma_{\text{comp}}^2 k_s (A_{66} + A_{55}) \left( -w_1 \ddot{N}_{t4} \ddot{N}_{t1} + \beta_{y1} \ddot{N}_{t4} \ddot{N}_{t2} \right. \right. \\
& \left. \left. - w_2 \ddot{N}_{t4} \ddot{N}_{t3} + \beta_{y2} \ddot{N}_{t4} \ddot{N}_{t4} \right) \right] dx
\end{aligned} \tag{A.28}$$

$$\begin{aligned}
\frac{\partial U_{BS}}{\partial q_8} = \int_0^L & \left[ \frac{L^2}{24} \Gamma_{\text{comp}} B_{16} k_s \left( -w_1 \dot{\dot{N}}_{t4} \dot{N}_{r1} + \beta_{y1} \dot{\dot{N}}_{t4} \dot{N}_{r2} - w_2 \dot{\dot{N}}_{t4} \dot{N}_{r3} \right. \right. \\
& \left. \left. + \beta_{y2} \dot{\dot{N}}_{t4} \dot{N}_{r4} \right) \right. \\
& + D_{11} (v_1 \dot{N}_{r4} \dot{N}_{r1} + \beta_{z1} \dot{N}_{r4} \dot{N}_{r2} + v_2 \dot{N}_{r4} \dot{N}_{r3} \\
& \left. + \beta_{z2} \dot{N}_{r4} \dot{N}_{r4} \right) + \frac{L^2}{24} \Gamma_{\text{comp}} B_{16} k_s \left( w_1 \dot{N}_{r4} \dot{\dot{N}}_{t1} - \beta_{y1} \dot{N}_{r4} \dot{\dot{N}}_{t2} \right. \\
& \left. + w_2 \dot{N}_{r4} \dot{\dot{N}}_{t3} - \beta_{y2} \dot{N}_{r4} \dot{\dot{N}}_{t4} \right) \\
& + \frac{L^4}{144} \Gamma_{\text{comp}}^2 k_s (A_{66} + A_{55}) \left( v_1 \dot{\dot{N}}_{t4} \dot{\dot{N}}_{t1} + \beta_{z1} \dot{\dot{N}}_{t4} \dot{\dot{N}}_{t2} \right. \\
& \left. \left. + v_2 \dot{\dot{N}}_{t4} \dot{\dot{N}}_{t3} + \beta_{z2} \dot{\dot{N}}_{t4} \dot{\dot{N}}_{t4} \right) \right] dx
\end{aligned} \tag{A.29}$$

## Appendix B

### Hierarchical shaft element formulation

The displacement field of hierarchical shaft element is [22]

$$v = v_1 f_1 + v_2 f_2 + \sum_{n=1}^N v_{n+2} f_{n+2} \quad (\text{B.1})$$

$$w = w_1 f_1 + w_2 f_2 + \sum_{n=1}^N w_{n+2} f_{n+2} \quad (\text{B.2})$$

$$\beta_y = \beta_{y1} f_1 + \beta_{y2} f_2 + \sum_{n=1}^N \beta_{y(n+2)} f_{n+2} \quad (\text{B.3})$$

$$\beta_z = \beta_{z1} f_1 + \beta_{z2} f_2 + \sum_{n=1}^N \beta_{z(n+2)} f_{n+2} \quad (\text{B.4})$$

The kinetic energy of the tapered composite shaft in terms of non-dimensional coordinate  $\xi$  is

$$\begin{aligned} T_{comp} = & \frac{L}{2} \int_0^1 m_c(\xi) (\dot{v}^2 + \dot{w}^2) d\xi + \frac{L}{2} \int_0^1 I_{dc}(\xi) (\dot{\beta}_y^2 + \dot{\beta}_z^2) d\xi \\ & - \int_0^1 L I_{pc}(\xi) \Omega \dot{\beta}_z \beta_y d\xi \end{aligned} \quad (\text{B.5})$$

The strain energy of the tapered composite shaft due to the axial load in terms of non-dimensional coordinate  $\xi$  is

$$U_F = \frac{1}{2L} \int_0^1 P \left[ \left( \frac{\partial v}{\partial \xi} \right)^2 + \left( \frac{\partial w}{\partial \xi} \right)^2 \right] d\xi \quad (\text{B.6})$$

The strain energy of tapered composite shaft due to bending moments and shear forces in term of non-dimensional coordinate  $\xi$  is

$$\begin{aligned} U_{BS} = \int_0^1 \left[ \frac{1}{2L} \bar{D}_{11} \left( \left( \frac{\partial \beta_y}{\partial \xi} \right)^2 + \left( \frac{\partial \beta_z}{\partial \xi} \right)^2 \right) \right. \\ + \bar{B}_{15} k_s \left( \beta_y \frac{\partial \beta_y}{\partial \xi} + \beta_z \frac{\partial \beta_z}{\partial \xi} + \frac{1}{L} \frac{\partial \beta_y}{\partial \xi} \frac{\partial w}{\partial \xi} - \frac{1}{L} \frac{\partial \beta_z}{\partial \xi} \frac{\partial v}{\partial \xi} \right) \\ + \frac{1}{2} \bar{B}_{16} k_s \left( \beta_z \frac{\partial \beta_y}{\partial \xi} - \beta_y \frac{\partial \beta_z}{\partial \xi} - \frac{1}{L} \frac{\partial \beta_y}{\partial \xi} \frac{\partial v}{\partial \xi} - \frac{1}{L} \frac{\partial \beta_z}{\partial \xi} \frac{\partial w}{\partial \xi} \right) \\ + \frac{1}{2} (\bar{A}_{66} + \bar{A}_{55}) \left( \frac{1}{L} \left( \frac{\partial v}{\partial \xi} \right)^2 + \frac{1}{L} \left( \frac{\partial w}{\partial \xi} \right)^2 + L \beta_y^2 + L \beta_z^2 + 2 \beta_y \frac{\partial w}{\partial \xi} \right. \\ \left. - 2 \beta_z \frac{\partial v}{\partial \xi} \right) \Big] d\xi \end{aligned} \quad (\text{B.7})$$

Substituting Equations (B.1) – (B.4) into Equations (B.5) – (B.7) and then applying Lagrange's equations, one can obtain the equations of motion of the tapered composite shaft.

The generalized co-ordinates for the shaft element are

$$\begin{array}{cccccc}
 q_1 = v_1 & q_2 = v_2 & q_3 = v_3 & \dots\dots & q_b = v_{N+2} \\
 q_{b+1} = w_1 & q_{b+2} = w_2 & q_{b+3} = w_3 & \dots\dots & q_{2b} = w_{N+2} \\
 q_{2b+1} = \beta_{y1} & q_{2b+2} = \beta_{y2} & q_{2b+3} = \beta_{y3} & \dots\dots & q_{3b} = \beta_{y(N+2)} \\
 q_{3b+1} = \beta_{z1} & q_{3b+2} = \beta_{z2} & q_{3b+3} = \beta_{z3} & \dots\dots & q_{4b} = \beta_{z(N+2)}
 \end{array} \tag{B.8}$$

Lagrange's equation is

$$\frac{d}{dt} \left( \frac{\partial L}{\partial \dot{q}} \right) - \frac{\partial L}{\partial q} = 0 \tag{B.9}$$

where

$$L = T_{comp} - (U_{BS} + U_F)$$

Applying Lagrange's equation gives

$$\begin{aligned}
 & \frac{d}{dt} \left[ \frac{\partial T_{comp}}{\partial \dot{q}_1} \right] - \frac{\partial T_{comp}}{\partial q_1} \\
 & = \int_0^1 L m_c(\xi) \left( \dot{v}_1 f_1 f_1 + \dot{v}_2 f_1 f_2 + \sum_{n=1}^N \dot{v}_{n+2} f_1 f_{2+n} \right) d\xi \tag{B.10}
 \end{aligned}$$

$$\begin{aligned}
 & \frac{d}{dt} \left[ \frac{\partial T_{comp}}{\partial \dot{q}_2} \right] - \frac{\partial T_{comp}}{\partial q_2} \\
 & = \int_0^1 L m_c(\xi) \left( \dot{v}_1 f_2 f_1 + \dot{v}_2 f_2 f_2 + \sum_{n=1}^N \dot{v}_{n+2} f_2 f_{2+n} \right) d\xi \tag{B.11}
 \end{aligned}$$

$\cdot$   $\cdot$   $\cdot$   
 $\vdots$   $\vdots$   $\vdots$   
 $\cdot$   $\cdot$   $\cdot$

$$\begin{aligned}
\frac{d}{dt} \left[ \frac{\partial T_{comp}}{\partial \dot{q}_b} \right] - \frac{\partial T_{comp}}{\partial q_b} &= \int_0^1 L m_c(\xi) \left( \dot{v}_1 f_{N+2} f_1 + \dot{v}_2 f_{N+2} f_2 \right. \\
&\quad \left. + \sum_{n=1}^N \dot{v}_{n+2} f_{N+2} f_{2+n} \right) d\xi
\end{aligned} \tag{B.12}$$

$$\begin{aligned}
\frac{d}{dt} \left[ \frac{\partial T_{comp}}{\partial \dot{q}_{b+1}} \right] - \frac{\partial T_{comp}}{\partial q_{b+1}} &= \int_0^1 L m_c(\xi) \left( \ddot{w}_1 f_1 f_1 + \ddot{w}_2 f_1 f_2 + \sum_{n=1}^N \ddot{w}_{n+2} f_1 f_{2+n} \right) d\xi
\end{aligned} \tag{B.13}$$

$$\begin{aligned}
\frac{d}{dt} \left[ \frac{\partial T_{comp}}{\partial \dot{q}_{b+2}} \right] - \frac{\partial T_{comp}}{\partial q_{b+2}} &= \int_0^1 L m_c(\xi) \left( \ddot{w}_1 f_2 f_1 + \ddot{w}_2 f_2 f_2 + \sum_{n=1}^N \ddot{w}_{n+2} f_2 f_{2+n} \right) d\xi
\end{aligned} \tag{B.14}$$

$$\begin{aligned}
&\vdots && \vdots && \vdots \\
&\vdots && \vdots && \vdots \\
&\vdots && \vdots && \vdots \\
\frac{d}{dt} \left[ \frac{\partial T_{comp}}{\partial \dot{q}_{2b}} \right] - \frac{\partial T_{comp}}{\partial q_{2b}} &= \int_0^1 L m_c(\xi) \left( \ddot{w}_1 f_{N+2} f_1 + \ddot{w}_2 f_{N+2} f_2 \right. \\
&\quad \left. + \sum_{n=1}^N \ddot{w}_{n+2} f_{N+2} f_{2+n} \right) d\xi
\end{aligned} \tag{B.15}$$

$$\begin{aligned}
& \frac{d}{dt} \left[ \frac{\partial T_{comp}}{\partial \dot{q}_{2b+1}} \right] - \frac{\partial T_{comp}}{\partial q_{2b+1}} \\
&= \int_0^1 L \left[ I_{dc}(\xi) \left( \ddot{\beta}_{y1} f_1 f_1 + \ddot{\beta}_{y2} f_1 f_2 \right. \right. \\
&\quad \left. \left. + \sum_{n=1}^N \ddot{\beta}_{y(n+2)} f_1 f_{n+2} \right) \right. \\
&\quad \left. + \Omega I_p(\xi) \left( \dot{\beta}_{z1} f_1 f_1 + \dot{\beta}_{z2} f_1 f_2 + \sum_{n=1}^N \dot{\beta}_{z(n+2)} f_1 f_{n+2} \right) \right] d\xi \quad (B.16)
\end{aligned}$$

$$\begin{aligned}
& \frac{d}{dt} \left[ \frac{\partial T_{comp}}{\partial \dot{q}_{2b+2}} \right] - \frac{\partial T_{comp}}{\partial q_{2b+2}} \\
&= \int_0^1 L \left[ I_{dc}(\xi) \left( \ddot{\beta}_{y1} f_2 f_1 + \ddot{\beta}_{y2} f_2 f_2 + \sum_{n=1}^N \ddot{\beta}_{y(n+2)} f_2 f_{n+2} \right) \right. \\
&\quad \left. + \Omega I_p(\xi) \left( \dot{\beta}_{z1} f_2 f_1 + \dot{\beta}_{z2} f_2 f_2 + \sum_{n=1}^N \dot{\beta}_{z(n+2)} f_2 f_{n+2} \right) \right] d\xi \quad (B.17)
\end{aligned}$$

$\cdot$   $\cdot$   $\cdot$   
 $\cdot$   $\cdot$   $\cdot$   
 $\cdot$   $\cdot$   $\cdot$

$$\begin{aligned}
& \frac{d}{dt} \left[ \frac{\partial T_{comp}}{\partial \dot{q}_{3b}} \right] - \frac{\partial T_{comp}}{\partial q_{3b}} \\
&= \int_0^1 L \left[ I_{dc}(\xi) \left( \ddot{\beta}_{y1} f_{N+2} f_1 + \ddot{\beta}_{y2} f_{N+2} f_2 \right. \right. \\
&\quad \left. \left. + \sum_{n=1}^N \ddot{\beta}_{y(n+2)} f_{N+2} f_{n+2} \right) \right. \\
&\quad \left. + \Omega I_p(\xi) \left( \dot{\beta}_{z1} f_{N+2} f_1 + \dot{\beta}_{z2} f_{N+2} f_2 \right. \right. \\
&\quad \left. \left. + \sum_{n=1}^N \dot{\beta}_{z(n+2)} f_{N+2} f_{n+2} \right) \right] d\xi
\end{aligned} \tag{B.18}$$

$$\begin{aligned}
& \frac{d}{dt} \left[ \frac{\partial T_{comp}}{\partial \dot{q}_{3b+1}} \right] - \frac{\partial T_{comp}}{\partial q_{3b+1}} \\
&= \int_0^1 L \left[ I_{dc}(\xi) \left( \ddot{\beta}_{z1} f_1 f_1 + \ddot{\beta}_{z2} f_1 f_2 + \sum_{n=1}^N \ddot{\beta}_{z(n+2)} f_1 f_{n+2} \right) \right. \\
&\quad \left. - \Omega I_p(\xi) \left( \dot{\beta}_{y1} f_1 f_1 + \dot{\beta}_{y2} f_1 f_2 + \sum_{n=1}^N \dot{\beta}_{y(n+2)} f_1 f_{n+2} \right) \right] d\xi
\end{aligned} \tag{B.19}$$

$$\begin{aligned}
& \frac{d}{dt} \left[ \frac{\partial T_{comp}}{\partial \dot{q}_{3b+2}} \right] - \frac{\partial T_{comp}}{\partial q_{3b+2}} \\
&= \int_0^1 L \left[ I_{dc}(\xi) \left( \ddot{\beta}_{z1} f_2 f_1 + \ddot{\beta}_{z2} f_2 f_2 + \sum_{n=1}^N \ddot{\beta}_{z(n+2)} f_2 f_{n+2} \right) \right. \\
&\quad \left. - \Omega I_p(\xi) \left( \dot{\beta}_{y1} f_2 f_1 + \dot{\beta}_{y2} f_2 f_2 + \sum_{n=1}^N \dot{\beta}_{y(n+2)} f_2 f_{n+2} \right) \right] d\xi
\end{aligned} \tag{B.20}$$

$\vdots$   $\vdots$   $\vdots$

$$\begin{aligned}
& \frac{d}{dt} \left[ \frac{\partial T_{comp}}{\partial \dot{q}_{4b}} \right] - \frac{\partial T_{comp}}{\partial q_{4b}} \\
&= \int_0^1 L \left[ I_{dc}(\xi) \left( \ddot{\beta}_{z1} f_{N+2} f_1 + \ddot{\beta}_{z2} f_{N+2} f_2 \right. \right. \\
&\quad \left. \left. + \sum_{n=1}^N \ddot{\beta}_{z(n+2)} f_{N+2} f_{n+2} \right) \right. \\
&\quad \left. - \Omega I_p(\xi) \left( \dot{\beta}_{y1} f_{N+2} f_1 + \dot{\beta}_{y2} f_{N+2} f_2 \right. \right. \\
&\quad \left. \left. + \sum_{n=1}^N \dot{\beta}_{y(n+2)} f_{N+2} f_{n+2} \right) \right] d\xi \tag{B.21}
\end{aligned}$$

$$\begin{aligned}
\frac{\partial U_{BS}}{\partial q_1} &= \int_0^1 \left[ -\frac{1}{2L} k_s \bar{B}_{16} \left( \beta_{y1} \dot{f}_1 \dot{f}_1 + \beta_{y2} \dot{f}_1 \dot{f}_2 + \sum_{n=1}^N \beta_{y(n+2)} \dot{f}_1 \dot{f}_{n+2} \right) \right. \\
&\quad \left. - \frac{1}{L} k_s \bar{B}_{15} \left( \beta_{z1} \dot{f}_1 \dot{f}_1 + \beta_{z2} \dot{f}_1 \dot{f}_2 + \sum_{n=1}^N \beta_{z(n+2)} \dot{f}_1 \dot{f}_{n+2} \right) \right. \\
&\quad \left. - k_s (\bar{A}_{66} + \bar{A}_{55}) \left( \beta_{z1} \dot{f}_1 f_1 + \beta_{z2} \dot{f}_1 f_2 + \sum_{n=1}^N \beta_{z(n+2)} \dot{f}_1 f_{n+2} \right) \right. \\
&\quad \left. + \frac{1}{L} k_s (\bar{A}_{66} + \bar{A}_{55}) \left( v_1 \dot{f}_1 \dot{f}_1 + v_2 \dot{f}_1 \dot{f}_2 \right. \right. \\
&\quad \left. \left. + \sum_{n=1}^N v_{(n+2)} \dot{f}_1 \dot{f}_{n+2} \right) \right] d\xi \tag{B.22}
\end{aligned}$$

$$\begin{aligned}
\frac{\partial U_{BS}}{\partial q_2} = & \int_0^1 \left[ -\frac{1}{2L} k_s \bar{B}_{16} \left( \beta_{y1} \dot{f}_2 \dot{f}_1 + \beta_{y2} \dot{f}_2 \dot{f}_2 + \sum_{n=1}^N \beta_{y(n+2)} \dot{f}_2 \dot{f}_{n+2} \right) \right. \\
& - \frac{1}{L} k_s \bar{B}_{15} \left( \beta_{z1} \dot{f}_2 \dot{f}_1 + \beta_{z2} \dot{f}_2 \dot{f}_2 + \sum_{n=1}^N \beta_{z(n+2)} \dot{f}_2 \dot{f}_{n+2} \right) \\
& - k_s (\bar{A}_{66} + \bar{A}_{55}) \left( \beta_{z1} \dot{f}_2 \dot{f}_1 + \beta_{z2} \dot{f}_2 \dot{f}_2 + \sum_{n=1}^N \beta_{z(n+2)} \dot{f}_2 \dot{f}_{n+2} \right) \\
& + \frac{1}{L} k_s (\bar{A}_{66} + \bar{A}_{55}) \left( v_1 \dot{f}_2 \dot{f}_1 + v_2 \dot{f}_2 \dot{f}_2 \right. \\
& \left. + \sum_{n=1}^N v_{(n+2)} \dot{f}_2 \dot{f}_{n+2} \right) \Big] d\xi \tag{B.23} \\
& \cdot \qquad \qquad \qquad \cdot \qquad \qquad \qquad \cdot \\
& \cdot \qquad \qquad \qquad \cdot \qquad \qquad \qquad \cdot \\
& \cdot \qquad \qquad \qquad \cdot \qquad \qquad \qquad \cdot
\end{aligned}$$

$$\begin{aligned}
\frac{\partial U_{BS}}{\partial q_b} = \int_0^1 & \left[ -\frac{1}{2L} k_s \bar{B}_{16} \left( \beta_{y1} \hat{f}_{N+2} \hat{f}_1 + \beta_{y2} \hat{f}_{N+2} \hat{f}_2 \right. \right. \\
& + \left. \sum_{n=1}^N \beta_{y(n+2)} \hat{f}_{N+2} \hat{f}_{n+2} \right) \\
& - \frac{1}{L} k_s \bar{B}_{15} \left( \beta_{z1} \hat{f}_{N+2} \hat{f}_1 + \beta_{z2} \hat{f}_{N+2} \hat{f}_2 \right. \\
& + \left. \sum_{n=1}^N \beta_{z(n+2)} \hat{f}_{N+2} \hat{f}_{n+2} \right) \\
& - k_s (\bar{A}_{66} + \bar{A}_{55}) \left( \beta_{z1} \hat{f}_{N+2} f_1 + \beta_{z2} \hat{f}_{N+2} f_2 \right. \\
& + \left. \sum_{n=1}^N \beta_{z(n+2)} \hat{f}_{N+2} f_{n+2} \right) \\
& + \frac{1}{L} k_s (\bar{A}_{66} + \bar{A}_{55}) \left( v_1 \hat{f}_{N+2} \hat{f}_1 + v_2 \hat{f}_{N+2} \hat{f}_2 \right. \\
& + \left. \sum_{n=1}^N v_{(n+2)} \hat{f}_{N+2} \hat{f}_{n+2} \right) \Big] d\xi
\end{aligned} \tag{B.24}$$

$$\begin{aligned}
\frac{\partial U_{BS}}{\partial q_{b+1}} = \int_0^1 & \left[ -\frac{1}{2L} k_s \bar{B}_{16} \left( \beta_{z1} \dot{f}_1 \dot{f}_1 + \beta_{z2} \dot{f}_1 \dot{f}_2 + \sum_{n=1}^N \beta_{z(n+2)} \dot{f}_1 \dot{f}_{n+2} \right) \right. \\
& + \frac{1}{L} k_s \bar{B}_{15} \left( \beta_{y1} \dot{f}_1 \dot{f}_1 + \beta_{y2} \dot{f}_1 \dot{f}_2 + \sum_{n=1}^N \beta_{y(n+2)} \dot{f}_1 \dot{f}_{n+2} \right) \\
& + k_s (\bar{A}_{66} + \bar{A}_{55}) \left( \beta_{y1} \dot{f}_1 \dot{f}_1 + \beta_{y2} \dot{f}_1 \dot{f}_2 \right. \\
& \left. + \sum_{n=1}^N \beta_{y(n+2)} \dot{f}_1 \dot{f}_{n+2} \right) \\
& + \frac{1}{L} k_s (\bar{A}_{66} + \bar{A}_{55}) \left( w_1 \dot{f}_1 \dot{f}_1 + w_2 \dot{f}_1 \dot{f}_2 \right. \\
& \left. + \sum_{n=1}^N w_{(n+2)} \dot{f}_1 \dot{f}_{n+2} \right) \Big] d\xi
\end{aligned} \tag{B.25}$$

$$\begin{aligned}
\frac{\partial U_{BS}}{\partial q_{b+2}} = \int_0^1 & \left[ -\frac{1}{2L} k_s \bar{B}_{16} \left( \beta_{z1} \dot{f}_2 \dot{f}_1 + \beta_{z2} \dot{f}_2 \dot{f}_2 + \sum_{n=1}^N \beta_{z(n+2)} \dot{f}_2 \dot{f}_{n+2} \right) \right. \\
& + \frac{1}{L} k_s \bar{B}_{15} \left( \beta_{y1} \dot{f}_2 \dot{f}_1 + \beta_{y2} \dot{f}_2 \dot{f}_2 + \sum_{n=1}^N \beta_{y(n+2)} \dot{f}_2 \dot{f}_{n+2} \right) \\
& + k_s (\bar{A}_{66} + \bar{A}_{55}) \left( \beta_{y1} \dot{f}_2 \dot{f}_1 + \beta_{y2} \dot{f}_2 \dot{f}_2 \right. \\
& + \left. \sum_{n=1}^N \beta_{y(n+2)} \dot{f}_2 \dot{f}_{n+2} \right) \\
& + \frac{1}{L} k_s (\bar{A}_{66} + \bar{A}_{55}) \left( w_1 \dot{f}_2 \dot{f}_1 + w_2 \dot{f}_2 \dot{f}_2 \right. \\
& + \left. \sum_{n=1}^N w_{(n+2)} \dot{f}_2 \dot{f}_{n+2} \right) \Big] d\xi \tag{B.26} \\
& \cdot \qquad \qquad \qquad \cdot \qquad \qquad \qquad \cdot \\
& \cdot \qquad \qquad \qquad \cdot \qquad \qquad \qquad \cdot \\
& \cdot \qquad \qquad \qquad \cdot \qquad \qquad \qquad \cdot
\end{aligned}$$

$$\begin{aligned}
\frac{\partial U_{BS}}{\partial q_{2b}} = \int_0^1 & \left[ -\frac{1}{2L} k_s \bar{B}_{16} \left( \beta_{z1} \dot{f}_{N+2} \dot{f}_1 + \beta_{z2} \dot{f}_{N+2} \dot{f}_2 \right. \right. \\
& + \sum_{n=1}^N \beta_{z(n+2)} \dot{f}_{N+2} \dot{f}_{n+2} \left. \right) \\
& + \frac{1}{L} k_s \bar{B}_{15} \left( \beta_{y1} \dot{f}_{N+2} \dot{f}_1 + \beta_{y2} \dot{f}_{N+2} \dot{f}_2 \right. \\
& + \sum_{n=1}^N \beta_{y(n+2)} \dot{f}_{N+2} \dot{f}_{n+2} \left. \right) \\
& + k_s (\bar{A}_{66} + \bar{A}_{55}) \left( \beta_{y1} \dot{f}_{N+2} f_1 + \beta_{y2} \dot{f}_{N+2} f_2 \right. \\
& + \sum_{n=1}^N \beta_{y(n+2)} \dot{f}_{N+2} f_{n+2} \left. \right) \\
& + \frac{1}{L} k_s (\bar{A}_{66} + \bar{A}_{55}) \left( w_1 \dot{f}_{N+2} \dot{f}_1 + w_2 \dot{f}_{N+2} \dot{f}_2 \right. \\
& \left. \left. + \sum_{n=1}^N w_{(n+2)} \dot{f}_{N+2} \dot{f}_{n+2} \right) \right] d\xi
\end{aligned} \tag{B.27}$$

$$\begin{aligned}
\frac{\partial U_{BS}}{\partial q_{2b+1}} = & \int_0^1 \left[ -\frac{1}{2L} k_s \bar{B}_{16} \left( v_1 \dot{f}_1 \dot{f}_1 + v_2 \dot{f}_1 \dot{f}_2 + \sum_{n=1}^N v_{(n+2)} \dot{f}_1 \dot{f}_{2+n} \right) \right. \\
& + \frac{1}{L} k_s \bar{B}_{15} \left( w_1 \dot{f}_1 \dot{f}_1 + w_2 \dot{f}_1 \dot{f}_2 + \sum_{n=1}^N w_{(n+2)} \dot{f}_1 \dot{f}_{n+2} \right) \\
& + k_s (\bar{A}_{66} + \bar{A}_{55}) \left( w_1 f_1 \dot{f}_1 + w_2 f_1 \dot{f}_2 + \sum_{n=1}^N w_{n+2} f_1 \dot{f}_{n+2} \right) \\
& + \frac{1}{L} \bar{D}_{11} \left( \beta_{y1} \dot{f}_1 \dot{f}_1 + \beta_{y2} \dot{f}_1 \dot{f}_2 + \sum_{n=1}^N \beta_{y(n+2)} \dot{f}_1 \dot{f}_{n+2} \right) \\
& + k_s \bar{B}_{15} \left( \beta_{y1} f_1 \dot{f}_1 + \beta_{y2} f_1 \dot{f}_2 + \sum_{n=1}^N \beta_{y(n+2)} f_1 \dot{f}_{n+2} \right) \\
& + k_s \bar{B}_{15} \left( \beta_{y1} \dot{f}_1 f_1 + \beta_{y2} \dot{f}_1 f_2 + \sum_{n=1}^N \beta_{y(n+2)} \dot{f}_1 f_{n+2} \right) \\
& + L k_s (\bar{A}_{66} + \bar{A}_{55}) \left( \beta_{y1} f_1 f_1 + \beta_{y2} f_1 f_2 + \sum_{n=1}^N \beta_{y(n+2)} f_1 f_{n+2} \right) \\
& + \frac{1}{2} k_s \bar{B}_{16} \left( \beta_{z1} \dot{f}_1 f_1 + \beta_{z2} \dot{f}_1 f_2 + \sum_{n=1}^N \beta_{z(n+2)} \dot{f}_1 f_{n+2} \right) \\
& \left. - \frac{1}{2} k_s \bar{B}_{16} \left( \beta_{z1} f_1 \dot{f}_1 + \beta_{z2} f_1 \dot{f}_2 + \sum_{n=1}^N \beta_{z(n+2)} f_1 \dot{f}_{n+2} \right) \right] d\xi \tag{B.28}
\end{aligned}$$

$$\begin{aligned}
\frac{\partial U_{BS}}{\partial q_{2b+2}} = & \int_0^1 \left[ -\frac{1}{2L} k_s \bar{B}_{16} \left( v_1 \dot{f}_2 \dot{f}_1 + v_2 \dot{f}_2 \dot{f}_2 + \sum_{n=1}^N v_{(n+2)} \dot{f}_2 \dot{f}_{2+n} \right) \right. \\
& + \frac{1}{L} k_s \bar{B}_{15} \left( w_1 \dot{f}_2 \dot{f}_1 + w_2 \dot{f}_2 \dot{f}_2 + \sum_{n=1}^N w_{(n+2)} \dot{f}_2 \dot{f}_{n+2} \right) \\
& + k_s (\bar{A}_{66} + \bar{A}_{55}) \left( w_1 f_2 \dot{f}_1 + w_2 f_2 \dot{f}_2 + \sum_{n=1}^N w_{n+2} f_2 \dot{f}_{n+2} \right) \\
& + \frac{1}{L} \bar{D}_{11} \left( \beta_{y1} \dot{f}_2 \dot{f}_1 + \beta_{y2} \dot{f}_2 \dot{f}_2 + \sum_{n=1}^N \beta_{y(n+2)} \dot{f}_2 \dot{f}_{n+2} \right) \\
& + k_s \bar{B}_{15} \left( \beta_{y1} f_2 \dot{f}_1 + \beta_{y2} f_2 \dot{f}_2 + \sum_{n=1}^N \beta_{y(n+2)} f_2 \dot{f}_{n+2} \right) \\
& + k_s \bar{B}_{15} \left( \beta_{y1} \dot{f}_2 f_1 + \beta_{y2} \dot{f}_2 f_2 + \sum_{n=1}^N \beta_{y(n+2)} \dot{f}_2 f_{n+2} \right) \\
& + L k_s (\bar{A}_{66} + \bar{A}_{55}) \left( \beta_{y1} f_2 f_1 + \beta_{y2} f_2 f_2 + \sum_{n=1}^N \beta_{y(n+2)} f_2 f_{n+2} \right) \\
& + \frac{1}{2} k_s \bar{B}_{16} \left( \beta_{z1} \dot{f}_2 f_1 + \beta_{z2} \dot{f}_2 f_2 + \sum_{n=1}^N \beta_{z(n+2)} \dot{f}_2 f_{n+2} \right) \\
& \left. - \frac{1}{2} k_s \bar{B}_{16} \left( \beta_{z1} f_2 \dot{f}_1 + \beta_{z2} f_2 \dot{f}_2 + \sum_{n=1}^N \beta_{z(n+2)} f_2 \dot{f}_{n+2} \right) \right] d\xi \quad (B.29) \\
& \cdot \qquad \qquad \qquad \cdot \qquad \qquad \qquad \cdot \\
& \cdot \qquad \qquad \qquad \cdot \qquad \qquad \qquad \cdot \\
& \cdot \qquad \qquad \qquad \cdot \qquad \qquad \qquad \cdot
\end{aligned}$$

$$\begin{aligned}
\frac{\partial U_{BS}}{\partial q_{3b}} = \int_0^1 & \left[ -\frac{1}{2L} k_s \bar{B}_{16} \left( v_1 \dot{f}_{N+2} \dot{f}_1 + v_2 \dot{f}_{N+2} \dot{f}_2 + \sum_{n=1}^N v_{(n+2)} \dot{f}_{N+2} \dot{f}_{n+2} \right) \right. \\
& + \frac{1}{L} k_s \bar{B}_{15} \left( w_1 \dot{f}_{N+2} \dot{f}_1 + w_2 \dot{f}_{N+2} \dot{f}_2 + \sum_{n=1}^N w_{(n+2)} \dot{f}_{N+2} \dot{f}_{n+2} \right) \\
& + k_s (\bar{A}_{66} + \bar{A}_{55}) \left( w_1 f_{N+2} \dot{f}_1 + w_2 f_{N+2} \dot{f}_2 \right. \\
& \left. + \sum_{n=1}^N w_{n+2} f_{N+2} \dot{f}_{n+2} \right) \\
& + \frac{1}{L} \bar{D}_{11} \left( \beta_{y1} \dot{f}_{N+2} \dot{f}_1 + \beta_{y2} \dot{f}_{N+2} \dot{f}_2 + \sum_{n=1}^N \beta_{y(n+2)} \dot{f}_{N+2} \dot{f}_{n+2} \right) \\
& + k_s \bar{B}_{15} \left( \beta_{y1} f_{N+2} \dot{f}_1 + \beta_{y2} f_{N+2} \dot{f}_2 + \sum_{n=1}^N \beta_{y(n+2)} f_{N+2} \dot{f}_{n+2} \right) \\
& + k_s \bar{B}_{15} \left( \beta_{y1} \dot{f}'_{N+2} f_1 + \beta_{y2} \dot{f}'_{N+2} f_2 + \sum_{n=1}^N \beta_{y(n+2)} \dot{f}'_{N+2} f_{n+2} \right) \\
& + L k_s (\bar{A}_{66} + \bar{A}_{55}) \left( \beta_{y1} f_{N+2} \dot{f}_1 + \beta_{y2} f_{N+2} \dot{f}_2 \right. \\
& \left. + \sum_{n=1}^N \beta_{y(n+2)} f_{N+2} \dot{f}_{n+2} \right) \\
& + \frac{1}{2} k_s \bar{B}_{16} \left( \beta_{z1} \dot{f}'_{N+2} f_1 + \beta_{z2} \dot{f}'_{N+2} f_2 + \sum_{n=1}^N \beta_{z(n+2)} \dot{f}'_{N+2} f_{n+2} \right) \\
& - \frac{1}{2} k_s \bar{B}_{16} \left( \beta_{z1} f_{N+2} \dot{f}_1 + \beta_{z2} f_{N+2} \dot{f}_2 \right. \\
& \left. + \sum_{n=1}^N \beta_{z(n+2)} f_{N+2} \dot{f}_{n+2} \right) \Big] d\xi
\end{aligned} \tag{B.30}$$

$$\begin{aligned}
\frac{\partial U_{BS}}{\partial q_{3b+1}} = & \int_0^1 \left[ -\frac{1}{L} k_s \bar{B}_{15} \left( v_1 \hat{f}_1 \hat{f}_1 + v_2 \hat{f}_1 \hat{f}_2 + \sum_{n=1}^N v_{(n+2)} \hat{f}_1 \hat{f}_{n+2} \right) \right. \\
& - k_s (\bar{A}_{66} + \bar{A}_{55}) \left( v_1 \hat{f}_1 \hat{f}_1 + v_2 \hat{f}_1 \hat{f}_2 + \sum_{n=1}^N v_{(n+2)} \hat{f}_1 \hat{f}_{n+2} \right) \\
& - \frac{1}{2L} k_s \bar{B}_{16} \left( w_1 \hat{f}_1 \hat{f}_1 + w_2 \hat{f}_1 \hat{f}_2 + \sum_{n=1}^N w_{(n+2)} \hat{f}_1 \hat{f}_{n+2} \right) \\
& + \frac{1}{2} k_s \bar{B}_{16} \left( \beta_{y1} f_1 \hat{f}_1 + \beta_{y2} f_1 \hat{f}_2 + \sum_{n=1}^N \beta_{y(n+2)} f_1 \hat{f}_{n+2} \right) \\
& - \frac{1}{2} k_s \bar{B}_{16} \left( \beta_{y1} \hat{f}_1 f_1 + \beta_{y2} \hat{f}_1 f_2 + \sum_{n=1}^N \beta_{y(n+2)} \hat{f}_1 f_{n+2} \right) \\
& + \frac{1}{L} \bar{D}_{11} \left( \beta_{z1} \hat{f}_1 \hat{f}_1 + \beta_{z2} \hat{f}_1 \hat{f}_2 + \sum_{n=1}^N \beta_{z(n+2)} \hat{f}_1 \hat{f}_{n+2} \right) \\
& + k_s \bar{B}_{15} \left( \beta_{z1} \hat{f}_1 f_1 + \beta_{z2} \hat{f}_1 f_2 + \sum_{n=1}^N \beta_{z(n+2)} \hat{f}_1 f_{n+2} \right) \\
& + k_s \bar{B}_{15} \left( \beta_{z1} f_1 \hat{f}_1 + \beta_{z2} f_1 \hat{f}_2 + \sum_{n=1}^N \beta_{z(n+2)} f_1 \hat{f}_{n+2} \right) \\
& + L k_s (\bar{A}_{66} + \bar{A}_{55}) \left( \beta_{z1} f_1 f_1 + \beta_{z2} f_1 f_2 \right. \\
& \left. + \sum_{n=1}^N \beta_{z(n+2)} f_1 f_{n+2} \right) \Big] d\xi
\end{aligned} \tag{B.31}$$

$$\begin{aligned}
\frac{\partial U_{BS}}{\partial q_{3b+2}} = & \int_0^1 \left[ -\frac{1}{L} k_s \bar{B}_{15} \left( v_1 \dot{f}_2 \dot{f}_1 + v_2 \dot{f}_2 \dot{f}_2 + \sum_{n=1}^N v_{(n+2)} \dot{f}_2 \dot{f}_{n+2} \right) \right. \\
& - k_s (\bar{A}_{66} + \bar{A}_{55}) \left( v_1 \dot{f}_2 \dot{f}_1 + v_2 \dot{f}_2 \dot{f}_2 + \sum_{n=1}^N v_{(n+2)} \dot{f}_2 \dot{f}_{n+2} \right) \\
& - \frac{1}{2L} k_s \bar{B}_{16} \left( w_1 \dot{f}_2 \dot{f}_1 + w_2 \dot{f}_2 \dot{f}_2 + \sum_{n=1}^N w_{(n+2)} \dot{f}_2 \dot{f}_{n+2} \right) \\
& + \frac{1}{2} k_s \bar{B}_{16} \left( \beta_{y1} \dot{f}_2 \dot{f}_1 + \beta_{y2} \dot{f}_2 \dot{f}_2 + \sum_{n=1}^N \beta_{y(n+2)} \dot{f}_2 \dot{f}_{n+2} \right) \\
& - \frac{1}{2} k_s \bar{B}_{16} \left( \beta_{y1} \dot{f}_2 \dot{f}_1 + \beta_{y2} \dot{f}_2 \dot{f}_2 + \sum_{n=1}^N \beta_{y(n+2)} \dot{f}_2 \dot{f}_{n+2} \right) \\
& + \frac{1}{L} \bar{D}_{11} \left( \beta_{z1} \dot{f}_2 \dot{f}_1 + \beta_{z2} \dot{f}_2 \dot{f}_2 + \sum_{n=1}^N \beta_{z(n+2)} \dot{f}_2 \dot{f}_{n+2} \right) \\
& + k_s \bar{B}_{15} \left( \beta_{z1} \dot{f}_2 \dot{f}_1 + \beta_{z2} \dot{f}_2 \dot{f}_2 + \sum_{n=1}^N \beta_{z(n+2)} \dot{f}_2 \dot{f}_{n+2} \right) \\
& + k_s \bar{B}_{15} \left( \beta_{z1} \dot{f}_2 \dot{f}_1 + \beta_{z2} \dot{f}_2 \dot{f}_2 + \sum_{n=1}^N \beta_{z(n+2)} \dot{f}_2 \dot{f}_{n+2} \right) \\
& + L k_s (\bar{A}_{66} + \bar{A}_{55}) \left( \beta_{z1} \dot{f}_2 \dot{f}_1 + \beta_{z2} \dot{f}_2 \dot{f}_2 \right. \\
& \left. + \sum_{n=1}^N \beta_{z(n+2)} \dot{f}_2 \dot{f}_{n+2} \right) \Big] d\xi
\end{aligned} \tag{B.32}$$

. . .  
. . .  
. . .

$$\begin{aligned}
\frac{\partial U_{BS}}{\partial q_{4b}} = \int_0^1 & \left[ -\frac{1}{L} k_s \bar{B}_{15} \left( v_1 \dot{f}_{N+2} \dot{f}_1 + v_2 \dot{f}_{N+2} \dot{f}_2 + \sum_{n=1}^N v_{(n+2)} \dot{f}_{N+2} \dot{f}_{n+2} \right) \right. \\
& - k_s (\bar{A}_{66} + \bar{A}_{55}) \left( v_1 \dot{f}_{N+2} \dot{f}_1 + v_2 \dot{f}_{N+2} \dot{f}_2 \right. \\
& \left. + \sum_{n=1}^N v_{(n+2)} \dot{f}_{N+2} \dot{f}_{n+2} \right) \\
& - \frac{1}{2L} k_s \bar{B}_{16} \left( w_1 \dot{f}_{N+2} \dot{f}_1 + w_2 \dot{f}_{N+2} \dot{f}_2 \right. \\
& \left. + \sum_{n=1}^N w_{(n+2)} \dot{f}_{N+2} \dot{f}_{n+2} \right) \\
& + \frac{1}{2} k_s \bar{B}_{16} \left( \beta_{y1} f_{N+2} \dot{f}_1 + \beta_{y2} f_{N+2} \dot{f}_2 + \sum_{n=1}^N \beta_{y(n+2)} f_{N+2} \dot{f}_{n+2} \right) \\
& - \frac{1}{2} k_s \bar{B}_{16} \left( \beta_{y1} \dot{f}_{N+2} f_1 + \beta_{y2} \dot{f}_{N+2} f_2 + \sum_{n=1}^N \beta_{y(n+2)} \dot{f}_{N+2} f_{n+2} \right) \\
& + \frac{1}{L} \bar{D}_{11} \left( \beta_{z1} \dot{f}_{N+2} \dot{f}_1 + \beta_{z2} \dot{f}_{N+2} \dot{f}_2 + \sum_{n=1}^N \beta_{z(n+2)} \dot{f}_{N+2} \dot{f}_{n+2} \right) \\
& + k_s \bar{B}_{15} \left( \beta_{z1} \dot{f}_{N+2} f_1 + \beta_{z2} \dot{f}_{N+2} f_2 + \sum_{n=1}^N \beta_{z(n+2)} \dot{f}_{N+2} f_{n+2} \right) \\
& + k_s \bar{B}_{15} \left( \beta_{z1} f_{N+2} \dot{f}_1 + \beta_{z2} f_{N+2} \dot{f}_2 + \sum_{n=1}^N \beta_{z(n+2)} f_{N+2} \dot{f}_{n+2} \right) \\
& + L k_s (\bar{A}_{66} + \bar{A}_{55}) \left( \beta_{z1} f_{N+2} f_1 + \beta_{z2} f_{N+2} f_2 \right. \\
& \left. + \sum_{n=1}^N \beta_{z(n+2)} f_{N+2} f_{n+2} \right) \Big] d\xi
\end{aligned} \tag{B.33}$$

$$\frac{\partial U_F}{\partial q_1} = \int_0^1 \frac{P}{L} \left( v_1 \dot{f}_1 \dot{f}_1 + v_2 \dot{f}_1 \dot{f}_2 + \sum_{n=1}^N v_{(n+2)} \dot{f}_1 \dot{f}_{2+n} \right) d\xi \quad (\text{B.34})$$

$$\frac{\partial U_F}{\partial q_2} = \int_0^1 \frac{P}{L} \left( v_1 \dot{f}_2 \dot{f}_1 + v_2 \dot{f}_2 \dot{f}_2 + \sum_{n=1}^N v_{(n+2)} \dot{f}_2 \dot{f}_{2+n} \right) d\xi \quad (\text{B.35})$$

⋮

$$\frac{\partial U_F}{\partial q_b} = \int_0^1 \frac{P}{L} \left( v_1 \dot{f}_{N+2} \dot{f}_1 + v_2 \dot{f}_{N+2} \dot{f}_2 + \sum_{n=1}^N v_{(n+2)} \dot{f}_{N+2} \dot{f}_{2+n} \right) d\xi \quad (\text{B.36})$$

$$\frac{\partial U_F}{\partial q_{b+1}} = \int_0^1 \frac{P}{L} \left( w_1 \dot{f}_1 \dot{f}_1 + w_2 \dot{f}_1 \dot{f}_2 + \sum_{n=1}^N w_{(n+2)} \dot{f}_1 \dot{f}_{2+n} \right) d\xi \quad (\text{B.37})$$

$$\frac{\partial U_F}{\partial q_{b+2}} = \int_0^1 \frac{P}{L} \left( w_1 \dot{f}_2 \dot{f}_1 + w_2 \dot{f}_2 \dot{f}_2 + \sum_{n=1}^N w_{(n+2)} \dot{f}_2 \dot{f}_{2+n} \right) d\xi \quad (\text{B.38})$$

⋮

$$\frac{\partial U_F}{\partial q_{2b}} = \int_0^1 \frac{P}{L} \left( w_1 \dot{f}_{N+2} \dot{f}_1 + w_2 \dot{f}_{N+2} \dot{f}_2 + \sum_{n=1}^N w_{(n+2)} \dot{f}_{N+2} \dot{f}_{2+n} \right) d\xi \quad (\text{B.39})$$

## Appendix C

### Lagrange's interpolation formulation

The displacement field for the shaft element with three nodes in terms of nodal displacements and shape functions is

$$v(x) = \sum_{i=1}^3 v_i(t) N_{ii}(x) \quad (C.1)$$

$$w(x) = \sum_{i=1}^3 w_i(t) N_{ii}(x) \quad (C.2)$$

$$\beta_y(x) = \sum_{i=1}^3 \beta_{yi}(t) N_{ii}(x) \quad (C.3)$$

$$\beta_z(x) = \sum_{i=1}^3 \beta_{zi}(t) N_{ii}(x) \quad (C.4)$$

The kinetic energy of the tapered composite shaft

$$\begin{aligned} T_{comp} = & \frac{1}{2} \int_0^L m_c(x) (\dot{v}^2 + \dot{w}^2) dx + \frac{1}{2} \int_0^L I_{dc}(x) (\dot{\beta}_y^2 + \dot{\beta}_z^2) dx \\ & - \int_0^L I_{pc}(x) \Omega \dot{\beta}_z \beta_y dx \end{aligned} \quad (C.5)$$

The strain energy of the tapered composite shaft due to axial load is

$$U_F = \frac{1}{2} \int_0^L P \left[ \left( \frac{\partial v}{\partial x} \right)^2 + \left( \frac{\partial w}{\partial x} \right)^2 \right] dx \quad (C.6)$$

The strain energy of tapered composite shaft due to bending moments and shear forces is

$$\begin{aligned} U_{BS} = \frac{1}{2} \int_0^L & \left[ \left( \frac{\partial \beta_y}{\partial x} \right) \left( \bar{D}_{11} \frac{\partial \beta_y}{\partial x} + \bar{B}_{15} k_s \left( \beta_y + \frac{\partial w}{\partial x} \right) + \frac{1}{2} \bar{B}_{16} k_s \left( \beta_z - \frac{\partial v}{\partial x} \right) \right) \right. \\ & + \left( \frac{\partial \beta_z}{\partial x} \right) \left( \bar{D}_{11} \frac{\partial \beta_z}{\partial x} - \bar{B}_{15} k_s \left( \frac{\partial v}{\partial x} - \beta_z \right) - \frac{1}{2} \bar{B}_{16} k_s \left( \beta_y + \frac{\partial w}{\partial x} \right) \right) \\ & + \left( \frac{\partial v}{\partial x} \right. \\ & \left. - \beta_z \right) k_s \left( \left( -\bar{B}_{15} \frac{\partial \beta_z}{\partial x} + \bar{A}_{55} \left( \frac{\partial v}{\partial x} - \beta_z \right) + \bar{A}_{56} \left( \beta_y + \frac{\partial w}{\partial x} \right) \right) \right. \\ & \left. - \left( \frac{1}{2} \bar{B}_{61} \frac{\partial \beta_y}{\partial x} + \bar{A}_{65} \left( \beta_y + \frac{\partial w}{\partial x} \right) + \bar{A}_{66} \left( \beta_z - \frac{\partial v}{\partial x} \right) \right) \right) \\ & + \left( \beta_y \right. \\ & \left. + \frac{\partial w}{\partial x} \right) k_s \left( \left( \bar{B}_{51} \frac{\partial \beta_y}{\partial x} + \bar{A}_{55} \left( \beta_y + \frac{\partial w}{\partial x} \right) + \bar{A}_{56} \left( \beta_z - \frac{\partial v}{\partial x} \right) \right) \right. \\ & \left. + \left( -\frac{1}{2} \bar{B}_{61} \frac{\partial \beta_z}{\partial x} + \bar{A}_{65} \left( \frac{\partial v}{\partial x} - \beta_z \right) + \bar{A}_{66} \left( \beta_y + \frac{\partial w}{\partial x} \right) \right) \right) \right] dx \quad (C.7) \end{aligned}$$

Substituting Equations (C.1) – (C.4) into Equations (C.5) – (C.7), and then applying Lagrange's equations, one can get the equations of motion of the tapered composite shaft.

The generalized co-ordinates for the shaft element are

$$\begin{aligned}
 q_1 &= v_1 & q_2 &= v_2 & q_3 &= v_3 \\
 q_4 &= w_1 & q_5 &= w_2 & q_6 &= w_3 \\
 q_7 &= \beta_{y1} & q_8 &= \beta_{y2} & q_9 &= \beta_{y3} \\
 q_{10} &= \beta_{z1} & q_{11} &= \beta_{z2} & q_{12} &= \beta_{z3}
 \end{aligned} \tag{C.8}$$

Using Lagrange's equation

$$\frac{d}{dt} \left( \frac{\partial L}{\partial \dot{q}} \right) - \frac{\partial L}{\partial q} = 0 \tag{C.9}$$

where

$$L = T_{comp} - (U_{BS} + U_F)$$

Applying Lagrange's equation gives

$$\frac{d}{dt} \left[ \frac{\partial T_{comp}}{\partial \dot{q}_1} \right] - \frac{\partial T_{comp}}{\partial q_1} = \int_0^L m_c(x) (\ddot{v}_1 N_{11} N_{11} + \ddot{v}_2 N_{11} N_{22} + \ddot{v}_3 N_{11} N_{33}) dx \tag{C.10}$$

$$\frac{d}{dt} \left[ \frac{\partial T_{comp}}{\partial \dot{q}_2} \right] - \frac{\partial T_{comp}}{\partial q_2} = \int_0^L m_c(x) (\ddot{v}_1 N_{22} N_{11} + \ddot{v}_2 N_{22} N_{22} + \ddot{v}_3 N_{22} N_{33}) dx \tag{C.11}$$

$$\frac{d}{dt} \left[ \frac{\partial T_{comp}}{\partial \dot{q}_3} \right] - \frac{\partial T_{comp}}{\partial q_3} = \int_0^L m_c(x) (\ddot{v}_1 N_{33} N_{11} + \ddot{v}_2 N_{33} N_{22} + \ddot{v}_3 N_{33} N_{33}) dx \tag{C.12}$$

$$\frac{d}{dt} \left[ \frac{\partial T_{comp}}{\partial \dot{q}_4} \right] - \frac{\partial T_{comp}}{\partial q_4} = \int_0^L m_c(x) (\ddot{w}_1 N_{11} N_{11} + \ddot{w}_2 N_{11} N_{22} + \ddot{w}_3 N_{11} N_{33}) dx \quad (C.13)$$

$$\frac{d}{dt} \left[ \frac{\partial T_{comp}}{\partial \dot{q}_5} \right] - \frac{\partial T_{comp}}{\partial q_5} = \int_0^L m_c(x) (\ddot{w}_1 N_{22} N_{11} + \ddot{w}_2 N_{22} N_{22} + \ddot{w}_3 N_{22} N_{33}) dx \quad (C.14)$$

$$\frac{d}{dt} \left[ \frac{\partial T_{comp}}{\partial \dot{q}_6} \right] - \frac{\partial T_{comp}}{\partial q_6} = \int_0^L m_c(x) (\ddot{w}_1 N_{33} N_{11} + \ddot{w}_2 N_{33} N_{22} + \ddot{w}_3 N_{33} N_{33}) dx \quad (C.15)$$

$$\begin{aligned} \frac{d}{dt} \left[ \frac{\partial T_{comp}}{\partial \dot{q}_7} \right] - \frac{\partial T_{comp}}{\partial q_7} &= \int_0^L [I_{dc}(x) (\ddot{\beta}_{y1} N_{11} N_{11} + \ddot{\beta}_{y2} N_{11} N_{22} + \ddot{\beta}_{y3} N_{11} N_{33}) \\ &\quad + \Omega I_p(x) (\dot{\beta}_{z1} N_{11} N_{11} + \dot{\beta}_{z2} N_{11} N_{22} + \dot{\beta}_{z3} N_{11} N_{33})] dx \end{aligned} \quad (C.16)$$

$$\begin{aligned} \frac{d}{dt} \left[ \frac{\partial T_{comp}}{\partial \dot{q}_8} \right] - \frac{\partial T_{comp}}{\partial q_8} &= \int_0^L [I_{dc}(x) (\ddot{\beta}_{y1} N_{22} N_{11} + \ddot{\beta}_{y2} N_{22} N_{22} + \ddot{\beta}_{y3} N_{22} N_{33}) \\ &\quad + \Omega I_p(x) (\dot{\beta}_{z1} N_{22} N_{11} + \dot{\beta}_{z2} N_{22} N_{22} + \dot{\beta}_{z3} N_{22} N_{33})] dx \end{aligned} \quad (C.17)$$

$$\begin{aligned} \frac{d}{dt} \left[ \frac{\partial T_{comp}}{\partial \dot{q}_9} \right] - \frac{\partial T_{comp}}{\partial q_9} &= \int_0^L [I_{dc}(x) (\ddot{\beta}_{y1} N_{33} N_{11} + \ddot{\beta}_{y2} N_{33} N_{22} + \ddot{\beta}_{y3} N_{33} N_{33}) \\ &\quad + \Omega I_p(x) (\dot{\beta}_{z1} N_{33} N_{11} + \dot{\beta}_{z2} N_{33} N_{22} + \dot{\beta}_{z3} N_{33} N_{33})] dx \end{aligned} \quad (C.18)$$

$$\begin{aligned}
& \frac{d}{dt} \left[ \frac{\partial T_{comp}}{\partial \dot{q}_{10}} \right] - \frac{\partial T_{comp}}{\partial q_{10}} \\
&= \int_0^L [I_{dc}(x) (\ddot{\beta}_{z1} N_{11} N_{11} + \ddot{\beta}_{z2} N_{11} N_{22} + \ddot{\beta}_{z3} N_{11} N_{33}) \\
&\quad - \Omega I_p(z) (\dot{\beta}_{y1} N_{11} N_{11} + \dot{\beta}_{y2} N_{11} N_{22} + \dot{\beta}_{y3} N_{11} N_{33})] dx \quad (C.19)
\end{aligned}$$

$$\begin{aligned}
& \frac{d}{dt} \left[ \frac{\partial T_{comp}}{\partial \dot{q}_{11}} \right] - \frac{\partial T_{comp}}{\partial q_{11}} \\
&= \int_0^L [I_{dc}(x) (\ddot{\beta}_{z1} N_{22} N_{11} + \ddot{\beta}_{z2} N_{22} N_{22} + \ddot{\beta}_{z3} N_{22} N_{33}) \\
&\quad - \Omega I_p(x) (\dot{\beta}_{y1} N_{22} N_{11} + \dot{\beta}_{y2} N_{22} N_{22} + \dot{\beta}_{y3} N_{22} N_{33})] dx \quad (C.20)
\end{aligned}$$

$$\begin{aligned}
& \frac{d}{dt} \left[ \frac{\partial T_{comp}}{\partial \dot{q}_{12}} \right] - \frac{\partial T_{comp}}{\partial q_{12}} \\
&= \int_0^L [I_{dc}(x) (\ddot{\beta}_{z1} N_{33} N_{11} + \ddot{\beta}_{z2} N_{33} N_{22} + \ddot{\beta}_{z3} N_{33} N_{33}) \\
&\quad - \Omega I_p(x) (\dot{\beta}_{y1} N_{33} N_{11} + \dot{\beta}_{y2} N_{33} N_{22} + \dot{\beta}_{y3} N_{33} N_{33})] dx \quad (C.21)
\end{aligned}$$

$$\begin{aligned}
\frac{\partial U_{BS}}{\partial q_1} = \int_0^L & \left[ k_s(\bar{A}_{66} + \bar{A}_{55})(v_1 \dot{N}_{11} \dot{N}_{11} + v_2 \dot{N}_{11} \dot{N}_{22} + v_3 \dot{N}_{11} \dot{N}_{33}) \right. \\
& - \frac{1}{2} k_s \bar{B}_{16} (\beta_{y1} \dot{N}_{11} \dot{N}_{11} + \beta_{y2} \dot{N}_{11} \dot{N}_{22} + \beta_{y3} \dot{N}_{11} \dot{N}_{33}) \\
& - k_s \bar{B}_{15} (\beta_{z1} \dot{N}_{11} \dot{N}_{11} + \beta_{z2} \dot{N}_{11} \dot{N}_{22} + \beta_{z3} \dot{N}_{11} \dot{N}_{33}) \\
& \left. - k_s(\bar{A}_{66} + \bar{A}_{55})(\beta_{z1} \dot{N}_{11} N_{11} + \beta_{z2} \dot{N}_{11} N_{22} + \beta_{z3} \dot{N}_{11} N_{33}) \right] dx \quad (C.22)
\end{aligned}$$

$$\begin{aligned}
\frac{\partial U_{BS}}{\partial q_2} = \int_0^L & \left[ k_s(\bar{A}_{66} + \bar{A}_{55})(v_1 \dot{N}_{22} \dot{N}_{11} + v_2 \dot{N}_{22} \dot{N}_{22} + v_3 \dot{N}_{22} \dot{N}_{33}) \right. \\
& - \frac{1}{2} k_s \bar{B}_{16} (\beta_{y1} \dot{N}_{22} \dot{N}_{11} + \beta_{y2} \dot{N}_{22} \dot{N}_{22} + \beta_{y3} \dot{N}_{22} \dot{N}_{33}) \\
& - k_s \bar{B}_{15} (\beta_{z1} \dot{N}_{22} \dot{N}_{11} + \beta_{z2} \dot{N}_{22} \dot{N}_{22} + \beta_{z3} \dot{N}_{22} \dot{N}_{33}) \\
& \left. - k_s(\bar{A}_{66} + \bar{A}_{55})(\beta_{z1} \dot{N}_{22} N_{11} + \beta_{z2} \dot{N}_{22} N_{22} + \beta_{z3} \dot{N}_{22} N_{33}) \right] dx \quad (C.23)
\end{aligned}$$

$$\begin{aligned}
\frac{\partial U_{BS}}{\partial q_3} = \int_0^L & \left[ k_s(\bar{A}_{66} + \bar{A}_{55})(v_1 \dot{N}_{33} \dot{N}_{11} + v_2 \dot{N}_{33} \dot{N}_{22} + v_3 \dot{N}_{33} \dot{N}_{33}) \right. \\
& - \frac{1}{2} k_s \bar{B}_{16} (\beta_{y1} \dot{N}_{33} \dot{N}_{11} + \beta_{y2} \dot{N}_{33} \dot{N}_{22} + \beta_{y3} \dot{N}_{33} \dot{N}_{33}) \\
& - k_s \bar{B}_{15} (\beta_{z1} \dot{N}_{33} \dot{N}_{11} + \beta_{z2} \dot{N}_{33} \dot{N}_{22} + \beta_{z3} \dot{N}_{33} \dot{N}_{33}) \\
& \left. - k_s(\bar{A}_{66} + \bar{A}_{55})(\beta_{z1} \dot{N}_{33} N_{11} + \beta_{z2} \dot{N}_{33} N_{22} + \beta_{z3} \dot{N}_{33} N_{33}) \right] dx \quad (C.24)
\end{aligned}$$

$$\begin{aligned}
\frac{\partial U_{BS}}{\partial q_4} = \int_0^L & \left[ k_s(\bar{A}_{66} + \bar{A}_{55})(w_1 \dot{N}_{11}\dot{N}_{11} + w_2 \dot{N}_{11}\dot{N}_{22} + w_3 \dot{N}_{11}\dot{N}_{33}) \right. \\
& + k_s\bar{B}_{15}(\beta_{y1} \dot{N}_{11}\dot{N}_{11} + \beta_{y2} \dot{N}_{11}\dot{N}_{22} + \beta_{y3}\dot{N}_{11}\dot{N}_{22}) \\
& + k_s(\bar{A}_{66} + \bar{A}_{55})(\beta_{y1}\dot{N}_{11}N_{11} + \beta_{y2}\dot{N}_{11}N_{22} + \beta_{y3}\dot{N}_{11}N_{33}) \\
& \left. - \frac{1}{2}k_s\bar{B}_{16}(\beta_{z1}\dot{N}_{11}\dot{N}_{11} + \beta_{z2} \dot{N}_{11}\dot{N}_{22} + \beta_{z3}\dot{N}_{11}\dot{N}_{33}) \right] dx \quad (C.25)
\end{aligned}$$

$$\begin{aligned}
\frac{\partial U_{BS}}{\partial q_5} = \int_0^L & \left[ k_s(\bar{A}_{66} + \bar{A}_{55})(w_1 \dot{N}_{22}\dot{N}_{11} + w_2 \dot{N}_{22}\dot{N}_{22} + w_3 \dot{N}_{22}\dot{N}_{33}) \right. \\
& + k_s\bar{B}_{15}(\beta_{y1} \dot{N}_{22}\dot{N}_{11} + \beta_{y2} \dot{N}_{22}\dot{N}_{22} + \beta_{y3}\dot{N}_{22}\dot{N}_{22}) \\
& + k_s(\bar{A}_{66} + \bar{A}_{55})(\beta_{y1}\dot{N}_{22}N_{11} + \beta_{y2}\dot{N}_{22}N_{22} + \beta_{y3}\dot{N}_{22}N_{33}) \\
& \left. - \frac{1}{2}k_s\bar{B}_{16}(\beta_{z1}\dot{N}_{22}\dot{N}_{11} + \beta_{z2} \dot{N}_{22}\dot{N}_{22} + \beta_{z3}\dot{N}_{22}\dot{N}_{33}) \right] dx \quad (C.26)
\end{aligned}$$

$$\begin{aligned}
\frac{\partial U_{BS}}{\partial q_6} = \int_0^L & \left[ k_s(\bar{A}_{66} + \bar{A}_{55})(w_1 \dot{N}_{33}\dot{N}_{11} + w_2 \dot{N}_{33}\dot{N}_{22} + w_3 \dot{N}_{33}\dot{N}_{33}) \right. \\
& + k_s\bar{B}_{15}(\beta_{y1} \dot{N}_{33}\dot{N}_{11} + \beta_{y2} \dot{N}_{33}\dot{N}_{22} + \beta_{y3}\dot{N}_{33}\dot{N}_{22}) \\
& + k_s(\bar{A}_{66} + \bar{A}_{55})(\beta_{y1}\dot{N}_{33}N_{11} + \beta_{y2}\dot{N}_{33}N_{22} + \beta_{y3}\dot{N}_{33}N_{33}) \\
& \left. - \frac{1}{2}k_s\bar{B}_{16}(\beta_{z1}\dot{N}_{33}\dot{N}_{11} + \beta_{z2} \dot{N}_{33}\dot{N}_{22} + \beta_{z3}\dot{N}_{33}\dot{N}_{33}) \right] dx \quad (C.27)
\end{aligned}$$

$$\begin{aligned}
\frac{\partial U_{BS}}{\partial q_7} = \int_0^L & \left[ -\frac{1}{2} k_s \bar{B}_{16} (v_1 \dot{N}_{11} \dot{N}_{11} + v_2 \dot{N}_{11} \dot{N}_{22} + v_3 \dot{N}_{11} \dot{N}_{33}) \right. \\
& + k_s \bar{B}_{15} (w_1 \dot{N}_{11} \dot{N}_{11} + w_2 \dot{N}_{11} \dot{N}_{22} + w_3 \dot{N}_{11} \dot{N}_{33}) \\
& + k_s (\bar{A}_{66} + \bar{A}_{55}) (w_1 N_{11} \dot{N}_{11} + w_2 N_{11} \dot{N}_{22} + w_3 N_{11} \dot{N}_{33}) \\
& + \bar{D}_{11} (\beta_{y1} \dot{N}_{11} \dot{N}_{11} + \beta_{y2} \dot{N}_{11} \dot{N}_{22} + \beta_{y3} \dot{N}_{11} \dot{N}_{33}) \\
& + k_s \bar{B}_{15} (\beta_{y1} \dot{N}_{11} N_{11} + \beta_{y2} \dot{N}_{11} N_{22} + \beta_{y3} \dot{N}_{11} N_{33}) \\
& + k_s \bar{B}_{15} (\beta_{y1} N_{11} \dot{N}_{11} + \beta_{y2} N_{11} \dot{N}_{22} + \beta_{y3} N_{11} \dot{N}_{33}) \\
& + k_s (\bar{A}_{66} + \bar{A}_{55}) (\beta_{y1} N_{11} N_{11} + \beta_{y2} N_{11} N_{22} + \beta_{y3} N_{11} N_{33}) \\
& + \frac{1}{2} k_s \bar{B}_{16} (\beta_{z1} \dot{N}_{11} N_{11} + \beta_{z2} \dot{N}_{11} N_{22} + \beta_{z3} \dot{N}_{11} N_{33}) \\
& \left. - \frac{1}{2} k_s \bar{B}_{16} (\beta_{z1} N_{11} \dot{N}_{11} + \beta_{z2} N_{11} \dot{N}_{22} + \beta_{z3} N_{11} \dot{N}_{33}) \right] dx \quad (C.28)
\end{aligned}$$

$$\begin{aligned}
\frac{\partial U_{BS}}{\partial q_8} = \int_0^L & \left[ -\frac{1}{2} k_s \bar{B}_{16} (v_1 \dot{N}_{22} \dot{N}_{11} + v_2 \dot{N}_{22} \dot{N}_{22} + v_3 \dot{N}_{22} \dot{N}_{33}) \right. \\
& + k_s \bar{B}_{15} (w_1 \dot{N}_{22} \dot{N}_{11} + w_2 \dot{N}_{22} \dot{N}_{22} + w_3 \dot{N}_{22} \dot{N}_{33}) \\
& + k_s (\bar{A}_{66} + \bar{A}_{55}) (w_1 N_{22} \dot{N}_{11} + w_2 N_{22} \dot{N}_{22} + w_3 N_{22} \dot{N}_{33}) \\
& + \bar{D}_{11} (\beta_{y1} \dot{N}_{22} \dot{N}_{11} + \beta_{y2} \dot{N}_{22} \dot{N}_{22} + \beta_{y3} \dot{N}_{22} \dot{N}_{33}) \\
& + k_s \bar{B}_{15} (\beta_{y1} \dot{N}_{22} N_{11} + \beta_{y2} \dot{N}_{22} N_{22} + \beta_{y3} \dot{N}_{22} N_{33}) \\
& + k_s \bar{B}_{15} (\beta_{y1} N_{22} \dot{N}_{11} + \beta_{y2} N_{22} \dot{N}_{22} + \beta_{y3} N_{22} \dot{N}_{33}) \\
& + k_s (\bar{A}_{66} + \bar{A}_{55}) (\beta_{y1} N_{22} N_{11} + \beta_{y2} N_{22} N_{22} + \beta_{y3} N_{22} N_{33}) \\
& + \frac{1}{2} k_s \bar{B}_{16} (\beta_{z1} \dot{N}_{22} N_{11} + \beta_{z2} \dot{N}_{22} N_{22} + \beta_{z3} \dot{N}_{22} N_{33}) \\
& \left. - \frac{1}{2} k_s \bar{B}_{16} (\beta_{z1} N_{22} \dot{N}_{11} + \beta_{z2} N_{22} \dot{N}_{22} + \beta_{z3} N_{22} \dot{N}_{33}) \right] dx \quad (C.29)
\end{aligned}$$

$$\begin{aligned}
\frac{\partial U_{BS}}{\partial q_9} = \int_0^L & \left[ -\frac{1}{2} k_s \bar{B}_{16} (v_1 \dot{N}_{33} \dot{N}_{11} + v_2 \dot{N}_{33} \dot{N}_{22} + v_3 \dot{N}_{33} \dot{N}_{33}) \right. \\
& + k_s \bar{B}_{15} (w_1 \dot{N}_{33} \dot{N}_{11} + w_2 \dot{N}_{33} \dot{N}_{22} + w_3 \dot{N}_{33} \dot{N}_{33}) \\
& + k_s (\bar{A}_{66} + \bar{A}_{55}) (w_1 N_{33} \dot{N}_{11} + w_2 N_{33} \dot{N}_{22} + w_3 N_{33} \dot{N}_{33}) \\
& + \bar{D}_{11} (\beta_{y1} \dot{N}_{33} \dot{N}_{11} + \beta_{y2} \dot{N}_{33} \dot{N}_{22} + \beta_{y3} \dot{N}_{33} \dot{N}_{33}) \\
& + k_s \bar{B}_{15} (\beta_{y1} \dot{N}_{33} N_{11} + \beta_{y2} \dot{N}_{33} N_{22} + \beta_{y3} \dot{N}_{33} N_{33}) \\
& + k_s \bar{B}_{15} (\beta_{y1} N_{33} \dot{N}_{11} + \beta_{y2} N_{33} \dot{N}_{22} + \beta_{y3} N_{33} \dot{N}_{33}) \\
& + k_s (\bar{A}_{66} + \bar{A}_{55}) (\beta_{y1} N_{33} N_{11} + \beta_{y2} N_{33} N_{22} + \beta_{y3} N_{33} N_{33}) \\
& + \frac{1}{2} k_s \bar{B}_{16} (\beta_{z1} \dot{N}_{33} N_{11} + \beta_{z2} \dot{N}_{33} N_{22} + \beta_{z3} \dot{N}_{33} N_{33}) \\
& \left. - \frac{1}{2} k_s \bar{B}_{16} (\beta_{z1} N_{33} \dot{N}_{11} + \beta_{z2} N_{33} \dot{N}_{22} + \beta_{z3} N_{33} \dot{N}_{33}) \right] dx \quad (C.30)
\end{aligned}$$

$$\begin{aligned}
\frac{\partial U_{BS}}{\partial q_{10}} = \int_0^L & \left[ -k_s \bar{B}_{15} (v_1 \dot{N}_{11} \dot{N}_{11} + v_2 \dot{N}_{11} \dot{N}_{22} + v_3 \dot{N}_{11} \dot{N}_{33}) \right. \\
& - k_s (\bar{A}_{66} + \bar{A}_{55}) (v_1 N_{11} \dot{N}_{11} + v_2 N_{11} \dot{N}_{22} + v_3 N_{11} \dot{N}_{33}) \\
& - \frac{1}{2} k_s \bar{B}_{16} (w_1 \dot{N}_{11} \dot{N}_{11} + w_2 \dot{N}_{11} \dot{N}_{22} + w_3 \dot{N}_{11} \dot{N}_{33}) \\
& - \frac{1}{2} k_s \bar{B}_{16} (\beta_{y1} \dot{N}_{11} N_{11} + \beta_{y2} \dot{N}_{11} N_{22} + \beta_{y3} \dot{N}_{11} N_{33}) \\
& + \frac{1}{2} k_s \bar{B}_{16} (\beta_{y1} N_{11} \dot{N}_{11} + \beta_{y2} N_{11} \dot{N}_{22} + \beta_{y3} N_{11} \dot{N}_{33}) \\
& + \bar{D}_{11} (\beta_{z1} \dot{N}_{11} \dot{N}_{11} + \beta_{z2} \dot{N}_{11} \dot{N}_{22} + \beta_{z3} \dot{N}_{11} \dot{N}_{33}) \\
& + k_s \bar{B}_{15} (\beta_{z1} \dot{N}_{11} N_{11} + \beta_{z2} \dot{N}_{11} N_{22} + \beta_{z3} \dot{N}_{11} N_{33}) \\
& + k_s \bar{B}_{15} (\beta_{z1} N_{11} \dot{N}_{11} + \beta_{z2} N_{11} \dot{N}_{22} + \beta_{z3} N_{11} \dot{N}_{33}) \\
& \left. + k_s (\bar{A}_{66} + \bar{A}_{55}) (\beta_{z1} N_{11} N_{11} + \beta_{z2} N_{11} N_{22} + \beta_{z3} N_{11} N_{33}) \right] dx \quad (C.31)
\end{aligned}$$

$$\begin{aligned}
\frac{\partial U_{BS}}{\partial q_{11}} = \int_0^L & \left[ -k_s \bar{B}_{15} (v_1 \dot{N}_{22} \dot{N}_{11} + v_2 \dot{N}_{22} \dot{N}_{22} + v_3 \dot{N}_{22} \dot{N}_{33}) \right. \\
& - k_s (\bar{A}_{66} + \bar{A}_{55}) (v_1 N_{22} \dot{N}_{11} + v_2 N_{22} \dot{N}_{22} + v_3 N_{22} \dot{N}_{33}) \\
& - \frac{1}{2} k_s \bar{B}_{16} (w_1 \dot{N}_{22} \dot{N}_{11} + w_2 \dot{N}_{22} \dot{N}_{22} + w_3 \dot{N}_{22} \dot{N}_{33}) \\
& - \frac{1}{2} k_s \bar{B}_{16} (\beta_{y1} \dot{N}_{22} N_{11} + \beta_{y2} \dot{N}_{22} N_{22} + \beta_{y3} \dot{N}_{22} N_{33}) \\
& + \frac{1}{2} k_s \bar{B}_{16} (\beta_{y1} N_{22} \dot{N}_{11} + \beta_{y2} N_{22} \dot{N}_{22} + \beta_{y3} N_{22} \dot{N}_{33}) \\
& + \bar{D}_{11} (\beta_{z1} \dot{N}_{22} \dot{N}_{11} + \beta_{z2} \dot{N}_{22} \dot{N}_{22} + \beta_{z3} \dot{N}_{22} \dot{N}_{33}) \\
& + k_s \bar{B}_{15} (\beta_{z1} \dot{N}_{22} N_{11} + \beta_{z2} \dot{N}_{22} N_{22} + \beta_{z3} \dot{N}_{22} N_{33}) \\
& + k_s \bar{B}_{15} (\beta_{z1} N_{22} \dot{N}_{11} + \beta_{z2} N_{22} \dot{N}_{22} + \beta_{z3} N_{22} \dot{N}_{33}) \\
& \left. + k_s (\bar{A}_{66} + \bar{A}_{55}) (\beta_{z1} N_{22} N_{11} + \beta_{z2} N_{22} N_{22} + \beta_{z3} N_{22} N_{33}) \right] dx \quad (C.32)
\end{aligned}$$

$$\begin{aligned}
\frac{\partial U_{BS}}{\partial q_{12}} = \int_0^L \bigg[ & -k_s \bar{B}_{15} (v_1 \dot{N}_{33} \dot{N}_{11} + v_2 \dot{N}_{33} \dot{N}_{22} + v_3 \dot{N}_{33} \dot{N}_{33}) \\
& - k_s (\bar{A}_{66} + \bar{A}_{55}) (v_1 N_{33} \dot{N}_{11} + v_2 N_{33} \dot{N}_{22} + v_3 N_{33} \dot{N}_{33}) \\
& - \frac{1}{2} k_s \bar{B}_{16} (w_1 \dot{N}_{33} \dot{N}_{11} + w_2 \dot{N}_{33} \dot{N}_{22} + w_3 \dot{N}_{33} \dot{N}_{33}) \\
& - \frac{1}{2} k_s \bar{B}_{16} (\beta_{y1} \dot{N}_{33} N_{11} + \beta_{y2} \dot{N}_{33} N_{22} + \beta_{y3} \dot{N}_{33} N_{33}) \\
& + \frac{1}{2} k_s \bar{B}_{16} (\beta_{y1} N_{33} \dot{N}_{11} + \beta_{y2} N_{33} \dot{N}_{22} + \beta_{y3} N_{33} \dot{N}_{33}) \\
& + \bar{D}_{11} (\beta_{z1} \dot{N}_{33} \dot{N}_{11} + \beta_{z2} \dot{N}_{33} \dot{N}_{22} + \beta_{z3} \dot{N}_{33} \dot{N}_{33}) \\
& + k_s \bar{B}_{15} (\beta_{z1} \dot{N}_{33} N_{11} + \beta_{z2} \dot{N}_{33} N_{22} + \beta_{z3} \dot{N}_{33} N_{33}) \\
& + k_s \bar{B}_{15} (\beta_{z1} N_{22} \dot{N}_{11} + \beta_{z2} N_{22} \dot{N}_{22} + \beta_{z3} N_{22} \dot{N}_{33}) \\
& + k_s (\bar{A}_{66} + \bar{A}_{55}) (\beta_{z1} N_{22} N_{11} + \beta_{z2} N_{22} N_{22} + \beta_{z3} N_{22} N_{33}) \bigg] dx \quad (C.33)
\end{aligned}$$

$$\frac{\partial U_F}{\partial q_1} = \int_0^L P (v_1 \dot{N}_{11} \dot{N}_{11} + v_2 \dot{N}_{11} \dot{N}_{22} + v_3 \dot{N}_{11} \dot{N}_{33}) dx \quad (C.34)$$

$$\frac{\partial U_F}{\partial q_2} = \int_0^L P (v_1 \dot{N}_{22} \dot{N}_{11} + v_2 \dot{N}_{22} \dot{N}_{22} + v_3 \dot{N}_{22} \dot{N}_{33}) dx \quad (C.35)$$

$$\frac{\partial U_F}{\partial q_3} = \int_0^L P (v_1 \dot{N}_{33} \dot{N}_{11} + v_2 \dot{N}_{33} \dot{N}_{22} + v_3 \dot{N}_{33} \dot{N}_{33}) dx \quad (C.36)$$

$$\frac{\partial U_F}{\partial q_4} = \int_0^L P (w_1 \dot{N}_{11} \dot{N}_{11} + w_2 \dot{N}_{11} \dot{N}_{22} + w_3 \dot{N}_{11} \dot{N}_{33}) dx \quad (\text{C.37})$$

$$\frac{\partial U_F}{\partial q_5} = \int_0^L P (w_1 \dot{N}_{22} \dot{N}_{11} + w_2 \dot{N}_{22} \dot{N}_{22} + w_3 \dot{N}_{22} \dot{N}_{33}) dx \quad (\text{C.38})$$

$$\frac{\partial U_F}{\partial q_6} = \int_0^L P (w_1 \dot{N}_{33} \dot{N}_{11} + w_2 \dot{N}_{33} \dot{N}_{22} + w_3 \dot{N}_{33} \dot{N}_{33}) dx \quad (\text{C.39})$$

$$\frac{\partial U_F}{\partial q_7} = \frac{\partial U_F}{\partial q_8} = \frac{\partial U_F}{\partial q_9} = \frac{\partial U_F}{\partial q_{10}} = \frac{\partial U_F}{\partial q_{11}} = \frac{\partial U_F}{\partial q_{12}} = 0 \quad (\text{C.40})$$

## Appendix D

### Conventional finite element

The displacement field of the shaft element in terms of nodal displacements and shape functions is

$$\begin{bmatrix} v \\ w \\ \beta_y \\ \beta_z \end{bmatrix} = \begin{bmatrix} N_{t1} & 0 & 0 & N_{t2} & N_{t3} & 0 & 0 & N_{t4} \\ 0 & N_{t1} & -N_{t2} & 0 & 0 & N_{t3} & -N_{t4} & 0 \\ 0 & -N_{r1} & N_{r2} & 0 & 0 & -N_{r3} & N_{r4} & 0 \\ N_{r1} & 0 & 0 & N_{r2} & N_{r3} & 0 & 0 & N_{r4} \end{bmatrix} \begin{bmatrix} v_1 \\ w_1 \\ \beta_{y1} \\ \beta_{z1} \\ v_2 \\ w_2 \\ \beta_{y2} \\ \beta_{z2} \end{bmatrix} \quad (\text{D.1})$$

The kinetic energy of tapered composite shaft is

$$\begin{aligned} T_{comp} = & \frac{1}{2} \int_0^L m_c(x) (\dot{v}^2 + \dot{w}^2) dx + \frac{1}{2} \int_0^L I_{dc}(x) (\dot{\beta}_y^2 + \dot{\beta}_z^2) dx \\ & - \int_0^L I_{pc}(x) \Omega \dot{\beta}_z \beta_y dx \end{aligned} \quad (\text{D.2})$$

The strain energy of the tapered composite shaft due to axial load is

$$U_F = \frac{1}{2} \int_0^L P \left[ \left( \frac{\partial v}{\partial x} \right)^2 + \left( \frac{\partial w}{\partial x} \right)^2 \right] dx \quad (\text{D.3})$$

The strain energy of the tapered composite shaft due to bending moments and shear forces is

$$\begin{aligned}
U_{BS} = \frac{1}{2} \int_0^L & \left[ \left( \frac{\partial \beta_y}{\partial x} \right) \left( \bar{D}_{11} \frac{\partial \beta_y}{\partial x} - \bar{B}_{15} k_s \left( \frac{\Gamma_1}{6} \frac{\partial^3 w}{\partial x^3} + \frac{\Gamma_2}{2} \frac{\partial^2 w}{\partial x^2} \right) \right. \right. \\
& + \frac{1}{2} \bar{B}_{16} k_s \left( \frac{\Gamma_1}{6} \frac{\partial^3 v}{\partial x^3} + \frac{\Gamma_2}{2} \frac{\partial^2 v}{\partial x^2} \right) \\
& + \left( \frac{\partial \beta_z}{\partial x} \right) \left( \bar{D}_{11} \frac{\partial \beta_z}{\partial x} + \bar{B}_{15} k_s \left( \frac{\Gamma_1}{6} \frac{\partial^3 v}{\partial x^3} + \frac{\Gamma_2}{2} \frac{\partial^2 v}{\partial x^2} \right) \right. \\
& + \frac{1}{2} \bar{B}_{16} k_s \left( \frac{\Gamma_1}{6} \frac{\partial^3 w}{\partial x^3} + \frac{\Gamma_2}{2} \frac{\partial^2 w}{\partial x^2} \right) \\
& - \left. \left. \left( \frac{\Gamma_1}{6} \frac{\partial^3 v}{\partial x^3} + \frac{\Gamma_2}{2} \frac{\partial^2 v}{\partial x^2} \right) k_s \left( \left( -\bar{B}_{51} \frac{\partial \beta_z}{\partial x} - \bar{A}_{55} \left( \frac{\Gamma_1}{6} \frac{\partial^3 v}{\partial x^3} + \frac{\Gamma_2}{2} \frac{\partial^2 v}{\partial x^2} \right) \right) \right. \right. \right. \\
& - \left. \left. \left( \frac{1}{2} \bar{B}_{61} \frac{\partial \beta_y}{\partial x} + \bar{A}_{66} \left( \frac{\Gamma_1}{6} \frac{\partial^3 v}{\partial x^3} + \frac{\Gamma_2}{2} \frac{\partial^2 v}{\partial x^2} \right) \right) \right) \right) \\
& - \left( \frac{\Gamma_1}{6} \frac{\partial^3 w}{\partial x^3} \right. \\
& + \left. \left. \frac{\Gamma_2}{2} \frac{\partial^2 w}{\partial x^2} \right) k_s \left( \left( \bar{B}_{51} \frac{\partial \beta_y}{\partial x} - \bar{A}_{55} \left( \frac{\Gamma_1}{6} \frac{\partial^3 w}{\partial x^3} + \frac{\Gamma_2}{2} \frac{\partial^2 w}{\partial x^2} \right) \right) \right. \right. \\
& + \left. \left. \left( -\frac{1}{2} \bar{B}_{61} \frac{\partial \beta_z}{\partial x} - \bar{A}_{66} \left( \frac{\Gamma_1}{6} \frac{\partial^3 w}{\partial x^3} + \frac{\Gamma_2}{2} \frac{\partial^2 w}{\partial x^2} \right) \right) \right) \right] dx
\end{aligned} \tag{D.4}$$

Substituting Equation (D.1) into Equations (D.2) – (D.4), and then applying Lagrange's equations, one can obtain the equations of motion of the tapered composite shaft. The generalized co-ordinates for the shaft element are

$$\{q\} = \{v_1 \quad w_1 \quad \beta_{y1} \quad \beta_{z1} \quad v_2 \quad w_2 \quad \beta_{y2} \quad \beta_{z2}\}^T \quad (D.5)$$

Using Lagrange's equation

$$\frac{d}{dt} \left( \frac{\partial L}{\partial \dot{q}} \right) - \frac{\partial L}{\partial q} = 0 \quad (D.6)$$

where

$$L = T_{comp} - (U_{BS} + U_F)$$

Applying Lagrange's equation gives

$$\begin{aligned} & \frac{d}{dt} \left[ \frac{\partial T_{comp}}{\partial \dot{q}_1} \right] - \frac{\partial T_{comp}}{\partial q_1} \\ &= \int_0^L [m_c(x) (\ddot{v}_1 N_{t1} N_{t1} + \ddot{\beta}_{z1} N_{t1} N_{t2} + \ddot{v}_2 N_{t1} N_{t3} \\ &+ \ddot{\beta}_{z2} N_{t1} N_{t4}) \\ &+ I_d(x) (\ddot{v}_1 N_{r1} N_{r1} + \ddot{\beta}_{z1} N_{r1} N_{r2} + \ddot{v}_2 N_{r1} N_{r3} \\ &+ \ddot{\beta}_{z2} N_{r1} N_{r4}) \\ &- I_p(x) (-\dot{w}_1 N_{r1} N_{r1} + \dot{\beta}_{y1} N_{r1} N_{r2} - \dot{w}_2 N_{r1} N_{r3} \\ &+ \dot{\beta}_{y2} N_{r1} N_{r4})] dx \quad (D.7) \end{aligned}$$

$$\begin{aligned}
& \frac{d}{dt} \left[ \frac{\partial T_{comp}}{\partial \dot{q}_2} \right] - \frac{\partial T_{comp}}{\partial q_2} \\
&= \int_0^L [m_c(x) (\ddot{w}_1 N_{t1} N_{t1} - \ddot{\beta}_{y1} N_{t1} N_{t2} + \ddot{w}_2 N_{t1} N_{t3} \\
&\quad - \ddot{\beta}_{y2} N_{t1} N_{t4}) \\
&\quad + I_d(x) (\ddot{w}_1 N_{r1} N_{r1} - \ddot{\beta}_{y1} N_{r1} N_{r2} + \ddot{w}_2 N_{r1} N_{r3} - \ddot{\beta}_{y2} N_{r1} N_{r4}) \\
&\quad - I_p(x) (\dot{v}_1 N_{r1} N_{r1} + \dot{\beta}_{z1} N_{r1} N_{r2} + \dot{v}_2 N_{r1} N_{r3} + \dot{\beta}_{z2} N_{r1} N_{r4})] dx \quad (D.8)
\end{aligned}$$

$$\begin{aligned}
& \frac{d}{dt} \left[ \frac{\partial T_{comp}}{\partial \dot{q}_3} \right] - \frac{\partial T_{comp}}{\partial q_3} \\
&= \int_0^L [m_c(x) (-\ddot{w}_1 N_{t2} N_{t1} + \ddot{\beta}_{y1} N_{t2} N_{t2} - \ddot{w}_2 N_{t2} N_{t3} \\
&\quad + \ddot{\beta}_{y2} N_{t2} N_{t4}) \\
&\quad + I_d(x) (-\ddot{w}_1 N_{r2} N_{r1} + \ddot{\beta}_{y1} N_{r2} N_{r2} - \ddot{w}_2 N_{r2} N_{r3} + \ddot{\beta}_{y2} N_{r2} N_{r4}) \\
&\quad + I_p(x) (\dot{v}_1 N_{r2} N_{r1} + \dot{\beta}_{z1} N_{r2} N_{r2} + \dot{v}_2 N_{r2} N_{r3} + \dot{\beta}_{z2} N_{r2} N_{r4})] dx \quad (D.9)
\end{aligned}$$

$$\begin{aligned}
& \frac{d}{dt} \left[ \frac{\partial T_{comp}}{\partial \dot{q}_4} \right] - \frac{\partial T_{comp}}{\partial q_4} \\
&= \int_0^L [m_c(x) (\dot{v}_1 N_{t2} N_{t1} + \dot{\beta}_{z1} N_{t2} N_{t2} + \dot{v}_2 N_{t2} N_{t3} + \dot{\beta}_{z2} N_{t2} N_{t4}) \\
&\quad + I_d(x) (\dot{v}_1 N_{r2} N_{r1} + \dot{\beta}_{z1} N_{r2} N_{r2} + \dot{v}_2 N_{r2} N_{r3} + \dot{\beta}_{z2} N_{r2} N_{r4}) \\
&\quad - I_p(x) (-\dot{w}_1 N_{r2} N_{r1} + \dot{\beta}_{y1} N_{r2} N_{r2} - \dot{w}_2 N_{r2} N_{r3} \\
&\quad + \dot{\beta}_{y2} N_{r2} N_{r4})] dx \quad (D.10)
\end{aligned}$$

$$\begin{aligned}
& \frac{d}{dt} \left[ \frac{\partial T_{comp}}{\partial \dot{q}_5} \right] - \frac{\partial T_{comp}}{\partial q_5} \\
&= \int_0^L [m_c(x) (\dot{v}_1 N_{t3} N_{t1} + \ddot{\beta}_{z1} N_{t3} N_{t2} + \dot{v}_2 N_{t3} N_{t3} \\
&\quad + \ddot{\beta}_{z2} N_{t3} N_{t4}) \\
&\quad + I_d(x) (\dot{v}_1 N_{r3} N_{r1} + \ddot{\beta}_{z1} N_{r3} N_{r2} + \dot{v}_2 N_{r3} N_{r3} \\
&\quad + \ddot{\beta}_{z2} N_{r3} N_{r4}) \\
&\quad - I_p(x) (-\dot{w}_1 N_{r3} N_{r1} + \dot{\beta}_{y1} N_{r3} N_{r2} - \dot{w}_2 N_{r3} N_{r3} \\
&\quad + \dot{\beta}_{y2} N_{r3} N_{r4})] dx \tag{D.11}
\end{aligned}$$

$$\begin{aligned}
& \frac{d}{dt} \left[ \frac{\partial T_{comp}}{\partial \dot{q}_6} \right] - \frac{\partial T_{comp}}{\partial q_6} \\
&= \int_0^L [m_c(x) (\ddot{w}_1 N_{t3} N_{t1} - \ddot{\beta}_{y1} N_{t3} N_{t2} + \ddot{w}_2 N_{t3} N_{t3} \\
&\quad - \ddot{\beta}_{y2} N_{t3} N_{t4}) \\
&\quad + I_d(x) (\ddot{w}_1 N_{r3} N_{r1} - \ddot{\beta}_{y1} N_{r3} N_{r2} + \ddot{w}_2 N_{r3} N_{r3} - \ddot{\beta}_{y2} N_{r3} N_{r4}) \\
&\quad - I_p(x) (\dot{v}_1 N_{r3} N_{r1} + \dot{\beta}_{z1} N_{r3} N_{r2} + \dot{v}_2 N_{r3} N_{r3} + \dot{\beta}_{z2} N_{r3} N_{r4})] dx \tag{D.12}
\end{aligned}$$

$$\begin{aligned}
& \frac{d}{dt} \left[ \frac{\partial T_{comp}}{\partial \dot{q}_7} \right] - \frac{\partial T_{comp}}{\partial q_7} \\
&= \int_0^L [m_c(x) (-\ddot{w}_1 N_{t4} N_{t1} + \ddot{\beta}_{y1} N_{t4} N_{t2} - \ddot{w}_2 N_{t4} N_{t3} \\
&\quad + \ddot{\beta}_{y2} N_{t4} N_{t4}) \\
&\quad + I_d(x) (-\ddot{w}_1 N_{r4} N_{r1} + \ddot{\beta}_{y1} N_{r4} N_{r2} - \ddot{w}_2 N_{r4} N_{r3} + \ddot{\beta}_{y2} N_{r4} N_{r4}) \\
&\quad + I_p(x) (\dot{v}_1 N_{r4} N_{r1} + \dot{\beta}_{z1} N_{r4} N_{r2} + \dot{v}_2 N_{r4} N_{r3} + \dot{\beta}_{z2} N_{r4} N_{r4})] dx \tag{D.13}
\end{aligned}$$

$$\begin{aligned}
& \frac{d}{dt} \left[ \frac{\partial T_{comp}}{\partial \dot{q}_8} \right] - \frac{\partial T_{comp}}{\partial q_8} \\
&= \int_0^L [m_c(x)(\ddot{v}_1 N_{t4} N_{t1} + \ddot{\beta}_{z1} N_{t4} N_{t2} + \ddot{v}_2 N_{t4} N_{t3} + \ddot{\beta}_{z2} N_{t4} N_{t3}) \\
&+ I_d(x)(\ddot{v}_1 N_{r4} N_{r1} + \ddot{\beta}_{z1} N_{r4} N_{r2} + \ddot{v}_2 N_{r4} N_{r3} + \ddot{\beta}_{z2} N_{r4} N_{r4}) \\
&- I_p(x)(-\dot{w}_1 N_{r4} N_{r1} + \dot{\beta}_{y1} N_{r4} N_{r2} - \dot{w}_2 N_{r4} N_{r3} \\
&+ \dot{\beta}_{y2} N_{r4} N_{r4})] dx \tag{D.14}
\end{aligned}$$

$$\begin{aligned}
\frac{\partial U_{BS}}{\partial q_1} &= \int_0^L \left[ \frac{\Gamma_1}{12} \bar{B}_{16} k_s \left( -w_1 \dot{\dot{N}}_{t1} \dot{N}_{r1} + \beta_{y1} \dot{\dot{N}}_{t1} \dot{N}_{r2} - w_2 \dot{\dot{N}}_{t1} \dot{N}_{r3} + \beta_{y2} \dot{\dot{N}}_{t1} \dot{N}_{r4} \right) \right. \\
&+ \frac{\Gamma_2}{4} \bar{B}_{16} k_s \left( -w_1 \dot{N}_{t1} \dot{N}_{r1} + \beta_{y1} \dot{N}_{t1} \dot{N}_{r2} - w_2 \dot{N}_{t1} \dot{N}_{r3} \right. \\
&+ \left. \beta_{y2} \dot{N}_{t1} \dot{N}_{r4} \right) \\
&+ \bar{D}_{11} (v_1 \dot{N}_{r1} \dot{N}_{r1} + \beta_{z1} \dot{N}_{r1} \dot{N}_{r2} + v_2 \dot{N}_{r1} \dot{N}_{r3} + \beta_{z2} \dot{N}_{r1} \dot{N}_{r4}) \\
&+ \frac{\Gamma_1}{6} \bar{B}_{15} k_s \left( v_1 \left( \dot{\dot{N}}_{t1} \dot{N}_{r1} + \dot{N}_{r1} \dot{\dot{N}}_{t1} \right) + \beta_{z1} \left( \dot{\dot{N}}_{t2} \dot{N}_{r1} + \dot{N}_{r2} \dot{\dot{N}}_{t1} \right) \right. \\
&+ \left. v_2 \left( \dot{\dot{N}}_{t3} \dot{N}_{r1} + \dot{N}_{r3} \dot{\dot{N}}_{t1} \right) + \beta_{z2} \left( \dot{\dot{N}}_{t4} \dot{N}_{r1} + \dot{N}_{r4} \dot{\dot{N}}_{t1} \right) \right) \\
&+ \frac{\Gamma_2}{2} \bar{B}_{15} k_s \left( v_1 \left( \dot{N}_{t1} \dot{N}_{r1} + \dot{N}_{r1} \dot{N}_{t1} \right) + \beta_{z1} \left( \dot{N}_{t2} \dot{N}_{r1} + \dot{N}_{r2} \dot{N}_{t1} \right) \right. \\
&+ \left. v_2 \left( \dot{N}_{t3} \dot{N}_{r1} + \dot{N}_{r3} \dot{N}_{t1} \right) + \beta_{z2} \left( \dot{N}_{t4} \dot{N}_{r1} + \dot{N}_{r4} \dot{N}_{t1} \right) \right) \\
&+ \frac{\Gamma_1}{12} \bar{B}_{16} k_s \left( w_1 \dot{N}_{r1} \dot{\dot{N}}_{t1} - \beta_{y1} \dot{N}_{r1} \dot{\dot{N}}_{t2} + w_2 \dot{N}_{r1} \dot{\dot{N}}_{t3} - \beta_{y2} \dot{N}_{r1} \dot{\dot{N}}_{t4} \right) \\
&+ \left. \frac{\Gamma_2}{4} \bar{B}_{16} k_s \left( w_1 \dot{N}_{r1} \dot{\dot{N}}_{t1} - \beta_{y1} \dot{N}_{r1} \dot{\dot{N}}_{t2} + w_2 \dot{N}_{r1} \dot{\dot{N}}_{t3} - \beta_{y2} \dot{N}_{r1} \dot{\dot{N}}_{t4} \right) \right]
\end{aligned}$$

$$\begin{aligned}
& + \frac{\Gamma_1^2}{36} k_s (\bar{A}_{66} + \bar{A}_{55}) \left( v_1 \dot{N}_{t1} \dot{N}_{t1} + \beta_{z1} \dot{N}_{t1} \dot{N}_{t2} + v_2 \dot{N}_{t1} \dot{N}_{t3} + \beta_{z2} \dot{N}_{t1} \dot{N}_{t4} \right) \\
& + \frac{\Gamma_1 \Gamma_2}{12} k_s (\bar{A}_{66} + \bar{A}_{55}) \left( v_1 \left( \dot{N}_{t1} \dot{N}_{t1} + \dot{N}_{t1} \dot{N}_{t1} \right) \right. \\
& + \beta_{z1} \left( \dot{N}_{t1} \dot{N}_{t2} + \dot{N}_{t1} \dot{N}_{t2} \right) + v_2 \left( \dot{N}_{t1} \dot{N}_{t3} + \dot{N}_{t1} \dot{N}_{t3} \right) \\
& \left. + \beta_{z2} \left( \dot{N}_{t1} \dot{N}_{t4} + \dot{N}_{t1} \dot{N}_{t4} \right) \right) \\
& + \frac{\Gamma_2^2}{4} k_s (\bar{A}_{66} + \bar{A}_{55}) \left( v_1 \dot{N}_{t1} \dot{N}_{t1} + \beta_{z1} \dot{N}_{t1} \dot{N}_{t2} + v_2 \dot{N}_{t1} \dot{N}_{t3} \right. \\
& \left. + \beta_{z2} \dot{N}_{t1} \dot{N}_{t4} \right) \Big] dx \tag{D.15}
\end{aligned}$$

$$\begin{aligned}
\frac{\partial U_{BS}}{\partial q_2} = \int_0^L \Big[ & \bar{D}_{11} (w_1 \dot{N}_{r1} \dot{N}_{r1} - \beta_{y1} \dot{N}_{r1} \dot{N}_{r2} + w_2 \dot{N}_{r1} \dot{N}_{r3} - \beta_{y2} \dot{N}_{r1} \dot{N}_{r4}) \\
& - \frac{\Gamma_1}{6} \bar{B}_{15} k_s \left( -w_1 \left( \dot{N}_{t1} \dot{N}_{r1} + \dot{N}_{r1} \dot{N}_{t1} \right) + \beta_{y1} \left( \dot{N}_{t1} \dot{N}_{r2} + \dot{N}_{r1} \dot{N}_{t2} \right) \right. \\
& \left. - w_2 \left( \dot{N}_{t1} \dot{N}_{r3} + \dot{N}_{r1} \dot{N}_{t3} \right) + \beta_{y2} \left( \dot{N}_{t1} \dot{N}_{r4} + \dot{N}_{r1} \dot{N}_{t4} \right) \right) \\
& - \frac{\Gamma_2}{2} \bar{B}_{15} k_s \left( -w_1 \left( \dot{N}_{t1} \dot{N}_{r1} + \dot{N}_{r1} \dot{N}_{t1} \right) + \beta_{w1} \left( \dot{N}_{t1} \dot{N}_{r2} + \dot{N}_{r1} \dot{N}_{t2} \right) \right. \\
& \left. - w_2 \left( \dot{N}_{t1} \dot{N}_{r3} + \dot{N}_{r1} \dot{N}_{t3} \right) + \beta_{y2} \left( \dot{N}_{t1} \dot{N}_{r4} + \dot{N}_{r1} \dot{N}_{t4} \right) \right) \\
& - \frac{\Gamma_1}{12} \bar{B}_{16} k_s \left( v_1 \dot{N}_{r1} \dot{N}_{t1} + \beta_{z1} \dot{N}_{r1} \dot{N}_{t2} + v_2 \dot{N}_{r1} \dot{N}_{t3} + \beta_{z2} \dot{N}_{r1} \dot{N}_{t4} \right) \\
& \left. - \frac{\Gamma_2}{4} \bar{B}_{16} k_s \left( v_1 \dot{N}_{r1} \dot{N}_{t1} + \beta_{z1} \dot{N}_{r1} \dot{N}_{t2} + v_2 \dot{N}_{r1} \dot{N}_{t3} + \beta_{z2} \dot{N}_{r1} \dot{N}_{t4} \right) \right]
\end{aligned}$$

$$\begin{aligned}
& \frac{\Gamma_1}{12} \bar{B}_{16} k_s \left( v_1 \dot{\dot{N}}_{t1} \dot{N}_{r1} + \beta_{z1} \dot{\dot{N}}_{t1} \dot{N}_{r2} + v_2 \dot{\dot{N}}_{t1} \dot{N}_{r3} + \beta_{z2} \dot{\dot{N}}_{t1} \dot{N}_{r4} \right) \\
& + \frac{\Gamma_2}{4} \bar{B}_{16} k_s \left( v_1 \dot{N}_{t1} \dot{N}_{r1} + \beta_{z1} \dot{N}_{t1} \dot{N}_{r2} + v_2 \dot{N}_{t1} \dot{N}_{r3} + \beta_{z2} \dot{N}_{t1} \dot{N}_{r4} \right) \\
& + \frac{\Gamma_1^2}{36} k_s (\bar{A}_{66} + \bar{A}_{55}) \left( w_1 \dot{\dot{N}}_{t1} \dot{\dot{N}}_{t1} - \beta_{y1} \dot{\dot{N}}_{t1} \dot{\dot{N}}_{t2} + w_2 \dot{\dot{N}}_{t1} \dot{\dot{N}}_{t3} \right. \\
& \left. - \beta_{y2} \dot{\dot{N}}_{t1} \dot{\dot{N}}_{t4} \right) \\
& + \frac{\Gamma_1 \Gamma_2}{12} k_s (\bar{A}_{66} + \bar{A}_{55}) \left( w_1 \left( \dot{N}_{t1} \dot{N}_{t1} + \dot{N}_{t1} \dot{\dot{N}}_{t1} \right) \right. \\
& \left. - \beta_{y1} \left( \dot{N}_{t1} \dot{N}_{t2} + \dot{N}_{t1} \dot{\dot{N}}_{t2} \right) + w_2 \left( \dot{N}_{t1} \dot{N}_{t3} + \dot{N}_{t1} \dot{\dot{N}}_{t3} \right) \right. \\
& \left. - \beta_{y2} \left( \dot{N}_{t1} \dot{N}_{t4} + \dot{N}_{t1} \dot{\dot{N}}_{t4} \right) \right) \\
& + \frac{\Gamma_2^2}{4} k_s (\bar{A}_{66} + \bar{A}_{55}) \left( w_1 \dot{N}_{t1} \dot{N}_{t1} - \beta_{y1} \dot{N}_{t1} \dot{N}_{t2} + w_2 \dot{N}_{t1} \dot{N}_{t3} \right. \\
& \left. - \beta_{y2} \dot{N}_{t1} \dot{N}_{t4} \right) \Big] dx
\end{aligned} \tag{D.16}$$

$$\begin{aligned}
\frac{\partial U_{BS}}{\partial q_3} &= \int_0^L \left[ \bar{D}_{11} \left( -w_1 \dot{N}_{r2} \dot{N}_{r1} + \beta_{y1} \dot{N}_{r2} \dot{N}_{r2} - w_2 \dot{N}_{r2} \dot{N}_{r3} + \beta_{y2} \dot{N}_{r2} \dot{N}_{r4} \right) \right. \\
& \left. - \frac{\Gamma_1}{6} \bar{B}_{15} k_s \left( w_1 \left( \dot{\dot{N}}_{t2} \dot{N}_{r1} + \dot{N}_{r2} \dot{\dot{N}}_{t1} \right) - \beta_{y1} \left( \dot{\dot{N}}_{t2} \dot{N}_{r2} + \dot{N}_{r2} \dot{\dot{N}}_{t2} \right) \right. \right. \\
& \left. \left. + w_2 \left( \dot{\dot{N}}_{t2} \dot{N}_{r3} + \dot{N}_{r2} \dot{\dot{N}}_{t3} \right) - \beta_{y2} \left( \dot{\dot{N}}_{t2} \dot{N}_{r4} + \dot{N}_{r2} \dot{\dot{N}}_{t4} \right) \right) \right]
\end{aligned}$$

$$\begin{aligned}
& -\frac{\Gamma_2}{2} \bar{B}_{15} k_s \left( w_1 \left( \dot{N}_{t2} \dot{N}_{r1} + \dot{N}_{r2} \dot{N}_{t1} \right) - \beta_{y1} \left( \dot{N}_{t2} \dot{N}_{r2} + \dot{N}_{r2} \dot{N}_{t2} \right) \right. \\
& \quad \left. + w_2 \left( \dot{N}_{t2} \dot{N}_{r3} + \dot{N}_{r2} \dot{N}_{t3} \right) - \beta_{y2} \left( \dot{N}_{t2} \dot{N}_{r4} + \dot{N}_{r2} \dot{N}_{t4} \right) \right) \\
& \quad + \frac{\Gamma_1}{12} \bar{B}_{16} k_s \left( v_1 \dot{N}_{r2} \dot{N}_{t1} + \beta_{z1} \dot{N}_{r2} \dot{N}_{t2} + v_2 \dot{N}_{r2} \dot{N}_{t3} + \beta_{z2} \dot{N}_{r2} \dot{N}_{t4} \right) \\
& \quad + \frac{\Gamma_2}{4} \bar{B}_{16} k_s \left( v_1 \dot{N}_{r2} \dot{N}_{t1} + \beta_{z1} \dot{N}_{r2} \dot{N}_{t2} + v_2 \dot{N}_{r2} \dot{N}_{t3} + \beta_{z2} \dot{N}_{r2} \dot{N}_{t4} \right) \\
& \quad - \frac{\Gamma_1}{12} \bar{B}_{16} k_s \left( v_1 \dot{N}_{t2} \dot{N}_{r1} + \beta_{z1} \dot{N}_{t2} \dot{N}_{r2} + v_2 \dot{N}_{t2} \dot{N}_{r3} + \beta_{z2} \dot{N}_{t2} \dot{N}_{r4} \right) \\
& \quad - \frac{\Gamma_2}{4} \bar{B}_{16} k_s \left( v_1 \dot{N}_{t2} \dot{N}_{r1} + \beta_{z1} \dot{N}_{t2} \dot{N}_{r2} + v_2 \dot{N}_{t2} \dot{N}_{r3} + \beta_{z2} \dot{N}_{t2} \dot{N}_{r4} \right) \\
& \quad + \frac{\Gamma_1^2}{36} k_s (\bar{A}_{66} + \bar{A}_{55}) \left( -w_1 \dot{N}_{t2} \dot{N}_{t1} + \beta_{y1} \dot{N}_{t2} \dot{N}_{t2} - w_2 \dot{N}_{t2} \dot{N}_{t3} \right. \\
& \quad \left. + \beta_{y2} \dot{N}_{t2} \dot{N}_{t4} \right) \\
& \quad + \frac{\Gamma_1 \Gamma_2}{12} k_s (\bar{A}_{66} + \bar{A}_{55}) \left( -w_1 \left( \dot{N}_{t2} \dot{N}_{t1} + \dot{N}_{t2} \dot{N}_{t1} \right) \right. \\
& \quad \left. + \beta_{y1} \left( \dot{N}_{t2} \dot{N}_{t2} + \dot{N}_{t2} \dot{N}_{t2} \right) - w_2 \left( \dot{N}_{t2} \dot{N}_{t3} + \dot{N}_{t2} \dot{N}_{t3} \right) \right. \\
& \quad \left. + \beta_{y2} \left( \dot{N}_{t2} \dot{N}_{t4} + \dot{N}_{t2} \dot{N}_{t4} \right) \right) \\
& \quad + \frac{\Gamma_2^2}{4} k_s (\bar{A}_{66} + \bar{A}_{55}) \left( -w_1 \dot{N}_{t2} \dot{N}_{t1} + \beta_{y1} \dot{N}_{t2} \dot{N}_{t2} - w_2 \dot{N}_{t2} \dot{N}_{t3} \right. \\
& \quad \left. + \beta_{y2} \dot{N}_{t2} \dot{N}_{t4} \right) \Big] dx
\end{aligned}$$

(D.17)

$$\begin{aligned}
\frac{\partial U_{BS}}{\partial q_4} = & \int_0^L \left[ \frac{\Gamma_1}{12} \bar{B}_{16} k_s \left( -w_1 \dot{\dot{N}}_{t2} \dot{N}_{r1} + \beta_{y1} \dot{\dot{N}}_{t2} \dot{N}_{r2} - w_2 \dot{\dot{N}}_{t2} \dot{N}_{r3} + \beta_{y2} \dot{\dot{N}}_{t2} \dot{N}_{r4} \right) \right. \\
& + \frac{\Gamma_2}{4} \bar{B}_{16} k_s \left( -w_1 \dot{N}_{t2} \dot{N}_{r1} + \beta_{y1} \dot{N}_{t2} \dot{N}_{r2} - w_2 \dot{N}_{t2} \dot{N}_{r3} \right. \\
& + \left. \beta_{y2} \dot{N}_{t2} \dot{N}_{r4} \right) \\
& + \bar{D}_{11} \left( v_1 \dot{N}_{r2} \dot{N}_{r1} + \beta_{z1} \dot{N}_{r2} \dot{N}_{r2} + v_2 \dot{N}_{r2} \dot{N}_{r3} + \beta_{z2} \dot{N}_{r2} \dot{N}_{r4} \right) \\
& + \frac{\Gamma_1}{6} \bar{B}_{15} k_s \left( v_1 \left( \dot{\dot{N}}_{t1} \dot{N}_{r2} + \dot{N}_{r1} \dot{\dot{N}}_{t2} \right) + \beta_{z1} \left( \dot{\dot{N}}_{t2} \dot{N}_{r2} + \dot{N}_{r2} \dot{\dot{N}}_{t2} \right) \right. \\
& + v_2 \left( \dot{\dot{N}}_{t3} \dot{N}_{r2} + \dot{N}_{r3} \dot{\dot{N}}_{t2} \right) + \beta_{z2} \left( \dot{\dot{N}}_{t4} \dot{N}_{r2} + \dot{N}_{r4} \dot{\dot{N}}_{t2} \right) \left. \right) \\
& + \frac{\Gamma_2}{2} \bar{B}_{15} k_s \left( v_1 \left( \dot{N}_{t1} \dot{N}_{r2} + \dot{N}_{r1} \dot{N}_{t2} \right) + \beta_{z1} \left( \dot{N}_{t2} \dot{N}_{r2} + \dot{N}_{r2} \dot{N}_{t2} \right) \right. \\
& + v_2 \left( \dot{N}_{t3} \dot{N}_{r2} + \dot{N}_{r3} \dot{N}_{t2} \right) + \beta_{z2} \left( \dot{N}_{t4} \dot{N}_{r2} + \dot{N}_{r4} \dot{N}_{t2} \right) \left. \right) \\
& + \frac{\Gamma_1}{12} \bar{B}_{16} k_s \left( w_1 \dot{N}_{r2} \dot{\dot{N}}_{t1} - \beta_{y1} \dot{N}_{r2} \dot{\dot{N}}_{t2} + w_2 \dot{N}_{r2} \dot{\dot{N}}_{t3} - \beta_{y2} \dot{N}_{r2} \dot{\dot{N}}_{t4} \right) \\
& + \frac{\Gamma_2}{4} \bar{B}_{16} k_s \left( w_1 \dot{N}_{r2} \dot{N}_{t1} - \beta_{y1} \dot{N}_{r2} \dot{N}_{t2} + w_2 \dot{N}_{r2} \dot{N}_{t3} - \beta_{y2} \dot{N}_{r2} \dot{N}_{t4} \right) \\
& + \frac{\Gamma_1^2}{36} k_s (\bar{A}_{66} + \bar{A}_{55}) \left( v_1 \dot{\dot{N}}_{t2} \dot{\dot{N}}_{t1} + \beta_{z1} \dot{\dot{N}}_{t2} \dot{\dot{N}}_{t2} + v_2 \dot{\dot{N}}_{t2} \dot{\dot{N}}_{t3} \right. \\
& + \left. \beta_{z2} \dot{\dot{N}}_{t2} \dot{\dot{N}}_{t4} \right) \\
& + \frac{\Gamma_1 \Gamma_2}{12} k_s (\bar{A}_{66} + \bar{A}_{55}) \left( v_1 \left( \dot{\dot{N}}_{t2} \dot{N}_{t1} + \dot{N}_{t2} \dot{\dot{N}}_{t1} \right) \right. \\
& + \beta_{z1} \left( \dot{\dot{N}}_{t2} \dot{N}_{t2} + \dot{N}_{t2} \dot{\dot{N}}_{t2} \right) + v_2 \left( \dot{\dot{N}}_{t2} \dot{N}_{t3} + \dot{N}_{t2} \dot{\dot{N}}_{t3} \right) \\
& + \left. \beta_{z2} \left( \dot{\dot{N}}_{t2} \dot{N}_{t4} + \dot{N}_{t2} \dot{\dot{N}}_{t4} \right) \right) \\
& \left. + \frac{\Gamma_2^2}{4} k_s (\bar{A}_{66} + \bar{A}_{55}) \left( v_1 \dot{N}_{t2} \dot{N}_{t1} + \beta_{z1} \dot{N}_{t2} \dot{N}_{t2} + v_2 \dot{N}_{t2} \dot{N}_{t3} + \beta_{z2} \dot{N}_{t2} \dot{N}_{t4} \right) \right] dx \quad (D.18)
\end{aligned}$$

$$\begin{aligned}
\frac{\partial U_{BS}}{\partial q_5} = & \int_0^L \left[ \frac{\Gamma_1}{12} \bar{B}_{16} k_s \left( -w_1 \dot{\dot{N}}_{t3} \dot{N}_{r1} + \beta_{y1} \dot{\dot{N}}_{t3} \dot{N}_{r2} - w_2 \dot{\dot{N}}_{t3} \dot{N}_{r3} + \beta_{y2} \dot{\dot{N}}_{t3} \dot{N}_{r4} \right) \right. \\
& + \frac{\Gamma_2}{4} \bar{B}_{16} k_s \left( -w_1 \dot{\dot{N}}_{t3} \dot{N}_{r1} + \beta_{y1} \dot{\dot{N}}_{t3} \dot{N}_{r2} - w_2 \dot{\dot{N}}_{t3} \dot{N}_{r3} \right. \\
& + \left. \beta_{y2} \dot{\dot{N}}_{t3} \dot{N}_{r4} \right) \\
& + \bar{D}_{11} (v_1 \dot{N}_{r3} \dot{N}_{r1} + \beta_{z1} \dot{N}_{r3} \dot{N}_{r2} + v_2 \dot{N}_{r3} \dot{N}_{r3} + \beta_{z2} \dot{N}_{r3} \dot{N}_{r4}) \\
& + \frac{\Gamma_1}{6} \bar{B}_{15} k_s \left( v_1 \left( \dot{\dot{N}}_{t1} \dot{N}_{r3} + \dot{N}_{r1} \dot{\dot{N}}_{t3} \right) + \beta_{z1} \left( \dot{\dot{N}}_{t2} \dot{N}_{r3} + \dot{N}_{r2} \dot{\dot{N}}_{t3} \right) \right. \\
& + \left. v_2 \left( \dot{\dot{N}}_{t3} \dot{N}_{r3} + \dot{N}_{r3} \dot{\dot{N}}_{t3} \right) + \beta_{z2} \left( \dot{\dot{N}}_{t4} \dot{N}_{r3} + \dot{N}_{r4} \dot{\dot{N}}_{t3} \right) \right) \\
& + \frac{\Gamma_2}{2} \bar{B}_{15} k_s \left( v_1 \left( \dot{\dot{N}}_{t1} \dot{N}_{r3} + \dot{N}_{r1} \dot{\dot{N}}_{t3} \right) + \beta_{z1} \left( \dot{\dot{N}}_{t2} \dot{N}_{r3} + \dot{N}_{r2} \dot{\dot{N}}_{t3} \right) \right. \\
& + \left. v_2 \left( \dot{\dot{N}}_{t3} \dot{N}_{r3} + \dot{N}_{r3} \dot{\dot{N}}_{t3} \right) + \beta_{z2} \left( \dot{\dot{N}}_{t4} \dot{N}_{r3} + \dot{N}_{r4} \dot{\dot{N}}_{t3} \right) \right) \\
& + \frac{\Gamma_1}{12} \bar{B}_{16} k_s \left( w_1 \dot{N}_{r3} \dot{\dot{N}}_{t1} - \beta_{y1} \dot{N}_{r3} \dot{\dot{N}}_{t2} + w_2 \dot{N}_{r3} \dot{\dot{N}}_{t3} - \beta_{y2} \dot{N}_{r3} \dot{\dot{N}}_{t4} \right) \\
& + \frac{\Gamma_2}{4} \bar{B}_{16} k_s \left( w_1 \dot{N}_{r3} \dot{\dot{N}}_{t1} - \beta_{y1} \dot{N}_{r3} \dot{\dot{N}}_{t2} + w_2 \dot{N}_{r3} \dot{\dot{N}}_{t3} - \beta_{y2} \dot{N}_{r3} \dot{\dot{N}}_{t4} \right) \\
& + \frac{\Gamma_1^2}{36} k_s (\bar{A}_{66} + \bar{A}_{55}) \left( v_1 \dot{\dot{N}}_{t3} \dot{\dot{N}}_{t1} + \beta_{z1} \dot{\dot{N}}_{t3} \dot{\dot{N}}_{t2} + v_2 \dot{\dot{N}}_{t3} \dot{\dot{N}}_{t3} \right. \\
& + \left. \beta_{z2} \dot{\dot{N}}_{t3} \dot{\dot{N}}_{t4} \right)
\end{aligned}$$

$$\begin{aligned}
& + \frac{\Gamma_1 \Gamma_2}{12} k_s (\bar{A}_{66} + \bar{A}_{55}) \left( v_1 \left( \dot{\dot{N}}_{t3} \dot{N}_{t1} + \dot{N}_{t3} \dot{\dot{N}}_{t1} \right) + \beta_{z1} \left( \dot{\dot{N}}_{t3} \dot{N}_{t2} + \dot{N}_{t3} \dot{\dot{N}}_{t2} \right) \right. \\
& \quad \left. + v_2 \left( \dot{\dot{N}}_{t3} \dot{N}_{t3} + \dot{N}_{t3} \dot{\dot{N}}_{t3} \right) + \beta_{z2} \left( \dot{\dot{N}}_{t3} \dot{N}_{t4} + \dot{N}_{t3} \dot{\dot{N}}_{t4} \right) \right) \\
& \quad + \frac{\Gamma_2^2}{4} k_s (\bar{A}_{66} + \bar{A}_{55}) \left( v_1 \dot{N}_{t3} \dot{N}_{t1} + \beta_{z1} \dot{N}_{t3} \dot{N}_{t2} + v_2 \dot{N}_{t3} \dot{N}_{t3} \right. \\
& \quad \left. + \beta_{z2} \dot{N}_{t3} \dot{N}_{t4} \right) \Big] dx \tag{D.19}
\end{aligned}$$

$$\begin{aligned}
\frac{\partial U_{BS}}{\partial q_6} = \int_0^L \Big[ & \bar{D}_{11} (w_1 \dot{N}_{r3} \dot{N}_{r1} - \beta_{y1} \dot{N}_{r3} \dot{N}_{r2} + w_2 \dot{N}_{r1} \dot{N}_{r3} - \beta_{y2} \dot{N}_{r1} \dot{N}_{r4}) \\
& - \frac{\Gamma_1}{6} \bar{B}_{15} k_s \left( -w_1 \left( \dot{\dot{N}}_{t3} \dot{N}_{r1} + \dot{N}_{r3} \dot{\dot{N}}_{t1} \right) + \beta_{y1} \left( \dot{\dot{N}}_{t3} \dot{N}_{r2} + \dot{N}_{r3} \dot{\dot{N}}_{t2} \right) \right. \\
& \quad \left. - w_2 \left( \dot{\dot{N}}_{t3} \dot{N}_{r3} + \dot{N}_{r3} \dot{\dot{N}}_{t3} \right) + \beta_{y2} \left( \dot{\dot{N}}_{t3} \dot{N}_{r4} + \dot{N}_{r3} \dot{\dot{N}}_{t4} \right) \right) \\
& - \frac{\Gamma_2}{2} \bar{B}_{15} k_s \left( -w_1 \left( \dot{\dot{N}}_{t3} \dot{N}_{r1} + \dot{N}_{r3} \dot{\dot{N}}_{t1} \right) + \beta_{w1} \left( \dot{\dot{N}}_{t3} \dot{N}_{r2} + \dot{N}_{r3} \dot{\dot{N}}_{t2} \right) \right. \\
& \quad \left. - w_2 \left( \dot{\dot{N}}_{t3} \dot{N}_{r3} + \dot{N}_{r3} \dot{\dot{N}}_{t3} \right) + \beta_{y2} \left( \dot{\dot{N}}_{t3} \dot{N}_{r4} + \dot{N}_{r3} \dot{\dot{N}}_{t4} \right) \right) \\
& - \frac{\Gamma_1}{12} \bar{B}_{16} k_s \left( v_1 \dot{N}_{r3} \dot{\dot{N}}_{t1} + \beta_{z1} \dot{N}_{r3} \dot{\dot{N}}_{t2} + v_2 \dot{N}_{r3} \dot{\dot{N}}_{t3} + \beta_{z2} \dot{N}_{r3} \dot{\dot{N}}_{t4} \right) \\
& - \frac{\Gamma_2}{4} \bar{B}_{16} k_s \left( v_1 \dot{N}_{r3} \dot{N}_{t1} + \beta_{z1} \dot{N}_{r3} \dot{N}_{t2} + v_2 \dot{N}_{r3} \dot{N}_{t3} + \beta_{z2} \dot{N}_{r3} \dot{N}_{t4} \right) \\
& + \frac{\Gamma_1}{12} \bar{B}_{16} k_s \left( v_1 \dot{\dot{N}}_{t3} \dot{N}_{r1} + \beta_{z1} \dot{\dot{N}}_{t3} \dot{N}_{r2} + v_2 \dot{\dot{N}}_{t3} \dot{N}_{r3} + \beta_{z2} \dot{\dot{N}}_{t3} \dot{N}_{r4} \right) \\
& + \frac{\Gamma_2}{4} \bar{B}_{16} k_s \left( v_1 \dot{N}_{t3} \dot{N}_{r1} + \beta_{z1} \dot{N}_{t3} \dot{N}_{r2} + v_2 \dot{N}_{t3} \dot{N}_{r3} + \beta_{z2} \dot{N}_{t3} \dot{N}_{r4} \right)
\end{aligned}$$

$$\begin{aligned}
& + \frac{\Gamma_1^2}{36} k_s (\bar{A}_{66} + \bar{A}_{55}) \left( w_1 \dot{\dot{N}}_{t3} \dot{\dot{N}}_{t1} - \beta_{y1} \dot{\dot{N}}_{t3} \dot{\dot{N}}_{t2} + w_2 \dot{\dot{N}}_{t3} \dot{\dot{N}}_{t3} - \beta_{y2} \dot{\dot{N}}_{t3} \dot{\dot{N}}_{t4} \right) \\
& + \frac{\Gamma_1 \Gamma_2}{12} k_s (\bar{A}_{66} + \bar{A}_{55}) \left( w_1 \left( \dot{\dot{N}}_{t3} \dot{\dot{N}}_{t1} + \dot{\dot{N}}_{t3} \dot{\dot{N}}_{t1} \right) \right. \\
& - \beta_{y1} \left( \dot{\dot{N}}_{t3} \dot{\dot{N}}_{t2} + \dot{\dot{N}}_{t3} \dot{\dot{N}}_{t2} \right) + w_2 \left( \dot{\dot{N}}_{t3} \dot{\dot{N}}_{t3} + \dot{\dot{N}}_{t3} \dot{\dot{N}}_{t3} \right) \\
& \left. - \beta_{y2} \left( \dot{\dot{N}}_{t3} \dot{\dot{N}}_{t4} + \dot{\dot{N}}_{t3} \dot{\dot{N}}_{t4} \right) \right) \\
& + \frac{\Gamma_2^2}{4} k_s (A_{44} + A_{55}) \left( w_1 \dot{\dot{N}}_{t3} \dot{\dot{N}}_{t1} - \beta_{y1} \dot{\dot{N}}_{t3} \dot{\dot{N}}_{t2} + w_2 \dot{\dot{N}}_{t3} \dot{\dot{N}}_{t3} \right. \\
& \left. - \beta_{y2} \dot{\dot{N}}_{t3} \dot{\dot{N}}_{t4} \right) \Big] dx \tag{D.20}
\end{aligned}$$

$$\begin{aligned}
\frac{\partial U_{BS}}{\partial q_7} &= \int_0^L \left[ \bar{D}_{11} (-w_1 \dot{N}_{r4} \dot{N}_{r1} + \beta_{y1} \dot{N}_{r4} \dot{N}_{r2} - w_2 \dot{N}_{r4} \dot{N}_{r3} + \beta_{y2} \dot{N}_{r2} \dot{N}_{r4}) \right. \\
& - \frac{\Gamma_1}{6} \bar{B}_{15} k_s \left( w_1 \left( \dot{\dot{N}}_{t4} \dot{N}_{r1} + \dot{N}_{r4} \dot{\dot{N}}_{t1} \right) - \beta_{y1} \left( \dot{\dot{N}}_{t4} \dot{N}_{r2} + \dot{N}_{r4} \dot{\dot{N}}_{t2} \right) \right. \\
& \left. + w_2 \left( \dot{\dot{N}}_{t4} \dot{N}_{r3} + \dot{N}_{r4} \dot{\dot{N}}_{t3} \right) - \beta_{y2} \left( \dot{\dot{N}}_{t4} \dot{N}_{r4} + \dot{N}_{r4} \dot{\dot{N}}_{t4} \right) \right) \\
& - \frac{\Gamma_2}{2} \bar{B}_{15} k_s \left( w_1 \left( \dot{\dot{N}}_{t4} \dot{N}_{r1} + \dot{N}_{r4} \dot{\dot{N}}_{t1} \right) - \beta_{y1} \left( \dot{\dot{N}}_{t4} \dot{N}_{r2} + \dot{N}_{r4} \dot{\dot{N}}_{t2} \right) \right. \\
& \left. + w_2 \left( \dot{\dot{N}}_{t4} \dot{N}_{r3} + \dot{N}_{r4} \dot{\dot{N}}_{t3} \right) - \beta_{y2} \left( \dot{\dot{N}}_{t4} \dot{N}_{r4} + \dot{N}_{r4} \dot{\dot{N}}_{t4} \right) \right) \\
& + \frac{\Gamma_1}{12} \bar{B}_{16} k_s \left( v_1 \dot{N}_{r4} \dot{\dot{N}}_{t1} + \beta_{z1} \dot{N}_{r4} \dot{\dot{N}}_{t2} + v_2 \dot{N}_{r4} \dot{\dot{N}}_{t3} + \beta_{z2} \dot{N}_{r4} \dot{\dot{N}}_{t4} \right) \\
& \left. + \frac{\Gamma_2}{4} \bar{B}_{16} k_s \left( v_1 \dot{N}_{r4} \dot{\dot{N}}_{t1} + \beta_{z1} \dot{N}_{r4} \dot{\dot{N}}_{t2} + v_2 \dot{N}_{r4} \dot{\dot{N}}_{t3} + \beta_{z2} \dot{N}_{r4} \dot{\dot{N}}_{t4} \right) \right]
\end{aligned}$$

$$\begin{aligned}
& -\frac{\Gamma_1}{12} \bar{B}_{16} k_s \left( v_1 \dot{\dot{N}}_{t4} \dot{N}_{r1} + \beta_{z1} \dot{\dot{N}}_{t4} \dot{N}_{r2} + v_2 \dot{\dot{N}}_{t4} \dot{N}_{r3} + \beta_{z2} \dot{\dot{N}}_{t4} \dot{N}_{r4} \right) \\
& -\frac{\Gamma_2}{4} \bar{B}_{16} k_s \left( v_1 \dot{N}_{t4} \dot{N}_{r1} + \beta_{z1} \dot{N}_{t4} \dot{N}_{r2} + v_2 \dot{N}_{t4} \dot{N}_{r3} + \beta_{z2} \dot{N}_{t4} \dot{N}_{r4} \right) \\
& + \frac{\Gamma_1^2}{36} k_s (\bar{A}_{66} + \bar{A}_{55}) \left( -w_1 \dot{\dot{N}}_{t4} \dot{\dot{N}}_{t1} + \beta_{y1} \dot{\dot{N}}_{t4} \dot{\dot{N}}_{t2} - w_2 \dot{\dot{N}}_{t4} \dot{\dot{N}}_{t3} \right. \\
& \left. + \beta_{y2} \dot{\dot{N}}_{t4} \dot{\dot{N}}_{t4} \right) \\
& + \frac{\Gamma_1 \Gamma_2}{12} k_s (\bar{A}_{66} + \bar{A}_{55}) \left( -w_1 \left( \dot{N}_{t4} \dot{N}_{t1} + \dot{N}_{t4} \dot{N}_{t1} \right) \right. \\
& \left. + \beta_{y1} \left( \dot{N}_{t4} \dot{N}_{t2} + \dot{N}_{t4} \dot{N}_{t2} \right) - w_2 \left( \dot{N}_{t4} \dot{N}_{t3} + \dot{N}_{t4} \dot{N}_{t3} \right) \right. \\
& \left. + \beta_{y2} \left( \dot{N}_{t4} \dot{N}_{t4} + \dot{N}_{t4} \dot{N}_{t4} \right) \right) \\
& + \frac{\Gamma_2^2}{4} k_s (\bar{A}_{66} + \bar{A}_{55}) \left( -w_1 \dot{N}_{t4} \dot{N}_{t1} + \beta_{y1} \dot{N}_{t4} \dot{N}_{t2} - w_2 \dot{N}_{t4} \dot{N}_{t3} \right. \\
& \left. + \beta_{y2} \dot{N}_{t4} \dot{N}_{t4} \right) \Big] dx
\end{aligned} \tag{D.21}$$

$$\begin{aligned}
\frac{\partial U_{BS}}{\partial q_8} &= \int_0^L \left[ \frac{\Gamma_1}{12} \bar{B}_{16} k_s \left( -w_1 \dot{\dot{N}}_{t4} \dot{N}_{r1} + \beta_{y1} \dot{\dot{N}}_{t4} \dot{N}_{r2} - w_2 \dot{\dot{N}}_{t4} \dot{N}_{r3} + \beta_{y2} \dot{\dot{N}}_{t4} \dot{N}_{r4} \right) \right. \\
& + \frac{\Gamma_2}{4} \bar{B}_{16} k_s \left( -w_1 \dot{N}_{t4} \dot{N}_{r1} + \beta_{y1} \dot{N}_{t4} \dot{N}_{r2} - w_2 \dot{N}_{t4} \dot{N}_{r3} \right. \\
& \left. + \beta_{y2} \dot{N}_{t4} \dot{N}_{r4} \right) \\
& \left. + \bar{D}_{11} \left( v_1 \dot{N}_{r4} \dot{N}_{r1} + \beta_{z1} \dot{N}_{r4} \dot{N}_{r2} + v_2 \dot{N}_{r4} \dot{N}_{r3} + \beta_{z2} \dot{N}_{r4} \dot{N}_{r4} \right) \right] dx
\end{aligned}$$

$$\begin{aligned}
& + \frac{\Gamma_1}{6} \bar{B}_{15} k_s \left( v_1 \left( \dot{\dot{N}}_{t1} \dot{N}_{r4} + \dot{N}_{r1} \dot{\dot{N}}_{t4} \right) + \beta_{z1} \left( \dot{\dot{N}}_{t2} \dot{N}_{r4} + \dot{N}_{r2} \dot{\dot{N}}_{t4} \right) \right. \\
& \quad \left. + v_2 \left( \dot{\dot{N}}_{t3} \dot{N}_{r4} + \dot{N}_{r3} \dot{\dot{N}}_{t4} \right) + \beta_{z2} \left( \dot{\dot{N}}_{t4} \dot{N}_{r4} + \dot{N}_{r4} \dot{\dot{N}}_{t4} \right) \right) \\
& + \frac{\Gamma_2}{2} \bar{B}_{15} k_s \left( v_1 \left( \dot{N}_{t1} \dot{N}_{r4} + \dot{N}_{r1} \dot{N}_{t4} \right) + \beta_{z1} \left( \dot{N}_{t2} \dot{N}_{r4} + \dot{N}_{r2} \dot{N}_{t4} \right) \right. \\
& \quad \left. + v_2 \left( \dot{N}_{t3} \dot{N}_{r4} + \dot{N}_{r3} \dot{N}_{t4} \right) + \beta_{z2} \left( \dot{N}_{t4} \dot{N}_{r4} + \dot{N}_{r4} \dot{N}_{t4} \right) \right) \\
& + \frac{\Gamma_1}{12} \bar{B}_{16} k_s \left( w_1 \dot{N}_{r4} \dot{\dot{N}}_{t1} - \beta_{y1} \dot{N}_{r4} \dot{\dot{N}}_{t2} + w_2 \dot{N}_{r4} \dot{\dot{N}}_{t3} - \beta_{y2} \dot{N}_{r4} \dot{\dot{N}}_{t4} \right) \\
& + \frac{\Gamma_2}{4} \bar{B}_{16} k_s \left( w_1 \dot{N}_{r4} \dot{N}_{t1} - \beta_{y1} \dot{N}_{r4} \dot{N}_{t2} + w_2 \dot{N}_{r4} \dot{N}_{t3} - \beta_{y2} \dot{N}_{r4} \dot{N}_{t4} \right) \\
& + \frac{\Gamma_1^2}{36} k_s (\bar{A}_{66} + \bar{A}_{55}) \left( v_1 \dot{\dot{N}}_{t4} \dot{\dot{N}}_{t1} + \beta_{z1} \dot{\dot{N}}_{t4} \dot{\dot{N}}_{t2} + v_2 \dot{\dot{N}}_{t4} \dot{\dot{N}}_{t3} \right. \\
& \quad \left. + \beta_{z2} \dot{\dot{N}}_{t4} \dot{\dot{N}}_{t4} \right) \\
& + \frac{\Gamma_1 \Gamma_2}{12} k_s (\bar{A}_{66} + \bar{A}_{55}) \left( v_1 \left( \dot{\dot{N}}_{t4} \dot{N}_{t1} + \dot{N}_{t4} \dot{\dot{N}}_{t1} \right) \right. \\
& \quad \left. + \beta_{z1} \left( \dot{\dot{N}}_{t4} \dot{N}_{t2} + \dot{N}_{t4} \dot{\dot{N}}_{t2} \right) + v_2 \left( \dot{\dot{N}}_{t4} \dot{N}_{t3} + \dot{N}_{t4} \dot{\dot{N}}_{t3} \right) \right. \\
& \quad \left. + \beta_{z2} \left( \dot{\dot{N}}_{t4} \dot{N}_{t4} + \dot{N}_{t4} \dot{\dot{N}}_{t4} \right) \right) + \frac{\Gamma_2^2}{4} k_s (\bar{A}_{66} + \bar{A}_{55}) \left( v_1 \dot{N}_{t4} \dot{N}_{t1} \right. \\
& \quad \left. + \beta_{z1} \dot{N}_{t4} \dot{N}_{t2} + v_2 \dot{N}_{t4} \dot{N}_{t3} + \beta_{z2} \dot{N}_{t4} \dot{N}_{t4} \right) \Big] dx
\end{aligned}$$

(D.22)